PSL UNIVERSITÉ PARIS

THÈSE DE DOCTORAT

DE L'UNIVERSITÉ PSL

Préparée à Mines Paris - PSL

Optimisation Stochastique Distribuée pour la Gestion de Centrales Virtuelles Complexes : Valorisation de la Flexibilité d'une Chaîne de Centrales Hydrauliques au Fil de l'Eau pour l'Intégration des Énergies Renouvelables

Distributed Stochastic Optimization for Operating Complex Virtual Power Plants: Leveraging Cascaded Run-of-the-River Hydropower Flexibility for Renewable Energy Integration

Soutenue par

Luca SANTOSUOSSO

Le 27/01/2025

Dirigée par

Georges KARINIOTAKIS

Co-encadrée par

Simon CAMAL

École doctorale n°621

Ingénierie des Systèmes, Matériaux, Mécanique, Energétique

Spécialité

Energétique et procédés

MINES PARIS | PSL

Composition du jury :

Luce BROTCORNE	Directrice de recherche, INRIA, Université de Lille	*Présidente*
Gianfranco CHICCO	Professor, Politecnico di Torino	*Rapporteur*
Lennart SÖDER	Professor, KTH Royal Institute of Technology	*Rapporteur*
Asgeir TOMASGARD	Professor, Norwegian University of Science and Technology - NTNU	*Rapporteur*
Jalal KAZEMPOUR	Professor, Technical University of Denmark - DTU	*Examinateur*
Malcolm MCCULLOCH	Professor, University of Oxford	*Examinateur*
Simon CAMAL	Chargé de recherche, Mines Paris - PSL	*Examinateur*
Georges KARINIOTAKIS	Directeur de recherche, Mines Paris - PSL	*Directeur de thèse*

No human investigation can be called
real knowledge if it does not pass
through mathematical demonstrations.

Leonardo da Vinci

Acknowledgments

I would like to thank Mines Paris - PSL for providing me the opportunity to conduct this research and for offering outstanding technical and personal support. This institution has given me the kind of environment every student hopes for. I am deeply grateful to my thesis director, Georges Kariniotakis, for entrusting me with this challenging project. His mentorship and friendship have guided me throughout this journey, inspired my passion for academia, and created the ideal conditions for pursuing my work. I am equally thankful to my thesis co-director, Simon Camal, whose mentorship dates back to my master's studies. His thoughtful guidance and technical expertise have been invaluable in shaping this thesis and making this research possible. I am also thankful to Guillaume Bontron for his guidance and dedicated efforts in supporting this work, as well as to Arthur Lett for the engaging technical discussions.

A part of this work was carried out during a research stay at the Technical University of Denmark, Department of Wind and Energy Systems (DTU Wind). In this regard, I am deeply thankful to Jalal Kazempour for hosting me in his department, offering guidance throughout my stay, providing insightful feedback on this work, and inspiring me with his exceptional professionalism and humanity.

My gratitude also extends to the friends and colleagues at the Procédés, Energies Renouvelables et Systèmes Énergétiques (PERSEE) Centre at Mines Paris, with whom I am proud to have shared this journey. I thank Panagiotis Andrianesis for his feedback from the outset of this research and for his guidance in helping me find my path forward. I also thank Andrea Michiorri, one of the first individuals to make my arrival at Mines Paris possible. Among my colleagues, I especially thank Lukas, Sergio, Eleni, Stefano, and Konstantinos for their friendship. I am grateful to my former colleague Akylas Stratigakos, who was like an older brother when I began this journey. His friendship and inspiring research have meant a lot to me. Finally, I would like to acknowledge all the staff and people at Mines Paris whose assistance and support made this journey possible.

I would like to express my gratitude to the esteemed members of my thesis jury for their insightful feedback and engaging discussion during the defense.

Finally, I am deeply grateful to my family, whose unwavering support extends far beyond this academic journey.

Financial Support

I gratefully acknowledge the financial support of Compagnie Nationale du Rhône and the Smart4RES Project (Grant No. 864337), funded under the Horizon 2020 Framework Programme, for providing part of the data. A part of this work was carried out during a research stay at the Technical University of Denmark, Department of Wind and Energy Systems (DTU Wind), with support from the Erasmus+ Programme and the Mines Paris Mobility Programme.

Contents

List of Figures viii

List of Tables xii

List of Acronyms xiv

Nomenclature xvi

1 Introduction 1
- 1.1 Context . . . 2
  - 1.1.1 The Energy Transition . . . 2
  - 1.1.2 Leveraging Power System Flexibility to Enhance Renewable Energy Integration . . . 3
  - 1.1.3 The Virtual Power Plant Paradigm . . . 3
  - 1.1.4 The Evolution of Virtual Power Plants into Large-Scale Systems with Complex Dynamics . . . 5
  - 1.1.5 Mathematical Decomposition Methods for the Optimal Operation of a Complex Virtual Power Plant . . . 7
  - 1.1.6 Virtual Power Plants Participation in the Electricity Markets . . . 9
  - 1.1.7 The Emergence of Complex Virtual Power Plants: A Case Study of Compagnie Nationale du Rhône . . . 10
- 1.2 Challenges, Objectives, and Contributions . . . 11
- 1.3 Structure of the Thesis . . . 14
- 1.4 List of Publications . . . 16
- 1.5 Notation . . . 17

2 Virtual Power Plants: Conceptual Framework and Case Study of Compagnie Nationale du Rhône 18
- 2.1 Introduction . . . 19
- 2.2 An Overview of the Virtual Power Plant Paradigm . . . 20
  - 2.2.1 Definition and Evolution of the Virtual Power Plant Concept . . . 20
  - 2.2.2 Classification of Virtual Power Plants . . . 21
  - 2.2.3 Navigating Uncertainties in Virtual Power Plant Operations . . . 22
  - 2.2.4 The Energy Management of a Virtual Power Plant . . . 23
  - 2.2.5 Virtual Power Plants Participation in the Electricity Markets . . . 28
  - 2.2.6 Virtual Power Plants in Practice: Real-World Applications . . . 31
- 2.3 Case Study: The Virtual Power Plant of Compagnie Nationale du Rhône . . . 33
  - 2.3.1 General Description of the Company . . . 33

2.3.2 Structure of the Hydropower Systems . . . 37
2.3.3 Market Participation at Compagnie Nationale du Rhône . . . 38
2.3.4 Modeling . . . 39
2.3.5 Operational Strategies and Management . . . 45
2.3.6 Input Data Description and Characterization . . . 47
2.3.7 Insights from the Compagnie Nationale du Rhône Case Study in the Broader Evolution of Virtual Power Plants . . . 58

3 The Integrated Bidding Problem: Modeling, Optimization and Control Methods for a Complex Virtual Power Plant 62
3.1 Introduction . . . 63
3.1.1 Positioning Within the Related Literature . . . 64
3.1.2 Chapter Outline . . . 70
3.2 Mathematical Background . . . 70
3.2.1 Deterministic Optimization . . . 70
3.2.2 Stochastic Programming . . . 70
3.2.3 Scenario-Based Stochastic Programming . . . 72
3.2.4 Model Predictive Control . . . 72
3.3 Methodology . . . 75
3.3.1 Formulation of the Bidding Problem . . . 75
3.3.2 Modeling a Complex Virtual Power Plant Participating in the Day-Ahead Energy Market . . . 77
3.3.3 A Fully Stochastic Two-Level Decision-Making Framework for Optimizing Complex Virtual Power Plant Participation in the Day-Ahead Market . . . 84
3.3.4 Evaluating the Proposed Energy Management Strategy for Complex Virtual Power Plants . . . 90
3.4 The Case Study of Compagnie Nationale du Rhône . . . 94
3.4.1 Application of the Proposed Modeling and Energy Management Strategies to the Case Study of Compagnie Nationale du Rhône . . . 95
3.4.2 Results from the Case Study of Compagnie Nationale du Rhône . . . 98

4 Decomposition Methods for the Optimal Bidding of a Complex Virtual Power Plant 112
4.1 Introduction . . . 113
4.1.1 Positioning Within the Related Literature . . . 116
4.1.2 Chapter Outline . . . 118
4.2 Mathematical Background . . . 119
4.3 Methodology . . . 121
4.3.1 A Scenario-Spatial Decomposition with a Performance Guarantee for Scheduling in Complex Virtual Power Plants . . . 122
4.3.2 Distributed Economic Model Predictive Control for Dispatch in Complex Virtual Power Plants . . . 135
4.4 A Small Illustrative Example . . . 140
4.4.1 A Small Illustrative Example: Case Study Description . . . 140
4.4.2 A Small Illustrative Example: Results . . . 142
4.5 The Case Study of Compagnie Nationale du Rhône . . . 144
4.5.1 Distributed Scheduling Results: A Stylized Illustrative Example . . . 146
4.5.2 Distributed Scheduling Results: Full Scale Case Study . . . 146
4.5.3 Distributed Dispatch Results . . . 149

5 Extension to Multi-Market Trading **151**
5.1 Introduction . . . 152
5.1.1 Chapter Outline . . . 154
5.2 Methodology . . . 155
5.2.1 Formulating the Complex Virtual Power Plant Participation in Day-Ahead and Ancillary Services Markets . . . 155
5.2.2 A Fully Stochastic Two-Level Decision-Making Framework for Optimizing Complex Virtual Power Plant Participation in the Day-Ahead and Ancillary Services Markets . . . 158
5.3 Case Study Description and Results . . . 163

6 Conclusions and Future Directions **169**

Bibliography **174**

List of Figures

1.1 Physical and cyber layers managed by VPPs [14]. 4
1.2 Distribution of the mathematical optimization models used for VPPs (2011–2020) [28]. **MINLP**: Mixed-integer nonlinear programming models; **NLP**: Nonlinear programming models; **MILP**: Mixed-integer linear programming models; **LP**: Linear programming models. 7
1.3 Distribution of the types of markets included in the VPPs (2011–2020) [28]. . . . 9
1.4 Overview of the structure of the thesis. 15

2.1 Illustration of the VPP paradigm. 21
2.2 Main contributing factors of the three uncertainties sources in VPP operations, as analyzed in [61]. 22
2.3 A standard energy management strategy for operating a VPP. 25
2.4 Sequence of electricity markets, as detailed in [28]. 30
2.5 Map of the Rhône River and its watershed (highlighted in yellow) [134]. 33
2.6 Map of the assets operated by Compagnie Nationale du Rhône. 36
2.7 Schematic representation of a typical hydropower system operated by Compagnie Nationale du Rhône. 38
2.8 Forebay and tailrace water levels in the proposed hydropower cascade model. . . 40
2.9 Example of operational curve of a hydropower system operated by Compagnie Nationale du Rhône. 42
2.10 The hydropower generation function (bilinear surface), along with its corresponding McCormick approximation. 45
2.11 The energy management strategy employed by Compagnie Nationale du Rhône to operate its VPP. 46
2.12 The solar farms for which data are provided by Compagnie Nationale du Rhône, organized into four distinct areas. 48
2.13 Boxplots of total external water inflow for each hour of the day in February, March, and April 2017 are shown in the top, middle, and bottom subplots, respectively. In each subplot, the box represents the interquartile range, the line inside indicates the median, and the whiskers extend to the minimum and maximum values (0th and 100th percentiles) of the data. 52
2.14 Boxplot of the normalized hourly CRPS for total external water inflow forecasts of each hydropower system within the lower Rhône cascade. The box represents the interquartile range, the line inside indicates the median, and the whiskers extend to the 5th and 95th percentiles of the data. The outliers are plotted as individual points beyond the whiskers. The hourly CRPS values are normalized by the corresponding water inflow observations for each respective hydropower system. 53

2.15 Boxplots of total wind energy (top subplot) and total solar energy (bottom subplot) outputs for each hour of the day during the simulation period (February-April 2017). In each subplot, the box represents the interquartile range, the line inside indicates the median, and the whiskers extend to the minimum and maximum values (0th and 100th percentiles) of the data. 54
2.16 Boxplots of normalized hourly CRPS of solar power forecasts (left subplot) and wind power forecasts (right subplot) for each month in the simulation period (February-April 2017). In each subplot, the box represents the interquartile range, the line inside indicates the median, and the whiskers extend to the 5th and 95th percentiles of the data. The outliers are plotted as individual points beyond the whiskers. The hourly CRPS values are normalized by the corresponding observed power outputs. 55
2.17 Boxplot of the energy prices in the day-ahead market for each hour of the day during the simulation period (February–April 2017). The box represents the interquartile range, the line inside indicates the median, and the whiskers extend to the minimum and maximum values (0th and 100th percentiles) of the data. . . 56
2.18 Boxplot of the normalized hourly CRPS of energy price forecasts in the day-ahead market for each month of the simulation period (February–April 2017). In each subplot, the box represents the interquartile range, the line inside indicates the median, and the whiskers extend to the 5th and 95th percentiles of the data. The outliers are plotted as individual points beyond the whiskers. The hourly CRPS values are normalized by the corresponding observed energy prices. 57

3.1 Illustration of a discrete reference-tracking MPC scheme. 74
3.2 Diagram of a branch and a cluster of energy resources in the proposed model for a complex VPP. **CHP**: Combined heat and power generation; **ESS**: Energy storage system; **EV**: Electric vehicles; **HPP**: Hydropower plant; **LC**: Load curtailment demand response program; **LS**: Load shifting demand response program; **TSS**: Thermal storage system. 79
3.3 Example of price-quantity bidding curve for a give time step $t = \bar{t}$ [178]. 83
3.4 The proposed stochastic economic MPC strategy for short-term dispatch of a complex VPP. 87
3.5 The proposed fully stochastic, scenario-based, two-level decision-making framework for optimizing complex VPPs participation in the day-ahead market. 89
3.6 A visual representation of the evaluation process adopted in this chapter. 91
3.7 Comparison between the current strategy of Compagnie Nationale du Rhône, characterized by uncoordinated energy management (top part of the figure), and the proposed coordinated energy management strategy (bottom part of the figure). Following to the proposed modeling approach, detailed in Section 3.3, the VPP is organized into distinct clusters while clearly identifying the coupling constraints of the coordinated energy management problem. 96
3.8 Out-of-sample validation results for the scheduling problem, considering 2000 testing scenarios. **MILP**: Mixed-integer programming problem (3.27); **LP**: Linear relaxation of (3.27). 99
3.9 Example of day-ahead market energy price forecasting scenarios generated by Compagnie Nationale du Rhône and used as inputs for the proposed day-ahead scheduling strategy (3.15). 100
3.10 Example of price-quantity bidding curves derived via the proposed day-ahead scheduling strategy (3.15). Peak price periods are highlighted in red. 101

3.11 Examples of price-quantity bidding curves for one hour when varying numbers of scenarios. This is equivalent to projecting the 3D price-quantity bidding curve from Fig. 3.10 onto the time domain. The breaking points of the curves are highlighted by red dots. 102
3.12 Example of real-time operation of a hydropower plant in the cascaded system. . . 103
3.13 Illustration of real-time operation of a hydropower plant within the cascaded system during low flow and energetic periods. 104
3.14 Illustration of real-time operation of a hydropower plant within the cascaded system during flood periods. 104
3.15 Average daily external water inflow and corresponding storage capacity of the hydropower cascade throughout the simulation period, calculated for a smaller cascaded system consisting only of the PR, SV, and BV assets in the lower Rhône cascade (refer to Table 2.3). 107
3.16 Example of energy volumes offered in the day-ahead market during energetic periods when operating cascaded hydropower and vRES in a coordinated manner. The results shown are based on 20 scenarios and fixed price levels maintained throughout each hour of the day. 108
3.17 Example of energy volumes offered in the day-ahead market during flood periods when operating cascaded hydropower and vRES in a coordinated manner. The results shown are based on 20 scenarios and fixed price levels maintained throughout each hour of the day. 110
3.18 Sensitivity of VPP profit to the integration of wind units. The reported profit per MWh of VPP energy capacity is normalized to the ex-post profit when no wind is integrated, with 100% representing the profit of the VPP without wind. Wind capacities are shown as a percentage of the total capacity of the hydropower cascade, where 100% indicates that the wind capacity within the VPP is equal to that of the cascaded hydropower system. No solar units are included in this aggregation. 111

4.1 Centralized, decentralized, hierarchical, and distributed structures of the VPP decision-making tool, based on the terminology of [38]. 114
4.2 Decomposition of the proposed fully stochastic, scenario-based, two-level decision-making framework illustrated in Fig. 3.5. 121
4.3 Example of decomposed structure of problem (3.27) when reformulated as the consensus problem (4.24) (**combined scenario-spatial decomposition**). The edges in the bipartite graph represent the consistency constraint linking global variables with their local copies. 125
4.4 Illustration of the functioning of the proposed novel, trustworthy ADMM-based distributed algorithm. 129
4.5 Illustration of the proposed trustworthy CADMMB Algorithm 2. 132
4.6 Diagram of the hybrid system for this illustrative case study. 140
4.7 Convergence of the proposed decomposition coordination algorithms (ATC, ADMM and APP) to the optimal objective function value of the centralized optimization (CO) approach. 143
4.8 Sensitivity of ADMM Algorithm 1 to the choice of the step-size parameter τ. The optimal value of the step-size parameter is denoted by τ^*. 144
4.9 Sensitivity of ATC [221] to the choice of the step-size parameter τ. The optimal value of the step-size parameter is denoted by τ^*. 144
4.10 Example of convergence of the standard consensus ADMM Algorithm 1 for various initial penalty parameter values, when considering 5 scenarios. 145

4.11 Example of convergence of the proposed trustworthy CADMMB Algorithm 2 for various initial penalty parameter values, when considering 5 scenarios. 146
4.12 Example of ADMM Algorithm 1 performance when considering 20 scenarios. . . 147
4.13 Example of trustworthy CADMMB Algorithm 2 performance when considering 20 scenarios. 147
4.14 Comparison between centralized MILP, consensus ADMM Algorithm 1, and the proposed trustworthy CADMMB Algorithm 2 based on average runtime per scheduling period and failure rates (% of total simulation days), as a function of the number of scenarios. 148
4.15 Example of coordination between the hydropower cascade and vRES under various inflow conditions when the proposed trustworthy CADMMB Algorithm 2 is employed. 148
4.16 Sensitivity to parameters tuning of the proposed APP-based distributed economic MPC Algorithm 3. **CEMPC**: Centralized Economic MPC (3.19); **DEMPC**: APP-based Distributed Economic MPC Algorithm 3. 150

5.1 Frequency control scheme implemented in Europe [232]. 154
5.2 Schematic representation of a balancing product, highlighting 1) gate closure distance to delivery, 2) minimum and 3) maximum time definitions, and 4) minimum and 5) maximum bid sizes. Further requirements can be set for 6) ramping and 7) de-ramping rates [235]. 156
5.3 Illustration of the impact of integrating an additional market (ancillary services market) into the distributed VPP decision-making strategy depicted in Fig. 4.3. The subproblems of the proposed distributed structure influenced by this modification are highlighted in red. 162
5.4 Illustration of the impact of integrating an additional dispatchable unit (hydropower system $n = 4$) into the distributed VPP decision-making strategy depicted in Fig. 4.3. The subproblems of the proposed distributed structure influenced by this modification are highlighted in red. 163
5.5 Example of BESS State of Charge (SoC) variations with the proposed SDA+SEMPC when providing energy and FCR. For each hour, the figure provides market prices, the initial BESS SoC, the energy offer, activated FCR balancing energy, and the total output of the aggregated system. Energy values are normalized by the nominal capacity of the aggregated system. 166
5.6 Impact of the short-term vRES energy forecast error on the mean and standard deviation of the normalized ex-post day-ahead objective function value, i.e., ex-post value of J^{DA} defined in (5.8). Values are in RON/MW/h since J^{DA} is normalized by the nominal capacity of the aggregated system. 167

List of Tables

2.1 Classification of the most common objectives in energy management problems for VPPs, as analyzed in [61]. . . . 24
2.2 An overview of some prominent VPP projects from around the world. . . . 32
2.3 Characterization of the hydropower systems operated by Compagnie Nationale du Rhône [135]. . . . 34
2.4 Characterization of daily external water inflow observations, including average, minimum, maximum, and standard deviation (std) values, for each hydropower system in the lower Rhône cascade. . . . 54

3.1 Comparison of the proposed generic modeling approach for complex VPPs presented in this chapter with the relevant related literature. **DA**: Day-ahead market; **ID**: Intraday market; **RT**: Real-time balancing market; **AS**: Ancillary services market. . . . 65
3.2 Comparison of the proposed fully stochastic, two-level energy management strategy in this chapter with relevant related literature. All referenced contributions provide solutions to bidding problems for energy producers or prosumers. **EMPC**: Economic model predictive control; **HS**: Hybrid system; **MG**: Microgrid; **RTMPC**: Reference-tracking model predictive control; **SBSP**: Scenario-based stochastic programming; **SEMPC**: Stochastic economic model predictive control; **SMPC**: Stochastic model predictive control. . . . 69
3.3 Characterization of day-ahead forecasts generated by Compagnie Nationale du Rhône, used as inputs for the proposed decision-making framework. . . . 99
3.4 Comparison between ex-post profit with fixed hourly bids and price-quantity bidding curves. In brackets, the relative difference with respect to fixed hourly bids. 101
3.5 Ex-post energy imbalances and profit for various dispatch strategies in the reference case (20 scenarios). Hourly average values normalized by VPP power generation. In brackets, the relative difference with respect to reference-tracking MPC. **DEMPC**: Deterministic economic MPC; **RTMPC**: Reference-tracking MPC; **SEMPC**: Stochastic economic MPC (proposed method); **UEMPC**: Uncoordinated economic MPC. . . . 106
3.6 Ex-post profit for uncoordinated and coordinated operation of cascaded hydropower and wind farms. These results are calculated for a smaller cascaded system consisting solely of the PR, SV, and BV assets in the lower Rhône (refer to Table 2.3). Hourly average values are normalized by the VPP power generation, with the relative difference compared to the uncoordinated approach indicated in brackets. . 107

4.1 Comparison between centralized, decentralized, hierarchical, and distributed structures of the VPP decision-making tool in terms of scalability, accuracy, and robustness against single-point communication failures. **Legend**: $\star \rightarrow$ poor; $\star\star \rightarrow$ medium; $\star\star\star \rightarrow$ good. 115
4.2 Comparison of the proposed trustworthy distributed algorithm with the relevant related literature, focusing specifically on the optimal operation of cascaded hydropower systems, which form the primary case study of this thesis. The studies employing augmented Lagrangian relaxation-based algorithms are denoted by the * symbol. **AGG**: Aggregation; **CCO**: Chance constrained optimization; **DECOM**: Decomposition; **IP**: Interval programming; **OPTIM**: Optimization; **RO**: Robust optimization; **SP**: Stochastic programming. 118
4.3 Parameter values used in the simulation. 142
4.4 Comparison between the proposed decomposition coordination algorithms in terms of relative error with respect to the optimal objective function value of the centralized (CO) approach (obj. relative error), number of iterations and time (when the algorithm is implemented in a sequential or parallel mode) required to meet the desired accuracy ϵ or reach the allowed maximum number of iterations ($\overline{I}$=30). 142
4.5 Comparison of computational performance between the classical centralized economic MPC (3.19) and the proposed APP-based distributed economic MPC Algorithm 3. The error is measured relative to the objective function value of the centralized MPC. 149

5.1 Comparison between the proposed SDA+SEMPC and the benchmark approaches. 164
5.2 Normalized revenue and BESS degradation when participating in the energy and balancing ancillary services markets. Hourly mean value and standard deviation (in brackets). Values are in RON/MW/h since the energy generation is normalized by both the nominal capacity of the aggregated system and the number of hours in the simulation period. 164
5.3 Normalized energy imbalances, FCR deficit and aFRR deficits, when participating in the day-ahead energy and balancing ancillary services markets. Hourly mean value and standard deviation (in brackets). Values are in MWh/MW/h since imbalances and deficits are normalized by both the nominal capacity of the system and the number of hours in the simulation period. 165

List of Acronyms

ADMM	Alternating Direction Method of Multipliers
aFRR	automatic Frequency Restoration Reserve
APP	Auxiliary Problem Principle
ATC	Analytical Target Cascading
BASMP	Balancing Ancillary Services Market Penalty
BASMR	Balancing Ancillary Services Market Remuneration
BESS	Battery Energy Storage System
BRP	Balancing Responsible Party
BSP	Balancing Service Provider
CADMMB	Consensus Alternating Direction Method of Multipliers with Bounds
CDF	Cumulative Distribution Function
CRPS	Continuous Ranked Probability Score
DDA+DEMPC	Deterministic Day-Ahead + Deterministic Economic Model Predictive Control algorithm
DDA+RTMPC	Deterministic Day-Ahead + Deterministic Reference-Tracking Model Predictive Control algorithm
DER	Distributed Energy Resource
ENTSO-E	European Network of Transmission System Operators for Electricity
FCR	Frequency Containment Reserve
LP	Linear Programming
mFRR	manual Frequency Restoration Reserve
MILP	Mixed-Integer Linear Programming
MINLP	Mixed-Integer Nonlinear Programming

MPC	Model Predictive Control
MIQP	Mixed-Integer Quadratic Programming
NLP	Nonlinear Programming
QP	Quadratic Programming
RR	Replacement Reserve
SDA+SEMPC	Stochastic Day-Ahead + Stochastic Economic Model Predictive Control algorithm
VPP	Virtual Power Plant
vRES	variable Renewable Energy Sources

Nomenclature

Superscripts

DA	Variables and parameters of the day-ahead scheduling problem
ST	Variables and parameters of the short-term dispatch problem
VPPBR	Variables and parameters of branches in the proposed VPP model
VPPCL	Variables and parameters of clusters in the proposed VPP model

Indices and Sets

$\boldsymbol{N}$	Set of hydropower systems, indexed by n
$\boldsymbol{N}^{\mathbf{BESS}}$	Set of BESSs, indexed by j
$\boldsymbol{N}^{\mathbf{VPPBR}}$	Set of branches in the VPP model, indexed by b
$\boldsymbol{N}_b^{\mathbf{VPPCL}}$	Set of clusters of branch b in the VPP model, indexed by c
$\boldsymbol{S}_n^{\mathbf{oc}}$	Set of inflow segments for the piecewise linear approximation of hydropower system n's operational curve, indexed by s
$\boldsymbol{T}$	Set of time steps in the day-ahead scheduling problem, indexed by t
$\boldsymbol{K}$	Set of time steps in the short-term dispatch problem, indexed by k
$\boldsymbol{\Omega}$	Set of scenarios, indexed by ω
i	Index for iteration of the distributed algorithms

Physical Constants

g	Acceleration due to gravity (m/s^2)
w	Water density (kg/m^3)

Parameters

E_t	Energy to be delivered in real-time by the VPP at time t (MWh)
$\overline{H}_n$	Maximum hydraulic head of hydropower system n (m)
$\underline{H}_n$	Minimum hydraulic head of hydropower system n (m)
P_ω	Probability associated with scenario ω (-)
$\overline{P}_j^{\mathrm{BESS,C}}$	Charging capacity of BESS j (MW)
$\overline{P}_j^{\mathrm{BESS,D}}$	Discharging capacity of BESS j (MW)
$\overline{P}_n^{\mathrm{H}}$	Capacity of hydropower system n (MW)
$\hat{P}_{\omega,t}^{\mathrm{S}}$	Solar power generation in scenario ω at time t (MW)
$\hat{P}_{\omega,t}^{\mathrm{vRES}}$	vRES power generation in scenario ω at time t (MW)
$\overline{P}^{\mathrm{vRES}}$	vRES installed capacity (MW)

$\overline{P}^{\mathrm{VPPCL,lin}}_{c,b}$	Maximum power flow on the line upstream of cluster c in VPP branch b (MW)
$\hat{P}^{\mathrm{W}}_{\omega,t}$	Wind power generation in scenario ω at time t (MW)
$\hat{P}^{\mathrm{D}}_{t}$	Power demand to be met by the VPP at time t (MW)
$\underline{Q}^{\mathrm{br}}_{n}$	Minimum barrage discharge of hydropower system n (m^3/s)
$\hat{Q}^{\mathrm{ext}}_{n,\omega,t}$	External inflow (from river and its tributaries) to hydropower system n in scenario ω at time t (m^3/s)
$Q^{\mathrm{in}}_{n,s}$	s-th inflow segment in the piecewise linear approximation of hydropower system n's operational curve (m^3/s)
$\overline{Q}^{\mathrm{tr}}_{n}$	Maximum turbines discharge of hydropower system n (m^3/s)
$\underline{Q}^{\mathrm{tr}}_{n}$	Minimum turbines discharge of hydropower system n (m^3/s)
R^{FCR}_{t}	Capacity reserved by the VPP for FCR at time t (MW)
$R^{\mathrm{aFRR}\uparrow}_{t}$	Capacity reserved by the VPP for upward aFRR at time t (MW)
$R^{\mathrm{aFRR}\downarrow}_{t}$	Capacity reserved by the VPP for downward aFRR at time t (MW)
$S_{n,\omega,t}$	n-th hydropower system surface area in scenario ω at time t (m^2)
$\overline{X}^{\mathrm{BESS}}_{j}$	Capacity of BESS j (MW)
$Z^{\mathrm{fbl},0}_{n}$	Initial forebay water level of hydropower system n (m)
$\overline{Z}^{\mathrm{fbl}}_{n,s}$	Maximum forebay water level corresponding to the s-th inflow segment in the piecewise linear approximation of hydropower system n's operational curve (m)
$\underline{Z}^{\mathrm{fbl}}_{n,s}$	Minimum forebay water level corresponding to the s-th inflow segment in the piecewise linear approximation of hydropower system n's operational curve (m)
Z^{tlr}_{n}	Tailrace water level of hydropower system n (m)
Δ_T	Sampling period of the day-ahead scheduling problem (s)
Δ_K	Sampling period of the short-term dispatch problem (s)
$\Delta q^{\mathrm{tr}}_{n}$	Turbines outflow ramp limit of hydropower system n (m^3/s)
$\hat{\alpha}^{\mathrm{aFRR}\uparrow}_{\omega,t}$	Upward aFRR activation signal in scenario ω at time t (-)
$\hat{\alpha}^{\mathrm{aFRR}\downarrow}_{\omega,t}$	Downward aFRR activation signal in scenario ω at time t (-)
$\hat{\alpha}^{\mathrm{FCR}}_{\omega,t}$	FCR activation signal in scenario ω at time t (-)
$\eta^{\mathrm{BESS,C}}_{j}$	Charging efficiency of BESS j (-)
$\eta^{\mathrm{BESS,D}}_{j}$	Discharging efficiency of BESS j (-)
η^{tr}_{n}	Turbine efficiency of hydropower system n (-)
$\hat{\pi}^{\mathrm{aFRR}\uparrow}_{\omega,t}$	Upward aFRR price in scenario ω at time t (€/MW)
$\hat{\pi}^{\mathrm{aFRR}\downarrow}_{\omega,t}$	Downward aFRR price in scenario ω at time t (€/MW)
$\hat{\pi}^{\mathrm{aFRR,bal}\uparrow}_{\omega,t}$	Price of upward aFRR activated balancing energy in scenario ω at time t (€/MWh)
$\hat{\pi}^{\mathrm{aFRR,bal}\downarrow}_{\omega,t}$	Downward aFRR activated balancing energy price in scenario ω at time t (€/MWh)
$\hat{\pi}^{\mathrm{aFRR,comp}\uparrow}_{\omega,t}$	Composite price of upward aFRR in scenario ω at time t (€/MW)
$\hat{\pi}^{\mathrm{aFRR,comp}\downarrow}_{\omega,t}$	Composite price of downward aFRR in scenario ω at time t (€/MW)
$\pi^{\mathrm{BESS}}_{j,t}$	Weight of degradation cost of BESS j at time t (€/MWh)

$\hat{\pi}^{\mathrm{E}}_{\omega,t}$	Day-ahead energy price in scenario ω at time t (€/MWh)
$\hat{\pi}^{\mathrm{E}\uparrow}_{\omega,t}$	Positive imbalance penalty price in scenario ω at time t (€/MWh)
$\hat{\pi}^{\mathrm{E}\downarrow}_{\omega,t}$	Negative imbalance penalty price in scenario ω at time t (€/MWh)
$\hat{\pi}^{\mathrm{FCR}}_{\omega,t}$	FCR price in scenario ω at time t (€/MW)
$\hat{\pi}^{\delta\mathrm{aFRR}\uparrow}_{\omega,t}$	Penalty price of upward aFRR deficit in scenario ω at time t (€/MW)
$\hat{\pi}^{\delta\mathrm{aFRR}\downarrow}_{\omega,t}$	Penalty price of downward aFRR deficit in scenario ω at time t (€/MW)
$\hat{\pi}^{\delta\mathrm{aFRR,comp}\uparrow}_{\omega,t}$	Composite penalty price of upward aFRR deficit in scenario ω at time t (€/MW)
$\hat{\pi}^{\delta\mathrm{aFRR,comp}\downarrow}_{\omega,t}$	Composite penalty price of downward aFRR deficit in scenario ω at time t (€/MW)
$\hat{\pi}^{\delta\mathrm{FCR}}_{\omega,t}$	Penalty price of FCR deficit in scenario ω at time t (€/MW)
$\tau^{\mathrm{br}}_{a,b}$	Barrage water travel time from hydropower system a to b (s)
$\tau^{\mathrm{tr}}_{a,b}$	Turbined water travel time from hydropower system a to b (s)

Notation for the Proposed Distributed Algorithms

$\overline{I}$	Maximum number of iterations allowed (-)
J	Objective function (€)
J^{LB}	Lower bound on the problem's global optimum in the CADMMB algorithm (€)
J^{UB}	Upper bound on the problem's global optimum in the CADMMB algorithm (€)
J^{gap}	Gap between upper and lower bounds in the CADMMB algorithm (%)
$\boldsymbol{r}$	Vector of primal residuals
$\boldsymbol{s}$	Vector of dual residuals
$\boldsymbol{z}^{\mathrm{prj}}$	Vector of decision variables resulting from the quasi-projection step of the CADMMB algorithm
ϵ	Tolerance parameter of termination criterion in the consensus ADMM algorithm (%)
ϵ^{gap}	Tolerance parameter of termination criterion in the CADMMB algorithm (%)
ϵ^{UB}	Tolerance parameter of upper bound update in the CADMMB algorithm (%)
$\boldsymbol{\lambda}$	Vector of dual variables associated with the consensus constraints
μ	Tolerance parameter of penalty parameter update (-)
ρ	Penalty parameter (-)
τ	Step-size of the penalty parameter update (-)

Variables

$b^{\mathrm{BESS,C}}_{j,t}$	Binary variable associated with the charging of BESS j at time t (-)
$b^{\mathrm{BESS,D}}_{j,t}$	Binary variable associated with the discharging of BESS j at time t (-)
$b^{\mathrm{br}}_{n,\omega,t}$	Binary variable associated with the barrage safety constraint of hydropower system n in scenario ω at time t (-)
$b^{\mathrm{oc}}_{n,\omega,t,s}$	Binary variable of the s-th segment in the piecewise linear approximation of hydropower system n's operational curve in scenario ω at time t (-)
c^{S}_{t}	Solar power curtailment as a percentage of solar power generation at time t (%)
c^{W}_{t}	Wind power curtailment as a percentage of wind power generation at time t (%)

$e_{\omega,t}$	Energy offer in scenario ω at time t (MWh)
$h_{n,\omega,t}$	Hydraulic head of hydropower system n in scenario ω at time t (m)
$o_{\omega,t}$	Incremental energy quantity offered at price $\hat{\pi}^{\mathrm{E}}_{\omega,t}$ in the price-quantity bidding curve formulated by the VPP at time t in scenario ω (MWh)
$p^{\mathrm{BESS,C}}_{j,t}$	Power charged to BESS j at time t (MW)
$p^{\mathrm{BESS,D}}_{j,t}$	Power discharged from BESS j at time t (MW)
p^{exp}_{t}	Power exported from the VPP to the grid at time t (MW)
$p^{\mathrm{H}}_{n,\omega,t}$	Output of hydropower system n in scenario ω at time t (MW)
p^{imp}_{t}	Power imported by the VPP from the grid at time t (MW)
$p^{\mathrm{VPPCL,ext}}_{c,b,\omega,t}$	External power flow of cluster c in the VPP branch b at time t in scenario ω (MW)
$p^{\mathrm{VPPCL,int}}_{c,b,\omega,t}$	Internal power flow of cluster c in the VPP branch b at time t in scenario ω (MW)
$p^{\mathrm{VPPCL,lin}}_{c,b,\omega,t}$	Power flow on the line upstream of cluster c in the VPP branch b at time t in scenario ω (MW)
$q^{\mathrm{br}}_{n,\omega,t}$	Outflow of barrage n in scenario ω at time t (m^3/s)
$q^{\mathrm{in}}_{n,\omega,t}$	Inflow of hydropower system n in scenario ω at time t (m^3/s)
$q^{\mathrm{out}}_{n,\omega,t}$	Outflow of hydropower system n in scenario ω at time t (m^3/s)
$q^{\mathrm{tr}}_{n,\omega,t}$	Outflow of turbines n in scenario ω at time t (m^3/s)
$r^{\mathrm{aFRR}\uparrow}_{t}$	Upward aFRR offer at time t (MW)
$r^{\mathrm{aFRR}\downarrow}_{t}$	Downward aFRR offer at time t (MW)
r^{FCR}_{t}	FCR offer at time t (MW)
$\boldsymbol{u}$	Vector of control variables in the short-term dispatch MPC strategy
$v_{n,t}$	Water reservoir volume of hydropower system n at time t (m^3)
$x^{\mathrm{BESS}}_{j,t}$	State of charge of BESS j at time t (MWh)
$\boldsymbol{z}$	Vector of decision variables
$z^{\mathrm{fbl}}_{n,\omega,t}$	Forebay level of hydropower system n in scenario ω at time t (m)
$\delta^{\mathrm{aFRR}\uparrow}_{\omega,t}$	Upward aFRR deficit in scenario ω at time t (MW)
$\delta^{\mathrm{aFRR}\downarrow}_{\omega,t}$	Downward aFRR deficit in scenario ω at time t (MW)
$\delta^{\mathrm{E}\uparrow}_{\omega,t}$	Positive energy imbalance in scenario ω at time t (MWh)
$\delta^{\mathrm{E}\downarrow}_{\omega,t}$	Negative energy imbalance in scenario ω at time t (MWh)
$\delta^{\mathrm{FCR}}_{\omega,t}$	FCR deficit in scenario ω at time t (MW)

Chapter 1

Introduction

Résumé en Français

Cette thèse se focalise sur la gestion optimisée des centrales électriques virtuelles complexes, qui représentent des systèmes énergétiques de grande échelle intégrant des ressources géographiquement dispersées et hétérogènes, soumises à des dynamiques non linéaires et à des sources d'incertitude variées. L'objectif principal est de développer des algorithmes d'optimisation et de contrôle adaptés à la planification et au dispatch quasi temps réel de ces centrales dans un cadre de marché libéralisé. Les modèles de gestion existants, souvent conçus pour des cas spécifiques, peinent à capturer la complexité inhérente à ces systèmes, notamment en ce qui concerne l'interaction entre diverses ressources énergétiques et leur participation simultanée à plusieurs marchés. De plus, la planification et le dispatch sont généralement traités séparément, ce qui limite l'efficacité des solutions adoptées et peut conduire à des décisions sous-optimales. Cette thèse propose un cadre de décision stochastique à deux niveaux, intégrant de manière cohérente les phases de planification et de dispatch dans un problème séquentiel unifié. Afin de surmonter les limites des approches conventionnelles qui se concentrent principalement sur une seule dimension du problème, une décomposition simultanée selon les dimensions spatiale et scénariale est introduite. Sur le plan algorithmique, des méthodes de résolution avancées sont développées pour garantir une gestion efficace des centrales électriques virtuelles. En particulier, des algorithmes distribués basés sur la relaxation lagrangienne augmentée sont conçus pour résoudre des problèmes convexes, tandis qu'une approche de décomposition et de coordination alternée est mise en œuvre pour traiter des modèles non convexes, notamment ceux impliquant la programmation linéaire en nombres entiers mixtes. Ces algorithmes assurent une performance optimale en fournissant des bornes supérieures et inférieures, permettant ainsi une évaluation rigoureuse des solutions distribuées. Enfin, cette thèse introduit un cadre élargi pour la gestion multi-marchés, facilitant la prise en compte simultanée de plusieurs horizons temporels et mécanismes de marché.

1.1 Context

1.1.1 The Energy Transition

The Earth is warming at an alarming rate. According to a temperature analysis by the National Aeronautics and Space Administration's Goddard Institute for Space Studies, the average global temperature has increased by at least 1.1°C since 1880—a phenomenon widely referred to as *global warming* [1]. This rise in temperature is not just melting polar ice caps and raising sea levels but also driving a range of climate changes, including desertification and an increase in extreme weather events such as hurricanes, floods, and wildfires. In response, the international community convened in Paris in December 2015, where a historic agreement was reached at the Climate Change Conference (COP21). This accord set the ambitious goal of limiting global warming to well below 2°C above pre-industrial levels, with a strong preference for capping it at 1.5°C. Failure to meet these targets could lead to catastrophic environmental, social, and economic consequences, fundamentally altering the habitability of our planet.

The overwhelming scientific consensus is that the primary driver of global warming is the emission of greenhouse gases, largely stemming from human activities. Among these gases, carbon dioxide plays a dominant role, with the energy sector being the primary contributor. This sector, which includes electricity generation, industrial processes, and transportation, accounts for over 70% of global greenhouse gas emissions [2]. As such, addressing the energy sector's emissions is critical to mitigating global warming and achieving climate goals. This ongoing *energy transition* consists in a global shift from fossil fuel-based energy systems to more sustainable, low-carbon systems. Central to this transition is the large-scale integration of variable renewable energy sources (vRES), such as wind and solar power, into modern power grids, with the ultimate aim of displacing conventional fossil-fuel-based power generation. This transformation promises numerous benefits, including environmental sustainability, decarbonization, energy security, public health improvements, rural electrification, and broader access to energy [3]. Additionally, the cost of vRES technologies has dropped significantly in recent years, making them increasingly competitive with traditional fossil fuel generation.

However, the integration of renewable energy on a large scale presents significant technical challenges. Renewable energy sources are inherently intermittent and variable, causing fluctuations in power supply that can lead to imbalances between supply and demand. These fluctuations threaten the stability and reliability of electricity networks, which were traditionally designed around flexible, controllable thermal units that could be adjusted to maintain grid balance. As the share of renewables increases, the role of conventional power plants is diminishing, and vRES must increasingly contribute to essential grid services such as frequency regulation, voltage control, and balancing reserves. Concurrently, energy producers incorporating vRES into their portfolios must navigate new challenges to optimize profits while managing multiple sources of uncertainty.

1.1.2 Leveraging Power System Flexibility to Enhance Renewable Energy Integration

To address the challenges associated with vRES integration, the solution lies in *power system flexibility*, which refers to the power producer's (consumer's) capability to modify its production (consumption) level or state in response to an activation signal [4]. Emerging technologies, such as energy storage systems, demand response programs, flexible generation and consumption units, provide this much-needed flexibility. In this context, the energy landscape is transitioning from a system dominated by large, centralized conventional power plants to one composed of millions of decentralized generation units and flexibility resources. These distributed energy resources (DERs) often operate independently or in small groups, making their participation in energy markets difficult and limiting their potential. In response, a new class of problems has emerged in the power system field, centered on the optimal control of stochastic energy resources by means of controllable units. In essence, vRES are *aggregated* with dispatchable units, providing the necessary flexibility to fully unlock their potential for grid services and maximizing their market value. Without this coordination, the fragmented integration of vRES and flexible resources risks destabilizing the power system, leading to inefficiencies and energy imbalances.

This evolving energy landscape has spurred the emergence of a new role: the *aggregator* [5]. Aggregators pool multiple energy resources potentially from various customers and manage them as a single entity to participate in the electricity markets or provide services to the grid. On a small scale, this aggregation manifests in systems like microgrids and hybrid systems. A *microgrid* is a localized energy system that can operate autonomously or in conjunction with the main power grid [6]. It typically includes DERs and is equipped with control systems that balance energy supply and demand within its boundaries. Microgrids can function in islanded mode (independently) or in grid-connected mode [7]. Meanwhile, a *hybrid system* combines multiple energy generation technologies, usually incorporating renewable and dispatchable sources, to optimize energy availability, reduce costs, and enhance energy security, especially in off-grid or rural areas [8]. Alternatively, aggregations can take the form of community-based systems, where the aggregated portfolio is operated collectively rather than through a centralized entity. For example, an *energy community* consists of individuals or organizations that collaborate to produce, consume, and manage energy locally [9]. These communities often strive for self-sufficiency, sustainability, and equitable distribution of energy resources [10].

1.1.3 The Virtual Power Plant Paradigm

As the scale and complexity of these aggregations grow, they increasingly evolve into *virtual power plants* (VPPs) [11]. A VPP aggregates geographically dispersed and heterogeneous energy resources to operate them as a single entity, providing grid services and participating in multiple electricity markets. In contrast to microgrids and energy communities, which typically operate on a local scale and focus on energy autonomy and social benefits, VPPs offer a broader and more flexible approach to energy management. By aggregating energy resources across wide

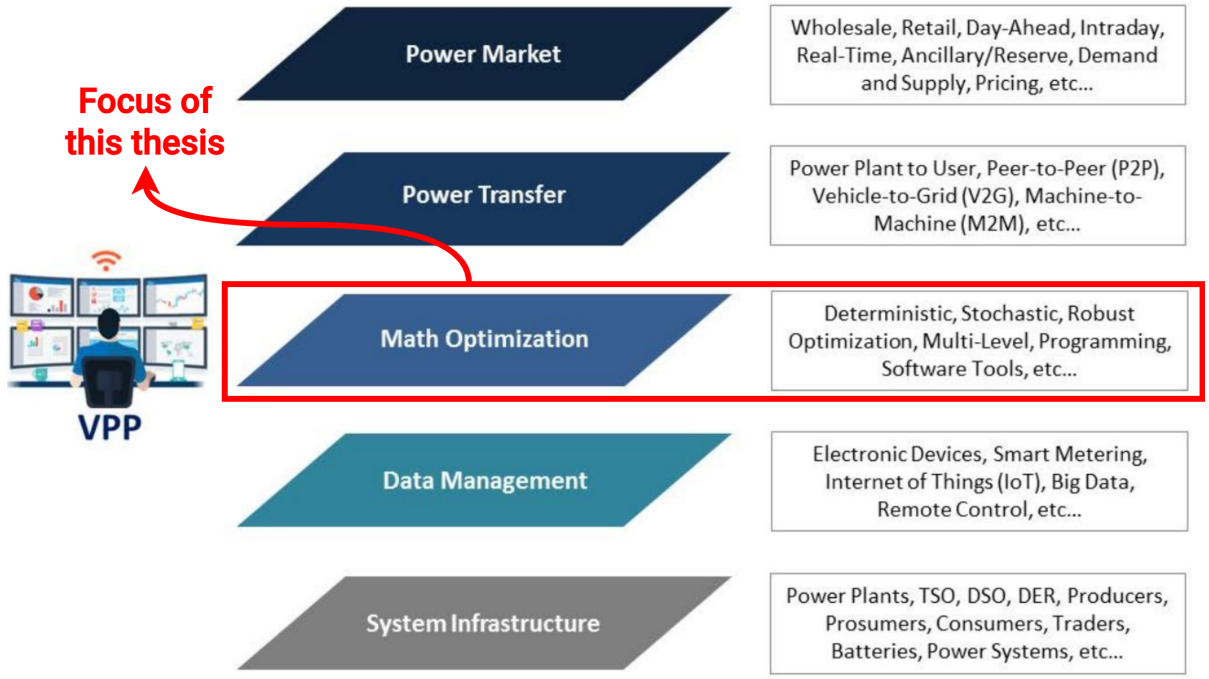

Figure 1.1: Physical and cyber layers managed by VPPs [14].

geographical areas, VPPs optimize their operation to participate in multiple electricity markets and provide ancillary services to the grid. A VPP may encompass hybrid systems and micro-grids within its energy resource portfolio, enhancing its capability to respond to varying market demands and grid conditions [12]. The most common classification of virtual power plants divides them into *commercial VPPs* and *technical VPPs* [13]. While technical VPPs primarily focus on grid support and operational stability, commercial VPPs are centered on maximizing profitability by optimizing asset operation and market participation. This thesis focuses on aggregators managing VPPs for commercial purposes, with particular attention to their participation in multiple electricity markets and strategies for optimizing profits while navigating the complexities of market bidding and assets coordination.

A VPP is generally structured into multiple layers, each with distinct roles, spanning from system infrastructure to data management and market interactions [14]. Fig. 1.1 provides an overview of the physical and cyber layers managed by the VPP. This thesis focuses on the mathematical models employed by the aggregator to operate the VPP, referred to as the *math optimization* layer in Fig. 1.1. The primary objective of this layer is to equip the VPP with decision-making tools that efficiently manage both internal and external energy dispatch while optimizing the aggregator's objectives in electricity markets under multiple sources of uncertainty. Traditionally, mathematical optimization has been the standard approach for solving such problems. However, in recent years, alternative methods have emerged, including heuristic/meta-heuristic approaches [15] and machine learning techniques [16]. While classical mathematical programming continues to offer strong theoretical guarantees and accuracy, it often faces computational challenges, especially when applied to large-scale and complex optimization problems, such

as those encountered in modern VPP management. In contrast, heuristic methods provide greater flexibility and can significantly reduce the computational burden, typically relying on simulation-based techniques that iteratively search for solutions, either by following specific rules or through random exploration. Machine learning-based methods, on the other hand, aim to deliver faster and more scalable solutions by leveraging historical data to inform future decisions [17]. However, heuristic methods lack solution guarantees, which is a significant drawback when managing critical infrastructure like VPPs. Similarly, machine learning approaches often suffer from limited theoretical guarantees, poor interpretability, and the need for extensive datasets for training. For these reasons, this thesis focuses on classical mathematical optimization methods to support decision-making within VPPs, with a particular emphasis on retaining the theoretical guarantees of these approaches while providing scalable and fast solutions.

1.1.4 The Evolution of Virtual Power Plants into Large-Scale Systems with Complex Dynamics

When employing mathematical optimization methods, the first step is to develop a model of the system's physical dynamics. For VPPs, the existing literature has primarily focused on case-specific models that describe the internal dynamics of the VPP and its external interactions with the grid and/or electricity markets, e.g., in [18]. To address the limitations of such case-specific models, the authors in [19] were the first to generalize the VPP modeling approach, accounting for what they termed *large-scale VPPs*—large aggregations of energy resources. However, in modern VPPs, the size of the energy portfolio is only one aspect of the overall *complexity* in managing such systems. This complexity arises not only from the sheer number of aggregated energy units but also from the interactions and *coupling constraints* between these typically heterogeneous assets, nonconvex individual dynamics, and the various sources of uncertainty linked to both the types of units involved and the VPP's objectives and roles. In short, modern VPPs are evolving into more than just large-scale systems; they are complex aggregations with intricate internal and external dynamics. This evolving paradigm, referred to here as the *complex VPP*, is the target system for both the modeling approach and the decision-making algorithms proposed in this thesis.

Once a model for the VPP is developed, operational decisions can be made based on this model across multiple time stages. Typically, the operation of a VPP is structured into three distinct phases:

- *Planning*: Planning involves making long-term strategic decisions over extended time horizons, often spanning months to years [20]. It centers on high-level objectives like capacity expansion, investments in new assets, maintenance scheduling, and setting overarching operational strategies for energy production and consumption.

- *Scheduling*: Scheduling is a medium-term decision-making process focused on optimizing VPP asset operations over shorter periods, such as daily, weekly, or monthly intervals [21]. For commercial VPPs, the primary goal of scheduling is to optimize market bids while

accommodating VPP constraints and managing uncertainties, including market prices and vRES power generation.

- *Dispatch*: Dispatch is the real-time or near-real-time decision-making process that adjusts the actual output of the VPP's assets based on real-time observations [22]. It is concerned with executing the operational schedule created during the scheduling phase while responding to unexpected deviations (such as forecast errors, equipment failures, or real-time market signals). Dispatch is a reactive process that ensures the VPP meets its obligations in energy markets and balances supply and demand dynamically, often using automated control systems.

This thesis primarily focuses on the scheduling and dispatch phases, which are intricately linked in the real-world operation of VPPs. The process is divided into two distinct modules: the *scheduling module*, which optimizes market bids, and the *dispatch module*, which handles deviations between actual VPP generation and consumption and the original schedule. Both modules rely on forecasts as inputs and use stochastic optimization and control methods to tackle complex VPP operations at multiple time stages, under various sources of uncertainty.

Methods for managing uncertainty in VPP optimization problems can be classified into four main approaches [23]: robust optimization [24], interval optimization [25], chance-constrained programming [26], and scenario-based stochastic programming [27]. *Robust optimization* seeks solutions that remain feasible under worst-case uncertainty realizations, ensuring reliability but often leading to overly conservative decisions that may sacrifice optimality. *Interval optimization*, meanwhile, optimizes within predefined uncertainty bounds, striking a balance between conservatism and flexibility by considering intervals rather than fixed values. *Chance-constrained programming* introduces a probabilistic trade-off, ensuring that constraints are satisfied with a specified likelihood, allowing for controlled risk in exchange for potential performance gains. *Scenario-based stochastic programming*, however, stands out by modeling uncertainty across multiple scenarios, enabling decision-making that minimizes expected costs or risks. This method is especially well-suited to handle unbounded uncertainty sources such as prices, and demand. Compared to chance-constrained programming, it offers greater flexibility by accounting for a broader range of potential outcomes rather than focusing solely on probability thresholds. It is also more straightforward to implement, as it does not require reformulating constraints into probabilistic terms, which can be challenging in highly complex systems. Furthermore, compared to robust and interval optimization, scenario-based stochastic programming delivers less conservative solutions by avoiding worst-case or fixed-bound restrictions, making it a more practical choice in settings with diverse, unbounded, and numerous uncertainty sources. Given its flexibility and suitability for handling complex uncertainty profiles, scenario-based stochastic programming is the chosen method in this thesis for addressing uncertainty in VPP energy management problems. Nonetheless, its main drawback lies in its computational complexity, particularly when large scenario sets are required to represent uncertainty comprehensively.

In the context of mathematical optimization methods applied to the decision-making chain of VPPs, existing contributions typically focus on either the scheduling [29] or the dispatch [30]

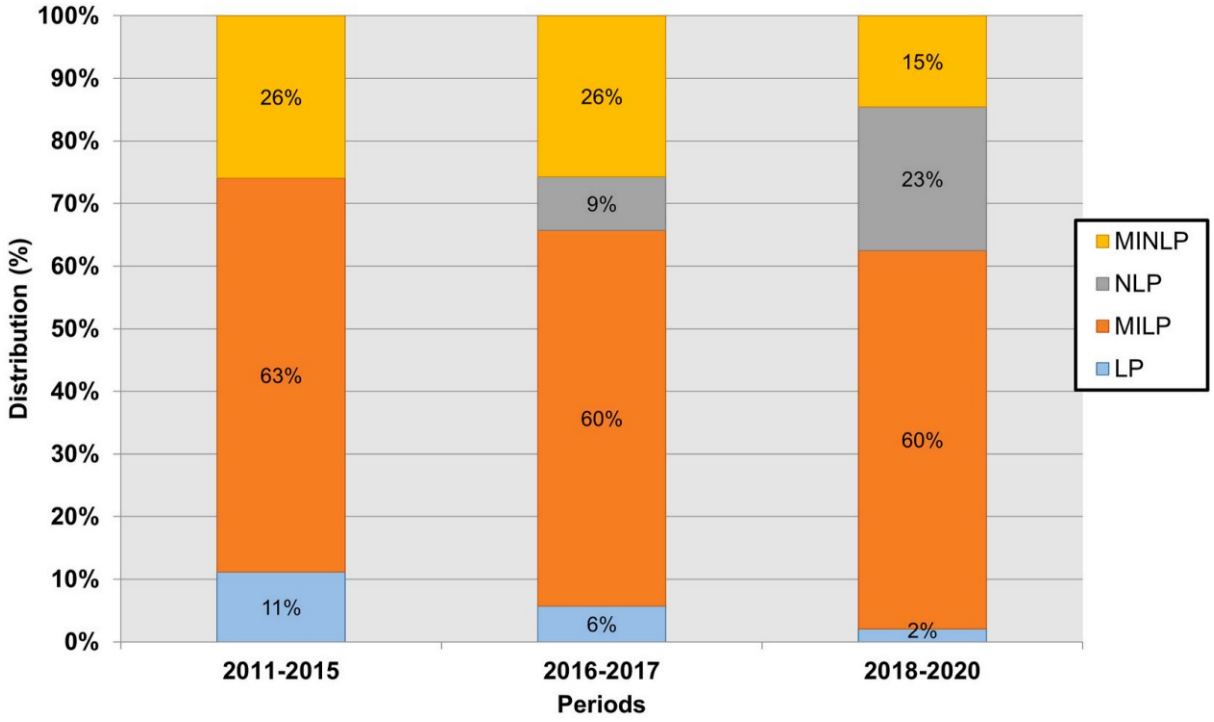

Figure 1.2: Distribution of the mathematical optimization models used for VPPs (2011–2020) [28]. **MINLP**: Mixed-integer nonlinear programming models; **NLP**: Nonlinear programming models; **MILP**: Mixed-integer linear programming models; **LP**: Linear programming models.

of the aggregated system separately. Only a limited number of works address both phases as an integrated multi-level problem, such as in [31]. A comprehensive approach that simultaneously integrates scheduling and dispatch for VPPs participating in multiple electricity markets, while also accounting for the numerous uncertainties involved, is still largely absent in current research. More importantly, several review studies have identified the increasing complexity of optimization models used to manage modern VPPs. For instance, an analysis conducted in [28], which reviews over 120 articles focusing on VPP scheduling and dispatch problems, underscores a growing interest in mixed-integer linear programming (MILP) and nonlinear programming (NLP) models, while showing a corresponding decline in the use of simpler methods like linear programming (LP) models. This transition, depicted in Fig. 1.2, highlights the growing complexity of modern VPP optimization models. These models require more advanced and scalable techniques to manage their intricacy and prevent intractability, particularly in cases involving nonconvex dynamics and numerous scenarios employed to represent possible outcomes of multiple sources of uncertainty.

1.1.5 Mathematical Decomposition Methods for the Optimal Operation of a Complex Virtual Power Plant

As discussed in the previous section, scheduling and dispatch in modern VPPs often lead to complex optimization and control problems, characterized by intricate coupling constraints, nonconvex internal dynamics, and multiple sources of uncertainty. When scenario-based stochastic

programming is applied to address uncertainty in a nonconvex optimization model—a common approach in the current literature, as shown in Fig. 1.2—the resulting optimization and control problems for centralized VPP energy management can become computationally intractable. To address this issue, researchers have increasingly turned to *mathematical decomposition methods*, which divide the centralized problem into multiple subproblems that can be solved concurrently, ultimately converging to the optimal solution of the original centralized problem [32].

Two primary strategies identified in the literature [33] are *scenario decomposition* and *spatial decomposition*. Scenario decomposition techniques, such as Benders decomposition [34], split the stochastic problem into multiple deterministic subproblems, typically one for each scenario. Spatial decomposition, often implemented through Lagrangian relaxation techniques like the alternating direction method of multipliers (ADMM) [35], divides the problem by units or groups of units. Both approaches offer significant advantages over traditional centralized methods [36]. By leveraging parallelization, decomposition methods can improve solution speed and scalability compared to centralized strategies. Moreover, while centralized approaches are vulnerable to single-point failures, decomposition methods enhance robustness and resilience while also offering the potential to protect data privacy. However, existing studies typically focus on either spatial or scenario decomposition in isolation, addressing only a single dimension of the problem's complexity. This limits the potential scalability benefits of decomposition methods when applied to complex VPP energy management.

Once the original centralized problem is decomposed into multiple subproblems managed by local agents, specific algorithms exist to coordinate the individual solutions of these subproblems [37]. These algorithms facilitate the exchange of information among local agents to iteratively guide the solution toward the global optimum (if any) of the original problem. In the following, the terminology from [38] is adopted to classify these methods, distinguishing between *distributed algorithms*, also referred to as *fully-distributed algorithms*, where each local agent communicates with its neighbors without a centralized controller, and *hierarchical algorithms*, where computations are carried out by agents that communicate with higher-level agents in a hierarchical structure. For example, the ADMM, which is among the most popular mathematical decomposition methods, in its standard form is a hierarchical algorithm, as it requires a central coordinator to manage the dual variable update step [39]. However, hierarchical methods might encounter scalability issues and challenges in terms of robustness and privacy, due to the existence of a central coordinator. Consequently, several ADMM variants [40], like proximal message passing [41] and consensus ADMM [42], have been developed to reach a distributed structure. A significant limitation of ADMM, and many other augmented Lagrangian relaxation-based methods, when applied to nonconvex problems like those under consideration, is that convergence to the global optimum of the centralized problem is generally not guaranteed [43]. Even in the case of mixed-integer programming problems, a straightforward application of ADMM can only provide heuristic solutions. While these solutions often offer strong practical performance, they still lack formal performance guarantees in the mixed-integer case [44].

To clarify the upcoming discussion, it is important to distinguish both hierarchical and distributed methods from *decentralized* or *uncoordinated* approaches. In decentralized methods,

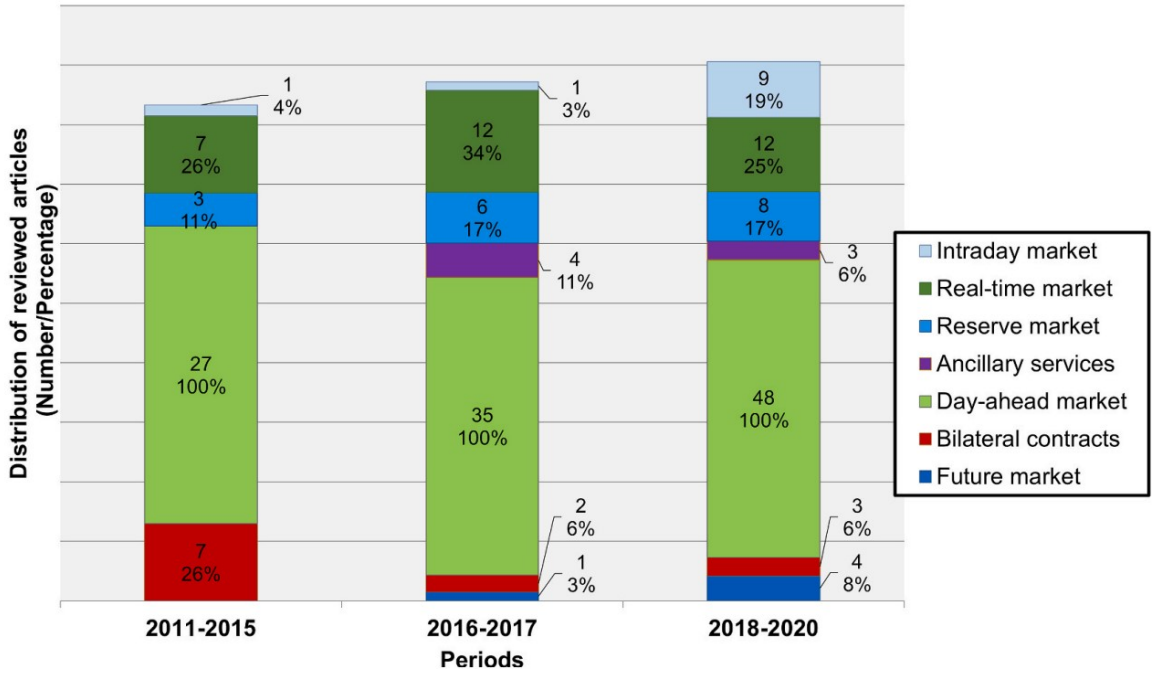

Figure 1.3: Distribution of the types of markets included in the VPPs (2011–2020) [28].

each subproblem is solved independently by local agents without any communication between them [38]. Consequently, decentralized methods typically result in a global optimum that differs from that of the original centralized problem.

1.1.6 Virtual Power Plants Participation in the Electricity Markets

The increasing complexity of optimization models for VPPs is closely tied to the ongoing evolution of electricity markets, which offer aggregators new opportunities for revenue generation. Over the past few decades, numerous countries have undertaken substantial market liberalization and deregulation efforts, with the primary goals of improving the economic efficiency of electricity companies, encouraging infrastructure investment, and ultimately reducing consumer electricity costs [45]. These regulatory changes have transformed the electricity sector, shifting from a vertically integrated structure—where generation, transmission, distribution, and retail were controlled by a single entity—to a decentralized framework, in which these activities are now managed independently [46]. Liberalization efforts, which gained significant momentum in the late 20th century, initially led to the establishment of short-term wholesale markets, where electricity buyers and sellers set prices through competitive auctions [47]. Examples of these developments can be seen in markets such as Texas, under the guidance of the Federal Energy Regulatory Commission, as well as in Scandinavia through NordPool, and the UK with the New Electricity Trading Agreements. In today's mature markets, trading mechanisms often extend beyond day-ahead markets to include forward and futures contracts, offering participants tools to hedge against price volatility and manage financial risks more effectively.

At the same time, the increasing integration of vRES into power systems has further complicated market operations. VPPs have become critical actors in addressing these challenges

by aggregating DERs and facilitating their collective participation in wholesale markets. This aggregation enables asset owners to access markets more efficiently and increase profitability. Despite the significant focus on optimizing VPP participation in single markets, particularly the day-ahead market [48], a gap persists in the literature concerning the optimization of VPP strategies across multiple electricity markets. A growing interest in multi-market trading problems involving VPPs is evidenced in recent studies, particularly those exploring the integration of day-ahead, intraday, and real-time balancing markets [28]. This trend, as depicted in Fig. 1.3, underscores the shift toward more sophisticated VPP operations, which now account for a broader range of revenue streams, more complex interactions with external entities, and multi-objective problems. In short, the growing complexity of modern VPPs analyzed in this thesis extends beyond the integration of increasingly diverse and intricate units; it also underscores the new constraints and challenges associated with simultaneous participation in multiple markets.

1.1.7 The Emergence of Complex Virtual Power Plants: A Case Study of Compagnie Nationale du Rhône

To validate the modeling and optimization methods developed in this thesis, a real-world case study from the French energy producer Compagnie Nationale du Rhône is employed. The company operates a cascade of 19 run-of-the-river hydropower plants along the Rhône River, with a total installed capacity of approximately 3 GW [49]. These facilities generate around 16 TWh of electricity annually, representing 25% of France's hydropower output and accounting for 3% of the nation's total electricity consumption. Additionally, Compagnie Nationale du Rhône oversees 59 wind farms and 59 solar power plants across France, contributing an extra 1 GW of renewable capacity.

Currently, the hydropower cascade is operated independently from the company's wind and solar assets. Managing the cascade alone is a highly complex task due to the nonconvex dynamics of each hydropower plant, strict safety constraints, and the intricate hydraulic coupling between plants. Furthermore, the cascade must be operated under uncertainty, considering variable water inflows from the river and its tributaries, as well as fluctuating market prices. However, despite its limited storage capacity, the hydropower cascade can be exploited to mitigate the stochasticity of wind and solar units, thereby significantly enhancing the market value of the energy portfolio. Thus, the company has begun exploring the potential benefits of combining cascaded hydropower plants with both wind and solar units to operate them as a single entity in the electricity markets. Moreover, the rise of modern electricity markets provides new opportunities. For instance, the fast-ramping capability of hydropower could be particularly advantageous for providing ancillary services to the grid operator. Clearly, this transition represents the evolution of this VPP into a larger and, more importantly, increasingly complex system that integrates heterogeneous energy sources, both stochastic and dispatchable, to maximize their value in multiple markets.

The transition to such a complex VPP requires significant investment and must be well justified. The primary objective of Compagnie Nationale du Rhône is to demonstrate the benefits of integrating its hydropower, wind, and solar assets into a unified system under various operational

scenarios, such as normal inflow conditions, where hydropower flexibility is available, and extreme conditions (e.g., flood or low-flow periods) where the hydropower plants are constrained to operate in pure run-of-the-river mode, without any available storage capacity. If the aggregation proves to enhance market value, the next challenge lies in managing the increased complexity of optimization and control tasks. In particular, the integration of cascaded hydropower with wind and solar units not only introduces additional sources of uncertainty but also creates new forms of coupling within the VPP. These include hydraulic coupling between hydropower plants, power balancing among hydropower, wind, and solar assets, as well as scenario coupling to ensure consistency across representations of multiple sources of uncertainty—namely vRES power generation, water inflows, and market prices—in the stochastic optimization and control problems. Furthermore, it is unrealistic to expect the company to overhaul its existing energy management tools in a short period. Therefore, the transition must be facilitated through the development of optimization and control methods that minimize disruptions to current practices, allowing for seamless integration and future adaptability as the VPP continues to evolve.

In summary, the rise of such a complex VPP must first be strongly justified in terms of potential benefits. Second, since the added complexity significantly increases the computational burden of the associated optimization and control problems, advanced methods must be developed that are both scalable and robust while minimizing the impact on existing operational strategies. These challenges are commonly faced by real-world aggregators transitioning their current systems into modern, complex VPPs.

1.2 Challenges, Objectives, and Contributions

This thesis addresses the energy management of complex VPPs, defined as large-scale systems that aggregate geographically dispersed and heterogeneous energy resources with complex interactions and intricate individual dynamics, all subject to multiple sources of uncertainty. The main objective is to develop optimization and control algorithms for both the scheduling and near-real-time dispatch of complex commercial VPPs participating in the energy market. Several challenges arise in this context. First, existing modeling approaches for complex VPPs are often case-specific (e.g., [18]), with limited efforts directed toward generalizing these models. The few attempts at generalization have focused primarily on large-scale systems (e.g., [19]), rather than addressing the broader category of complex VPPs. Furthermore, VPP scheduling and dispatch problems are typically addressed independently, as seen for example in [50] and [51]. When both phases are considered together, the interaction of the VPP is typically restricted to a single market, and the system is simplified to an aggregation of limited energy resources, such as vRES and energy storage systems (e.g., [52]). A comprehensive stochastic decision-making framework that jointly addresses the scheduling and dispatch of complex VPPs participating in multiple electricity markets remains absent in current literature. Such a framework involves solving highly complex optimization and control problems, characterized by nonconvex dynamics, intricate coupling constraints across both spatial and scenario dimensions, and various sources of uncertainty. In response, researchers have shown increasing interest in

the application of mathematical decomposition methods to VPPs operational algorithms [53]. Among these methods, augmented Lagrangian relaxation techniques, particularly the ADMM, stand out for their efficiency, ease of implementation, and adaptability across a broad range of problems [40]. However, two key challenges emerge when applying these methods to complex VPP operations. First, existing contributions typically decompose the VPP's stochastic optimization problem along either the scenario or spatial dimension in isolation [33], limiting the parallelization potential of the decomposition method. Second, when applied to nonconvex models—such as MILP, the most prevalent class of models in the literature as detailed in Fig. 1.2—the direct application of ADMM results in heuristic solutions without performance guarantees, meaning the quality of the final solution is not assured in these cases [43].

It is worth mentioning that the challenges and gaps identified in the analysis of the current state-of-the-art regarding the evolving role, structure, and operations of VPPs align with those highlighted in several recent review studies. For example, the analysis conducted in [28] reveals that "*the complexity of mathematical models has been growing, and more nonlinear problems have been formulated. This is the result of incorporating more realistic approximations of the VPPs and including more complex interactions in the mathematical models between agents and markets.*" This study also emphasizes that "*the integration of distributed generation in the VPP has contributed to more active participation in different types of markets*," underscoring the evolution of modern commercial VPPs into complex systems with expanded trading horizons. Additionally, in relation to VPP scheduling and dispatch problems, [12] points out that "*none of the previous studies considered all technical and economic constraints, along with different kinds of uncertainties simultaneously*," while [15] remarks that "*researchers have concentrated more on the deterministic formulation type than on the stochastic one.*" These observations underline the necessity of a comprehensive approach that treats scheduling and dispatch as a unified multi-stage problem, addressing multiple sources of uncertainty. Furthermore, [54] highlights that in modern VPPs, "*complex interrelationships between heterogeneous distributed energy resources negatively impact the ability to use centralized models*," emphasizing the limitations of traditional centralized optimization approaches in managing complex VPP operations. Similarly, [55] forecasts that "*the future VPP model incorporates a distributed control environment that enables a decentralized system to operate somewhat autonomously across all interconnected networks*," illustrating the growing interest in distributed control strategies to tackle the increasing complexity of VPP optimization problems. In this context, identifying new methods to derive performance guarantees for distributed optimization approaches, particularly when applied to nonconvex problems, has been already recognized as a significant area for future research [56]. The intricate nonconvex problems associated with the complex VPPs energy management offer a compelling opportunity to drive forward the investigation of distributed methods in this direction.

Finally, from the perspective of Compagnie Nationale du Rhône, whose transition to a complex VPP is used as a case study to validate the proposed optimization and control algorithms, two key **research questions** arise:

Q1. Does the integrated operation of cascaded run-of-the-river hydropower plants, wind, and

solar units offer advantages in electricity market trading compared to operating these units separately?

Q2. What methods can be implemented to manage the complexity of combined scheduling and dispatch of these units, while ensuring scalability, performance guarantee and minimizing disruptions to the company's existing tools?

The **general objective** of this thesis is to tackle the emerging challenges posed by the rise of complex VPPs. The focus is on developing modeling and decision-making tools that ensure scalability and adaptability to the dynamic nature of complex VPPs—such as accommodating participation in multiple electricity markets or the evolving composition of the VPP portfolio—while maintaining the secure and feasible operation of these critical systems. The **contributions of this thesis** in achieving this objective and addressing the aforementioned challenges are summarized as follows:

C1. **A generic modeling approach**: A modular modeling approach for large-scale, complex VPPs is developed, wherein the energy resources within the VPP are organized into generic clusters that are interconnected through coupling constraints. By identifying common coupling constraints within the physical model of the VPP, this approach lays the groundwork for subsequent decomposition methods aimed at decoupling the identified sources of coupling.

C2. **A comprehensive fully-stochastic decision-making framework**: Building on the modeling approach of C1, a two-level fully stochastic decision-making framework is developed by integrating scenario-based stochastic programming and stochastic predictive control. This framework addresses both the scheduling of complex VPPs in the day-ahead market and near-real-time dispatch, efficiently handling multiple sources of uncertainty at various stages of the VPP energy management problem.

C3. **A scenario-spatial decomposition**: The proposed two-level stochastic decision-making framework of C2 is reformulated as a general form consensus problem to enable simultaneous decomposition across both spatial and scenario dimensions, enabling full-scale parallelization and improving scalability compared to existing methods, which typically limit decomposition to either the spatial or scenario dimension alone.

C4. **A distributed method for the convex case**: Augmented Lagrangian relaxation-based stochastic distributed algorithms are developed to solve the reformulated decision-making framework of C3 in the convex case.

C5. **A trustworthy distributed method for the mixed-integer case**: An ADMM-based stochastic distributed algorithm is developed to address the reformulated decision-making framework of C3 in the MILP case. Since a direct application of ADMM inherently results in a heuristic approach for such problems [43], a novel *trustworthy* distributed algorithm is proposed. This approach iteratively updates upper and lower bounds throughout the algorithm's execution to approximate the global optimum of the original centralized model.

By quantifying the "distance" between these bounds, the algorithm evaluates the quality of the distributed solution, ensuring a performance guarantee.

C6. **Proof of bounds existence and validity**: A mathematical proof is provided to demonstrate the existence and validity of the upper and lower bounds derived by the trustworthy distributed method for MILP models.

C7. **Extension for multi-market trading**: The proposed two-level stochastic decision-making framework is extended to handle multi-market trading, allowing the complex VPP to operate across multiple electricity markets as a unified entity.

Contributions C1 and C2 establish a standardized modeling and stochastic decision-making framework for complex VPP operations within the day-ahead energy market. Contribution C3 reformulates the problem to facilitate the implementation of augmented Lagrangian relaxation-based algorithms. Building on this foundation, C4 develops tools for distributed solutions in the convex case, while C5 and C6 provide similar tools for the mixed-integer case, complete with a performance guarantee. Finally, C7 extends these methods to support simultaneous participation in multiple electricity markets.

Regarding the research questions posed by Compagnie Nationale du Rhône, contributions C1, C2, and C7 address Q1 by exploring trading strategies in both single and multiple electricity markets, while contributions C3-C6 focus on answering Q2 within both convex and nonconvex models of the VPP.

1.3 Structure of the Thesis

The remainder of this manuscript is structured as follows. Chapter 2 presents an overview of the VPP paradigm and introduces the case study of Compagnie Nationale du Rhône, which provides a basis for simulation results, testing of the proposed optimization and control methods, and examination of research questions Q1 and Q2. Although this chapter does not introduce specific novel contributions, it establishes the foundation for subsequent chapters by motivating their contributions and outlining both the input data and physical models used by Compagnie Nationale du Rhône. Chapter 3 transitions from the existing VPP paradigm to the proposed complex VPP paradigm. In particular, after defining the concept of a complex VPP, this chapter proposes a generic modeling approach along with a stochastic, two-level decision-making framework for addressing scheduling and dispatch for a complex VPP in the day-ahead market (**contributions C1 and C2**). Chapter 4 decomposes the centralized two-level decision-making framework of Chapter 3 to enable a distributed approach for scheduling and dispatching complex VPPs. A spatial-scenario decomposition approach is introduced, enabling the development of distributed algorithms designed to address both convex and MILP problems (**contributions C3, C4, and C5**). Additionally, a mathematical proof is provided to ensure a performance guarantee for the proposed distributed algorithm in the nonconvex case (**contribution C6**). Chapter 5 then extends the findings of Chapters 3 and 4 to encompass multi-market trading

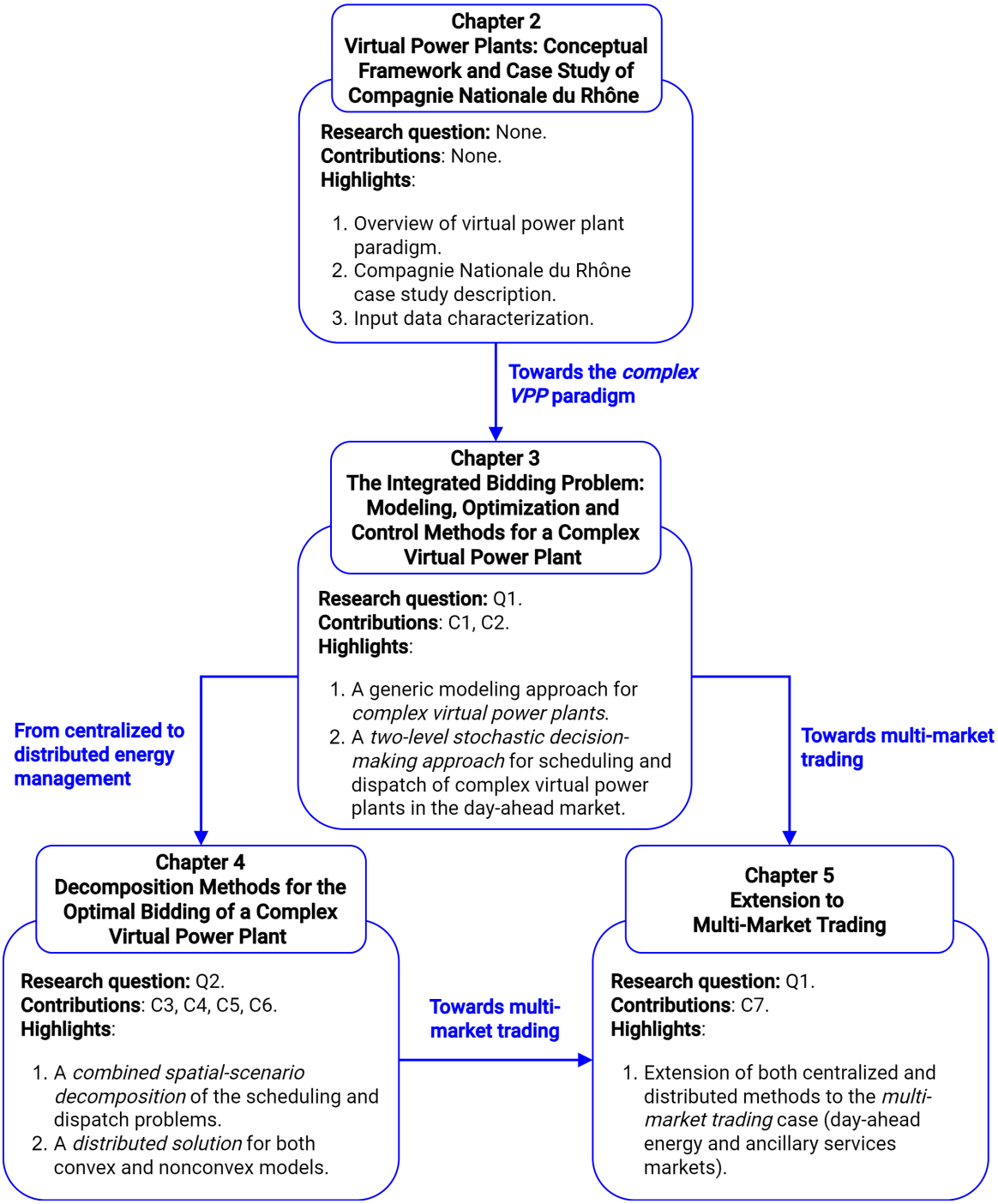

Figure 1.4: Overview of the structure of the thesis.

(**contribution C7**). Finally, Chapter 6 concludes the thesis. A visual overview of the thesis structure is provided in Fig. 1.4.

1.4 List of Publications

The present thesis led to the following publications.

Journal Publications

[J1] **L. Santosuosso**, S. Camal, A. Lett, G. Bontron, and G. Kariniotakis, "Distributed economic model predictive control for the joint energy dispatch of wind farms and run-of-the-river hydropower plants," *Electric Power Systems Research*, vol. 235, pp. 110805, 2024. Special Issue *Proceedings of the 23rd Power Systems Computation Conference (PSCC 2024)*. Available at: https://www.sciencedirect.com/science/article/abs/pii/S0378779624006916.

[J2] **L. Santosuosso**, S. Camal, A. Di Giorgio, F. Liberati, A. Michiorri, and G. Kariniotakis, "Stochastic economic model predictive control for trading energy and ancillary services with storage," *Sustainable Energy, Grids and Networks*, vol. 38, pp.101373, 2024. Available at: https://www.sciencedirect.com/science/article/abs/pii/S2352467724001024.

Journal Papers Under Review

[J3] **L. Santosuosso**, S. Camal, A. Lett, G. Bontron, J. Kazempour, and G. Kariniotakis, "A scenario-spatial decomposition approach with a performance guarantee for the combined bidding of cascaded hydropower and renewables," submitted to *IEEE Transactions on Power Systems* (**under review**). Preprint available at: https://hal.science/hal-04738929v1.

Conference Publications (Peer Reviewed)

1. **L. Santosuosso**, S. Camal, A. Di Giorgio, F. Liberati, A. Michiorri, G. Bontron, and G. Kariniotakis, "Economic model predictive control for the energy management problem of a virtual power plant including resources at different voltage levels," in *27th International Conference on Electricity Distribution (CIRED)*, Rome, Italy, 2023. Available at: https://ieeexplore.ieee.org/document/10267715 and https://hal.science/hal-04210514.

Conference Presentations

- **L. Santosuosso**, S. Camal, A. Lett, G. Bontron, and G. Kariniotakis, "Run-of-river hydropower to improve the market value of wind: A case study in France," in *2023 WindEurope Technology Workshop*, Lyon, France, 2023. Available at: https://hal.science/hal-04917973.
- **L. Santosuosso**, S. Camal, A. Lett, G. Bontron, and G. Kariniotakis, "Optimization of large-scale virtual power plants integrating wind farms," in *2023 WindEurope Annual Event*, Copenhagen, Denmark, 2023. Available at: https://hal.science/hal-04162057.

- **L. Santosuosso**, S. Camal, A. Di Giorgio, F. Liberati, A. Michiorri, and G. Kariniotakis, "Advanced model predictive control strategies for the provision of energy and ancillary services by wind farms coupled with storage," in *2022 WindEurope Technology Workshop*, Bruxelles, Belgium, 2022. Available at: https://hal.science/hal-03710704.

1.5 Notation

In the following, sets and vectors are represented by boldfaced letters, e.g., $\boldsymbol{z}$, while matrices are denoted by boldfaced uppercase letters, e.g., $\mathbf{M}$. The cardinality (i.e., the number of elements) of a set $\boldsymbol{S}$ is denoted by $|\boldsymbol{S}|$.

Chapter 2

Virtual Power Plants: Conceptual Framework and Case Study of Compagnie Nationale du Rhône

Résumé en Français

Ce chapitre explore le concept de centrale électrique virtuelle en mettant en lumière son rôle dans la gestion des systèmes électriques modernes, marqués par l'intégration de ressources énergétiques variées. L'intérêt croissant pour les centrales électriques virtuelles réside dans leur capacité à optimiser l'exploitation des ressources énergétiques distribuées, à améliorer leur visibilité sur les marchés de l'électricité et à renforcer la durabilité du secteur énergétique. Une centrale électrique virtuelle est une agrégation de ressources hétérogènes gérées de manière flexible pour participer aux marchés ou fournir des services au réseau. Le chapitre aborde l'évolution du concept de centrale électrique virtuelle, en examinant ses origines, ses progrès technologiques et son rôle actuel dans les systèmes électriques. Il distingue les centrales électriques virtuelles commerciales, axées sur l'optimisation des agrégateurs sur les marchés de l'électricité, des centrales électriques virtuelles techniques, qui assurent des services essentiels pour la sécurité du réseau. Le chapitre décrit également les stratégies pour surmonter ces incertitudes et optimiser les performances des centrales électriques virtuelles. Il se concentre sur leur participation aux marchés de l'électricité, en abordant les interactions avec ces derniers et en analysant des exemples concrets de projets réussis. Enfin, le chapitre présente une étude de cas sur la Compagnie Nationale du Rhône, qui exploite une centrale électrique virtuelle en France, et examine la gestion de son portefeuille énergétique diversifié, comprenant des unités hydroélectriques, éoliennes et photovoltaïques.

2.1 Introduction

The increasing complexity of modern power systems, driven by the integration of several heterogeneous energy resources, has necessitated the development of innovative energy management approaches [57]. Among these, the concept of the VPP has emerged as a transformative framework for coordinating and optimizing the operation of DERs [58]. The growing interest in VPPs is driven by several factors, including their potential to increase the visibility of DERs in electricity markets, enable the active participation of vRES in providing essential grid services—a role traditionally fulfilled by large-scale power plants—and ultimately enhance the sustainability of the energy sector [59].

This chapter provides a comprehensive exploration of VPPs, delving into their definition, classifications, and the strategies employed to address the challenges inherent to VPP operations. A VPP is fundamentally an aggregation of heterogeneous energy resources, managed as a unified and flexible entity to participate in electricity markets or provide grid services [28]. The discussion begins by tracing the evolution of the VPP concept, examining its origins, key technological advancements, and the milestones that have defined its current role in modern power systems. It then transitions to the classification of VPPs based on their primary objectives and roles, distinguishing between commercially oriented VPPs, which aim to optimize aggregator participation in electricity markets, and technically oriented VPPs, which focus on delivering services essential for maintaining secure and reliable grid operation [60].

A central theme of the chapter is the challenge of managing uncertainties within VPP operations [61]. These uncertainties arise from various sources, including the stochastic nature of vRES, fluctuating market conditions, and dynamic consumer behavior. Effective energy management strategies are crucial to mitigating these uncertainties and optimizing VPP performance. The discussion includes an overview of the main stages involved in VPP operations and the methodologies commonly employed to achieve optimal performance. Given the focus of this thesis on VPP participation in electricity markets, particular attention is given to the mechanisms through which VPPs interact with these markets. To bridge theoretical concepts with practical applications, the proposed overview concludes by examining real-world implementations and projects regarding VPPs (e.g., [62]), highlighting their operational successes and challenges.

Building on this foundational overview, the chapter transitions to a detailed description of the primary case study featured in this thesis: the VPP operated by Compagnie Nationale du Rhône, a leading producer of renewable energy in France [49]. This case study examines how Compagnie Nationale du Rhône has implemented and managed its VPP, addressing the distinct challenges and opportunities associated with its diverse energy portfolio, which includes hydropower units, wind farms, and solar power plants. The chapter further introduces the mathematical formulation of the physical dynamics governing the VPP, specifically the intricate cascaded hydropower system managed by the company [63], and analyzes the input data, with a particular focus on the forecasting inputs for market prices, vRES power generation, and water inflows into its hydropower assets. The relevance of this case study is then placed within the

broader context of the VPP paradigm evolution.

Rather than proposing novel contributions, this chapter aims to equip the reader with the foundational knowledge required to engage with the models and methods proposed in the subsequent chapters.

2.2 An Overview of the Virtual Power Plant Paradigm

This section offers an overview of the VPP concept, detailing its definition, classifications, and the diverse strategies employed for energy management within this framework. Furthermore, it delves into the inherent uncertainties that VPPs must navigate and underscores their growing significance in modern electricity markets. Additionally, real-world applications are examined to illustrate their practical implementation and operational challenges.

2.2.1 Definition and Evolution of the Virtual Power Plant Concept

The VPP paradigm emerged in 1997, initially introduced as the *virtual utility* [64]. Since its inception, this paradigm has evolved considerably, attracting widespread attention due to its potential to enhance the management and visibility of DERs. The evolving definitions and classifications of VPPs reflect the changing landscape of energy markets and the increasing complexity of power systems.

The VPP concept was initially defined as "*a framework to enhance the visibility and control of DERs to system operators and other market actors by providing an appropriate interface between these system components*" [64]. Since then, scholars have proposed definitions for VPPs based on their role in the electricity markets, like in [65], where achieving the greatest profit for the owners of DERs is seen as the primary objective of a VPP; while others focused on the ability of VPPs to contribute in enhancing grid reliability and safety, like in [66], where VPPs are seen as a framework to participate in power system operation, reducing power losses and peak loads.

The VPP conceptualization process has followed distinct paths in different countries and regions. Accordingly to [67], in the European Union, the term VPP generally refers to a collective of supply-side resources that are managed as a single entity in the electricity markets. Differently, in the United States, a VPP typically involves demand response and critical peak pricing programs that, when amalgamated, can reproduce the ability of conventional power plants to contribute in deliver peak capacity and grid reliability services [68]. Overall, the primary appeal of VPPs lies in their ability to enhance controllability over non-dispatchable units, such as vRES, enabling these resources to take on roles that have traditionally—and still largely—been filled by large-scale thermal power plants, such as contributing to the provision of ancillary services [69].

Bringing these perspectives together, a VPP integrates and manages heterogeneous energy resources spread across different locations, enabling them to function collectively as a single entity. The resources within a VPP can be traded on the market, utilized to support the power grid, or both. A key concept within the VPP framework is flexibility [70]. Through

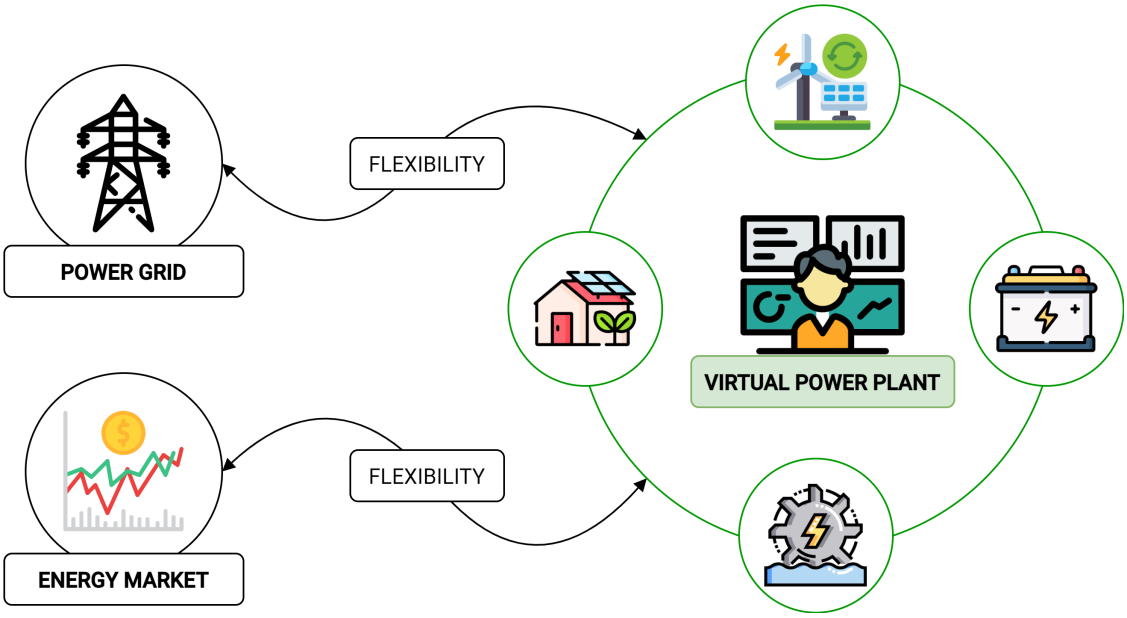

Figure 2.1: Illustration of the VPP paradigm.

the coordinated operation of both dispatchable and non-dispatchable units, the primary goal of VPPs is to enhance the controllability of the system by leveraging the flexibility gained through the aggregation. Fig. 2.1 provides an illustration of the VPP concept.

2.2.2 Classification of Virtual Power Plants

The classification of VPPs is intricately linked to their functionalities and the specific objectives they are designed to achieve. Generally, VPPs are categorized into two primary types, each with distinct operational focuses [71]:

- A *commercial VPP* focuses on the economic optimization of its resource portfolio within electricity markets [72]. This entails formulating and implementing optimal bidding strategies, facilitating the market integration of DERs, and ensuring a fair allocation of revenues and costs among DER owners. Operating as a market-oriented entity, this type of VPP emphasizes financial performance and profit maximization. Participation in electricity markets requires commercial VPPs to manage imbalances—defined as discrepancies between scheduled and actual real-time power injection or consumption [73]. As discussed in the following chapter, addressing the penalties associated with these imbalances constitutes a central objective for such VPPs.

- A *technical VPP* focuses on the operational and technical management of energy resources [28]. Its primary objective is to ensure the efficient and secure operation of these resources by considering technical constraints, safety requirements, asset dynamics, and grid stability. It plays a critical role in maintaining the reliability of the power grid, providing essential services such as frequency regulation, voltage support, and load balancing.

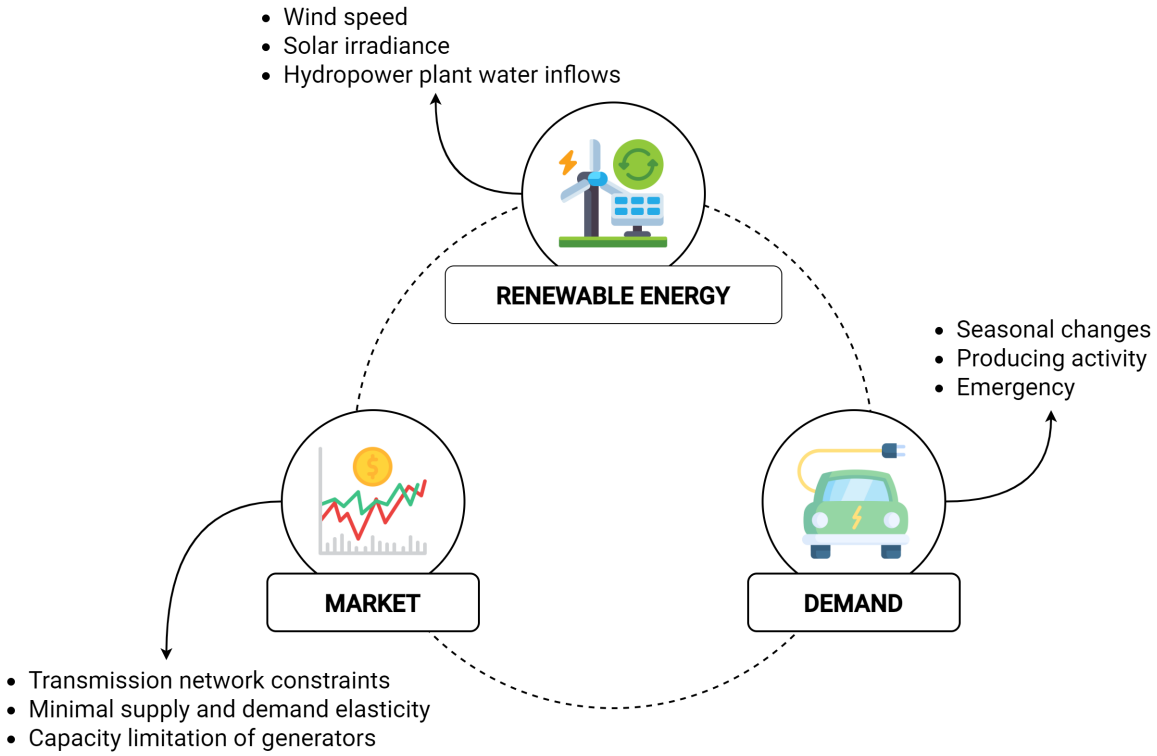

Figure 2.2: Main contributing factors of the three uncertainties sources in VPP operations, as analyzed in [61].

While commercial VPPs and technical VPPs can function independently, there is a growing trend toward integrating their operations to achieve optimal performance, as discussed for example in [74]. This integrated approach allows for the holistic management of both the economic and technical aspects of the VPP, thereby maximizing its overall efficiency and effectiveness within the energy system.

2.2.3 Navigating Uncertainties in Virtual Power Plant Operations

Optimization challenges in VPP operations are profoundly influenced by various uncertainties, particularly in complex large-scale systems with significant integration of vRES. As such, it is imperative to identify the primary sources of these uncertainties, appropriately characterize them, and select robust models to mitigate their impacts.

As detailed in Fig. 2.2, the three main sources of uncertainty typically recognized in VPP operations are as follows [61]:

- *Renewable energy generation*: The uncertainty associated with renewable energy generation arises predominantly from the intermittent and variable nature of resources such as wind and solar power [75]. Although forecasting methods have advanced [76], the accuracy of predictions for these energy sources remains limited, with forecast errors typically ranging from 10% and 15% [77]. This uncertainty is further complicated by its influence on other aspects of the system, such as market prices, making it a critical area of focus in

optimization models. For economically driven problems, such as those commonly faced by commercial VPPs, the significant economic value of vRES forecasting has been extensively established [78].

- *Market*: Market prices constitute another critical source of uncertainty when VPPs engage in the energy trading [79]. These prices are subject to fluctuations driven by a multitude of factors, including transmission network constraints, local demand variations, climatic conditions, and regulatory policies. Unlike most conventional commodities, electricity prices can experience extreme volatility, with fluctuations reaching up to approximately 360% in some cases within the United States [80]. Additionally, participation in ancillary service markets introduces further uncertainties, such as those related to power grid frequency, which can significantly impact bidding strategies and are challenging to predict well in advance [81].

- *Demand*: Uncertainty in electricity demand represents a common and significant challenge in VPP optimization problems [82]. This uncertainty can be decomposed into a deterministic component, largely influenced by predictable factors such as time of day and seasonal climatic patterns, and a stochastic component, which arises from various unpredictable influences, including consumer behavior, emergency situations, and broader economic conditions. The increasing integration of emerging technologies, particularly controllable loads like electric vehicles, further accentuates the challenges posed by demand uncertainty [83]. Depending on their integration and management within the grid, these technologies can either mitigate or intensify such uncertainties.

The various sources of uncertainty in VPP operations are not isolated; rather, they often exhibit significant interdependencies [84]. For instance, fluctuations in renewable energy generation can directly impact market prices by altering the supply-demand balance. Similarly, both renewable generation and electricity demand can be influenced by external factors such as weather conditions, which further complicates forecasting and planning. These interdependencies necessitate a holistic approach to uncertainty management, where the interconnected nature of different uncertainties is considered in the modeling and optimization process to fully exploit the advantages of aggregated systems [85].

2.2.4 The Energy Management of a Virtual Power Plant

The energy management of a VPP involves all the activities necessary to optimize the operation of the VPP. These activities are implemented by the *energy management system*, which functions as the central component of the VPP. The energy management system gathers data from various sources, including markets, energy resources, consumers, loads, and the grid, and then develops its planning strategy based on this information. This section explores the formulation of the energy management problem for VPPs, the standard optimization-based approach commonly used by energy management systems, and various methods for addressing the energy management challenges within VPPs.

Type	List of most common objectives
Generation units	· Generation income · Spinning reserve income · Capital cost · Operational cost
Main grid	· Income from electricity markets · Incentives to support renewables
End customers	· Retail energy income · Demand response income/cost · Penalty cost
Energy storage	· Storage cost · Battery degradation
Miscellany	· System net load · Abandoned energy cost · Risk cost · Load shedding cost

Table 2.1: Classification of the most common objectives in energy management problems for VPPs, as analyzed in [61].

2.2.4.1 Energy Management Problem formulation

The energy management of VPPs is a complex, multi-objective problem, with its formulation varying significantly based on the specific characteristics of each plant. Typically, it involves both economic and technical objectives and constraints. Economically, the primary objective is to maximize the profits of DER owners while minimizing associated costs. On the technical side, it is essential to consider the physical constraints of each asset, the interactions among DERs, and the dynamics of individual components. The primary goals in VPP optimization problems generally revolve around maximizing revenue or minimizing costs. The specific formulation of the objective function is influenced by various factors, including the components of the VPP, market conditions, regulatory policies, environmental requirements, and risk considerations. Table 2.1 presents a classification of the most common objectives in energy management problems for VPPs, as analyzed in [61].

A VPP may aggregate a diverse array of resources. To ensure its secure and reliable operation, the energy management system must consider the physical constraints of generators, such as power generation limits, ramping restrictions, or start-up/shut-down requirements. It must also account for energy storage systems, which should avoid simultaneous charging and discharging, and demand response mechanisms, which may involve limits on curtailed power. Furthermore, constraints are necessary to model the dynamics of time-varying components, such as energy storage and electric vehicles, as well as the balance between power generation and load consumption. Additionally, various other constraints may be incorporated to address technical limits, such as network constraints, safety requirements, and market regulations, including rules that enforce single bidding curves and manage risk. Typically, the energy management formulation involves *non-anticipativity constraints*, which are used to ensure that decisions made in advance are consistent with future conditions [86]. These constraints enforce the principle that

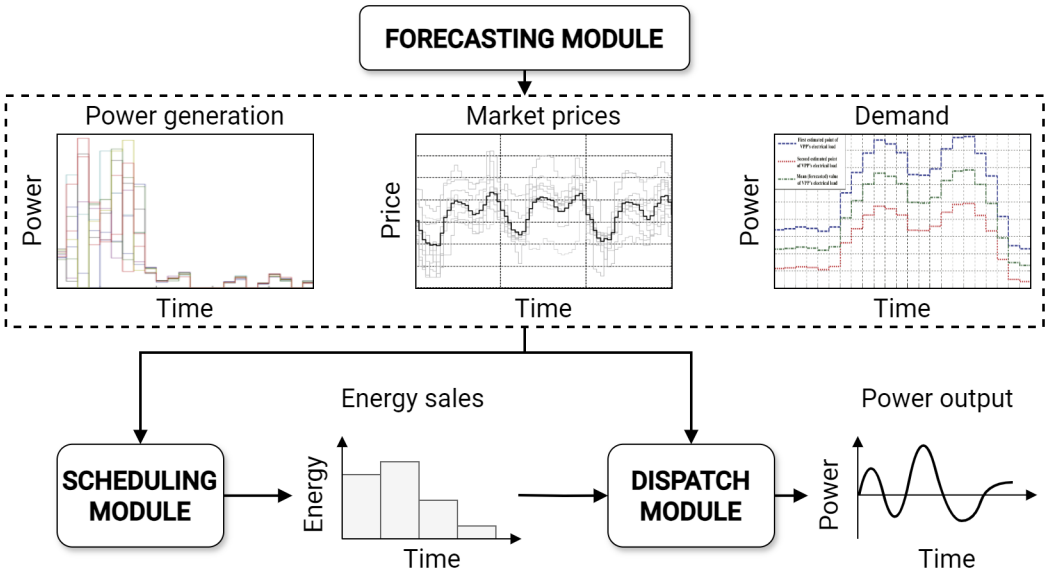

Figure 2.3: A standard energy management strategy for operating a VPP.

operational strategies, such as bidding curves or scheduling decisions, must be formulated without foreknowledge of future events or market outcomes. Essentially, they ensure that decisions are based on current information and do not assume any information that would be available only at a later time. This approach is crucial for maintaining the realism and feasibility of planning and optimization processes, reflecting the uncertainty inherent in energy markets and operational conditions.

A detailed overview of the primary objectives, components, and constraints addressed by energy management systems in VPPs is provided in [61].

2.2.4.2 Energy Management Strategy and Methods

A conventional energy management strategy consists of three distinct modules [28]:

- The *forecasting module* is responsible for predicting future uncertainties, including variations in energy demand and supply. Accurate forecasting is essential, as it provides the foundational data for subsequent decisions. This prediction process covers multiple time horizons, ranging from short-term to long-term, to address the inherent variability in energy systems.

- The *scheduling module* allocates energy resources to the market using long- to medium-term forecasts. This process involves optimizing resource deployment to meet anticipated demand and/or maximize profit while adhering to market constraints and regulations. The primary aim is to efficiently balance supply and demand, thereby reducing operational costs and enhancing economic performance.

- The *dispatch module* focuses on refining and adjusting the VPP schedule (established by the scheduling module) using short-term forecasts and real-time observations. It employs

control strategies to manage and correct deviations from the initially planned schedule. These adjustments are necessary due to unexpected changes in demand and supply conditions that may occur after the scheduling phase. The dispatch strategy aims to ensure that operations remain aligned with the forecasted plan, minimizing discrepancies and maintaining system reliability.

Fig. 2.3 illustrates a typical energy management strategy for operating a VPP, organized into the aforementioned modules. The energy management strategy typically covers several time stages.

In the domain of energy management for VPPs, various methods have been employed to address the complex challenges involved. These methods can generally be categorized into several broad types [87]:

- *Mathematical programming* is a fundamental approach for formulating and solving operational problems in VPPs. These problems often need to account for complex nonlinear dynamics, frequently resulting in mixed-integer nonlinear programming (MINLP) formulations [88]. However, a significant limitation of MINLP models is the lack of readily available off-the-shelf solvers capable of handling these formulations efficiently. This practical constraint poses a barrier to the widespread application of MINLP models in the VPP domain. To address this challenge, researchers have explored various methods to simplify these models. A common approach involves applying linearization or convexification techniques to approximate the original nonlinear dynamics, resulting in LP models [89]. LP models are straightforward to implement and solve but often provide overly simplistic approximations of the VPP's physical dynamics. Another widely used approach is MILP, which strikes a balance between computational tractability and modeling accuracy [90]. As discussed in Chapter 1 and illustrated in Fig. 1.2, MILP models remain the most prevalent modeling framework in the VPP context. However, there is growing interest in nonlinear models, reflecting the increasing demand for greater precision in capturing the inherent complexities of VPP operations. Besides the nature of the mathematical programming model, a critical aspect of VPP problems—and optimization problems in the power system domain more broadly—is the approach used to handle uncertainties. As this is central to the discussion presented in this thesis, a detailed review of these methods is provided in the context of the specific problems addressed in the following chapters. For a comprehensive overview of power system optimization under uncertainty, the reader is referred to [23].

- *Heuristic methods* offer a practical alternative to mathematical programming which aims at providing a balance between solution accuracy and computational efficiency. These methods do not guarantee optimal solutions but can reduce the computational effort compared to classical optimization techniques. In this context, *meta-heuristic methods* represent a higher level of abstraction designed to find optimal or near-optimal solutions in complex problems with incomplete or imperfect information [91]. Commonly used heuristics include genetic algorithms [92] and particle swarm optimization [93]. These methods

have garnered attention for their ability to provide solutions in cases where traditional mathematical programming approaches lead to intractable problems. However, skepticism remains regarding their widespread application in real-world settings, particularly in critical domains such as power system operations, where ensuring system safety and reliability is often a paramount concern.

- *Learning-based methods* such as artificial intelligence and machine learning techniques have gained prominence in energy management, offering fast, scalable, and efficient solutions. Machine learning approaches are generally classified into three main categories [94]: supervised learning, unsupervised learning, and reinforcement learning. Among these, reinforcement learning has shown particular promise for energy management in VPPs [95]. This method trains algorithms through iterative interactions with an environment, where actions result in rewards or penalties, and the system's state evolves accordingly. This makes reinforcement learning particularly well-suited to modeling the complex decision-making processes inherent in energy management systems [96]. Despite their potential, the practical application of learning-based methods in this domain remains limited. These approaches often require extensive datasets for effective training, which can be challenging to obtain in energy systems. Furthermore, learning-based methods generally suffer from poor interpretability and lack theoretical guarantees regarding the accuracy and reliability of the solutions they produce. This has spurred growing interest in simpler machine learning algorithms, such as decision trees, which aim to harness the scalability of machine learning while preserving interpretability in the decision-making process [97].

Moreover, *control theory* [98] provides attractive methods to tackle VPP decision-making problems, especially for the dispatch module of the VPP energy management strategy (see Fig. 2.3), which operates near to real-time and thus requires fast effective algorithms. In this context, the literature highlights a range of applications, from simple feedback-based control methods, such as proportional–integral–derivative controllers [99], to more advanced approaches. Notably, two branches of control theory are particularly relevant for modern VPP problems:

- *Optimal control* [100], which focuses on designing control strategies to optimize a specific performance criterion, subject to system dynamics and constraints. This approach assumes precise knowledge of the system model and external disturbances, aiming to achieve the best performance under nominal conditions.

- *Robust control* [101], which prioritizes maintaining acceptable performance and stability in the presence of uncertainties in the system model or external disturbances. It emphasizes reliability and resilience, ensuring the system can handle worst-case scenarios effectively.

Given the increasing emphasis on optimizing system operations under uncertainty, recent advances in control theory have extended optimal control methods to address uncertain environments. Among these, *model predictive control* (MPC) [102] has emerged as a highly effective and sophisticated approach. MPC leverages a system model to predict future states and optimize

control actions over a finite time horizon, continuously adapting to new data and evolving conditions [103]. By extending the offline decision-making capabilities of traditional mathematical programming to real-time control, MPC provides a flexible and scalable framework [104]. MPC's ability to incorporate diverse system dynamics and multiple objectives, alongside its integration with forecasting tools, makes it exceptionally well-suited to managing the dynamic and complex nature of modern VPPs [105].

2.2.5 Virtual Power Plants Participation in the Electricity Markets

From the end of the 20th century, several countries have started a process of liberalization and openness to competition in their electricity markets. This has brought a transformation of the energy sector, where energy generation, transmission, distribution and retailing now operate independently. Nowadays, market participants can operate in various electricity markets, whose market sessions take place either *long before dispatch* (e.g., bilateral contracts, future markets) or the *day before dispatch* (e.g., day-ahead market) or *during the day of dispatch* (e.g., intraday market, balancing market) [28]. A comprehensive description of these electricity markets is beyond the scope of this review; however, the following provides an overview of the various markets in which VPPs can participate:

- *Bilateral contracts* (*power purchase agreement*): Bilateral contracts, often structured as power purchase agreements, involve direct negotiations between electricity generators and buyers to establish terms such as price, quantity, and contract duration [106]. These agreements typically span power exchanges over periods of 5 to 20 years and have gained popularity due to increased market volatility and the growing penetration of renewable energy. They offer both parties protection against uncertainties related to vRES and price fluctuations. For VPPs, power purchase agreements provide a stable income stream by securing long-term sales contracts [107]. Moreover, VPPs can aggregate and supply energy through these agreements, helping to balance supply and demand and reducing reliance on the spot market, where prices are more volatile [108].

- *Futures and forward markets*: The futures and forward markets provide mechanisms for electricity market participants to hedge against price volatility by locking in energy prices for delivery at a future date. *Futures contracts* are typically standardized and traded on exchanges, while *forward contracts* are more flexible and negotiated directly between parties. Forward contracts typically have durations of multiple years, while futures contracts generally have shorter time horizons. By engaging in futures and forward contracts, VPPs can stabilize their revenue streams, making their operations more financially predictable [109]. Additionally, VPPs exploit arbitrage opportunities between futures markets and day-ahead markets, buying low in one and selling high in the other to maximize their operating profits [110].

- *Day-ahead market*: The day-ahead market is a critical component of electricity markets and, in most cases, represents the only fully liquid market, where energy transactions

are scheduled for each hour of the following day based on bids submitted by market participants. VPPs play a significant role in this market by enabling small-scale generators and consumers to participate directly [111]. For generators, VPPs consolidate the output of multiple DERs and sell it in the day-ahead market, often at prices that reflect the expected supply-demand balance for the next day. Consumers, on the other hand, can use VPPs to manage self-consumption and sell excess energy back to the grid. Although VPPs typically act as price-takers [112], accepting market prices rather than setting them, some models suggest that VPPs can influence market prices through strategic bidding, effectively becoming price-makers [113]. This ability to impact market prices, even marginally, can be advantageous, allowing VPPs to optimize their revenue based on expected market conditions.

- *Ancillary services market*: Ancillary services are crucial for maintaining the reliability and security of the electricity grid, particularly as the penetration of vRES increases. The ancillary services market facilitates the trading of a diverse range of services, such as frequency regulation [114] and voltage control, which ensure the real-time balance between generation and consumption. Through the aggregation of heterogeneous energy resources, integrated systems can efficiently provide these services [115], often leveraging energy storage systems capable of rapid responses to grid condition changes [116]. As the liquidity of these markets improves, the economic viability of VPPs is expected to grow, enhancing their attractiveness for managing grid stability. Furthermore, by participating in these markets, VPPs mitigate the variability of renewable energy generation, enabling vRES to contribute to services traditionally dominated by large-scale conventional thermal power plants [117]. More broadly, the market-based procurement of power system flexibility has garnered significant attention in recent years and is widely acknowledged as an area where aggregation can play a pivotal role [118].

- *Reserve market*: Reserve markets, like ancillary services markets, are designed to enhance grid reliability [119]. However, the focus of reserve markets is primarily on ensuring sufficient backup generation or load-shedding capacity is available to address unexpected imbalances or contingencies, such as the sudden loss of a generation unit or a sharp increase in demand. Unlike ancillary services, which directly support the real-time secure operation of the grid, reserve markets are more oriented towards preparing the system to handle larger, less frequent disruptions. For VPPs, participation in reserve markets provides an opportunity to generate additional revenue by monetizing system capacity that is not already committed to other markets [120]. The profitability of participating in reserve markets, however, depends on several factors, including market demand, the availability of renewable energy, and the opportunity costs of forgoing participation in the day-ahead market. During periods of high demand or low renewable generation, reserve market prices tend to rise, making participation particularly attractive. Conversely, when renewable generation is abundant, reserve market prices may drop, and VPPs might find it more advantageous to sell energy in the day-ahead market or use storage systems to

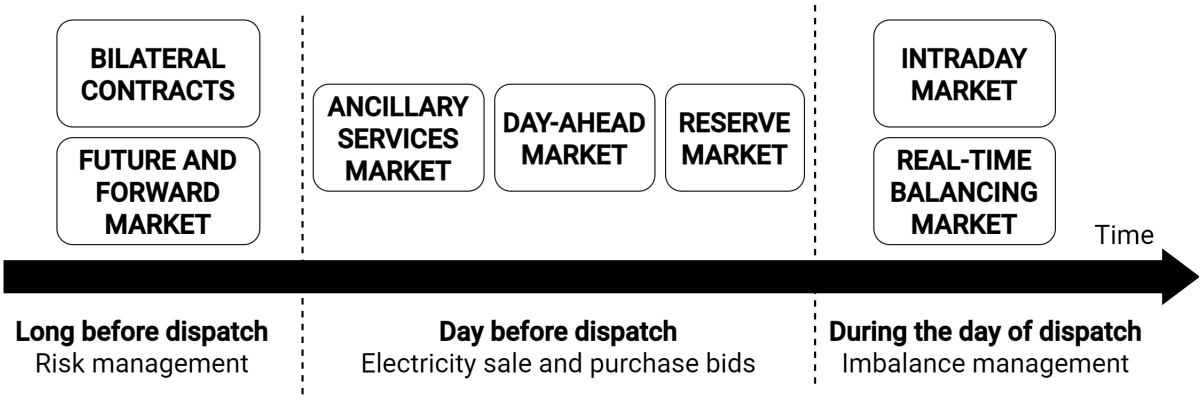

Figure 2.4: Sequence of electricity markets, as detailed in [28].

capture excess energy for later use. As such, the decision to commit resources to reserve markets requires careful consideration of market conditions and operational constraints.

- *Intraday market*: Intraday markets enable participants to adjust their energy positions established in the day-ahead market, allowing them to buy or sell electricity closer to the time of delivery [121]. Typically, these markets operate within a time horizon of a few hours to as little as 15 minutes before delivery, depending on the market structure. Intraday trading is crucial for managing the variability and uncertainty associated with renewable energy production, which can significantly deviate from forecasts made in the day-ahead timeframe [122]. For VPPs, intraday markets provide an opportunity to fine-tune their energy portfolios as more accurate information about generation and demand becomes available. For instance, if a VPP anticipates that one of its distributed generators will underperform, it can purchase additional energy in the intraday market to cover the shortfall, thereby avoiding penalties for failing to deliver the contracted amount of energy. The ability to adjust positions in near-real-time makes intraday markets an indispensable tool for VPPs to manage risk, address imbalances, and optimize their operations [123].

- *Real-time balancing market*: The real-time balancing market provides the final opportunity for market participants to reconcile their supply and demand positions before energy is delivered to the grid [124]. Operating on very short timeframes, this market typically has gate closures just minutes before delivery. VPPs engage in real-time balancing markets to correct any imbalances that remain after the intraday market, ensuring their actual generation aligns with their commitments [125]. When permitted by market regulations, VPP participation in these markets is especially valuable for managing vRES, as unexpected weather changes can cause significant discrepancies between forecasted and actual generation [120]. By participating in the real-time balancing market, VPPs can reduce imbalance penalties and enhance overall system stability.

Fig. 2.4 provides an overview of the sequence of electricity markets.

Overall, the VPP concept brings several advantages to both market participants and system operators. For instance, while various incentive mechanisms have been proposed to enhance

the visibility of small-scale units in modern electricity markets [126], the VPP paradigm effectively addresses this challenge by providing a technical solution to aggregate and manage these resources. Additionally, the coalition of heterogeneous resources within a VPP improves the ability to manage imbalances, boosting the profitability of these assets while contributing to the secure operation of the power grid. According to [28], most research on VPPs in electricity markets has focused on optimizing bidding strategies for the day-ahead market (see Fig. 1.3). However, due to the increasing penetration of renewable energy sources, the growing interest in ancillary services markets (to trade flexibility) and bilateral contracts (to hedge against the risk of price volatility) is notable. Few studies have considered VPP participation in multiple electricity markets, which provides an attractive opportunity to enhance VPP profitability and hedge against trading risk.

2.2.6 Virtual Power Plants in Practice: Real-World Applications

The practical implementation of VPPs varies significantly across different regions, reflecting the unique characteristics of each market, including regulatory frameworks, energy mixes, and specific energy challenges.

Europe has been a leader in the development and implementation of VPPs, driven by ambitious climate goals, a high penetration of renewable energy, and supportive regulatory environments. Two key projects illustrate the diversity of VPP applications in Europe:

- *FENIX Project* [127]: The Flexible Electricity Network to Integrate the Expected energy evolution project was a pioneering initiative funded by the European Union. It aimed to develop a technical, economic, and regulatory framework to enable DERs to actively participate in the electricity market and support grid operations. The project demonstrated how DERs, such as small-scale wind turbines, photovoltaic systems, and combined heat and power units, could be aggregated into a VPP to provide ancillary services, such as frequency regulation and load balancing, to the grid. The FENIX project highlighted the potential of VPPs to enhance grid stability and integrate a higher share of renewable energy.

- *Kombikraftwerk2* [128]: The Kombikraftwerk2 project in Germany showcased the ability of VPPs to create a balanced energy system using only renewable energy sources. By aggregating wind, solar, biogas, and hydropower plants into a VPP, the project demonstrated that it is possible to reliably supply electricity to the grid without fossil fuels. The project also emphasized the role of advanced forecasting and real-time control technologies in managing the variability of renewable energy generation. This project underscored the importance of VPPs in supporting Germany's energy transition, known as the Energiewende, towards a low-carbon energy system.

In the United States, VPPs have been explored as a means to enhance grid resilience and integrate DERs within a more deregulated and competitive electricity market. One notable example is the *ConEdison VPP* [55]. ConEdison, a major utility in New York, launched a VPP

Reference	Location	Components	Markets	Period
[127]	UK	· Cogeneration units	Day-ahead, intraday	2007/2008
[127]	Spain	· Cogeneration units · Renewable energy	Day-ahead, intraday	2007/2008
[128]	Germany	· Cogeneration units · Energy storage · Renewable energy	Day-ahead	2012
[130]	Croatia	· Energy storage · Gas · Renewable energy	Day-ahead	7 days
[131]	Belgium	· Boiler · Cogeneration units · Renewable energy	Day-ahead	1 day
[132]	China	· Electric vehicles · Energy storage · Cogeneration units · Renewable energy	Fixed prices	1 day
[133]	Australia	· Energy storage · Gas · Renewable energy	Ancillary services	1 year

Table 2.2: An overview of some prominent VPP projects from around the world.

pilot program that aggregates residential battery storage systems to provide demand response and grid support services. By partnering with homeowners who install batteries alongside their solar panels, ConEdison can reduce peak demand on the grid and defer the need for costly infrastructure upgrades. This project highlights how VPPs can offer utilities a cost-effective way to enhance grid reliability while empowering customers to participate in energy markets and reduce their carbon footprint.

In the Asia-Pacific region, where energy systems are often characterized by rapid growth, diverse energy mixes, and varying degrees of market liberalization, VPPs are being deployed to address specific regional challenges. Australia has seen significant adoption of rooftop solar photovoltaic systems, leading to challenges in managing the grid. The *Decentralized Energy Exchange platform* [129], developed by GreenSync, facilitates the creation of VPPs by enabling DERs, such as solar photovoltaic systems, batteries, and electric vehicles, to participate in the energy market. The Decentralized Energy Exchange provides a marketplace where owners of DERs can offer their energy services to utilities and grid operators, helping to stabilize the grid and integrate more renewable energy. This project illustrates the role of VPPs in managing the decentralized energy landscape in Australia.

Table 2.2 provides an overview of some prominent VPP projects from around the world.

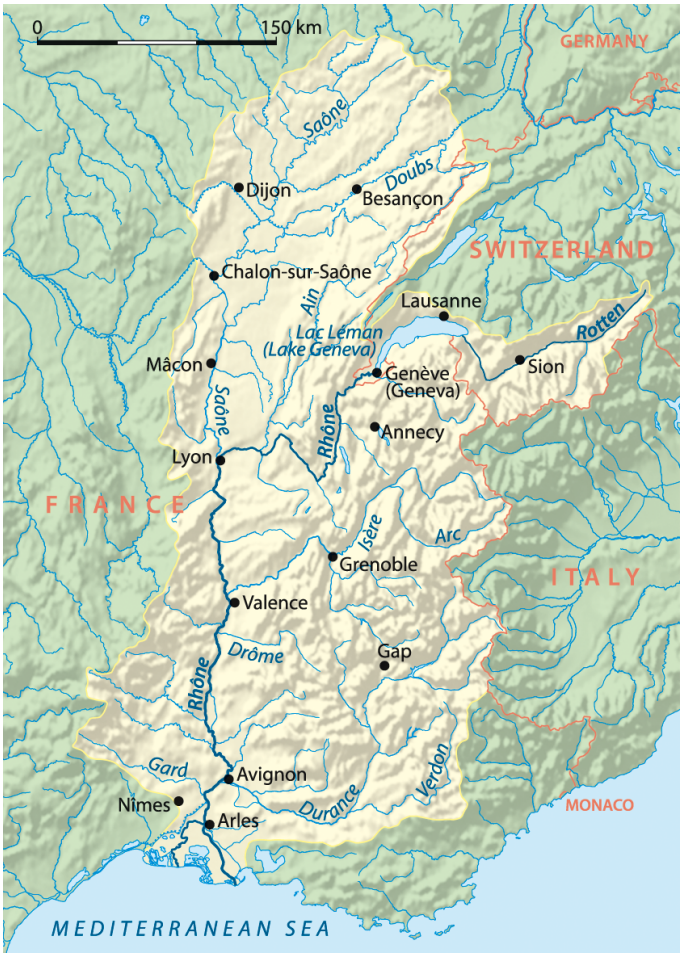

Figure 2.5: Map of the Rhône River and its watershed (highlighted in yellow) [134].

2.3 Case Study: The Virtual Power Plant of Compagnie Nationale du Rhône

This thesis centers on the case study of the VPP operated by Compagnie Nationale du Rhône. To provide a thorough understanding, this section begins with a general overview of the company and its role within the energy sector. Following this, the modeling of the VPP is detailed, including the input data utilized in the study. The section concludes by discussing the identified challenges and opportunities associated with this case study, as well as its significance within the broader context of the evolution of VPPs.

2.3.1 General Description of the Company

As a producer of 100% green energy, Compagnie Nationale du Rhône is a leading actor committed to advancing the energy transition. The French company, founded in 1933, operates primarily along the French section of the Rhône River, which is the most powerful and longest river in France, stretching over 812 kilometers from the Swiss Alps through southeastern France to the Mediterranean Sea. A map of the river is provided in Fig. 2.5.

Development	Output/year (GWh)	Head (m)	Capacity (MW)	Main tributaries
Upper Rhône				
Génissiat (GE)	1786	64.5	420	Arve, Valserine
Seyssel (SY)	166	7.5	45	Usses
Chautagne (CE)	449	17.0	90	Fier
Belley (BY)	453	16.7	90	-
Brégnier-Cordon (BC)	324	13.7	70	Séran
Sault-Brénaz (SB)	249	7.5	45	Guiers
Total upper Rhône	3427	126.9	760	-
Lower Rhône				
Pierre-Bénite (PB)	528	9.0	80	Ain, Saône
Vaugris (VS)	332	6.7	72	Gier
Péage-de-Roussilon (PR)	885	12.2	160	-
Saint-Vallier (SV)	668	11.5	120	-
Bourg-lès-Valence (BV)	1082	11.7	180	Doux, Isère
Beauchastel (BE)	1211	11.8	192	-
Baix-le-Logis-Neuf (LN)	1177	11.7	192	Eyrieux, Drôme, Ouvèze
Montélimar (MO)	1575	16.5	275	Roubion
Donzère-Mondragon (DM)	2032	22.5	349	-
Caderousse (CA)	843	8.6	187	Ardèche
Avignon (AV)	857	9.5	186	Cèze, Aygues
Vallabrègues (VA)	1269	11.3	210	Ouvèze, Durance
Total lower Rhône	12459	143.0	2203	-

Table 2.3: Characterization of the hydropower systems operated by Compagnie Nationale du Rhône [135].

The Rhône River is a critical natural resource, providing extensive opportunities for hydropower generation due to its significant flow and elevation drop. The company manages a cascade of 19 hydropower plants along the river, primarily consisting of run-of-the-river plants, with a total installed capacity of around 3 GW. The installed hydropower plants harness the river's flow to generate around 16 TWh of electricity annually, sufficient to supply the energy needs of approximately 4 million people, representing about 3% of France's total electricity consumption. The company's hydropower plants are complemented by an extensive network of 330 kilometers of canals and associated infrastructures that support the dual goals of energy production and river management. Beyond electricity generation, Compagnie Nationale du Rhône plays a pivotal role in managing the Rhône River's navigability, irrigation, and environmental protection. In addition to its core hydropower assets, the company has significantly diversified its renewable energy portfolio. Compagnie Nationale du Rhône operates 59 wind farms and 59 solar power plants across France, adding a further 1 GW of renewable energy capacity (around 2-3% of France's total combined wind and solar capacity). Together, these wind and solar units produce approximately 2 TWh of electricity annually. Fig. 2.6 illustrates a map of the assets operated by Compagnie Nationale du Rhône. Table 2.3 provides a characterization of the hydropower systems operated by the company, as detailed in [135]. The hydropower cascade is

divided into two sections: the *upper Rhône* and the *lower Rhône*. **This thesis focuses on the lower Rhône section**, examining the role of run-of-the-river hydropower plants in enhancing the market value of the company's wind and solar assets.

Compagnie Nationale du Rhône's operations are not limited to energy production; the company is also deeply involved in the integrated management of the Rhône River. This involves balancing the needs of energy production with those of navigation, agriculture, and environmental protection. In terms of financial performance, the company reports annual net sales of approximately €1.2 billion, primarily generated from the sale of electricity on the market. The company is primarily publicly owned, with 50.03% of its capital, while ENGIE is the main industrial shareholder, holding 49.97%.

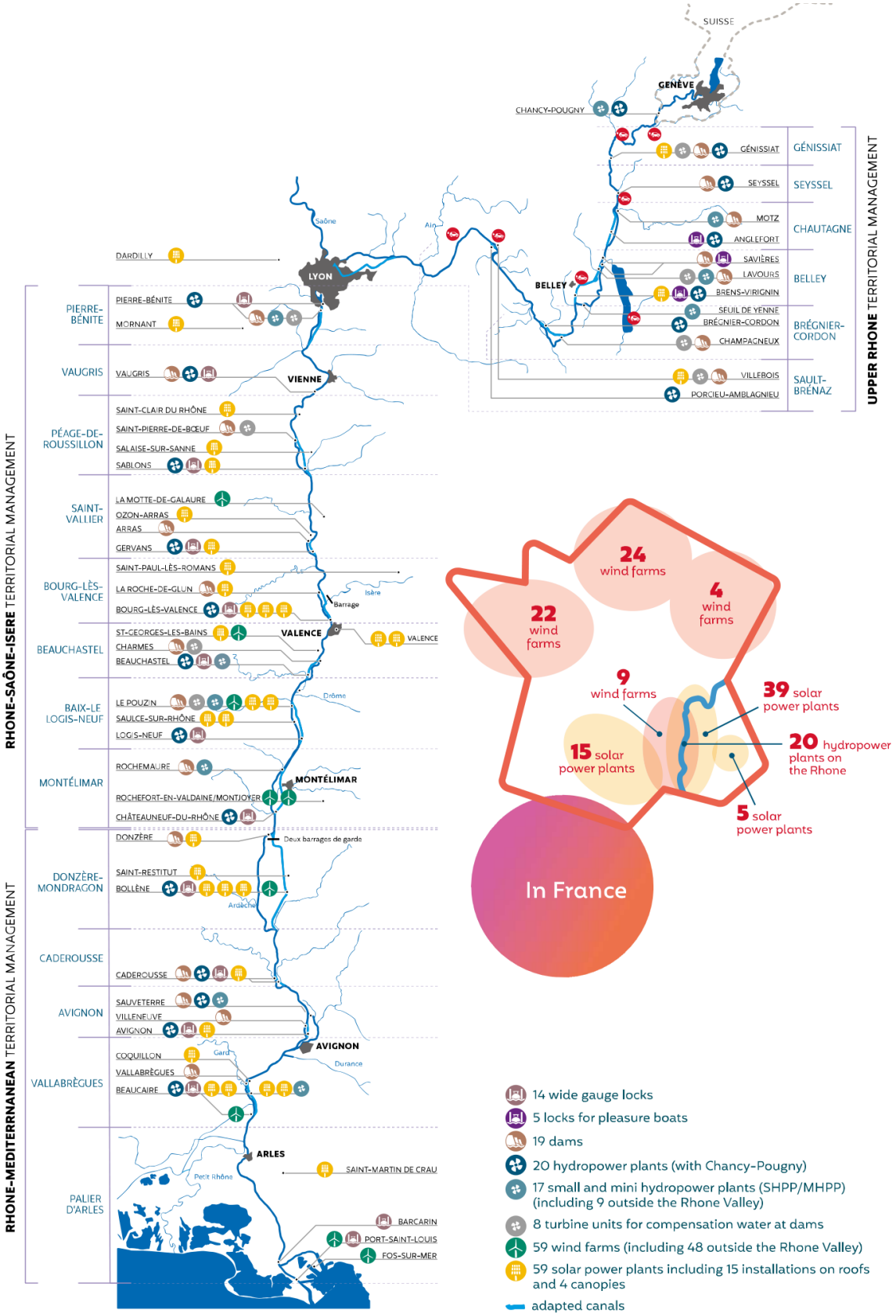

Figure 2.6: Map of the assets operated by Compagnie Nationale du Rhône.

2.3.2 Structure of the Hydropower Systems

Hydropower can be generally classified into three main types [136]:

- *Reservoir-based hydropower*: This type of hydropower plants involves large dams that create significant water storage capacity. By regulating the release of stored water, these systems can generate electricity on demand, making them highly responsive to fluctuations in energy demand. The potential energy of the stored water is converted into electricity as it flows through turbines housed within or near the dam.

- *Pumped-storage hydropower*: This type of hydropower plants operates on a different principle, utilizing two water reservoirs located at different elevations. During periods of low electricity demand, excess energy from the grid is used to pump water from the lower reservoir to the upper reservoir. When electricity demand peaks, the stored water is released back to the lower reservoir through turbines, generating electricity.

- *Run-of-the-river hydropower*: This type of hydropower plants differs from the other two types in that it typically involves minimal water storage capacity. Instead, it harnesses the natural flow and elevation gradient of a river to generate electricity. This generally has a lower environmental impact compared to reservoir-based systems since it does not require large dams or significant alterations to the river's natural state. However, due to their limited storage capacity, run-of-the-river facilities are more susceptible to seasonal and climatic variations in water flow, with their production being directly influenced by the water inflow.

The hydropower systems operated by Compagnie Nationale du Rhône are primarily run-of-the-river facilities, strategically located along sections of the Rhône River that naturally exhibit sufficient elevation gradients. Each hydropower system typically comprises a *barrage*, a *reservoir*, a *hydropower plant*, a *lock* (for navigation), and an interconnected system of channels. A *diversion channel* is engineered to concentrate the river's gradient at a specific location where the power station and lock are situated. The barrage, constructed along the natural course of the Rhône, diverts a substantial portion of the river's flow into the diversion channel, guiding it toward the hydropower plant. This arrangement creates an upstream reservoir, providing limited yet crucial storage capacity. After passing through the turbines, the water from the diversion channel is reintroduced into the Rhône downstream of the power station via the *discharge channel*. The portion of water that is not diverted to the power station flows over the barrage, where it is often harnessed by auxiliary hydropower units integrated into the barrage structure. To mitigate environmental and biodiversity impacts, a minimum ecological flow must be maintained continuously through the barrage, ensuring that the river's natural course does not dry out. During periods of high flow, the barrage functions as a spillway, releasing excess water once the hydropower plant's turbine capacity is exceeded. Fig. 2.7 provides a schematic representation of a typical hydropower system configuration.

Among the hydropower systems operated by Compagnie Nationale du Rhône, some notable exceptions exist:

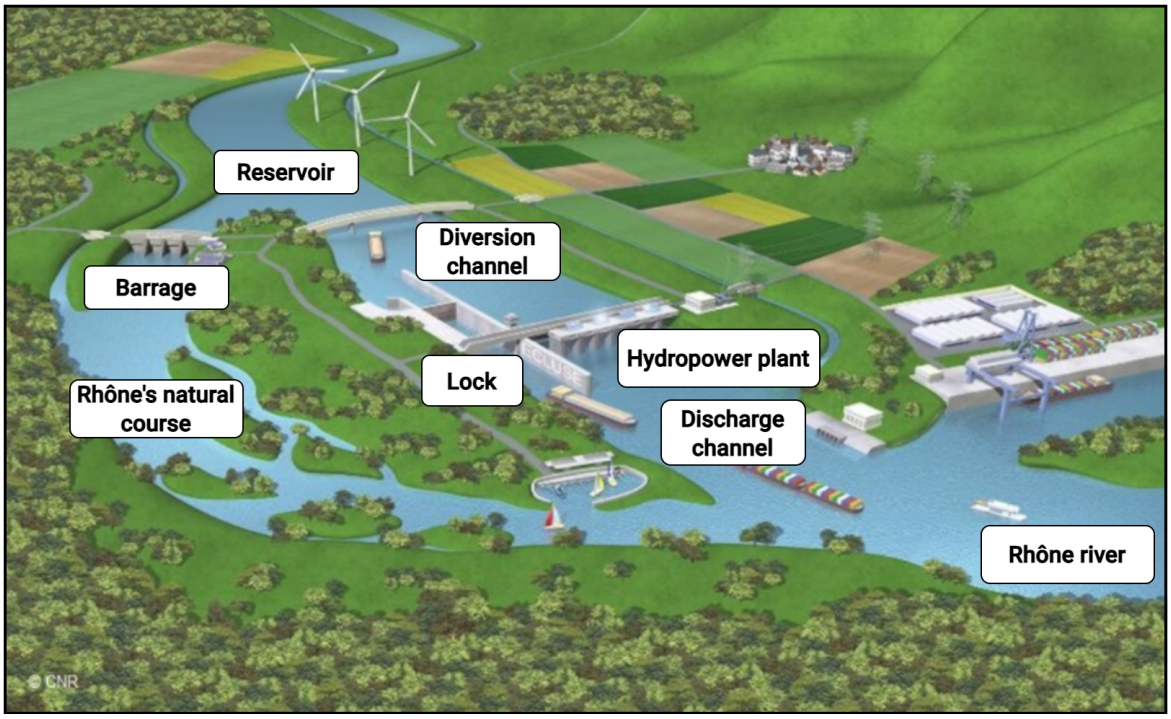

Figure 2.7: Schematic representation of a typical hydropower system operated by Compagnie Nationale du Rhône.

- The Génissiat hydropower system, located at the upstream end of the company's hydropower cascade, features a medium-head barrage and power station with a head height of 65 meters. This complex is unique within the cascade as it is the only reservoir-based hydropower system.
- At the Seyssel and Vaugris sites, the barrage and hydropower plant are integrated into a single structure, eliminating the need for a diversion channel.
- The Bourg-lès-Valence hydropower system includes an additional barrage, which manages the discharge of part of the flow from the river.
- The Avignon hydropower system incorporates an additional barrage-power station on the dead arm of the Barthelasse, effectively bypassing the primary diversion channel.

2.3.3 Market Participation at Compagnie Nationale du Rhône

The market participation of Compagnie Nationale du Rhône can be divided into long-term and short-term sales. Approximately 80% of its production is sold through long-term contracts, typically over-the-counter, with agreements spanning several hours, days, or even months. These contracts are structured around broader time frames and do not account for the short-term fluctuations in Rhône's production, which can vary over the course of just a few hours. The committed production volumes are based on long-term hydro-meteorological trends, drawing on past experience and risk management strategies.

The remaining 20% of Compagnie Nationale du Rhône's production is sold in short-term markets, either over-the-counter or on organized exchanges such as the day-ahead and intraday markets. As the company primarily operates cascaded hydropower plants, it is essential to jointly define the bidding strategy and the associated production schedule. This approach aims to schedule production in a way that meets operational constraints while also optimizing revenue by strategically timing electricity sales in the markets.

This thesis focuses on the operation of VPPs from the day-ahead to near-real-time/short-term horizons, which involves optimizing the aggregator's bidding strategy and then adjusting the actual dispatch to minimize imbalances. This strategy prioritizes the alignment of production with market opportunities, particularly by shifting production from periods of low prices to those with higher prices, both within the same day and across different hydropower plants.

Short-term optimization not only provides financial benefits but also helps align production with network demand, as high electricity prices typically correspond to peak consumption hours. Additionally, by maximizing short-term revenue, Compagnie Nationale du Rhône contributes to substituting renewable energy for more costly and carbon-intensive forms of energy, such as gas or coal, which are often required during peak periods. This allows Compagnie Nationale du Rhône to play a role in reducing the carbon footprint of electricity production while benefiting from market-driven opportunities.

2.3.4 Modeling

This section presents the modeling of the VPP operated by Compagnie Nationale du Rhône, which mainly consists of a series of hydropower plants arranged in a cascade system. The focus is to outline the key assumptions underlying the model, describe the dynamic behavior of each hydropower system, and explain their interactions within the cascade. It is important to note that a comprehensive model of the hydropower cascade operated by Compagnie Nationale du Rhône is beyond the scope of this thesis and has been addressed in detail in prior works, such as [135]. Instead, this section aims to derive a simplified yet sufficiently accurate model that captures the main complexities from an optimization perspective, enabling effective evaluation of the optimization and control strategies proposed in the following chapters.

Let $n \in \boldsymbol{N}$ denote an individual hydropower system within the cascade. The dynamics of the cascaded hydropower systems, as detailed below, are formulated in discrete time over a finite horizon, consisting of a set of time steps $t \in \boldsymbol{T}$, with a constant sampling period denoted by Δ_T. The uncertain parameters are denoted by the hat symbol, i.e., $\hat{\cdot}$.

2.3.4.1 Main Assumptions

The VPP consisting of the assets shown in Fig. 2.6 is modeled based on three **key assumptions**:

- *Assumption I*: Wind and solar units are considered non-dispatchable, with curtailment being the only possible action to modify their output. This assumption allows for a clearer

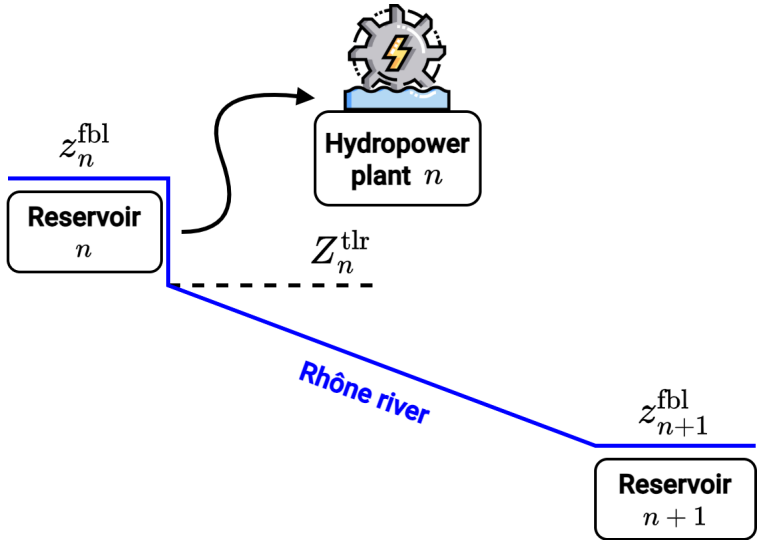

Figure 2.8: Forebay and tailrace water levels in the proposed hydropower cascade model.

analysis of the ability of the hydropower cascade to mitigate the inherent stochasticity of renewable power generation.

- *Assumption II*: Tailrace water levels are assumed to remain constant due to the negligible short-term impact of run-of-river hydropower plant discharge.
- *Assumption III*: All turbines within each hydropower plant are assumed to be of the same type, allowing the use of a single variable to represent the total turbine discharge.

2.3.4.2 Water Balancing

The fundamental equation governing the dynamics of water flow within a hydropower cascade is the water balance equation, or water conservation law. For each asset pair, a specific point between the two reservoirs, termed the *control point*, is selected, and the water balance at this point is calculated as follows:

$$\left(q_{n,t}^{\text{in}} - q_{n,t}^{\text{out}}\right) \Delta_T = v_{n,t} - v_{n,t-1}, \ \forall n, \forall t, \tag{2.1}$$

where $q_{n,t}^{\text{in}}, q_{n,t}^{\text{out}}$ and $v_{n,t}$ denote the inflow, outflow, and the reservoir volume of the hydropower plant n at time t, respectively.

Since the operational safety constraints set by the Compagnie Nationale du Rhône are based on reservoir water levels rather than volumes, the notion of surface area is employed to derive a state-space model that describes the water level dynamics in (2.1).

In this context, the forebay water level of hydropower plant n at time t, denoted by $z_{n,t}^{\text{fbl}}$, corresponds to the upstream water level of the hydropower plant, while the tailrace water level, denoted by Z_n^{tlr}, refers to the downstream water level. Under *Assumption II*, the tailrace water level remains constant. Fig. 2.8 illustrates the modeling of the forebay and tailrace water levels for a hydropower plant in the cascade.

Using the surface area of the reservoir, denoted by $S_{n,t}$, the forebay water level variation is related to the reservoir volume variation, as expressed by:

$$v_{n,t} - v_{n,t-1} = S_{n,t} \left(z^{\text{fbl}}_{n,t} - z^{\text{fbl}}_{n,t-1} \right), \ \forall n, \forall t, \tag{2.2}$$

where it is assumed that $S_{n,t} \approx S_{n,t-1}, \forall n, \forall t$.

By combining (2.1) with (2.2), the dynamics of the forebay water level $z^{\text{fbl}}_{n,t}$ can be computed as follows:

$$z^{\text{fbl}}_{n,t} = z^{\text{fbl}}_{n,t-1} + \frac{\left(q^{\text{in}}_{n,t} - q^{\text{out}}_{n,t} \right) \Delta_T}{S_{n,t}}, \ \forall n, \forall t, \tag{2.3a}$$

$$z^{\text{fbl}}_{n,0} = Z^{\text{fbl},0}_{n}, \ \forall n, \tag{2.3b}$$

$$z^{\text{fbl}}_{n,|\boldsymbol{T}|} = Z^{\text{fbl},0}_{n}, \ \forall n, \tag{2.3c}$$

where $Z^{\text{fbl},0}_{n}$ denotes the initial forebay water level of hydropower plant n at time t. For consistency, constraints (2.3c) are employed to enforce that the forebay water levels at the end of the operational period coincide with the levels observed at the beginning of the period.

The total inflow $q^{\text{in}}_{n,t}$ into the reservoir of hydropower plant n at time t consists of the water discharged from upstream hydropower plants via both the barrage and turbines, denoted by $q^{\text{br}}_{n,t}$ and $q^{\text{tr}}_{n,t}$, respectively, as well as the external water inflow (from the river and its tributaries), denoted by $\hat{Q}^{\text{ext}}_{n,t}$:

$$q^{\text{in}}_{n,t} = q^{\text{br}}_{n-1,t-\tau^{\text{br}}_{n-1,n}} + q^{\text{tr}}_{n-1,t-\tau^{\text{tr}}_{n-1,n}} + \hat{Q}^{\text{ext}}_{n,t}, \ \forall n, \forall t, \tag{2.4}$$

where $\tau^{\text{tr}}_{n-1,n}$ and $\tau^{\text{br}}_{n-1,n}$ represent the water propagation times from the upstream hydropower system $n-1$ to n through the turbines and barrage, respectively. Similarly, the outflow from each reservoir is defined as the sum of water discharged through the barrage and turbines, as given by:

$$q^{\text{out}}_{n,t} = q^{\text{br}}_{n,t} + q^{\text{tr}}_{n,t}, \ \forall n, \forall t. \tag{2.5}$$

Under *Assumption III*, a single variable $q^{\text{tr}}_{n,t}$ is used to represent the total discharge across all turbines of hydropower plant n at time t.

2.3.4.3 Operational Curves of the Hydropower Systems

The operational management of hydropower systems is subject to a rigorous regulatory framework focused on hydraulic safety [49]. Each system is operated accordingly to a specific operational curve, determined in compliance with guidelines approved by the relevant authorities. These guidelines consider multiple factors, including flood control, navigation, irrigation, nuclear safety, and various water uses such as environmental, agricultural, and recreational needs. An example of operational curve of a hydropower system operated by Compagnie Nationale du Rhône is shown in Fig. 2.9.

During *low flow periods*, the hydropower systems are operated with the forebay water level maintained at its maximum possible height to provide optimal draught for navigation. During

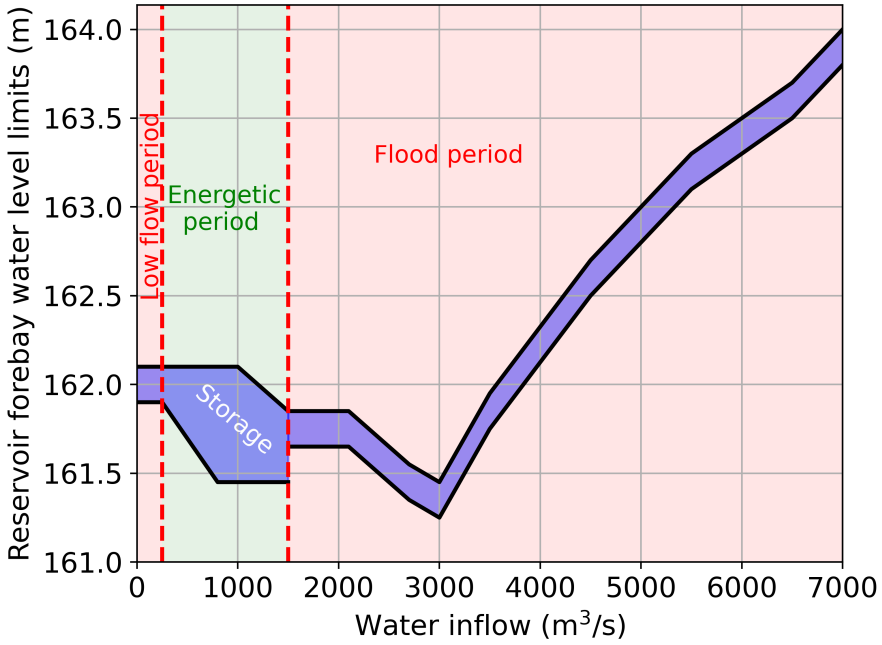

Figure 2.9: Example of operational curve of a hydropower system operated by Compagnie Nationale du Rhône.

flood periods, both forebay and tailrace water levels are adjusted to closely mimic the natural hydrological conditions that existed prior to dam construction. Only during *energetic periods* a limited storage capacity—typically fluctuating between 20 and 50 cm—is available to optimize the hydropower generation. Although this storage capacity is relatively small compared to the average discharge of the Rhône River (for example, at the Péage-de-Roussillon site, it accounts for less than 50 minutes of average flow), it plays a key role in optimizing the daily production schedule across the entire cascade of power plants.

Here, a piecewise linear approximation of the operational curves (e.g., Fig. 2.9) is considered. For each hydropower plant $n \in \boldsymbol{N}$, the inflow range of the operational curve is partitioned into segments $Q^{\text{in}}_{n,s}$, each corresponding to a fixed maximum and minimum forebay water level, denoted by $\underline{Z}^{\text{fbl}}_{n,s}$ and $\overline{Z}^{\text{fbl}}_{n,s}$, respectively. A specific set of inflow segments, $\boldsymbol{S}^{\mathbf{oc}}_n$, is calculated for each hydropower plant n. Then, the piecewise linear approximation is formulated as follows:

$$q^{\text{in}}_{n,t} \geq b^{\text{oc}}_{n,t,s} Q^{\text{in}}_{n,s},\ \forall s \in \boldsymbol{S}^{\mathbf{oc}}_n, \forall n, \forall t, \tag{2.6a}$$

$$q^{\text{in}}_{n,t} < b^{\text{oc}}_{n,t,s} Q^{\text{in}}_{n,s+1} + \left(1 - b^{\text{oc}}_{n,t,s}\right) M_1,\ \forall s \in \boldsymbol{S}^{\mathbf{oc}}_n, \forall n, \forall t. \tag{2.6b}$$

Here, M_1 is a large positive constant, and the binary variables $b^{\text{oc}}_{n,t,s} \in \{0,1\}, \forall n, \forall t, \forall s$, are constrained by the following consistency condition:

$$\sum_{s \in \boldsymbol{S}^{\mathbf{oc}}_n} b^{\text{oc}}_{n,t,s} = 1,\ \forall n, \forall t. \tag{2.7}$$

Then, upper and lower limits are enforced on the forebay water level $z^{\text{fbl}}_{n,t}$ as given by:

$$\sum_{s\in \boldsymbol{S}^{\mathbf{oc}}_n} \underline{Z}^{\text{fbl}}_{n,s} b^{\text{oc}}_{n,t,s} \leq z^{\text{fbl}}_{n,t} \leq \sum_{s\in \boldsymbol{S}^{\mathbf{oc}}_n} \overline{Z}^{\text{fbl}}_{n,s} b^{\text{oc}}_{n,t,s},\ \forall n, \forall t. \tag{2.8}$$

To mitigate excessive wear on the hydraulic equipment, specific constraints are applied. Firstly, the turbine discharge is restricted by the following ramp limit:

$$\left| q^{\text{tr}}_{n,t} - q^{\text{tr}}_{n,t-1} \right| \leq \Delta Q^{\text{tr}}_n,\ \forall n, \forall t. \tag{2.9}$$

Additionally, turbine discharge is constrained by the following upper and lower limits:

$$b^{\text{tr}}_{n,t} \underline{Q}^{\text{tr}}_n \leq q^{\text{tr}}_{n,t} \leq b^{\text{tr}}_{n,t} \overline{Q}^{\text{tr}}_n,\ \forall n, \forall t, \tag{2.10}$$

where $b^{\text{tr}}_{n,t} \in \{0,1\}$ are binary variables indicating whether the turbines are operational, while $\underline{Q}^{\text{tr}}_n$ and $\overline{Q}^{\text{tr}}_n$ denote the minimum and maximum turbine discharge values, respectively.

The operation of the barrage is permitted only under the following two conditions:

- The reservoir has reached its full capacity.
- The turbines have reached their maximum discharge capacity.

Due to the economic nature of the objective functions employed in the following optimization problems, and assuming positive energy prices, the optimal solution will always involve fully utilizing the turbines before the barrage is opened. Therefore, a constraint is introduced to enforce only the first condition, given by:

$$q^{\text{br}}_{n,t} \leq \begin{cases} 0 & \text{if} z^{\text{fbl}}_{n,t} < \sum_{s\in \boldsymbol{S}^{\mathbf{oc}}_n} \overline{Z}^{\text{fbl}}_{n,s} b^{\text{oc}}_{n,t,s} \\ \infty & \text{otherwise} \end{cases},\ \forall n, \forall t. \tag{2.11}$$

The safety constraints in (2.11) can be efficiently modeled using binary variables $b^{\text{br}}_{n,t} \in \{0,1\}, \forall n, \forall t$, as follows:

$$b^{\text{br}}_{n,t} \leq 1 - \frac{\sum_{s\in \boldsymbol{S}^{\mathbf{oc}}_n} \overline{Z}^{\text{fbl}}_{n,s} b^{\text{oc}}_{n,t,s} - z^{\text{fbl}}_{n,t}}{\overline{Z}^{\text{fbl,max}}_n},\ \forall n, \forall t, \tag{2.12a}$$

$$q^{\text{br}}_{n,t} \leq b^{\text{br}}_{n,t} M_2,\ \forall n, \forall t, \tag{2.12b}$$

$$q^{\text{br}}_{n,t} \geq b^{\text{br}}_{n,t} \underline{Q}^{\text{br}}_n,\ \forall n, \forall t, \tag{2.12c}$$

where $\underline{Q}^{\text{br}}_n$ denotes the minimum barrage discharge value, M_2 is a large positive constant, and $\overline{Z}^{\text{fbl,max}}_n$ is defined as follows:

$$\overline{Z}^{\text{fbl,max}}_n = \max\left(\left\{ \overline{Z}^{\text{fbl}}_{n,s} \right\}_{s\in \boldsymbol{S}^{\mathbf{oc}}_n} \right),\ \forall n. \tag{2.13}$$

Here, the operator $\max(\cdot)$ denotes the maximum value from the specified set.

2.3.4.4 Hydropower Generation Function

The power output of a hydropower plant is fundamentally dependent on three key variables: the turbines discharge, the net head, and the efficiency of the turbines. This relationship is expressed by:

$$p^{\mathrm{H}}_{n,t} = w\ g\ \eta^{\mathrm{tr}}_{n}\ q^{\mathrm{tr}}_{n,t}\ h_{n,t}\ 10^{-6},\ \forall n, \forall t. \tag{2.14}$$

Here, g denotes the acceleration due to gravity, w represents the density of water, η^{tr}_{n} signifies the efficiency of the turbines, and $h_{n,t}$ denotes the hydraulic head, defined as follows:

$$h_{n,t} = z^{\mathrm{fbl}}_{n,t} - Z^{\mathrm{tlr}}_{n},\ \forall n, \forall t. \tag{2.15}$$

In general, the efficiency of the turbines is a nonlinear function expressed in the Hill diagram [137]. For simplicity in this work, a constant efficiency value ranging between 0.7 and 0.9 is assumed for each hydropower plant.

The hydropower generation function (2.14) is inherently nonlinear due to its bilinear dependence on turbine discharge and hydraulic head. To manage this nonlinearity, various approximation techniques are employed, including piecewise linearization and envelope models [138]. Among these methods, a McCormick approximation [139] is employed here, which replaces the bilinear term in (2.14) with a convex envelope:

$$p^{\mathrm{H}}_{n,t} \geq 10^{-6} w g \eta^{\mathrm{tr}}_{n} \left(\underline{Q}^{\mathrm{tr}}_{n} h_{n,t} + \underline{H}_{n} q^{\mathrm{tr}}_{n,t} - \underline{Q}^{\mathrm{tr}}_{n} \underline{H}_{n} \right),\ \forall n, \forall t, \tag{2.16a}$$

$$p^{\mathrm{H}}_{n,t} \geq 10^{-6} w g \eta^{\mathrm{tr}}_{n} \left(\overline{Q}^{\mathrm{tr}}_{n} h_{n,t} + \overline{H}_{n} q^{\mathrm{tr}}_{n,t} - \overline{Q}^{\mathrm{tr}}_{n} \overline{H}_{n} \right),\ \forall n, \forall t, \tag{2.16b}$$

$$p^{\mathrm{H}}_{n,t} \leq 10^{-6} w g \eta^{\mathrm{tr}}_{n} \left(\underline{Q}^{\mathrm{tr}}_{n} h_{n,t} + \overline{H}_{n} q^{\mathrm{tr}}_{n,t} - \underline{Q}^{\mathrm{tr}}_{n} \overline{H}_{n} \right),\ \forall n, \forall t, \tag{2.16c}$$

$$p^{\mathrm{H}}_{n,t} \leq 10^{-6} w g \eta^{\mathrm{tr}}_{n} \left(\overline{Q}^{\mathrm{tr}}_{n} h_{n,t} + \underline{H}_{n} q^{\mathrm{tr}}_{n,t} - \overline{Q}^{\mathrm{tr}}_{n} \underline{H}_{n} \right),\ \forall n, \forall t. \tag{2.16d}$$

In (2.16), $\overline{P}^{\mathrm{H}}_{n}$ represents the maximum hydropower generation value, while $\underline{H}_{n}$ and $\overline{H}_{n}$ represent the minimum and maximum hydraulic head values, respectively. Fig. 2.10 illustrates the McCormick approximation of the hydropower generation function.

Finally, the hydropower generation is constrained by the following upper and lower limits:

$$0 \leq p^{\mathrm{H}}_{n,t} \leq \overline{P}^{\mathrm{H}}_{n},\ \forall n, \forall t. \tag{2.17}$$

2.3.4.5 Variable Renewable Energy Sources and Power Balancing

In addition to its hydropower cascade, Compagnie Nationale du Rhône manages approximately 1 GW of vRES, specifically wind and solar power plants, as outlined in Section 2.3.1. Under *Assumption I*, no active control is exerted over these vRES, aside from the possibility of curtailment. This assumption allows for a more thorough evaluation of the flexibility potential offered by the hydropower cascade, which, when aggregated with wind and solar farms, can be harnessed to mitigate the inherent stochasticity of renewable energy generation.

Furthermore, this thesis adopts the perspective of Compagnie Nationale du Rhône, acknowl-

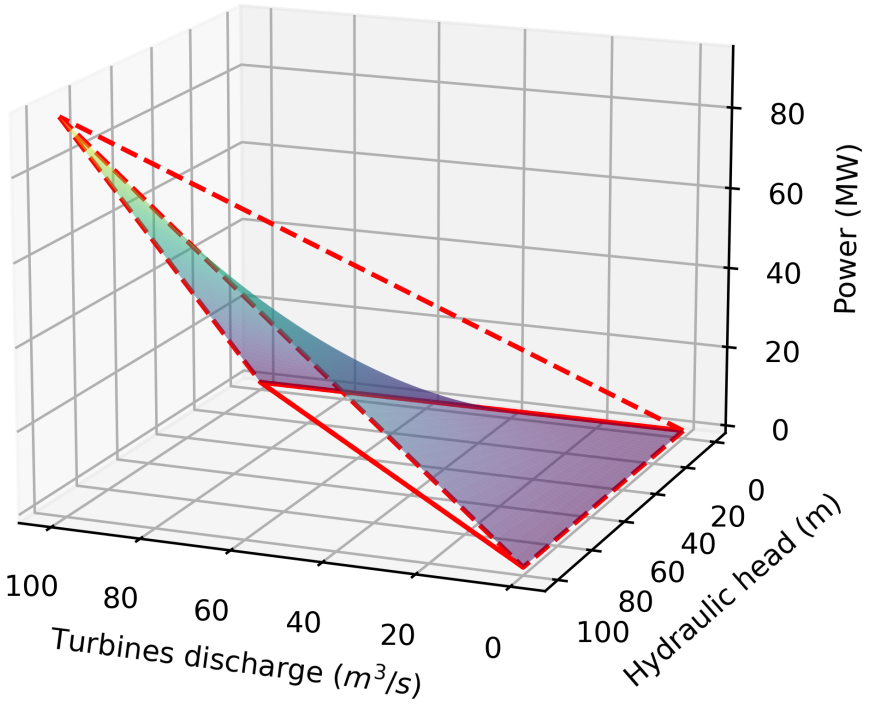

Figure 2.10: The hydropower generation function (bilinear surface), along with its corresponding McCormick approximation.

edging that the company does not participate in direct grid management in its real-world operations. Consequently, within the context of the VPP's energy management, the wind and solar power generation from the geographically distributed farms operated by the company can be aggregated. This aggregation simplifies the optimization and control problems, allowing the wind and solar power generation to be represented by single random variables, with their respective forecasts denoted as $\hat{P}_t^{\mathrm{W}}$ and $\hat{P}_t^{\mathrm{S}}$ in the following analysis.

Given these considerations, the power balance of the VPP is expressed by:

$$\hat{P}_t^{\mathrm{D}} - p_t^{\mathrm{imp}} + p_t^{\mathrm{exp}} = \sum_{n \in \boldsymbol{N}} p_{n,t}^{\mathrm{H}} + (1 - c_t^{\mathrm{W}})\hat{P}_t^{\mathrm{W}} + (1 - c_t^{\mathrm{S}})\hat{P}_t^{\mathrm{S}}, \ \forall t. \tag{2.18}$$

Here, $\hat{P}_t^{\mathrm{D}}$ represents the power demand to be met by the VPP, p_t^{imp} and p_t^{exp} denote the power imported from and exported to the grid, respectively. The variables $c_t^{\mathrm{W}} \in [0,1], \forall t$, and $c_t^{\mathrm{S}} \in [0,1], \forall t$, represent the percentage of wind and solar power curtailment, respectively.

2.3.5 Operational Strategies and Management

Following the standard energy management strategy for operating a VPP, as illustrated in Fig. 2.3, Compagnie Nationale du Rhône currently separates the scheduling and dispatch stages of its operations. The process is organized as follows:

- **Scheduling Module**: Compagnie Nationale du Rhône utilizes an internal simulation tool named GAIPAR for the scheduling stage. This tool enables operators to simulate the dy-

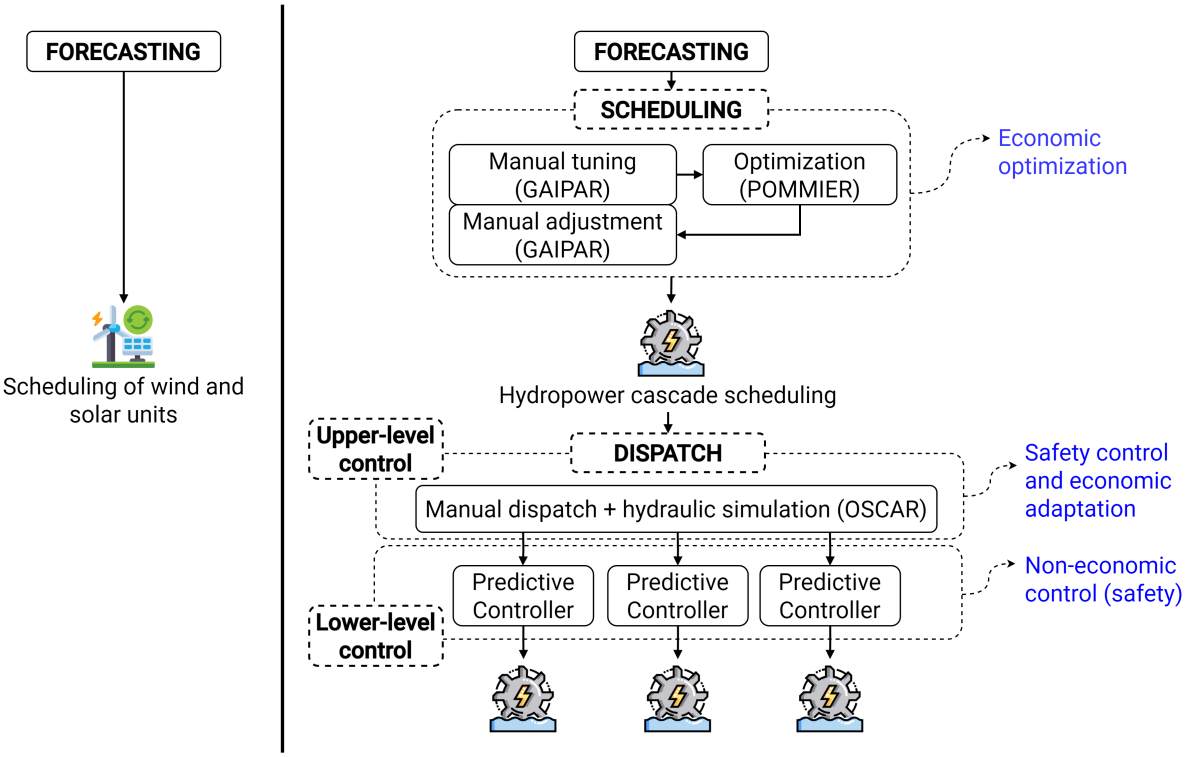

Figure 2.11: The energy management strategy employed by Compagnie Nationale du Rhône to operate its VPP.

namics of the hydropower cascade and generate production schedules based on a variety of factors, including anticipated prices, forecasted inflows, and the availability of hydropower production units. GAIPAR provides a visualization of the evolution of key variables within each hydropower system, such as water levels, volumes, and inflows and outflows, while accounting for the nonlinearity of hydropower generation and the operational constraints of individual units. Although this simulation tool facilitates the verification of the feasibility of proposed schedules, operators often spend considerable time generating production plans that may not align with the optimal operation of the hydropower cascade. To address this, an optimization and decision-support tool named the *Plateforme d'Optimisation et de Modulation Mutualisées pour l'Intégration des Energies Renouvelables* (POMMIER), which translates to *Platform for Shared Optimization and Modulation for the Integration of Renewable Energy* in English, has been developed. POMMIER determines the optimal scheduling strategy for Compagnie Nationale du Rhône's assets over a four-day horizon, optimizing starting from day $d+1$, where d represents the current day. The schedules provided by POMMIER aim to maximize the company's economic objectives within a simplified model of the hydropower cascade. The output from POMMIER is subsequently fed into GAIPAR to obtain the nearest feasible solution.

- **Dispatch Module**: The dispatch module operates close to real-time and primarily focuses on ensuring the safe operation of the hydropower assets, with secondary attention to optimizing the economic performance of the VPP. This module is structured as a two-step

process: an upper-level control strategy involving manual adjustment across the entire VPP, supported by a detailed hydraulic simulation tool (OSCAR) to ensure the consistency of the day-ahead scheduling with the hydraulic constraints of the hydropower systems. Then, a lower-level control strategy ensures the hydraulic safety of each hydropower systems locally, even in the event of a communication loss with the upper-level control, through the use of predictive controllers.

Fig. 2.11 depicts the energy management strategy employed by Compagnie Nationale du Rhône to operate its VPP.

It is worth noting that **Compagnie Nationale du Rhône currently manages its wind and solar power plants independently from the hydropower cascade in the market**. Specifically, while the hydropower cascade is managed through a combination of manual adjustments, simulation, and optimization tools, the vRES are simply bid into the market based on their forecasts, without the involvement of any optimization tools, as their controllability is considered negligible.

2.3.6 Input Data Description and Characterization

This section presents an overview and characterization of the input data provided by Compagnie Nationale du Rhône. These data are employed to assess the performance of the optimization and control methods proposed in subsequent chapters.

2.3.6.1 Input Data Description

The input data provided by Compagnie Nationale du Rhône include:

- Parameters used to model the dynamics of vRES and the hydropower plants in the cascade. A comprehensive description of these parameters is given in Section 2.3.4.
- Probabilistic forecasts of the three primary sources of uncertainty: external inflows, day-ahead market prices, and vRES power generation.

The probabilistic forecast data are structured into three distinct sets of scenarios:

- 50 scenarios, along with observations, of day-ahead energy market prices, generated for each hour throughout the simulation period.
- 51 scenarios, along with observations, of vRES (wind and solar) power generation, produced for each hour of the simulation period.
- 51 scenarios, along with observations, of external inflows, covering all tributaries associated with the hydropower cascade assets (refer to Table 2.3), generated for each hour of the simulation period.

It is worth notice that an analysis conducted by Compagnie Nationale du Rhône indicates that **these three sources of uncertainty exhibit very low correlation and can be**

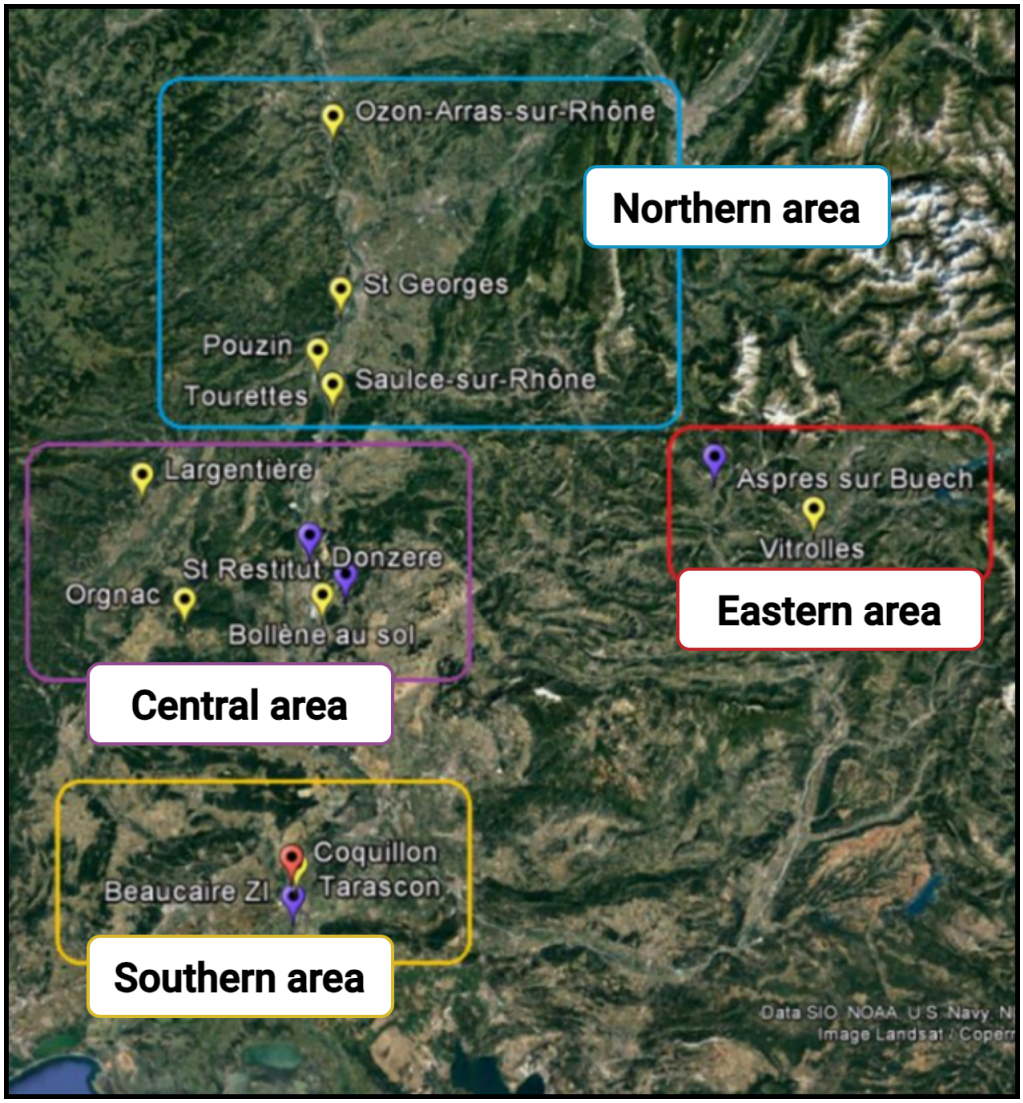

Figure 2.12: The solar farms for which data are provided by Compagnie Nationale du Rhône, organized into four distinct areas.

treated as independent random variables [135]. As a result, independent scenario sets are generated for each source of uncertainty and then randomly combined within the proposed optimization and control framework. The methodology employed to generate these forecasts is outlined in the following section.

The input data provided pertain to a subset of assets operated by Compagnie Nationale du Rhône. Specifically, the solar power generation forecast pertains to solar farms grouped into four distinct areas:

- *Northen area* (14.4 MWp of aggregated installed capacity) that gathers together 5 distinct solar power farms: Ozon (4.2 MWp), Saint Georges (2.4 MWp), Le Pouzin (3.4 MWp), Saulce sur Rhône (4.1 MWp), and Tourettes (0.3 MWp).
- *Eastern area* (8.4 MWp of aggregated installed capacity) that gathers together 2 distinct solar power farms: Aspres sur Buëch (5.5 MWp), and Vitrolles (2.9 MWp).

- *Central area* (24.2 MWp of aggregated installed capacity) that gathers together 5 distinct solar power farms: Largentières (12.0 MWp), Orgnac (1.3 MWp), Bollène (4.0 MWp), Donzère (3.9 MWp), and Saint Restitut (3.0 MWp).
- *Southern area* (13.8 MWp of aggregated installed capacity) that gathers together 3 distinct solar power farms: Beaucaire (9.6 MWp), Coquillon (1.2 MWp), and Tarascon (3.0 MWp).

Since each of these areas comprises multiple solar farms, the combined generation forecasts incorporate a smoothing effect. An illustration of the four areas is shown in Fig. 2.12.

Similarly, wind power generation forecasts are provided for six distinct areas, where the company's wind farms are grouped. The entire wind farm portfolio accounts for approximately 310 MW of installed capacity. Forecast data are supplied in two forms: without post-processing (i.e., without reliability guarantees) and with reliability post-processing and spatial coherence reconstruction.

Additionally, forecast data are provided for external inflows into the hydropower systems from the tributaries of the Rhône River, covering all assets within the hydropower cascade. As discussed in the previous sections, the hydropower cascade is divided into two parts: the upper Rhône and the lower Rhône (refer to Table 2.3). As the focus of this thesis is on the lower Rhône section of the hydropower cascade, the following analysis of the external inflow forecasts focuses exclusively on the lower Rhône developments.

2.3.6.2 Forecasting Process Overview

The primary objective of this thesis is to develop and evaluate optimization and control methods for the energy management of VPPs. While a detailed exploration of forecasting methodologies is outside the scope of this work, understanding the forecasting process employed by Compagnie Nationale du Rhône is relevant, as it serves as an input to the proposed methods. A detailed description of the forecasting process employed by the company is provided in [135].

Compagnie Nationale du Rhône's forecasting process is integral to effective production planning in hydropower systems and comprises several key components. Forecasting begins with predicting water inflows from tributaries and intermediate watersheds, which significantly influence hydraulic models. These inflows are uncertain due to their dependence on variable hydro-meteorological conditions and the operations of hydropower systems located in the section of the Rhône River outside of France. To manage this uncertainty, Compagnie Nationale du Rhône employs a structured forecasting process:

1. *Precipitation and snowmelt scenarios*: Scenarios are generated for liquid precipitation and snowmelt across the Rhône watershed, typically forecasting up to four days in advance. These scenarios are developed using observational data (such as rain gauge measurements and quantitative radar estimates) and predictive models (including several ensemble numerical weather prediction forecasts issued by national meteorological services, as well as in-house developed snowmelt models).

2. *Hydrological scenarios*: Based on the precipitation and snowmelt forecasts, hydrological scenarios are generated to predict flows from gauged natural tributaries and also from ungauged intermediate watersheds inflows. These scenarios, which provide detailed forecasts with high temporal resolution (hourly or half-hourly), are produced using hydrological models (rainfall-runoff models) and hydraulic models (flow propagation models), supported by a network of measurement stations.

3. *Influence of other hydropower systems operators on the Rhône watershed*: The Compagnie Nationale du Rhône exchanges hydrological forecasts with other operators within the Rhône catchment area. However, the operational schedules of these various entities mean that these exchanges often occur after the day-ahead market closes. As a result, forecasters at the Compagnie Nationale du Rhône develop their own predictions based on the forecasts received the previous day and their anticipation of the behavior of these third-party operators. In practice, this process remains deterministic, generating deterministic forecasts. For the purposes of this thesis, a specific probabilistic forecasting archive for these influenced tributaries has been reconstructed, incorporating an error model based on historical operational forecasts.

In addition to forecasting inflows, correction flows are employed to address limitations in the hydraulic model. Simplifications and measurement errors, typically ranging from 5% to 10%, require the inclusion of correction flows to ensure the model accurately reflects field observations. These correction flows are calibrated using historical data to align calculated and observed water levels. Since the calibrated correction inflows are not entirely random, they are projected for future periods, with adjustments made by operators as necessary.

Electricity prices are another key element of the forecasting process. Short-term price forecasts are made for up to seven days in advance, with day-ahead prices published daily around 12:30 PM. A dedicated team is responsible for forecasting these prices and making adjustments for forecasting imbalance settlement prices.

Finally, predictions also consider the availability of production units based on maintenance schedules and known issues.

2.3.6.3 Evaluating Probabilistic Forecasts

In general, the evaluation of probabilistic forecasts involves both qualitative and quantitative approaches. Probabilistic forecasts aim to capture the uncertainties in predictions by providing a distribution of possible outcomes rather than a single deterministic value. The performance of these forecasts is commonly assessed using key concepts such as *reliability*, and *sharpness*, as well as proper scoring rules like the *continuous ranked probability score* (CRPS).

Reliability measures the degree to which the predicted probability distribution aligns with the true underlying distribution of the observed variable. Let $\{F_l(x)\}_{l\in\boldsymbol{L}}$ represent a set of probabilistic forecasts and $\{y_l\}_{l\in\boldsymbol{L}}$ the corresponding observations. A forecast is considered reliable if the forecast probabilities, on average, match the observed frequencies of events. Since

the actual underlying distribution of the observations is not directly accessible, reliability is typically evaluated over a large sample of forecast-observation pairs [140].

Sharpness, in contrast, quantifies the concentration or spread of the forecast distribution, with sharper forecasts indicating lower uncertainty. Sharpness is a property of the forecast itself, independent of observations, and is crucial for assessing the confidence in the predicted outcomes [141].

The CRPS extends the concept of the *mean absolute error* from deterministic to probabilistic settings and is widely used for evaluating probabilistic forecasts [142]. For a single forecast F_l and an observation y_l, the CRPS is defined as:

$$\mathrm{CRPS}(F_l, y_l) = \int_{-\infty}^{\infty} \left(F_l(x) - \mathbb{I}(x \geq y_l)\right)^2 \, dx, \tag{2.19}$$

where $\mathbb{I}(\cdot)$ is the indicator function. This score measures the squared difference between the forecast *cumulative distribution function* (CDF) $F_l(x)$ and the observation y_l, integrated over all possible values x. The CRPS accounts for both reliability and sharpness, making it a proper scoring rule for probabilistic forecasts [141].

In the case of *ensemble forecasts*, where $|\boldsymbol{M}|$ members $(x_{l1}, \ldots, x_{l|\boldsymbol{M}|}) \in \mathbb{R}^{|\boldsymbol{M}|}$ are provided, the empirical CDF $F_l(x)$ can be expressed as:

$$F_l(x) = \sum_{m \in \boldsymbol{M}} p_m H(x - x_{lm}), \tag{2.20}$$

where $p_m \in [0, 1]$ represents the weight of each ensemble member, and $H(\cdot)$ is the Heaviside step function [143]. For equally weighted ensemble members, $p_m = \frac{1}{|\boldsymbol{M}|}$.

For ensemble forecasts, the CRPS simplifies to:

$$\mathrm{CRPS}(F_l, y_l) = \sum_{m \in \boldsymbol{M}} p_m |x_{lm} - y_l| - \frac{1}{2} \sum_{m \in \boldsymbol{M}} \sum_{m' \in \boldsymbol{M}} p_m p_{m'} |x_{lm} - x_{lm'}|. \tag{2.21}$$

This form is computationally efficient and commonly used to calculate the CRPS for ensemble forecasts [141].

The average CRPS over a set of $|\boldsymbol{L}|$ forecasts is computed as:

$$\mathrm{CRPS}_{\mathrm{avg}} = \frac{1}{|\boldsymbol{L}|} \sum_{l \in \boldsymbol{L}} \mathrm{CRPS}(F_l, y_l). \tag{2.22}$$

A lower average CRPS indicates better forecast quality, with a perfect deterministic forecast resulting in a CRPS of zero.

2.3.6.4 Analysis of the Input Data Provided by Compagnie Nationale du Rhône

This section reports an analysis of the input data provided by Compagnie Nationale du Rhône. Specifically, the CRPS metric detailed in the previous section is employed to validate the probabilistic forecast provided by the company. This analysis encompasses all three sources of uncertainty in the problem: external inflows, vRES power generation, and market prices. The

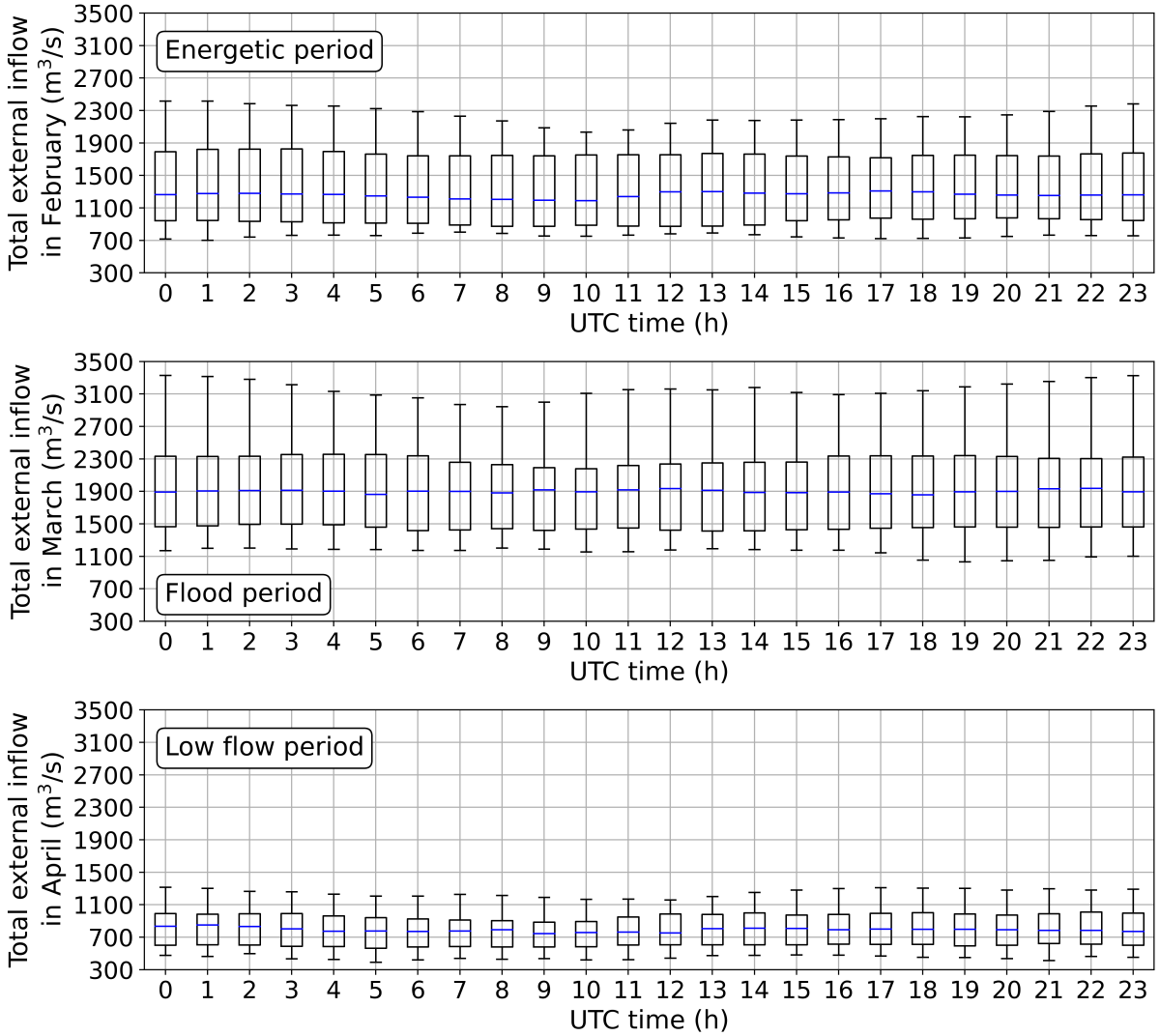

Figure 2.13: Boxplots of total external water inflow for each hour of the day in February, March, and April 2017 are shown in the top, middle, and bottom subplots, respectively. In each subplot, the box represents the interquartile range, the line inside indicates the median, and the whiskers extend to the minimum and maximum values (0th and 100th percentiles) of the data.

forecasts analyzed are issued with a 24-hour lead time and have hourly resolution over a three-month period from February to April 2017. This period was chosen because it presents a diverse range of inflow, vRES power generation, and market conditions experienced by the VPP.

Fig. 2.13 shows a boxplot of the observed total external water inflow for this three-month simulation period. The total external water inflow, denoted by $\hat{Q}_t^{\text{ext,tot}}$, is defined as follows:

$$\hat{Q}_t^{\text{ext,tot}} = \sum_{n \in \boldsymbol{N}} \hat{Q}_{n,t}^{\text{ext}}, \ \forall t. \tag{2.23}$$

The figure illustrates that the VPP encounters three distinct situations during this simulation: energetic, flood, and low-flow periods. The impact of these varying inflow conditions is significant, as it directly influences the storage capacity of the hydropower cascade, as outlined by

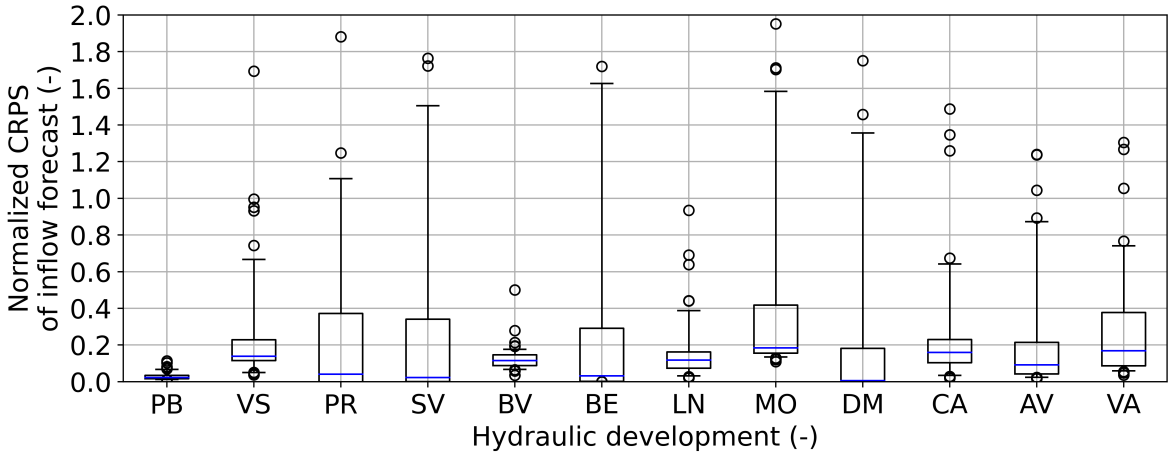

Figure 2.14: Boxplot of the normalized hourly CRPS for total external water inflow forecasts of each hydropower system within the lower Rhône cascade. The box represents the interquartile range, the line inside indicates the median, and the whiskers extend to the 5th and 95th percentiles of the data. The outliers are plotted as individual points beyond the whiskers. The hourly CRPS values are normalized by the corresponding water inflow observations for each respective hydropower system.

the operational curves in Fig. 2.9. Consequently, analyzing the VPP's behavior and market performance during this period is expected to provide valuable insights into the system's response under diverse conditions.

Fig. 2.14 presents an analysis of the probabilistic forecast for external water inflows, showing a boxplot of their normalized hourly CRPS values for each hydropower system within the lower Rhône cascade. The hourly CRPS values are normalized by the corresponding inflow observations for each respective hydropower system. As indicated in the figure, the median normalized CRPS is consistently below 0.2, meaning the median forecasting error is less than 20% of the observed inflow for each system. The best performance is observed for the first hydropower system (PB), while less accurate forecasts are seen for the PR, SV, BE, MO, and DM assets (refer to Table 2.2 for abbreviations and names of hydropower system). These larger error values are attributed to the very low average inflows observed for these developments, as detailed in Table 2.4. The inflow into PB, as detailed in this table, is notably high compared to that of the other hydropower systems because it not only includes contributions from PB's tributaries but also accumulates the inflows from the upstream hydropower system within the upper Rhône cascade.

A similar analysis is conducted for the input data corresponding to the wind and solar farms operated by Compagnie Nationale du Rhône. Fig. 2.15 characterizes the daily wind and solar power generation over the selected simulation period (February-April 2017). As with the external inflows, this figure highlights the diverse vRES power generation conditions observed during this period, offering valuable insights. Notably, wind power constitutes the most significant vRES contribution to the VPP's total power generation. Slight drops in wind energy output are observed during the morning and evening hours. It is interesting to note that the morning wind energy drop coincides with a rise in solar power generation, while the evening drop occurs during

Hydro. sys.	Average (m^3/s)	Min (m^3/s)	Max (m^3/s)	Std (m^3/s)
PB	883.81	177.28	2567.35	564.26
VS	2.69	0.72	20.70	2.57
PR	0.04	0.00	0.64	0.09
SV	0.15	0.00	3.70	0.42
BV	257.84	105.47	544.39	66.07
BE	0.82	0.00	14.30	2.00
LN	50.26	22.64	142.60	19.87
MO	2.97	0.01	35.40	2.56
DM	0.93	0.00	24.03	2.89
CA	81.82	13.33	35.40	59.92
AV	22.40	5.10	141.91	17.84
VA	68.76	23.20	312.24	54.98

Table 2.4: Characterization of daily external water inflow observations, including average, minimum, maximum, and standard deviation (std) values, for each hydropower system in the lower Rhône cascade.

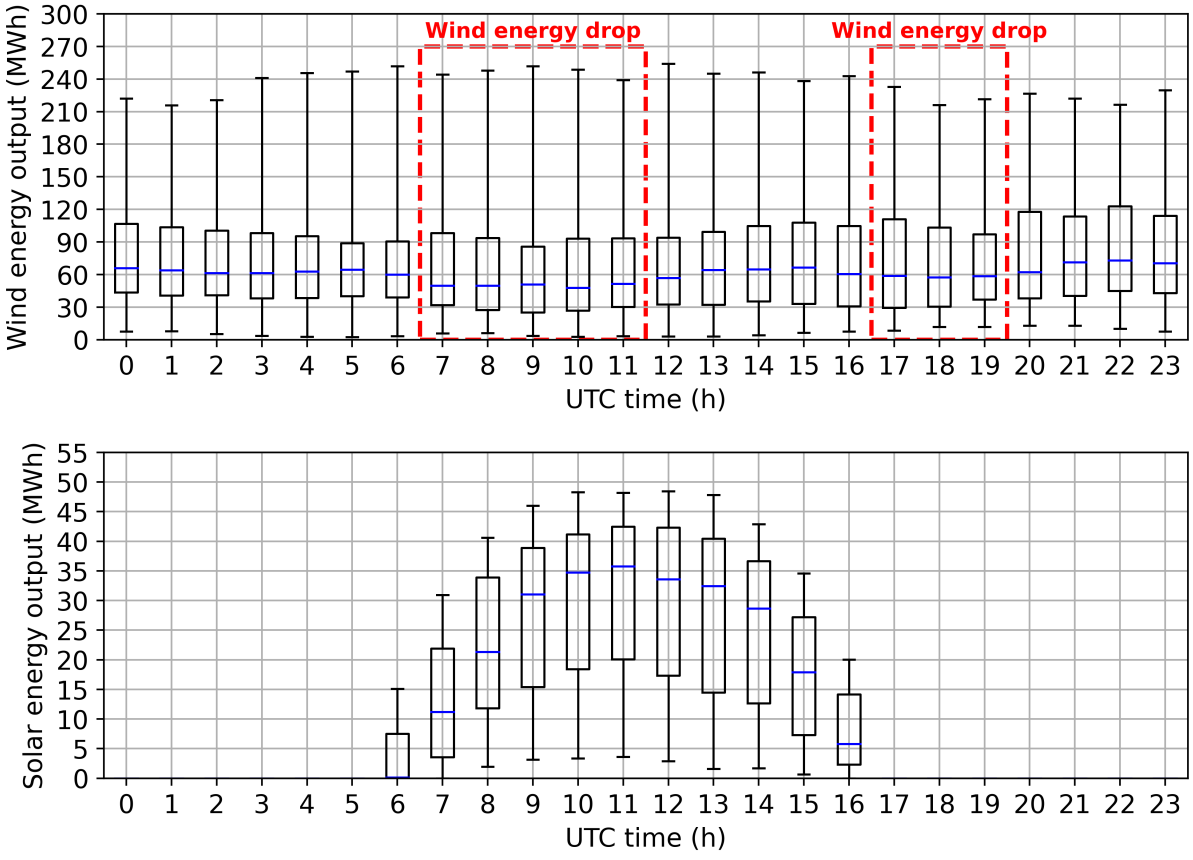

Figure 2.15: Boxplots of total wind energy (top subplot) and total solar energy (bottom subplot) outputs for each hour of the day during the simulation period (February-April 2017). In each subplot, the box represents the interquartile range, the line inside indicates the median, and the whiskers extend to the minimum and maximum values (0th and 100th percentiles) of the data.

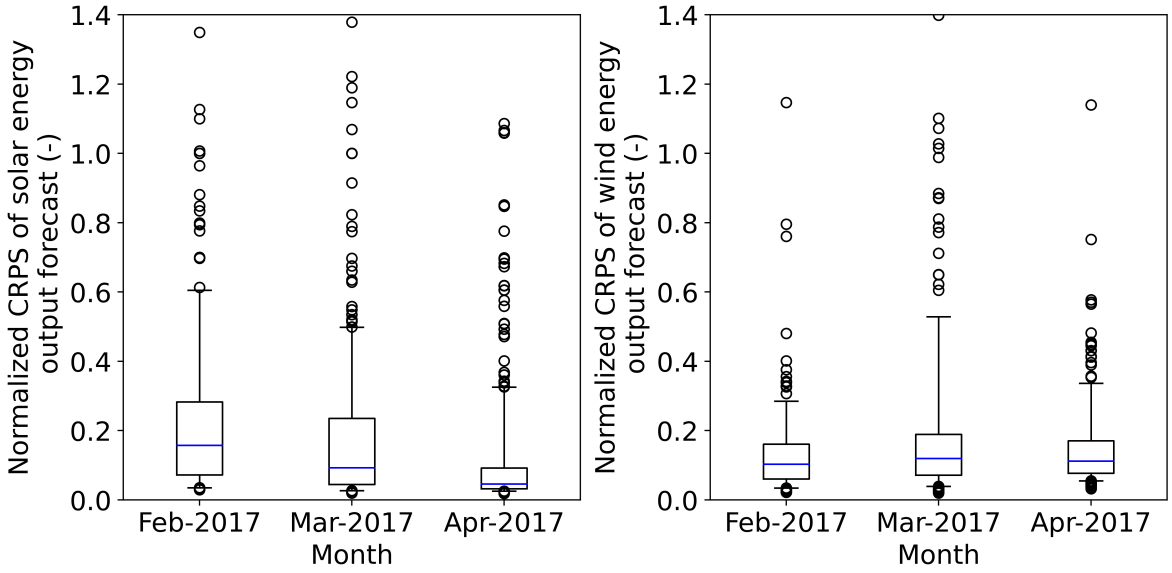

Figure 2.16: Boxplots of normalized hourly CRPS of solar power forecasts (left subplot) and wind power forecasts (right subplot) for each month in the simulation period (February-April 2017). In each subplot, the box represents the interquartile range, the line inside indicates the median, and the whiskers extend to the 5th and 95th percentiles of the data. The outliers are plotted as individual points beyond the whiskers. The hourly CRPS values are normalized by the corresponding observed power outputs.

periods of zero solar generation. As will be shown in subsequent sections, analyzing the behavior of the VPP during these periods offers interesting insights into the smoothing effects achieved when combining wind and solar farms.

Fig. 2.16 presents boxplots of the normalized hourly CRPS for both solar and wind power forecasts across the three months of the simulation period (February–April 2017). The CRPS values for wind and solar forecasts are normalized by the observed wind and solar power generations, respectively. The results indicate a comparable forecast quality for wind and solar power generation over these months. In all cases, the median normalized CRPS is below 0.2, meaning the median forecast error is less than 20% of the observed power generation.

The forecast performance for both wind and solar is slightly worse compared to inflow forecasting, both in terms of average performance and the number of outliers. This is expected due to the inherently higher variability in the uncertainty sources for wind and solar generation. The higher number of outliers in vRES forecasting compared to inflow forecasting suggests greater variability and uncertainty in predicting wind and solar power generation. This reflects the inherently volatile nature of vRES, where rapid changes in weather conditions pose challenges for forecasting models, particularly in predicting extreme values. The increased incidence of outliers indicates that these models struggle to accurately capture rare but significant deviations in power generation, leading to both underpredictions and overpredictions during periods of very low or very high output.

In contrast, inflow forecasts show fewer outliers, reflecting more reliable predictions. Inflows are influenced by longer-term weather patterns, which tend to be more stable and predictable.

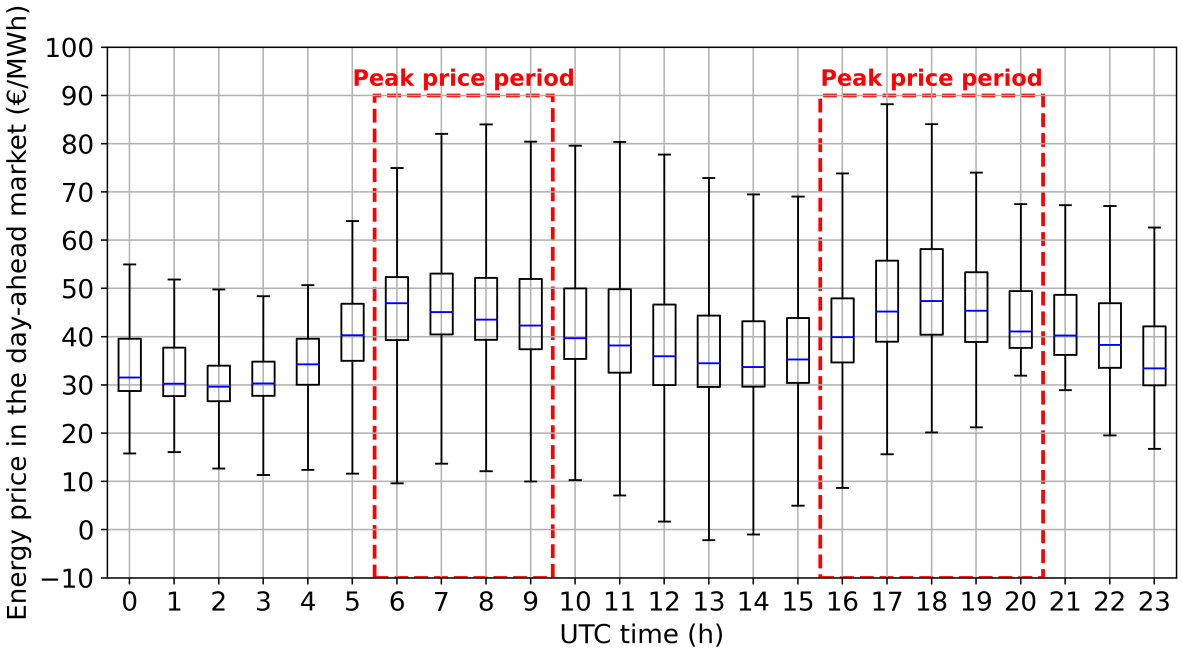

Figure 2.17: Boxplot of the energy prices in the day-ahead market for each hour of the day during the simulation period (February–April 2017). The box represents the interquartile range, the line inside indicates the median, and the whiskers extend to the minimum and maximum values (0th and 100th percentiles) of the data.

The lower number of outliers in inflow forecasting also suggests better model calibration and reduced uncertainty in these predictions. Furthermore, the flexibility offered by hydropower cascades can potentially be leveraged to mitigate the stochasticity of vRES (wind and solar power).

Fig. 2.17 presents a boxplot of the day-ahead market energy prices for each hour of the day over the simulation period (February–April 2017). The figure clearly shows two distinct peak price periods: one occurring in the morning and another in the evening. These peak periods coincide with typical demand surges, reflecting the inherent daily fluctuations in energy consumption. Analyzing the system's response to these specific market patterns is crucial for evaluating the performance of the proposed operational strategies. By focusing on how the VPP adapts to peak price periods, the analysis provides valuable insights into the system's ability to leverage favorable market conditions. The flexibility offered by the hydropower cascade, in particular, plays a pivotal role in optimizing market participation during these peak periods, where the price premiums can be maximized. The subsequent chapters will present a detailed assessment of the proposed optimization and control methods, highlighting their effectiveness in recognizing and responding to these peak price intervals. In particular, the results consistently show how the hydropower cascade's operational flexibility is strategically exploited to align power generation with high market prices, thereby capitalizing on these opportunities to enhance overall market performance.

Fig. 2.18 presents a boxplot of the normalized hourly CRPS for day-ahead market price forecasts throughout the simulation period from February to April 2017. The CRPS values are

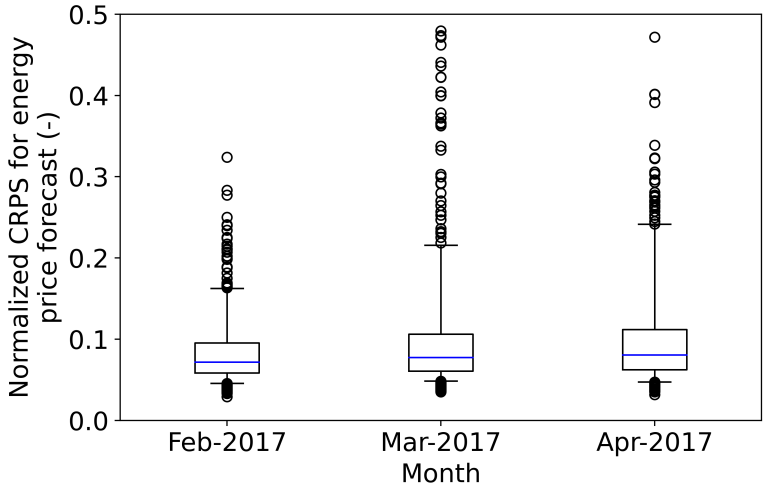

Figure 2.18: Boxplot of the normalized hourly CRPS of energy price forecasts in the day-ahead market for each month of the simulation period (February–April 2017). In each subplot, the box represents the interquartile range, the line inside indicates the median, and the whiskers extend to the 5th and 95th percentiles of the data. The outliers are plotted as individual points beyond the whiskers. The hourly CRPS values are normalized by the corresponding observed energy prices.

normalized by the corresponding observed energy prices. The figure illustrates that the median normalized CRPS remains below 0.1 across all analyzed months. This indicates that the error of the probabilistic price forecasting model is consistently less than 10% of the corresponding observed prices. The lower median normalized CRPS (<10%) and the thinner interquartile range observed in price forecasting, compared to vRES and inflow forecasting (both having a normalized CRPS median of <20%), suggest that price forecasts are not only more accurate but also exhibit less variability in the forecast errors. This indicates a higher degree of accuracy and consistency in the price forecasting model compared to the models used for vRES and inflow predictions. Such performance could be attributed to the presence of well-established market dynamics, where price variations may follow more predictable patterns driven by demand, generation mix, and regulatory structures.

Furthermore, the narrower interquartile range in price forecasting suggests lower forecast uncertainty, implying that the model consistently delivers accurate predictions with minimal variability across different forecast scenarios. This reduced variability indicates that extreme forecast errors—both underpredictions and overpredictions—are less frequent in price forecasting compared to vRES and inflow forecasting. Such consistency is expected, given that market prices, while subject to fluctuations, typically exhibit more structured behavior than the physical processes governing wind, solar, and hydrological inflows, which are inherently more volatile due to their dependence on rapidly changing weather conditions.

2.3.7 Insights from the Compagnie Nationale du Rhône Case Study in the Broader Evolution of Virtual Power Plants

The case study of Compagnie Nationale du Rhône offers a compelling perspective on the development of VPPs, particularly in the integration of hydropower with vRES, namely wind and solar power. This integration not only provides an opportunity to assess the flexibility potential of cascade hydropower but also necessitates the development of methods to manage the complexities of such an aggregation, which is subject to multiple uncertainties. This section explores the relevance of this case study within the broader evolution of VPPs.

2.3.7.1 Importance of Hydropower in Europe and Its Potential Role to Provide Flexibility

Hydropower plays a vital role in Europe's energy landscape [144], valued for its capacity to provide substantial flexibility and stability in power generation. The VPP operated by Compagnie Nationale du Rhône predominantly relies on a cascade of run-of-the-river hydraulic systems. Although these systems typically have limited storage capacity, they can still be strategically exploited to mitigate the intermittency and unpredictability of vRES, such as wind and solar.

Relevance to Broader Integration: Exploring the integration of cascaded hydropower into a VPP yields critical insights into optimizing flexibility within renewable energy systems. As Europe continues to expand its use of intermittent renewables, ensuring grid stability becomes a growing challenge. Hydropower, with its inherent fast-ramping capabilities, storage capacity, and inexpensive fuel, is an essential asset in addressing these challenges. Cascade hydropower, in particular, offers enhanced flexibility by utilizing the water flow at multiple points along a river, effectively maximizing the energy potential across different stages. This multi-point harnessing of water flow allows for a more adaptable and responsive system, especially during fluctuations in vRES production. Given the extensive presence of hydropower plants in European countries [144], such as Switzerland, Austria, France, and Italy, the case study at hand provides interesting insights on how to leverage existing hydropower infrastructure to provide system flexibility. By doing so, it reduces the immediate need for large investments in new technologies like battery storage systems, offering a cost-effective solution for enhancing the grid's flexibility.

Challenges: The operation of cascaded run-of-the-river hydropower systems presents several inherent challenges. A primary difficulty is the hydraulic interdependency among units (*spatial coupling*), which adds complexity to the system management. Each hydropower unit within the cascade influences the others, necessitating precise coordination to optimize both water use and energy generation. Moreover, run-of-the-river systems are highly reliant on natural river flows, which are subject to seasonal fluctuations, droughts, and other environmental variables. This dependence leads to periods of reduced energy output and limited storage capacity. Consequently, a comprehensive analysis of the system's performance across various scenarios—such as low-flow conditions, flood events, and normal inflow periods, in conjunction with stochastic vRES power generation—is essential. Such analysis is necessary to evaluate how wind, solar, and run-of-the-river cascaded hydropower can be integrated and optimized together to enhance

grid stability and operational efficiency.

2.3.7.2 A Virtual Power Plant with Only Renewable Energy Sources

The VPP operated by Compagnie Nationale du Rhône is distinguished by its exclusive reliance on renewable energy sources, including hydropower, wind, and solar power.

Relevance to Broader Integration: Analyzing a VPP powered entirely by renewables sheds light on the practical challenges and benefits of integrating diverse renewable energy sources into a single, cohesive system. It provides an opportunity to explore how different energy sources complement each other, their potential for smoothing out variability, and the overall efficiency of their coordination. This is particularly relevant to the European context, where the decarbonization of the energy sector and the shift to a low-carbon grid are critical policy objectives. The Compagnie Nationale du Rhône case offers key insights into how multiple renewable sources can be efficiently managed to contribute to grid stability and energy security.

Challenges: The integration of various renewable sources into a unified VPP presents several significant challenges, largely due to the stochastic nature of wind, solar, and even hydropower in some contexts. Ensuring a stable and reliable energy supply under these conditions requires advanced stochastic decision-making tools. Forecasting energy generation accurately across all sources is critical, but even with the best predictive techniques, uncertainties remain. This adds complexity to balancing supply and demand, as mismatches can significantly impact the aggregator's profitability and grid stability.

2.3.7.3 Trading in Multiple Electricity Markets

The VPP managed by Compagnie Nationale du Rhône can potentially operate across multiple energy markets, taking advantage of various trading opportunities and ancillary services.

Relevance to Broader Integration: Studying how multi-market trading is managed in this case study can provide valuable insights into maximizing economic benefits and grid services from VPPs. As European energy markets become increasingly interconnected and complex [28], understanding how to navigate these markets effectively is crucial for optimizing market participation and revenue generation. This case study serves as a practical example to assess the feasibility and performance of a renewable-based VPP operating across multiple electricity markets.

Challenges: Engaging in multi-market trading, however, presents several challenges. These include navigating complex and often divergent market regulations, understanding varied pricing mechanisms, and adhering to specific contractual obligations across different markets. Successful participation demands sophisticated market analysis and the development of strategic trading approaches that balance immediate revenue opportunities with long-term risk management. Moreover, Compagnie Nationale du Rhône's experience underscores the importance of building robust operational capabilities that can handle the volatility and financial risks inherent in multi-market trading. Ensuring regulatory compliance and minimizing exposure to market price fluctuations are critical for effective integration into this complex landscape.

2.3.7.4 Complexity of the System Stimulates the Development of Alternatives to Traditional Centralized Optimization Methods

The VPP operated by Compagnie Nationale du Rhône is characterized by significant complexity, driven by several factors. These include the hard nonlinear dynamics of hydropower generation, the spatial-temporal constraints associated with the combined operation of multiple hydropower systems and vRES, the hydraulic coupling among cascaded hydropower plants, the strict safety requirements of hydropower systems, and various sources of uncertainty in the management process. Traditional centralized optimization and control methods, may struggle to provide efficient solutions in such a complex environment.

Relevance to Broader Integration: Most VPPs are operated using centralized energy management strategies. However, as discussed in the following chapters, when applied to the complex VPP operated by Compagnie Nationale du Rhône, such centralized approaches may struggle to deliver solutions within the limited time available for market session decisions or may even lead to intractable problems due to the system's complexity. This limitation is generalizable to modern complex VPPs and highlights the need to explore alternative methods. Specifically, approaches that decompose the problem into smaller, more manageable components or utilize distributed optimization techniques could offer substantial benefits. Insights from the Compagnie Nationale du Rhône case study can inform the development and refinement of these strategies. Key benefits of exploring such methods include:

- *Modularity*: Distributed approaches provide substantial advantages in managing the evolving portfolio and energy management strategies of VPPs. They enable the seamless integration of new assets and adaptation to new markets by allowing components to be added or modified with minimal impact on the existing energy management system. Furthermore, distributed systems are well-suited to accommodate changes in market conditions or regulatory requirements through localized adjustments and updates. This modularity also facilitates the easy integration or removal of optimization tools within the distributed management framework, thereby minimizing the impact of transitioning to different tools or strategies.

- *Scalability*: Traditional centralized methods may struggle as the scale of the VPP increases, leading to inefficiencies or infeasibility in managing large and complex systems. Decomposition and distributed optimization approaches can better handle large-scale problems by breaking them down into smaller, more manageable sub-problems.

- *Robustness*: Centralized systems depend heavily on consistent communication between components and a central controller. In contrast, distributed optimization methods enhance robustness by enabling individual components or subsystems to operate using information received solely from neighboring components. This approach reduces the impact of communication failures, such as single-point failures, ensuring more reliable operation even during network disruptions.

- *Privacy*: Centralized optimization often involves aggregating sensitive data at a central

point, which may raise concerns about data privacy and security. Distributed approaches can improve privacy by keeping sensitive information localized within individual components or subsystems. This decentralization of data handling can help protect proprietary or confidential information while still enabling effective coordination and management of the VPP.

Challenges: Developing scalable solutions to the energy management challenges in such complex VPPs is inherently difficult. The first obstacle is the challenge of decoupling the problem, due to strong interconnections both in the *spatial dimension* (because of the hydraulic relationships among cascaded hydropower plants and the power balancing constraints) and in the *scenario dimension* (due to the need to maintain consistency across decisions made in each scenario within the uncertainty representation). Achieving full parallelization necessitates a decomposition method capable of scaling across both dimensions of complexity inherent to the problem. The nonconvex nature of the hydropower optimization problem adds another layer of complexity. Directly applying distributed approaches would often lead to heuristic methods. Therefore, it is crucial to develop methods that not only allow for decoupling but also maintain high-quality, reliable solutions, effectively balancing *scalability* with the need to ensure *feasibility* and *accuracy* of the decision-making process.

Chapter 3

The Integrated Bidding Problem: Modeling, Optimization and Control Methods for a Complex Virtual Power Plant

Résumé en Français

Ce chapitre traite du problème des enchères pour l'exploitation d'une centrale électrique virtuelle, en particulier sur le marché de l'électricité de la veille, où des incertitudes telles que les prix de l'énergie et la production d'énergie renouvelable doivent être prises en compte. Le chapitre adopte la perspective de la Compagnie Nationale du Rhône, en supposant que la centrale agit comme un *price-taker*, n'influençant pas les prix du marché. Une approche générique de modélisation est proposée pour les centrales électriques virtuelles complexes, tenant compte des dynamiques non linéaires et des multiples incertitudes. Ensuite, une stratégie de gestion de l'énergie à deux niveaux est introduite : un niveau de planification basé sur la programmation stochastique et un niveau de contrôle économique en quasi-temps réel. La validation de cette stratégie se fait par des tests hors échantillon et une analyse ex-post, fournissant une évaluation complète de sa robustesse et de ses performances. Enfin, les simulations montrent comment l'intégration de l'hydraulique en cascade avec les énergies renouvelables variables peut améliorer la flexibilité et les profits de la centrale, offrant ainsi une solution optimale pour l'exploitation de la centrale virtuelle.

3.1 Introduction

The bidding problem represents a central challenge in the operation of a VPP, particularly when dealing with complex systems that aggregate multiple energy units. The problem involves determining optimal bids for energy markets, typically the day-ahead market, while accounting for various uncertainties, including energy prices, demand fluctuations, and renewable energy generation [145]. Depending on the size and influence of the VPP, it may behave either as a *price-taker*, submitting bids without influencing market prices, or as a *price-maker*, where its bids directly affect the market clearing price. This distinction fundamentally alters the bidding strategy and the complexity of the decision-making process. This thesis adopts the perspective of Compagnie Nationale du Rhône within the French market, **assuming that the VPP functions as a price-taker in the day-ahead energy market**.

Addressing the bidding problem for a price-taker VPP involves several key challenges, starting with modeling the physical dynamics of the aggregated system and its interaction with the electricity market. While existing methods typically focus on case-specific models, this chapter aims to present a more generic modeling framework for VPPs. Previous contributions have introduced general modeling approaches for *large-scale VPPs*, concentrating on the difficulties related to aggregating numerous energy units. However, the **complex VPP** paradigm explored here goes beyond mere large-scale aggregation. In this case, complexity arises not only from the system's size but also from its hard nonlinear dynamics, multiple sources of uncertainty, and intricate coupling constraints that connect the diverse units within the aggregation. Building on existing modeling techniques, **this chapter provides a generic modeling approach tailored to complex VPPs** (**contribution C1** in Chapter 1). An analysis of current modeling methods and how the proposed approach fits within the existing literature is presented in Section 3.1.1.1.

Building on the generic modeling approach outlined in the first part of the chapter, the discussion moves to the proposed energy management strategy for operating the complex VPP in the day-ahead market. The goal is to provide a comprehensive solution that addresses multiple stages of the VPP energy management, including both scheduling and dispatch (see Fig. 2.3), while effectively managing the various sources of uncertainty, such as market prices, vRES generation, and water inflows into the hydropower systems, within the context of the complex aggregation operated by Compagnie Nationale du Rhône. To achieve this, **the chapter introduces a two-level, fully stochastic decision-making framework** (**contribution C2** in Chapter 1). The *first level* employs a scenario-based stochastic programming method to schedule the complex VPP for the day-ahead market using day-ahead forecasts. The *second level* features a stochastic economic MPC strategy, which governs the system in near-real time, incorporating short-term forecasts and observed realizations of uncertainties. A review of the existing literature and the positioning of the proposed method within this broader context are presented in Section 3.1.1.2.

Validation of the proposed two-level stochastic energy management strategy is carried out using out-of-sample validation and ex-post analysis. Out-of-sample validation evaluates the

robustness of the bidding strategy by simulating scenarios not used in the model's initial training, while ex-post analysis examines the performance of the strategy after market results are known, assessing metrics such as market profits, imbalances, and overall system behavior. Together, these methods provide a comprehensive assessment of the proposed optimization and control strategies, showing their practical relevance for real-world VPP operations.

From the perspective of Compagnie Nationale du Rhône, the strategies outlined in this chapter aim to address the first research question of this thesis (**research question Q1** in Chapter 1), which seeks to assess the flexibility potential of the VPP operated by Compagnie Nationale du Rhône and the potential benefits of combining cascaded hydropower with vRES to enhance the aggregator's market profit. This is explored through the simulations presented at the end of the chapter, particularly in relation to the impact of the operational curves (see Fig. 2.9) used by the aggregator to operate cascaded run-of-the-river hydropower on the flexibility potential of the aggregated system. Furthermore, the centralized decision-making methods introduced here provide the foundation for the decomposition approaches discussed in the following chapter.

3.1.1 Positioning Within the Related Literature

This section presents an overview of the literature concerning existing modeling and optimization methods for VPPs participation in the electricity markets. First, it provides an overview of the modeling approaches used to represent physical dynamics and interactions with the market. Subsequently, the discussion shifts to energy management methods aimed at handling uncertainties and optimizing the various stages involved in market participation, specifically focusing on day-ahead scheduling methods and near-real-time dispatch techniques.

3.1.1.1 Modeling Physical Dynamics and Power Market Interactions of a Complex Virtual Power Plants

Before developing bidding strategies for a VPP, a crucial preliminary step is to create a model that accurately represents the system's physical dynamics and its interaction with electricity markets. The ongoing evolution of the VPP paradigm has led to numerous contributions, each addressing different facets of this modeling challenge. Significant efforts have been made to model the diverse energy resources involved in VPP operations and their interactions with various power markets, as reviewed comprehensively in [14].

The most common approach is case-study-specific modeling of the VPP's physical dynamics and market interactions. In these models, the optimization framework is tailored to the particular case under study. The literature offers a variety of models that capture the physical dynamics of VPPs integrating vRES [18], energy storage systems [146], nuclear power plants [147], hydropower plants [148], gas turbines [149], combined heat and power units [150], electric vehicles [151], and controllable loads [152], among others. Similarly, different approaches have been developed to model VPP participation in the day-ahead market [153], intraday market [154], and ancillary services market [155]. Only a limited number of studies examine VPPs operating across multiple electricity markets, such as [156]. However, the main limitation of

Ref.	Trading in				Type of VPP modeled		
	DA	ID	RT	AS	Case-specific	Large-scale	Complex
[18]	✓	✓	×	×	✓	×	×
[146]	✓	×	✓	×	✓	×	×
[153]	✓	×	×	×	✓	×	×
[150]	✓	×	✓	×	✓	×	×
[154]	✓	✓	✓	×	✓	×	×
[155]	✓	×	✓	✓	✓	×	×
[19]	×	×	×	×	×	✓	×
[157]	✓	×	×	✓	×	✓	×
[158]	✓	×	×	×	×	✓	×
This chapter	✓	×	✓	×	×	×	✓

Table 3.1: Comparison of the proposed generic modeling approach for complex VPPs presented in this chapter with the relevant related literature. **DA**: Day-ahead market; **ID**: Intraday market; **RT**: Real-time balancing market; **AS**: Ancillary services market.

these methods is their dependence on the specific case study at hand. While many propose strategies with potential for broader generalization, their applicability remains constrained by the case-study-specific nature of the models, limiting their validation within the broader context of complex VPPs.

In response to the rise of large-scale VPPs, scholars have developed more generalized modeling approaches to overcome the limitations of traditional case-study-specific models. The first significant work in this direction, [19], proposed a flexible model for large-scale VPPs by grouping energy resources into clusters based on their point of common coupling with the upstream grid. Each cluster is modeled generically, accounting for common energy resources in VPPs, including conventional units, vRES and new flexibility technologies. For each cluster, both electrical and thermal components are considered. The dynamics of each energy resource are modeled in a simplified, generic manner to determine the power exchange of a cluster with the upstream grid. The power balance within the VPP is maintained by considering the power exchanges between clusters.

This modeling approach has been extended in two main directions. First, adaptations have been proposed to incorporate emerging technologies such as demand response programs [157]. Second, efforts have focused on improving the accuracy and realism of individual energy resource dynamics and providing a more detailed representation of market interactions [158]. While these developments offer a more generalized modeling framework that can be applied to a wide range of existing VPPs, they still fall short in effectively describing the complexities of large-scale VPPs.

In complex VPPs, the challenges extend beyond the dimensionality and heterogeneity of energy resources. A significant source of complexity arises from the intricate *spatial-scenario coupling* inherent in the VPP problem. While prior research on VPP modeling has primarily concentrated on asset types and their individual dynamics—focusing on large-scale VPPs and their heterogeneity—this thesis expands the modeling approach to address the case of a complex VPP. Specifically, the generic modeling framework proposed in [19] is enhanced to incorporate

not only a generic model of the individual physical dynamics of a large-scale portfolio of aggregated assets, but also a generic model of the main sources of coupling and interaction among the aggregated units in a complex VPP. These coupling constraints range from common power balancing constraints to physical coupling among assets (e.g., hydraulic coupling in a hydropower cascade), as well as the coupling between scenarios in the stochastic model. Additionally, the proposed model distinguishes between *dispatchable* and *non-dispatchable* energy resources in the complex VPP. This distinction is critical for evaluating the flexibility of the aggregated system—typically provided by the dispatchable units—as well as understanding the sources of uncertainty, which are linked to the nature of the energy units involved in the portfolio operated by the complex VPP.

Table 3.1 compares the modeling approach introduced in this section with relevant related literature. This chapter aims to generalize the modeling framework outlined in [19] for large-scale VPPs to encompass complex VPPs. A comprehensive analysis of the complex VPP's participation in multiple electricity markets is outside the scope of this discussion. Consequently, the focus is on VPP participation in the day-ahead market, which serves as the primary market for VPP operations. Extensions of the proposed modeling approach to the multi-market trading case are addressed in Chapter 5.

3.1.1.2 Optimizing Complex Virtual Power Plants Participation in the Energy Market

Once a model capturing the physical dynamics and interactions with electricity markets for complex VPPs is developed, it can be used to optimize the participation of these VPPs in the market. When addressing the day-ahead market participation of a complex VPP, this process typically involves two stages: the scheduling phase, where energy resources are traded in the market, and the dispatch phase, where real-time operations are reoptimized based on updated forecasts and realizations of the uncertainties. Various methods exist to address these stages, ranging from model-based approaches to machine learning techniques or hybrid methods. This thesis focuses on model-based approaches, emphasizing mathematical optimization and optimal control theory due to their established rigor, transparency, and interpretability when formulating decisions under uncertainty. While machine learning approaches offer promising alternatives for data-driven decision-making, model-based methods are preferred here for their ability to incorporate explicit system constraints and leverage domain knowledge effectively.

A critical step in optimizing the market participation of complex VPPs is the proper handling of uncertainty. In the case study under investigation, the primary uncertainties arise from market prices, vRES power generation, and water inflows in the hydropower cascade. Several established methods are available for addressing these uncertainties, with the most prominent being robust optimization [159], interval optimization [160], chance-constrained programming [161], and scenario-based stochastic programming [162].

Robust optimization [163] focuses on worst-case scenarios. It assumes that uncertainties lie within predefined bounds and seeks solutions that perform well under the worst possible realizations of these uncertainties. The key advantage of robust optimization is its conservative

nature, which guarantees feasibility under all possible outcomes within the uncertainty set. However, this approach can lead to overly conservative solutions, as it does not distinguish between different likelihoods of uncertainty realizations. In the context of VPPs with highly fluctuating market prices and vRES generation, robust optimization may result in suboptimal operational strategies due to its assumption of worst-case outcomes.

Interval optimization [164] extends robust optimization by considering uncertainty intervals for the input parameters. Solutions are sought that remain feasible across all values within these intervals. While interval optimization allows for a more flexible treatment of uncertainties than pure robust approaches, it still focuses on preserving feasibility across the entire range of possible outcomes, without considering the probabilistic nature of different uncertainty realizations. This can lead to conservative solutions similar to robust optimization, which may not be well-suited for market-driven applications where uncertain variables like prices exhibit high volatility and are often unbounded.

Chance-constrained programming [165] takes a more probabilistic approach to uncertainty management. Instead of ensuring feasibility under all possible scenarios, it guarantees that constraints are satisfied with a specified probability. This allows for balancing risk and conservatism by permitting small violations of the constraints in low-probability scenarios. The advantage of chance-constrained methods lies in their ability to manage uncertainty while avoiding the overly conservative solutions that arise in robust optimization. However, one limitation is the difficulty in specifying appropriate probabilities for constraint satisfaction, and the method's reliance on a precise characterization of the underlying probability distributions of the uncertainties, which may not always be available.

Scenario-based stochastic programming [166] is a flexible approach that models uncertainty by generating a set of discrete scenarios, each representing a possible realization of the uncertain parameters. This method allows for a detailed representation of the probability distributions and correlations between different uncertainties. The optimization problem is then solved across all scenarios, typically minimizing the expected cost while accounting for the potential variability across the different realizations. The main advantage of scenario-based stochastic programming is its ability to handle unbounded uncertainty sources—such as market prices—effectively, as it does not require predefining bounds or intervals for the uncertain variables. Additionally, it allows for modeling the full range of possible outcomes and their likelihoods, which provides a more nuanced approach to risk management than robust or interval optimization. A potential downside of this method is the computational complexity introduced by the need to solve the problem for multiple scenarios. This limitation prompts the exploration of the distributed approaches discussed in the next chapter of this thesis.

In this work, the day-ahead scheduling phase of the energy management system is formulated as a scenario-based stochastic programming problem. After establishing the day-ahead decisions using this scheduling tool, a near-real-time dispatch module becomes necessary to optimize the complex VPP scheduling in the balancing market, relying on updated forecasts and realizations of uncertainties. Optimal control theory is particularly well-suited for addressing this second phase of the problem, as it provides a systematic framework for making decisions that impact

the future behavior of dynamic systems, which is crucial for managing the complexities of VPP operations. By employing state-space representations, optimal control methods can effectively capture the dynamics of the VPP, seamlessly integrating both physical and market interactions.

In this context, MPC offers a practical implementation of optimal control by repeatedly solving an optimization problem at each time step while using the most recent system states and forecasts. The MPC framework inherently incorporates constraints on the system's inputs and states, ensuring that operational limits are respected during optimization.

Within the MPC framework, various strategies can be adopted depending on the nature of the control problem and the objectives tackled by the operator:

- *Reference-tracking model predictive control*: This variant focuses on tracking predefined trajectories or setpoints over time, allowing the VPP to follow desired operational profiles while minimizing deviations. This is particularly useful in scenarios where there are target outputs for power generation that need to be maintained in response to market signals or demand forecasts. Applications of this control method can be found in [167] for operating microgrids within energy markets and in [52], where this MPC approach is integrated into a two-level energy management strategy for operating hybrid systems.

- *Economic model predictive control*: This approach optimizes economic objectives such as profit maximization or cost minimization over the control horizon. By integrating market prices and operational costs into the MPC framework, economic MPC ensures that the VPP operates not only efficiently but also profitably, responding dynamically to fluctuations in the energy market. Examples of this control method are found in [168] and [169], where it is applied to solve bidding problems for microgrids and VPPs, respectively.

- *Stochastic model predictive control*: Extending the conventional MPC, stochastic MPC incorporates uncertainty directly into the optimization process by considering multiple scenarios or probabilistic forecasts. This method is particularly beneficial for VPPs facing uncertainties in market prices, renewable generation, and demand fluctuations. By modeling these uncertainties, stochastic MPC enhances the robustness of the control decisions, improving the VPP's adaptability to real-time market conditions. An example of this method is provided in [170], where a two-level stochastic energy management strategy combines scenario-based stochastic programming for energy bidding with stochastic MPC for real-time control under uncertainty.

While there has been considerable interest in the concepts of stochastic and economic MPC, relatively few efforts have been made to integrate both system uncertainties and economically driven objectives in the development of predictive controllers for optimizing the bidding strategies of aggregated systems. This integrated approach, which combines aspects of both economic and stochastic MPC, is referred to in the literature as *stochastic economic MPC*. An example can be found in [171], where a scenario-based stochastic economic MPC strategy is developed for the energy trading of a hybrid system. Additionally, [50] presents a sample-based stochastic economic MPC strategy aimed at minimizing real-time deviations from the original schedule

Ref.	System type	Two-level energy management strategy	
		First level (scheduling module)	Second level (dispatch module)
[167]	MG	×	RTMPC
[52]	HS	SBSP	RTMPC
[168]	MG	×	EMPC
[169]	VPP	×	EMPC
[170]	MG	SBSP	SMPC
[171]	HS	×	SEMPC
[50]	VPP	×	SEMPC
[51]	VPP	×	SEMPC
[172]	MG	SBSP	SEMPC
This chapter	Complex VPP	SBSP	SEMPC

Table 3.2: Comparison of the proposed fully stochastic, two-level energy management strategy in this chapter with relevant related literature. All referenced contributions provide solutions to bidding problems for energy producers or prosumers. **EMPC**: Economic model predictive control; **HS**: Hybrid system; **MG**: Microgrid; **RTMPC**: Reference-tracking model predictive control; **SBSP**: Scenario-based stochastic programming; **SEMPC**: Stochastic economic model predictive control; **SMPC**: Stochastic model predictive control.

for market participants, specifically addressing uncertainties in wind power generation. Similarly, [51] discusses the use of small controllable loads in a demand response program to trade energy on the day-ahead market, proposing a stochastic economic MPC approach to mitigate aggregator imbalances in the intraday market. In [172], stochastic economic MPC is utilized for the energy management of residential microgrids, where a comprehensive two-level architecture is introduced to trade energy in the day-ahead market while minimizing real-time imbalances, based on forecasts of load, weather, and prices.

In this chapter, a two-level fully stochastic energy management strategy is introduced to optimize the bidding strategy of a complex VPP in the day-ahead energy market. The first level, referred to as the scheduling module, applies a scenario-based stochastic programming model to determine bids for the day-ahead market, accounting for key uncertainties such as market prices, vRES power generation, and inflows, as considered in the primary case study. The second level, or dispatch module, receives the day-ahead decisions along with updated forecasts and utilizes stochastic economic MPC to optimize real-time control actions for the VPP. While the first level aims to maximize the expected profit of the VPP in the market, the primary objective of the second level is to minimize imbalance costs for the aggregated system. Although the methods used to formulate the proposed strategy are well-established in the literature, the purpose of this chapter is to integrate these approaches into a comprehensive strategy for optimizing the operation of an aggregated system in the market. Additionally, unlike most studies that focus on scheduling and dispatch for microgrids, hybrid systems, or case-specific VPPs, this chapter aims to generalize the two-level approach to the case of a complex VPP. Table 3.2 compares the energy management strategy presented in this chapter with the relevant related literature.

The proposed approach is evaluated on the full case study of Compagnie Nationale du Rhône,

which includes a series of cascaded hydropower plants aggregated with wind and solar units.

3.1.2 Chapter Outline

The remainder of this chapter is structured as follows. Section 3.2 outlines the mathematical foundations, emphasizing the optimization and control techniques applied in this chapter. Section 3.3 details the modeling approach for complex VPPs and introduces the proposed two-level fully stochastic energy management strategy for day-ahead market operations. Lastly, Section 3.4 presents the case study and discusses the obtained results.

3.2 Mathematical Background

This section offers a concise overview of the mathematical foundations essential for understanding the methods presented in this chapter. The proposed two-stage stochastic decision-making framework integrates stochastic optimization with optimal control theory. Thus, to provide the necessary background, this section begins by discussing optimization techniques for managing uncertainty, with a focus on scenario-based stochastic programming. It then proceeds to present an overview of MPC schemes, emphasizing reference-tracking MPC, economic MPC, and stochastic MPC.

3.2.1 Deterministic Optimization

Deterministic optimization assumes that all parameters and data involved in the problem are known with certainty. It seeks to find the optimal decision variables that minimize or maximize an objective function, subject to a set of constraints. The problem is typically formulated as follows:

$$\min_{\boldsymbol{x}} \quad J(\boldsymbol{x}) \tag{3.1a}$$

$$\text{subject to} \quad h(\boldsymbol{x}) = 0, \tag{3.1b}$$

$$g(\boldsymbol{x}) \leq 0, \tag{3.1c}$$

where $\boldsymbol{x}$ denotes the decision variable vector, $J(\cdot)$ is the objective function, $g(\cdot)$ is the equality constraint function, and $h(\cdot)$ is the inequality constraint function.

While deterministic optimization is highly efficient for problems with well-defined and predictable environments, it can be inadequate in real-world applications where uncertainty plays a significant role. Deterministic models often lead to suboptimal or even infeasible solutions when the actual system behavior deviates from the assumed conditions. As a result, deterministic optimization lacks the robustness required for decision-making in uncertain environments.

3.2.2 Stochastic Programming

To address the limitations of deterministic optimization, stochastic programming introduces uncertainty explicitly into the model. In stochastic programming, some of the parameters in the

objective function or constraints are considered random variables. Differently from deterministic optimization, the goal is to find decisions that are not only optimal for a single realization of the uncertainty but are robust across all possible outcomes.

The general form of a stochastic optimization problem is given by:

$$\min_{\boldsymbol{x}} \quad \mathbb{E}_{\hat{\boldsymbol{\xi}}}[J(\boldsymbol{x}, \hat{\boldsymbol{\xi}})] \tag{3.2a}$$

$$\text{subject to} \quad \mathbb{E}_{\hat{\boldsymbol{\xi}}}[h(\boldsymbol{x}, \hat{\boldsymbol{\xi}})] = 0, \tag{3.2b}$$

$$\mathbb{E}_{\hat{\boldsymbol{\xi}}}[g(\boldsymbol{x}, \hat{\boldsymbol{\xi}})] \leq 0, \tag{3.2c}$$

where $\hat{\boldsymbol{\xi}}$ is a random vector representing the uncertain parameters, and $\mathbb{E}_{\hat{\boldsymbol{\xi}}}$ denotes the expectation operator with respect to the random vector $\hat{\boldsymbol{\xi}}$.

A widely used formulation in stochastic programming is *two-stage stochastic programming* [23], which structures the decision-making process into two stages:

- In the *first stage*, decisions are made before the uncertainty is revealed. These decisions are typically irreversible or costly to adjust later.
- In the *second stage*, once the uncertainty is realized, additional recourse decisions are made to address the outcomes of the uncertainty.

The core concept of two-stage stochastic programming is that optimal decisions must be made based on information available at the time of decision-making, without relying on future realizations of uncertain parameters. A common formulation of two-stage optimization problems is given by:

$$\min_{\left\{\boldsymbol{x}, \boldsymbol{y}_{\hat{\boldsymbol{\xi}}}\right\}} \quad f^{\mathrm{F}}(\boldsymbol{x}) + \mathbb{E}_{\hat{\boldsymbol{\xi}}}\left[f^{\mathrm{S}}(\boldsymbol{x}, \boldsymbol{y}_{\hat{\boldsymbol{\xi}}}, \hat{\boldsymbol{\xi}})\right] \tag{3.3a}$$

$$\text{subject to} \quad h^{\mathrm{F}}(\boldsymbol{x}) = 0, \tag{3.3b}$$

$$g^{\mathrm{F}} \leq 0, \tag{3.3c}$$

$$h^{\mathrm{S}}\left(\boldsymbol{x}, \boldsymbol{y}_{\xi}, \hat{\boldsymbol{\xi}}\right) = 0, \tag{3.3d}$$

$$g^{\mathrm{S}}\left(\boldsymbol{x}, \boldsymbol{y}_{\hat{\boldsymbol{\xi}}}, \hat{\boldsymbol{\xi}}\right) \leq 0. \tag{3.3e}$$

Here, f^{F} and f^{S} represent the first-stage and second-stage costs, respectively. The first-stage and second-stage decisions are denoted by $\boldsymbol{x}$ and $\boldsymbol{y}_{\hat{\boldsymbol{\xi}}}$, respectively. Moreover, the first-stage constraint functions, denoted by g^{F} and h^{F}, are independent of the random vector $\hat{\boldsymbol{\xi}}$, in contrast to the second-stage constraint functions, denoted by g^{S} and h^{S}, which depend on the realization of the uncertainty parameter.

In summary, the first-stage decision, $\boldsymbol{x}$, referred to as the *here-and-now decision*, is made before the uncertain parameter $\hat{\boldsymbol{\xi}}$ is realized. Once $\hat{\boldsymbol{\xi}}$ is observed, the second-stage decision, $\boldsymbol{y}_{\hat{\boldsymbol{\xi}}}$, also known as the *wait-and-see decision*, is made in response to the realization of the uncertainty.

This two-stage formulation is particularly relevant for energy systems, where decisions often need to be made in the face of uncertainty about future demand, renewable energy generation,

or market prices. For instance, in power system operation, the first stage might involve the commitment of generation resources, while the second stage allows for adjustments based on actual demand or renewable generation outcomes.

Stochastic programming allows decision-makers to consider the expected performance of their decisions under uncertainty. However, solving these problems can be computationally challenging, especially when the uncertainty involves complex probability distributions or a large number of possible outcomes. The computational complexity of evaluating expectations and satisfying constraints for all possible realizations of the uncertainty motivates the development of scenario-based methods to approximate these expectations more tractably.

3.2.3 Scenario-Based Stochastic Programming

One effective way to handle uncertainty in stochastic programming is to use *scenario-based optimization*, where uncertainty is represented by a finite set $\mathbf{\Omega}$ of possible realizations of the uncertainty, called *scenarios*. Each scenario $\omega \in \mathbf{\Omega}$ represents a potential outcome of the random variable, and a probability is associated with each scenario, denoted by P_ω, where $\sum_{\omega \in \mathbf{\Omega}} P_\omega = 1$.

For stochastic problems in the form of (3.3) it is is common to leverage a sample average approximation to derive the following deterministic equivalent problem:

$$\min_{\{\boldsymbol{x}, \boldsymbol{y}_\omega\}_{\omega \in \mathbf{\Omega}}} \quad f^{\mathrm{F}}(\boldsymbol{x}) + \underbrace{\sum_{\omega \in \mathbf{\Omega}} P_\omega f^{\mathrm{S}}\left(\boldsymbol{x}, \boldsymbol{y}_\omega, \hat{\boldsymbol{\xi}}_\omega\right)}_{\approx \mathbb{E}_{\hat{\boldsymbol{\xi}}}\left[f^{\mathrm{S}}\left(\boldsymbol{x}, \boldsymbol{y}_{\hat{\boldsymbol{\xi}}}, \hat{\boldsymbol{\xi}}\right)\right]} \tag{3.4a}$$

$$\text{subject to} \quad h^{\mathrm{F}}(\boldsymbol{x}) = 0, \tag{3.4b}$$

$$g^{\mathrm{F}} \leq 0, \tag{3.4c}$$

$$h^{\mathrm{S}}\left(\boldsymbol{x}, \boldsymbol{y}_\omega, \hat{\boldsymbol{\xi}}_\omega\right) = 0, \ \forall \omega, \tag{3.4d}$$

$$g^{\mathrm{S}}\left(\boldsymbol{x}, \boldsymbol{y}_{\boldsymbol{\omega}}, \hat{\boldsymbol{\xi}}_\omega\right) \leq 0, \ \forall \omega. \tag{3.4e}$$

Here, $\hat{\boldsymbol{\xi}}_\omega$ represents the realization of the uncertain parameters in scenario ω.

In this approach, decision-makers optimize the expected performance of their decision across all scenarios, ensuring that the solution is robust against a range of potential future states. Scenario-based approaches are commonly used to generate tractable problem instances, allowing for more practical implementation of stochastic optimization in real-world applications. However, the quality of the solution depends heavily on the choice and accuracy of the scenarios. If the scenarios do not adequately represent the true distribution of uncertainty, the solution may still lack robustness. On the other hand, as the number of scenarios increases, so does the computational complexity of the problem, making it difficult to solve in real-time applications.

3.2.4 Model Predictive Control

MPC is a powerful optimization-based control strategy widely applied in engineering systems, particularly where the dynamics of the system need to be controlled over time [102]. The essence of MPC is to repeatedly solve an optimization problem over a finite prediction horizon, taking

into account system dynamics, constraints, and a performance objective. The prediction horizon keeps being shifted forward and for this reason MPC is also called *receding horizon control*. At each time step, an optimal control sequence is computed, but only the first control action is applied before the optimization is updated with new measurements or forecasts, making MPC inherently suitable for systems with uncertainty or varying conditions.

The basic principle of MPC is to iteratively minimize a cost function that depends on future predictions of the system's state by solving the following optimization problem at each time $t \in \boldsymbol{T}$:

$$\min_{\{\boldsymbol{x}(t+k|t),\boldsymbol{y}(t+k|t),\boldsymbol{u}(t+k|t)\}_{k\in\boldsymbol{K}}} \quad \sum_{k\in\boldsymbol{K}} \ell(\boldsymbol{x}(t+k|t),\boldsymbol{y}(t+k|t),\boldsymbol{u}(t+k|t)) \tag{3.5a}$$

$$\text{subject to} \quad \boldsymbol{x}(t+k+1|t) = f^{\mathrm{X}}(\boldsymbol{x}(t+k|t),\boldsymbol{u}(t+k|t)),\ \forall k \in \boldsymbol{K}, \tag{3.5b}$$

$$\boldsymbol{y}(t+k|t) = f^{\mathrm{Y}}(\boldsymbol{x}(t+k|t)),\ \forall k \in \boldsymbol{K}, \tag{3.5c}$$

$$\boldsymbol{x}(t+k|t) \in \boldsymbol{\Upsilon}^{\mathrm{X}},\ \forall k \in \boldsymbol{K}, \tag{3.5d}$$

$$\boldsymbol{u}(t+k|t) \in \boldsymbol{\Upsilon}^{\mathrm{U}},\ \forall k \in \boldsymbol{K}. \tag{3.5e}$$

Here, $\boldsymbol{x}(t+k|t)$ and $\boldsymbol{y}(t+k|t)$ and $\boldsymbol{u}(t+k|t)$ represent the system's state, output and control input at each sample time k in the prediction horizon $\boldsymbol{K}$, respectively. The feasible spaces for the system's state and control input are denoted by $\boldsymbol{\Upsilon}^{\mathrm{X}}$ and $\boldsymbol{\Upsilon}^{\mathrm{U}}$, respectively. The functions f^{X} and f^{Y} define the relationships between the system's state, output, and control input. The term $\ell(\boldsymbol{x}(t+k|t),\boldsymbol{y}(t+k|t),\boldsymbol{u}(t+k|t))$ is the stage cost. The notation $t+k \mid t$ signifies that decisions are made at time $t+k$, based on information available up to time t, i.e., the system's measurements at time t.

MPC has become a popular control strategy due to its ability to handle multivariable systems with constraints on inputs and outputs. However, its effectiveness depends on how well the system model predicts future behavior and how the performance criteria are defined. Several variants of MPC exist, depending on the specific control objectives, including reference-tracking MPC, economic MPC, and stochastic MPC, each of which poses unique challenges and benefits.

3.2.4.1 Reference-Tracking Model Predictive Control

In its most basic form, MPC is used for *reference-tracking*, where the control objective is to ensure that the system follows a predefined reference trajectory as closely as possible. The cost function in reference-tracking MPC typically penalizes the deviation between the system's predicted output and the desired reference:

$$\ell(\boldsymbol{x}\,(t+k|t),\boldsymbol{y}(t+k|t),\boldsymbol{u}(t+k|t)) = \|\boldsymbol{y}(t+k|t) - \boldsymbol{r}(t+k|t)\|^2_{\mathbf{Q}} + \|\boldsymbol{u}(t+k|t)\|^2_{\mathbf{R}}\,, \tag{3.6}$$

where $\boldsymbol{r}(t+k|t)$ denotes the reference signal, while $\mathbf{Q}$ is the weighting matrix for the output deviation and $\mathbf{R}$ is the weighting matrix for the control effort. The quadratic cost is widely used in control design to ensure stability of the controller and to impose greater penalties on large deviations from the desired setpoint [102]. Fig. 3.1 illustrates a discrete reference-tracking MPC

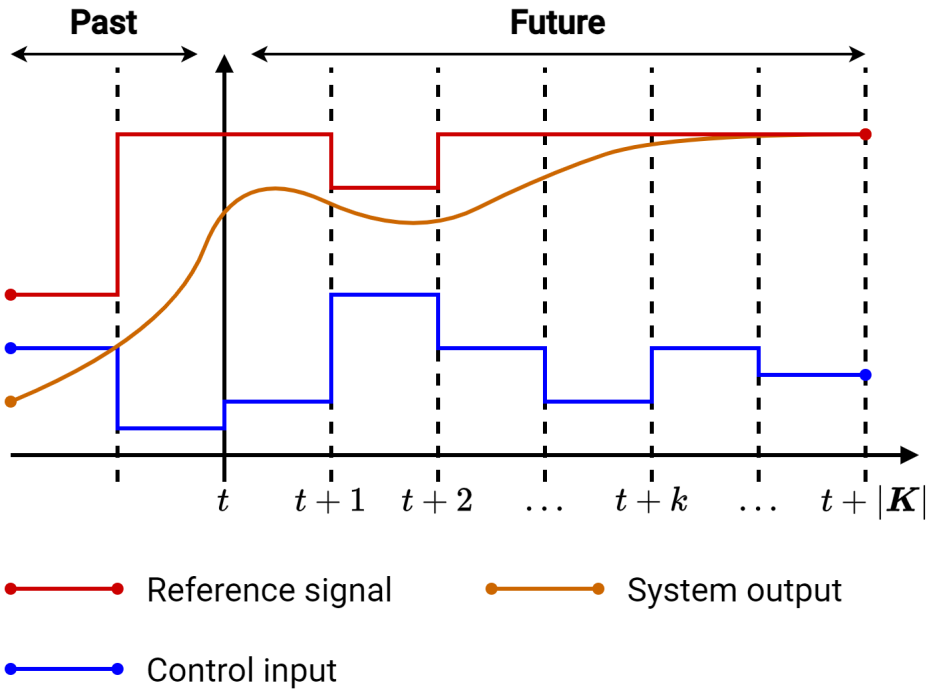

Figure 3.1: Illustration of a discrete reference-tracking MPC scheme.

scheme.

The main challenge with reference-tracking MPC lies in the need for accurate system models and reference trajectories. When the system model does not capture the true dynamics or the reference is unattainable due to external disturbances, the control performance may degrade. Additionally, it can be computationally demanding, especially for fast-changing systems with tight constraints.

3.2.4.2 Economic Model Predictive Control

While reference-tracking MPC focuses on following a predefined path, *economic* MPC directly incorporates the economic key performance indicators of the problem into the control objective [173]. Rather than minimizing the deviation from a reference, the goal is to optimize an economic criterion, such as minimizing operational costs or maximizing energy efficiency.

The main advantage of economic MPC is that it aligns the control objectives with economic performance, which is particularly useful in energy systems or industrial processes. However, this approach often introduces trade-offs between short-term gains and long-term system health or stability. The economic performance is closely tied to external factors like market prices, adding complexity to the optimization problem, especially in dynamic environments such as electricity markets.

3.2.4.3 Stochastic Model Predictive Control

To address uncertainty in system dynamics or external disturbances, *stochastic* MPC extends the traditional MPC framework by explicitly incorporating uncertainty in the optimization problem

[174]. The uncertainty is often modeled as random variables, and the cost function may include an expectation over the possible future scenarios:

$$\mathbb{E}_{\hat{\boldsymbol{\xi}}}\left[\sum_{k\in\boldsymbol{K}}\ell(\boldsymbol{x}(t+k|t),\boldsymbol{y}(t+k|t),\boldsymbol{u}(t+k|t),\hat{\boldsymbol{\xi}}(t+k))\right], \tag{3.7}$$

where $\hat{\boldsymbol{\xi}}(t+k)$ represents the random vector, and $\mathbb{E}_{\xi}$ denotes the expectation operator with respect to the random vector $\hat{\boldsymbol{\xi}}(t+k)$.

One of the key challenges of stochastic MPC is computational complexity. Evaluating the expected cost over all possible future realizations of uncertainty can be prohibitively expensive, especially in real-time control applications. Approximation techniques, such as scenario-based stochastic MPC, are often employed to reduce computational demands by sampling a finite number of scenarios. However, the quality of the solution depends heavily on the choice and representativeness of these scenarios, similar to stochastic programming. Stochastic MPC offers significant robustness compared to deterministic MPC, but this comes at the cost of increased computational burden.

3.3 Methodology

The methodology section of this chapter is organized as follows. Section 3.3.1 defines the bidding problem. Section 3.3.2 describes the proposed generic modeling approach for complex VPPs. Section 3.3.3 introduces the proposed stochastic two-level energy management strategy for operating complex VPPs in the day-ahead market. Finally, Section 3.3.4 outlines the evaluation methods proposed to assess the quality and performance of the proposed methods.

3.3.1 Formulation of the Bidding Problem

The aggregator's objective in the day-ahead market is to optimize its market participation through an effective bidding strategy, commonly known as the bidding problem [145]. In Europe's energy system, electricity is exchanged through various markets operating at different temporal scales, including intraday, balancing, and day-ahead markets [28]. Each of these markets is governed by specific regulatory frameworks and operates within distinct timeframes, which heavily influence the strategic decisions of market participants. While the proposed models are grounded in the mechanisms currently applied in Europe, a comprehensive discussion of the European electricity markets is outside the scope of this work. For an in-depth analysis of recent developments in European electricity markets readers can consult [175].

In this thesis, aggregators are tasked with managing and integrating a portfolio of diverse, geographically dispersed energy resources into a single market bid. These resources may include various generation assets—such as wind farms, solar photovoltaic systems, and energy storage technologies—which, despite their spatial separation, are collectively subject to the same *balancing perimeter*. As a *balancing responsible party* (BRP), the aggregator must ensure that its net energy position—the total energy injected into or withdrawn from the grid by all resources

within its balancing perimeter—remains balanced at all times. Deviations from this balance, whether caused by forecast inaccuracies or the inherent stochasticity of vRES, pose a risk to grid stability and lead to financial penalties. As a BRP, the aggregator is bound by strict imbalance settlement mechanisms, which impose substantial penalties for failure to maintain the required energy balance [176].

The integration of vRES into an aggregator's portfolio adds significant complexity due to the stochastic nature of renewable energy generation, which inherently increases uncertainty in power output. As a result, the aggregator is more likely to deviate from the energy schedule submitted to the day-ahead market, thereby facing imbalance penalties. These penalties occur because any shortfall or surplus in delivered energy, relative to the scheduled amount, disrupts the grid's energy balance. In this thesis, imbalance settlement follows a *dual pricing scheme*, wherein separate prices apply to positive imbalances (underproduction compared to the scheduled quantity) and negative imbalances (overproduction) [28]. This dual settlement structure presents both a challenge and an opportunity for the aggregator: while deviations from the schedule incur financial risks, strategic management of imbalances can also provide the potential to minimize losses or even exploit price differentials [177].

In the following, the energy volumes offered to the market are denoted by $e_{\omega,t}$, and the day-ahead energy price forecast by $\hat{\pi}^{\mathrm{E}}$. In a dual pricing settlement framework, distinct prices are applied to positive imbalances, $\delta^{\mathrm{E}\uparrow}$, and negative imbalances, $\delta^{\mathrm{E}\downarrow}$. The forecasted penalty prices for these imbalances are denoted by $\hat{\pi}^{\mathrm{E}\uparrow}$ and $\hat{\pi}^{\mathrm{E}\downarrow}$, respectively.

To mitigate the risk of penalties and manage uncertainties associated with vRES, aggregators can leverage the flexibility inherent in their portfolios. Flexibility sources, such as energy storage systems, play a pivotal role by enabling the aggregator to absorb or dispatch energy in real time, thereby buffering the variability of renewable generation. This capability is crucial for smoothing out deviations from the forecasted generation schedule, which directly reduces imbalance penalties. Moreover, aggregators with geographically and technologically diverse portfolios may further benefit from resource heterogeneity, as it dampens the impact of localized fluctuations. For instance, if solar generation underperforms in one region, excess wind power in another could help offset the shortfall, leading to a more balanced aggregated position.

From a system-wide perspective, not all BRPs will experience the same type of imbalance. While some BRPs may face positive imbalances, others may experience negative imbalances, where actual generation exceeds their market commitments. Across the market, these opposing imbalances may partially cancel each other out, reducing the net system imbalance. However, any residual imbalance that persists after this partial cancellation must be corrected through ancillary services such as frequency control. These services deploy balancing energy to restore grid frequency to its nominal level, typically 50 Hz in Europe. The reliance on such balancing mechanisms underscores the critical importance of accurate forecasting and precise bidding strategies for aggregators participating in the day-ahead market, as deviations not only incur financial penalties but also impact grid stability.

In European day-ahead markets, aggregators face regulatory constraints on how bids must be structured. Specifically, market rules typically require that supply bids submitted for the same

time interval be non-decreasing with respect to price [145]. This ensures that as prices rise, the quantities of energy offered also increase, reflecting rational economic behavior—generators are naturally more inclined to supply energy at higher prices. For aggregators, this constraint must be integrated into their optimization frameworks to ensure compliance with market regulations while maximizing potential profit. In this thesis, two mechanisms for formulating bids in the day-ahead market are examined: *fixed hourly bids* and *price-quantity bidding curves*. In the former, the aggregator offers a fixed energy volume for each hour, for all forecasted price levels. In the latter, an offering curve is generated for each hour, with the energy volume varying according to different price scenarios. A detailed discussion on these bid formulation approaches is provided in Section 3.3.2.2 of this chapter.

3.3.2 Modeling a Complex Virtual Power Plant Participating in the Day-Ahead Energy Market

This section outlines the proposed modeling approach for a complex VPP participating in the day-ahead market. Initially, a general modeling framework is introduced to describe the physical dynamics of the complex VPP, with a particular emphasis on the coupling constraints integral to the problem. These constraints will later be utilized to decompose the VPP energy management problem and develop a distributed solution. Subsequently, different bidding strategies for the day-ahead market are detailed, focusing on fixed hourly bids and price-quantity bidding curves. The coupling constraints associated with each bidding strategy are also discussed.

3.3.2.1 Modeling the Physical Dynamics of a Complex Virtual Power Plant

The complex VPP analyzed in this study is modeled as an interconnected set of energy resources linked to a public radial network, which is, in turn, connected to the upstream grid, as depicted in Fig. 3.2. The resources within the VPP are organized into *clusters*, each consisting of various components. These clusters can vary widely in nature, encompassing passive loads, composite power plants, or a combination of both, and may include energy storage systems. A set of clusters connected to the same public line forms a *branch* of the VPP. The boundary between each branch and the upstream network is defined by the *point of common coupling of the branch*, denoted by PCC^{br}.

Beyond the physical infrastructure, a property layer is defined by the ownership of generating, storage, and load resources, distinguishing energy facilities based on their respective owners. Although different companies may own these physical assets, operational control is delegated to a scheduling coordinator. This coordinator aggregates the resources within the VPP and manages them to optimize the total profit of the cluster. While the VPP is operated under a unified strategy, post-operational profit redistribution can occur among cluster participants, reflecting their contributions to the overall economic outcome.

The energy clusters are modeled as shown in Fig. 3.2. The model is designed to be highly adaptable and to accommodate a wide range of energy components. If a particular component is absent from a facility, the model simply sets the capability of that component to zero, without

altering the overall structure. Additionally, the model can simulate the presence of loads or producers outside the VPP, which are not subject to optimization, by treating them as independent entities with their own loads (positive or negative). Only active power is considered, as the network is assumed to be non-dissipative.

As illustrated in Fig. 3.2, each cluster contains both thermal and electrical components. The thermal section, connected to the thermal busbar, consists primarily of (a) a defined thermal load, which can be supplied by a combined heat and power plant, and (b) a boiler and/or a thermal storage system. If the thermal output from the combined heat and power plant exceeds the load and cannot be stored due to limitations in storage capacity or power, the surplus thermal energy is released into the atmosphere via a heat exchanger. Both the combined heat and power units and the boiler are powered by gas. The electrical section is divided into two parts. The first, referred to as the *internal* section, operates as a conventional energy producer, with its boundary with the distribution grid defined by an *internal point of common coupling*, denoted by PCC^{int}. This part, connected to the central busbar, primarily consists of an electrical load, which can be powered by the combined heat and power plant, along with an internal vRES and/or an energy storage system.

Many global feed-in tariff schemes only incentivize energy injected into the grid from certain vRES, such as small-scale wind farms, rather than the total energy produced. Therefore, installing such vRES within the VPP's internal network would limit the tariff to the energy produced beyond the local load, if any surplus exists. To maximize benefits, the aggregator would strategically install these vRES outside the internal section of the cluster, using a different point of common coupling, called *external point of common coupling* and denoted by PCC^{ext}, leading to the distinction between external vRES and internal vRES.

In this modeling framework, cogeneration units, boilers, thermal and energy storage systems, electric vehicles, controllable loads, and hydropower plants are identified as *dispatchable units*. These assets offer flexibility to the complex VPP, which can be leveraged to manage the inherent stochasticity of the *non-dispatchable units* of the complex VPP, specifically the vRES. Since the primary focus is on renewable energy integration, conventional power plants are excluded from the proposed model. A comprehensive model of the individual dynamics for each energy resource within the VPP cluster depicted in Fig. 3.2 is detailed in [19].

As illustrated in Fig. 3.2, the generic clusters of the complex VPP are organized into branches based on their point of common coupling with the upstream network. The complex VPP can thus be viewed as a unified entity formed by the aggregation of multiple branches, each of which is further subdivided into individual clusters that aggregate the energy resources managed by the VPP. Such a modular structure is particularly valuable for enabling parallelization of the operational algorithms. **Through this modular modeling approach, it becomes evident how the complex VPP can be spatially decomposed**, either per asset or by groups of assets, according to the point of common coupling of each resource cluster with the upstream network. This decoupling approach lays the foundation for the spatial-scenario decomposition approach described in Chapter 4.

This modeling approach specifically considers four types of **coupling constraints**: *electri-*

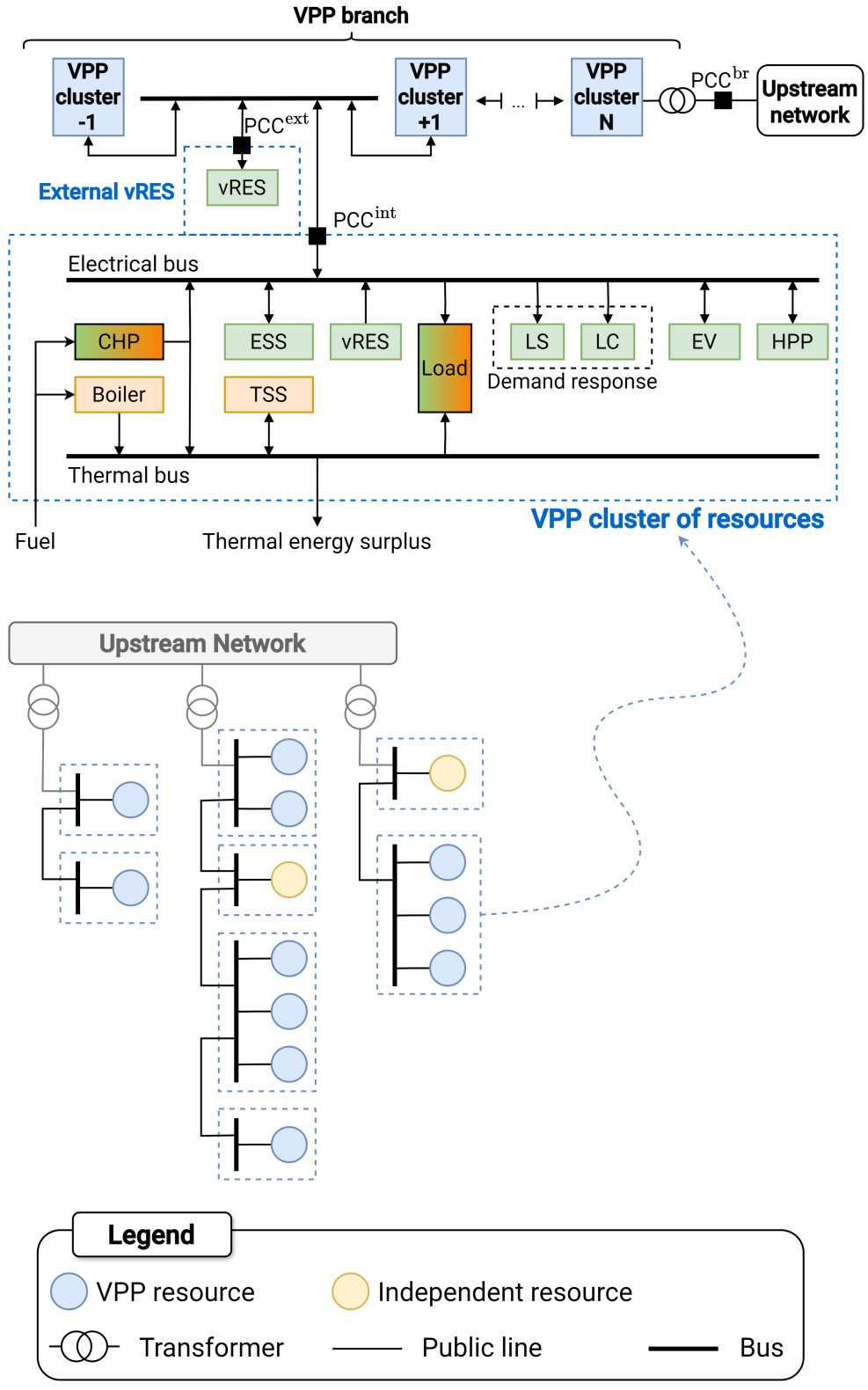

Figure 3.2: Diagram of a branch and a cluster of energy resources in the proposed model for a complex VPP. **CHP**: Combined heat and power generation; **ESS**: Energy storage system; **EV**: Electric vehicles; **HPP**: Hydropower plant; **LC**: Load curtailment demand response program; **LS**: Load shifting demand response program; **TSS**: Thermal storage system.

cal coupling, *thermal coupling*, *physical coupling*, and **scenario coupling constraints**. The first three establish a spatial connection between the energy resources operated by the complex VPP and are therefore referred to as the set of **spatial coupling constraints**. The fourth set, scenario coupling constraints, ensures consistency among the decision variables across all scenarios used to represent potential uncertainty outcomes in the subsequent stochastic programming problems. The formulation of these coupling constraints is detailed below:

- **Spatial coupling constraints: the electrical coupling**. Let $p^{\text{VPPCL,lin}}_{c,b,\omega,t} \in \mathbb{R}$ denotes the power flow on the line upstream of VPP cluster $c \in \boldsymbol{N}^{\mathbf{VPPCL}}_{b}$ in the VPP branch $b \in \boldsymbol{N}^{\mathbf{VPPBR}}$ at time $t \in \boldsymbol{T}$ under scenario $\omega \in \boldsymbol{\Omega}$. The power flow $p^{\text{VPPCL,lin}}_{c,b,\omega,t}$ is computed as a function of internal and external power injections/withdrawals from each VPP cluster, denoted by $p^{\text{VPPCL,int}}_{c,b,\omega,t} \in \mathbb{R}, \forall c, \forall b, \forall \omega, \forall t$ and $p^{\text{VPPCL,ext}}_{c,b,\omega,t} \in \mathbb{R}^{+}, \forall c, \forall b, \forall \omega, \forall t$, respectively:

$$p^{\text{VPPCL,lin}}_{c,b,\omega,t} = p^{\text{VPPCL,int}}_{c,b,\omega,t} + p^{\text{VPPCL,ext}}_{c,b,\omega,t} + \sum_{c'=1}^{c-1} \left(p^{\text{VPPCL,int}}_{c',b,\omega,t} + p^{\text{VPPCL,ext}}_{c',b,\omega,t} \right), \ \forall c, \forall b, \forall \omega, \forall t. \quad (3.8)$$

  The internal and external power flows of each VPP cluster represents the power exchange at the internal (PCC^{int}) and external (PCC^{ext}) points of common coupling, respectively, as illustrated in Fig. 3.2. The power flow on each line must comply with the thermal limit $\overline{P}^{\text{VPPCL,lin}}$:

$$\left| p^{\text{VPPCL,lin}}_{c,b,\omega,t} \right| \leq \overline{P}^{\text{VPPCL,lin}}_{c,b}, \ \forall c, \forall b, \forall \omega, \forall t. \quad (3.9)$$

  If the system operates in islanded mode, the power flow limit on the final line, which connects to the upstream network, is set to zero:

$$p^{\text{VPPCL,lin}}_{|\boldsymbol{N}^{\mathbf{VPPCL}}_{b}|,b,\omega,t} = 0, \ \forall b, \forall \omega, \forall t. \quad (3.10)$$

  During participation in the day-ahead market, the power balance of the complex VPP is expressed as:

$$\sum_{b \in \boldsymbol{N}^{\mathbf{VPPBR}}} \sum_{c \in \boldsymbol{N}^{\mathbf{VPPCL}}_{b}} \left(p^{\text{VPPCL,int}}_{c,b,\omega,t} + p^{\text{VPPCL,ext}}_{c,b,\omega,t} \right) \Delta_T - e_{\omega,t} - \delta^{\text{E}\downarrow}_{\omega,t} + \delta^{\text{E}\uparrow}_{\omega,t} = 0, \ \forall \omega, \forall t. \quad (3.11)$$

- **Spatial coupling constraints: the thermal coupling**. Thermal coupling refers to the sum of the thermal loads of the components within each cluster of the complex VPP, as illustrated in Fig. 3.2. If the thermal production exceeds the load and cannot be absorbed by storage due to power or energy limitations, the surplus thermal energy is released into the atmosphere via a heat exchanger. As this thesis focuses on the electrical components of the complex VPP, the mathematical formulation of these coupling constraints is omitted but can be easily derived using the same reasoning applied for the electrical coupling constraints.

- **Spatial coupling constraints: the physical coupling**. Physical coupling refers to the inherent physical interconnections between the various energy assets within a com-

plex VPP. These couplings arise from the interactions and dependencies between different physical units, which must be explicitly modeled in the optimization problem governing the VPP's operation. Given the diversity of energy resources integrated into such complex systems, these physical links can take many forms and must be carefully accounted for to ensure accurate and efficient coordination of the VPP. One prominent example is *mechanical coupling*, which can occur between generation units that are physically connected, such as turbines and generators in a combined-cycle power plant. In this case, the mechanical interaction imposes constraints on the operation of both units, necessitating a joint consideration of their dynamics within the optimization framework. Another critical form of physical coupling is *hydraulic coupling*, particularly relevant in hydropower systems. When multiple hydropower units are linked by shared water resources, the flow of water between upstream and downstream units creates a direct physical dependence. This hydraulic connection imposes constraints related to water balance, as the operations of upstream units influence the available water—and hence the potential power generation—of downstream units. In the context of this thesis, the primary focus is on the hydraulic coupling that arises from the operation of cascaded run-of-the-river hydropower plants. Specifically, the system operated by Compagnie Nationale du Rhône provides a clear example of hydraulic coupling, where water released by one plant impacts the inflow conditions of the next plant downstream. Properly managing these water flows, while respecting the constraints of water availability and operational limits, is critical for optimizing the overall performance of the cascaded system. A comprehensive treatment of the hydraulic coupling constraints for cascaded hydropower plants, including water balance considerations, is provided in Section 2.3.4.2 and forms a key part of the optimization model used in this study.

- **Scenario coupling constraints**. In stochastic programming, scenario coupling constraints are constraints that enforce coherency across different scenarios in a stochastic problem. These constraints arise when decision variables for different scenarios cannot vary independently because they are subject to some shared, real-world constraint. For example, in a two-stage stochastic programming problem, the first-stage decision variables (which represent decisions made before the uncertainty is revealed) are common to all scenarios. This introduces a coupling effect, as the decisions must be valid across all potential future outcomes (scenarios). The second-stage decisions, made after uncertainty is revealed, may differ across scenarios but can still be subject to certain coupling constraints, especially when physical, operational, or regulatory constraints need to hold across multiple scenarios. A typical example is in power systems optimization with renewables, where the scheduling of energy resources (like hydropower or wind) must respect capacity or operational limits, no matter which scenario materializes. The scenario coupling constraints ensure that the solution is feasible and coherent across all scenarios by imposing rules that govern the relationships between decisions under different uncertain outcomes. In this thesis, such coupling arises from the bid formulation in the day-ahead market. Depending on the strategy used—whether fixed hourly bids or price-quantity bidding curves—different scenario coupling constraints emerge. The formulation of bids and the resulting scenario

coupling constraints are discussed in Section 3.3.2.2.

3.3.2.2 Formulating Bids in the Day-Ahead Market

In the day-ahead market, the formulation of bids plays a pivotal role in determining the operational efficiency and financial outcomes of participants. This market operates as a structured platform where electricity producers and consumers schedule energy transactions for the following day. Two predominant bidding strategies are employed: *fixed hourly bids* and *price-quantity bidding curves*.

Fixed hourly bids involve submitting a constant energy offer across all price forecasting scenarios within a stochastic bidding framework. In this strategy, a participant commits to selling a predefined quantity of energy irrespective of the forecasted price fluctuations. The principal advantage of this method lies in its simplicity and ease of implementation. By selecting a static energy volume, participants can more easily estimate profits based on expected prices, which facilitates straightforward financial planning and risk management. This approach is particularly advantageous for smaller market players, as it provides consistent profit streams without requiring frequent adjustments to bids. However, the rigidity inherent in fixed hourly bids limits participants' ability to capitalize on sudden price surges or demand variations, potentially leading to suboptimal financial performance in volatile markets.

Conversely, price-quantity bidding curves enable participants to specify variable energy quantities at different price levels for each time step [178]. These curves are constructed by associating distinct energy volumes with corresponding price levels, allowing for a more dynamic response to anticipated market conditions. This strategy introduces a greater degree of flexibility, permitting participants to adjust their bids based on real-time market conditions and price signals.

Market price uncertainty is typically represented by a set of potential price scenarios, namely $\left\{\hat{\pi}^{\mathrm{E}}_{\omega,t}\right\}_{\omega\in\boldsymbol{\Omega},t\in\boldsymbol{T}}$, where each scenario is assigned a probability P_ω such that $\sum_{\omega\in\boldsymbol{\Omega}} P_\omega = 1$. For each price scenario, an optimal energy offer $e_{\omega,t}$ is determined. The complete set of price-quantity pairs, $\left\{\left(\hat{\pi}^{\mathrm{E}}_{\omega,t}, e_{\omega,t}\right)\right\}_{\omega\in\boldsymbol{\Omega},t\in\boldsymbol{T}}$, forms the producer's offer curve. To ensure that the curve is non-decreasing, the following condition must hold:

$$\left(\hat{\pi}^{\mathrm{E}}_{\omega,t} - \hat{\pi}^{\mathrm{E}}_{\omega',t}\right)\left(e_{\omega,t} - e_{\omega',t}\right) \geq 0,\ \forall\omega' \in \boldsymbol{\Omega}\setminus\omega,\ \forall\omega,\forall t. \tag{3.12}$$

Let $o_{\omega,t}$ represent the incremental energy quantity offered at price $\hat{\pi}^{\mathrm{E}}_{\omega,t}$. Fig. 3.3 illustrates an example of an offer curve with three offer blocks for a fixed time step $t = \bar{t}$. In this case, $\hat{\pi}^{\mathrm{E}}_{1,\bar{t}}$, $\hat{\pi}^{\mathrm{E}}_{2,\bar{t}}$, and $\hat{\pi}^{\mathrm{E}}_{3,\bar{t}}$ serve as both price scenarios and price offers. The producer offers $e_{1,\bar{t}}$ at price $\hat{\pi}^{\mathrm{E}}_{1,\bar{t}}$ as the first block and adds $o_{2,\bar{t}}$ at price $\hat{\pi}^{\mathrm{E}}_{2,\bar{t}}$ as the second block. The total energy quantity $e_{\omega,\bar{t}}$ corresponding to price $\hat{\pi}^{\mathrm{E}}_{\omega,\bar{t}}$ is computed as:

$$e_{\bar{t}} = \sum_{\omega\in\boldsymbol{\Omega}} \mathbf{B}_{\omega,\bar{t}}\, o_{\omega,\bar{t}},\ \forall\omega, \tag{3.13}$$

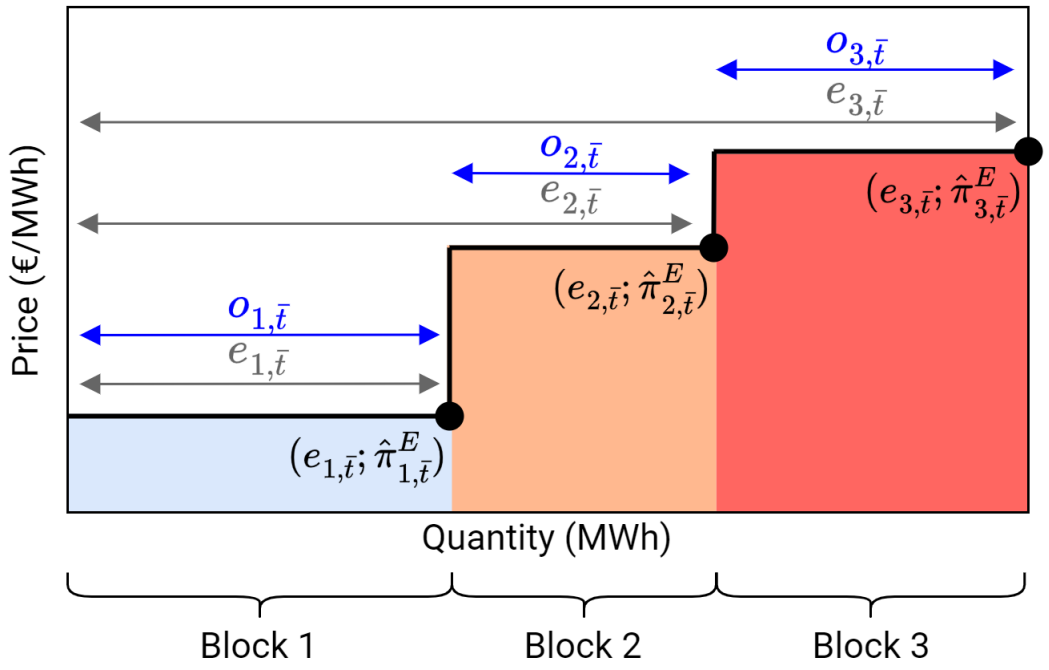

Figure 3.3: Example of price-quantity bidding curve for a give time step $t = \bar{t}$ [178].

where the acceptance matrix $\mathbf{B}_{\omega,\bar{t}}$ for time step $t = \bar{t}$ is defined as:

$$\mathbf{B}_{\omega,\bar{t}} = \begin{cases} 1, & \text{if } \pi^{\mathrm{E}}_{\bar{t}} \geq \hat{\pi}^{\mathrm{E}}_{\omega,\bar{t}} \\ 0, & \text{otherwise} \end{cases}, \ \forall \omega. \tag{3.14}$$

The matrix $\mathbf{B}_{\omega,\bar{t}}$ indicates whether the offer block $\left(\bar{\pi}^{\mathrm{E}}_{\omega,\bar{t}}, e_{\omega,\bar{t}}\right)$ is accepted, provided that the price realization is $\pi^{\mathrm{E}}_{\bar{t}}$. Notably, the bid described in (3.13) is scenario-independent, despite being constructed using scenario-dependent price-quantity bids.

Price-quantity bidding curves offer the advantage of responsiveness to market conditions and price elasticity. This adaptability allows participants to capture higher profits during peak demand and secure sales during off-peak periods, thus improving financial performance and market resilience. However, the complexity of constructing these curves necessitates advanced modeling techniques and computational resources, posing challenges for participants with limited operational capacity. Moreover, the dynamic nature of price-quantity bidding can result in increased transaction costs, as participants may need to update their strategies frequently in response to evolving market conditions.

When comparing fixed hourly bids with price-quantity bidding curves, several key differences emerge. Fixed hourly bids offer simplicity and operational stability, making them suitable for participants seeking predictable outcomes. However, this approach lacks the flexibility required to fully exploit fluctuating market prices. In contrast, price-quantity bidding curves provide the flexibility needed to optimize bids according to market conditions, offering greater potential for profit maximization and risk management. Nonetheless, the increased complexity and re-

source requirements associated with this approach can present obstacles, particularly for smaller market players. The selection of an appropriate bidding strategy should be informed by the participant's operational objectives, market environment, and available resources, as this decision can significantly impact competitiveness in the day-ahead market.

It is worth mentioning that (3.12) introduces a coupling between scenarios in the stochastic bidding problem, referred to here as scenario coupling. In other words, if these constraints could be solved independently for each scenario $\omega \in \mathbf{\Omega}$, rather than collectively for all forecasted outcomes of the random variable, the problem would become separable—or *decoupled*—with respect to the scenario coupling constraints. Building on this concept, Chapter 4 how to decompose the stochastic bidding problem formulated here.

3.3.3 A Fully Stochastic Two-Level Decision-Making Framework for Optimizing Complex Virtual Power Plant Participation in the Day-Ahead Market

This section introduces a fully stochastic, scenario-based, two-level decision-making framework for the participation of complex VPPs in the day-ahead market. The problem is structured around two time stages:

1. **Day-ahead step** (24 hours before energy injection/withdrawal), corresponding to the *bidding problem*, where the day-ahead scheduling of the complex VPP is optimized to compute energy market bids, with the objective of maximizing the aggregator's profit.

2. **Short-term step** (minutes before energy injection/withdrawal), corresponding to the *control problem*, where the near-real-time dispatch of the complex VPP is optimized to adjust actual energy generation, minimizing the cost of penalties arising from market imbalances.

In the following, decision variables and parameters associated with the day-ahead and short-term stages are denoted by superscripts DA and ST, respectively. Two sets of uncertainty scenarios are considered. A set of day-ahead scenarios, denoted by $\mathbf{\Omega^{DA}}$, is generated during the day-ahead step (24h before the uncertainty realization) to address the bidding problem. A set of short-term scenarios, denoted by $\mathbf{\Omega^{ST}}$, is generated during the short-term step (minutes before the uncertainty realization) to handle the control problem. As this thesis focuses on developing optimization and control methods for managing complex VPPs, forecasting techniques for the underlying uncertainties are not covered here. Instead, it is assumed that scenarios for the relevant random variables—ranging from price forecasts to vRES power generation, water inflows, and demand, depending on the VPP portfolio—are provided as input to the proposed optimization and control methods. For instance, in the case of the Compagnie Nationale du Rhône, specific scenario sets are generated according to the methods described in Chapter 2.

A two-level stochastic architecture is proposed, combining optimization-based approaches to address the bidding and control challenges. First, a stochastic day-ahead scheduling module uses scenario-based stochastic optimization for the bidding problem. Second, a scenario-based

stochastic economic MPC strategy is applied to handle the control problem during the short-term step. Together, these stochastic optimization and control tools form the proposed fully stochastic decision-making framework for the operation of complex VPPs.

Based on the generic modeling approach for complex VPPs outlined in Section 3.3.2, the **day-ahead scheduling strategy** for addressing the bidding problem of a complex VPP can be formulated as the following scenario-based stochastic optimization problem, solved at each time step $t \in \boldsymbol{T}$ with a sampling time Δ_T, across all day-ahead scenarios $\omega \in \boldsymbol{\Omega}^{\mathbf{DA}}$:

$$\underset{\boldsymbol{z}^{\mathbf{DA}}}{\text{argmin}} \quad J^{\mathrm{DA}} \tag{3.15a}$$

$$\text{subject to} \quad \sum_{b \in \boldsymbol{N}^{\mathbf{VPPBR}}} \sum_{c \in \boldsymbol{N}_b^{\mathbf{VPPCL}}} p_{c,b,\omega,t}^{\mathrm{VPPCL,DA}} \Delta_T - e_{\omega,t}^{\mathrm{DA}} - \delta_{\omega,t}^{\mathrm{E}\downarrow,\mathrm{DA}} + \delta_{\omega,t}^{\mathrm{E}\uparrow,\mathrm{DA}} = 0, \ \forall \omega, \forall t, \tag{3.15b}$$

$$\left(\hat{\pi}_{\omega,t}^{\mathrm{E}} - \hat{\pi}_{\omega',t}^{\mathrm{E}}\right)\left(e_{\omega,t}^{\mathrm{DA}} - e_{\omega',t}^{\mathrm{DA}}\right) \geq 0, \ \forall \omega' \in \boldsymbol{\Omega}^{\mathbf{DA}} \setminus \omega, \ \forall \omega, \forall t, \tag{3.15c}$$

$$\boldsymbol{z}_{c,b,\omega,t}^{\mathbf{VPPCL,DA}} \in \boldsymbol{\Phi}^{\mathbf{VPPCL,DA}}, \ \forall c, \forall b, \forall \omega, \forall t. \tag{3.15d}$$

Here, the set of *day-ahead decision variables*, denoted as $\boldsymbol{z}^{\mathbf{DA}}$, is defined as:

$$\boldsymbol{z}^{\mathbf{DA}} := \left\{ p_{c,b,\omega,t}^{\mathrm{VPPCL,DA}}, e_{\omega,t}^{\mathrm{DA}}, \boldsymbol{\delta}_{\omega,t}^{\mathbf{E,DA}}, \boldsymbol{z}_{c,b,\omega,t}^{\mathbf{VPPCL,DA}} \right\}_{b \in \boldsymbol{N}^{\mathbf{VPPBR}}, c \in \boldsymbol{N}_b^{\mathbf{VPPCL}}, \omega \in \boldsymbol{\Omega}^{\mathbf{DA}}, t \in \boldsymbol{T}}, \tag{3.16}$$

where $\boldsymbol{\delta}_{\omega,t}^{\mathbf{E,DA}}$ is given by:

$$\boldsymbol{\delta}_{\omega,t}^{\mathbf{E,DA}} := \left[\delta_{\omega,t}^{\mathrm{E}\uparrow,\mathrm{DA}}, \delta_{\omega,t}^{\mathrm{E}\downarrow,\mathrm{DA}}\right]^{\top}, \ \forall \omega, \forall t. \tag{3.17}$$

The day-ahead objective function of the aggregator is denoted by J^{DA}. Constraints (3.15b) ensure the power balance of the VPP, as explained in Section 3.3.2. Constraints (3.15c) enforce the non-decreasing form of the price-quantity bidding curves, as detailed in Section 3.3.2. Lastly, constraints (3.15d) ensure that the set of decision variables for each VPP cluster $c \in \boldsymbol{N}_b^{\mathbf{VPPCL}}$ within each VPP branch $b \in \boldsymbol{N}^{\mathbf{VPPBR}}$, denoted by $\boldsymbol{z}_{c,b,\omega,t}^{\mathbf{VPPCL,DA}}$, remains within its feasible space $\boldsymbol{\Phi}^{\mathbf{VPPCL,DA}}$.

Since the objective of the aggregator in this thesis is to maximize its profit from participation in the day-ahead market, the objective function J^{DA} is defined as follows:

$$\begin{aligned} J^{\mathrm{DA}} := & \sum_{\omega \in \boldsymbol{\Omega}^{\mathbf{DA}}} \sum_{t \in \boldsymbol{T}} P_{\omega}^{\mathrm{DA}} \left(\hat{\pi}_{\omega,t}^{\mathrm{E}\uparrow,\mathrm{DA}} \delta_{\omega,t}^{\mathrm{E}\uparrow,\mathrm{DA}} - \hat{\pi}_{\omega,t}^{\mathrm{E}\downarrow,\mathrm{DA}} \delta_{\omega,t}^{\mathrm{E}\downarrow,\mathrm{DA}} - \hat{\pi}_{\omega,t}^{\mathrm{E,DA}} e_{\omega,t}^{\mathrm{DA}} \right) \\ & + \frac{1}{\left|\boldsymbol{N}^{\mathbf{VPPBR}}\right|} \sum_{b \in \boldsymbol{N}^{\mathbf{VPPBR}}} \frac{1}{\left|\boldsymbol{N}_b^{\mathbf{VPPCL}}\right|} \sum_{c \in \boldsymbol{N}_b^{\mathbf{VPPCL}}} \sum_{\omega \in \boldsymbol{\Omega}^{\mathbf{DA}}} \sum_{t \in \boldsymbol{T}} P_{\omega}^{\mathrm{DA}} C_{c,b,\omega,t}^{\mathrm{VPPCL,DA}}. \end{aligned} \tag{3.18}$$

Here, $C^{\mathrm{VPPCL,DA}}$ is the day-ahead cost term that represents the operational costs of the energy resources within each cluster of the VPP, such as the degradation costs of energy storage systems. Meanwhile, P_{ω}^{DA} denotes the probability of the day-ahead scenario ω. The objective function (3.18) reflects the total cost incurred by the VPP in the day-ahead market, and minimizing this cost is equivalent to maximizing the VPP's profit.

In words, the optimization problem (3.15) seeks to maximize the profit (the difference be-

tween profit and costs) of the complex VPP, while satisfying the power balancing constraints (3.15b), ensuring that the obtained price-quantity bidding curves maintain a non-decreasing form as dictated by (3.15c), and adhering to the individual dynamics of each cluster of energy resources within the complex VPP, as specified by (3.15d). If the aggregator decides to compute fixed hourly bids instead of price-quantity bidding curves, as discussed in Section 3.3.2.2, the energy volumes offered in the day-ahead market will be constant across all scenarios. In this case, the energy volumes $e^{\mathrm{DA}}_{\omega,t}$ in (3.15) will simplify to e^{DA}_{t}, and constraints (3.15c) can be neglected.

After the aggregator submits its bids, the energy market clears, assigning the aggregator a specific energy delivery volume, denoted as E^{ST}_t. Between the day-ahead market closure and the actual real-time delivery, the aggregator reoptimizes both internal and external dispatch operations to maximize real-time profits. In this thesis, the **short-term dispatch strategy** is formulated as a MPC problem. At each time step $t \in \boldsymbol{T}$, the aggregator solves an optimization problem considering forecasts for all time steps k within the prediction horizon $\boldsymbol{K}$, with a sampling interval of Δ_K, across all short-term scenarios $\omega \in \boldsymbol{\Omega}^{\mathbf{ST}}$:

$$\underset{\boldsymbol{u}^{\mathbf{ST}}_{t|t}, \boldsymbol{z}^{\mathbf{ST}}}{\operatorname{argmin}} \quad J^{\mathrm{ST}} \tag{3.19a}$$

$$\text{subject to} \quad \sum_{b \in \boldsymbol{N}^{\mathbf{VPPBR}}} \sum_{c \in \boldsymbol{N}^{\mathbf{VPPCL}}_b} p^{\mathrm{VPPCL,ST}}_{c,b,\omega,t+k|t} \Delta_K - E^{\mathrm{ST}}_{t+k} - \delta^{\mathrm{E}\downarrow,\mathrm{ST}}_{\omega,t+k|t} + \delta^{\mathrm{E}\uparrow,\mathrm{ST}}_{\omega,t+k|t} = 0, \quad \forall \omega, \forall k, \tag{3.19b}$$

$$\left[\boldsymbol{u}^{\mathbf{VPP,ST}}_{\omega,t|t}, \boldsymbol{\delta}^{\mathbf{E,ST}}_{\omega,t|t}\right]^\top = \boldsymbol{u}^{\mathbf{ST}}_{t|t}, \ \forall \omega, \tag{3.19c}$$

$$\boldsymbol{z}^{\mathbf{VPPCL,ST}}_{c,b,\omega,t+k|t} \in \boldsymbol{\Phi}^{\mathbf{VPPCL,ST}}, \ \forall c, \forall b, \forall \omega, \forall k. \tag{3.19d}$$

Here, the set of *short-term decision variables*, denoted as $\boldsymbol{z}^{\mathbf{ST}}$, is defined as

$$\boldsymbol{z}^{\mathbf{ST}} := \left\{ p^{\mathrm{VPPCL,ST}}_{c,b,\omega,t+k|t}, \boldsymbol{\delta}^{\mathbf{E,ST}}_{\omega,t+k|t}, \boldsymbol{z}^{\mathbf{VPPCL,ST}}_{c,b,\omega,t+k|t} \right\}_{b \in \boldsymbol{N}^{\mathbf{VPPBR}}, c \in \boldsymbol{N}^{\mathbf{VPPCL}}_b, \omega \in \boldsymbol{\Omega}^{\mathbf{ST}}, k \in \boldsymbol{K}}, \tag{3.20}$$

where $\boldsymbol{\delta}^{\mathbf{E,ST}}_{\omega,t+k|t}$ is given by

$$\boldsymbol{\delta}^{\mathbf{E,ST}}_{\omega,t+k|t} := \left[\delta^{\mathrm{E}\uparrow,\mathrm{ST}}_{\omega,t+k|t}, \delta^{\mathrm{E}\downarrow,\mathrm{ST}}_{\omega,t+k|t}\right]^\top, \ \forall \omega, \forall k. \tag{3.21}$$

Moreover, $\boldsymbol{u}^{\mathbf{VPP,ST}}_{\omega,t+k|t}$ collects all the decision variables of problem (3.19), corresponding to the control actions applicable to the dispatchable units of the complex VPP (e.g., decision variables related to the charging and discharging power of an energy storage system), and is defined as:

$$\boldsymbol{u}^{\mathbf{VPP,ST}}_{\omega,t+k|t} := \left[\boldsymbol{u}^{\mathbf{VPPBR,ST}}_{1,\omega,t+k|t}, \ldots, \boldsymbol{u}^{\mathbf{VPPBR,ST}}_{b,\omega,t+k|t}, \ldots, \boldsymbol{u}^{\mathbf{VPPBR,ST}}_{|\boldsymbol{N}^{\mathbf{VPPBR}}|,\omega,t+k|t}\right]^\top, \ \forall \omega, \forall k, \tag{3.22}$$

where $\boldsymbol{u}^{\mathbf{VPPBR,ST}}_{b,\omega,t+k|t}$ includes all the decision variables corresponding to the control actions that can be applied to the dispatchable units within branch $b \in \boldsymbol{N}^{\mathbf{VPPBR}}$ of the complex VPP. These

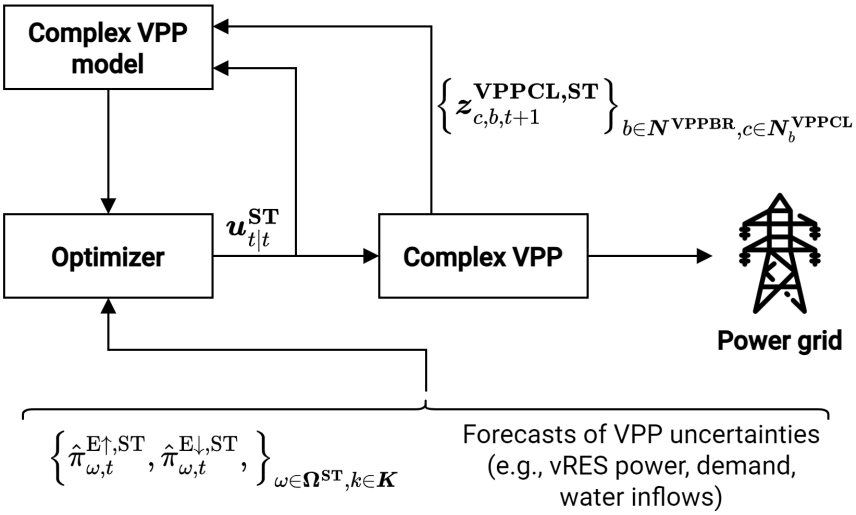

Figure 3.4: The proposed stochastic economic MPC strategy for short-term dispatch of a complex VPP.

decision variables represent the control actions applicable to the dispatchable units within each corresponding set of clusters of the complex VPP.

In (3.19), constraints (3.19b) are equivalent to those in (3.15b), while the constraints (3.19d) correspond to those in (3.15d). Additionally, the constraints (3.19c) are introduced to ensure that the control strategy remains consistent across all scenarios during the first prediction step of the MPC strategy. This consistency is necessary to guarantee the convergence properties of the MPC strategy, as shown in [171].

Once (3.19) is solved, only the first element $\boldsymbol{u}^{\mathbf{ST}}_{t|t}$ of the optimal control sequence is executed at time t, and this process is reiterated in the next time step $t+1$.

Since the objective of the aggregator in this thesis is to maximize its profit from participation in the day-ahead market, the objective function J^{ST} is defined as follows:

$$
\begin{aligned}
J^{\mathrm{ST}} := & \sum_{\omega \in \boldsymbol{\Omega}^{\mathbf{ST}}} \sum_{k \in \boldsymbol{K}} P^{\mathrm{ST}}_{\omega} \left(\hat{\pi}^{\mathrm{E}\uparrow,\mathrm{ST}}_{\omega,t+k} \delta^{\mathrm{E}\uparrow,\mathrm{ST}}_{\omega,t+k|t} - \hat{\pi}^{\mathrm{E}\downarrow,\mathrm{ST}}_{\omega,t+k} \delta^{\mathrm{E}\downarrow,\mathrm{ST}}_{\omega,t+k|t} \right) \\
& + \frac{1}{\left| \boldsymbol{N}^{\mathbf{VPPBR}} \right|} \sum_{b \in \boldsymbol{N}^{\mathbf{VPPBR}}} \frac{1}{\left| \boldsymbol{N}^{\mathbf{VPPCL}}_b \right|} \sum_{c \in \boldsymbol{N}^{\mathbf{VPPCL}}_b} \sum_{\omega \in \boldsymbol{\Omega}^{\mathbf{ST}}} \sum_{k \in \boldsymbol{K}} P^{\mathrm{ST}}_{\omega} C^{\mathrm{VPPCL,ST}}_{c,b,\omega,t+k|t} .
\end{aligned} \tag{3.23}
$$

Here, $C^{\mathrm{VPPCL,ST}}$ is the short-term cost term that represents the short-term operational costs of the energy resources within each cluster of the VPP. Meanwhile, P^{ST}_{ω} denotes the probability of the short-term scenario ω.

Fig. 3.4 depicts the proposed stochastic economic MPC strategy for the short-term dispatch of a complex VPP. At each time step $t \in \boldsymbol{T}$, the optimizer receives forecasts for market prices and other uncertain parameters, then solves the control problem (3.19) over the prediction horizon $\boldsymbol{K}$. However, only the first control action, $\boldsymbol{u}^{\mathbf{ST}}_{t|t}$, is implemented. After observing the system's response to this action, $\boldsymbol{z}^{\mathbf{VPPCL,ST}}_{c,b,t+1}, \forall b, \forall c$, the complex VPP model is updated, and the process is repeated for $t+1$.

The proposed fully stochastic, scenario-based, two-level decision-making framework for op-

timizing complex VPPs participation in the day-ahead market is depicted in Fig. 3.5.

As discussed in Section 3.3.2.1, one of the key objectives of the proposed formulation is to emphasize the coupling constraints typically encountered in optimization problems for complex VPPs. Specifically, in examining the generic optimization models (3.15) and (3.19), distinct sets of coupling constraints emerge:

- **Spatial coupling constraints**: In (3.15), the power balancing constraint (3.15b) introduces a coupling between the VPP clusters by incorporating the decision variables representing the power exchanges of all clusters with the upstream grid, denoted by $p^{\text{VPPCL,DA}}$. As a result, the optimization problem for each cluster cannot be solved independently, since enforcing the power balancing constraint requires consideration of the decision variables across all clusters. This is commonly referred to as *electrical coupling* between the units (or groups of units) within the complex VPP. Similarly, the constraints (3.19b) create an electrical coupling also in the short-term dispatch problem (3.19). In addition to electrical coupling, which is among the most prevalent types of coupling in VPP problems, other forms of spatial coupling constraints may arise depending on the energy resources involved, as detailed in Section 3.3.2.1. Specifically, in the case study of Compagnie Nationale du Rhône, a *hydraulic coupling* exists among the cascaded hydropower assets managed by the aggregator. In the generic optimization models (3.15) and (3.19), this coupling is embedded in the constraint sets (3.15d) and (3.19d), respectively.

- **Scenario coupling constraints**: In scenario-based stochastic programs, a scenario coupling arises to ensure consistency among the scenarios of potential uncertainty considered in the optimization problem. This coupling is expressed in constraints (3.15c) and (3.19c), in the optimization models (3.15) and (3.19), respectively. In the first case, the consistency between the price-quantity bidding curves produced by the aggregator introduces a scenario coupling, meaning that the energy bids resulting from the scheduling problem in the day-ahead market must be optimized across all scenarios of uncertainty. Similarly, constraints (3.19c) create a scenario coupling in the dispatch control problem, as the control actions imposed on the physical system must be consistent across all scenarios. In other words, the control actions for each dispatchable unit in the complex VPP cannot vary by scenario but are instead optimized across the entire prediction horizon of the controller, accounting for all potential uncertainty outcomes.

It is worth noting that if the aforementioned spatial and scenario coupling constraints were disregarded, the constraint set in the optimization model (3.15) would reduce to:

$$\boldsymbol{z}^{\mathbf{VPPCL,DA}}_{c,b,\omega,t} \in \boldsymbol{\Phi}^{\mathbf{VPPCL,DA}}_{c,b,\omega}, \ \forall c, \forall b, \forall \omega, \forall t, \tag{3.24}$$

where the feasible space of decision variables associated with the internal dynamics of each cluster becomes decoupled in both the spatial dimension (i.e., one per cluster) and the scenario dimension (i.e., one per scenario). **In other words, in this case, the scheduling module can be addressed in parallel, handling each cluster and each scenario separately**.

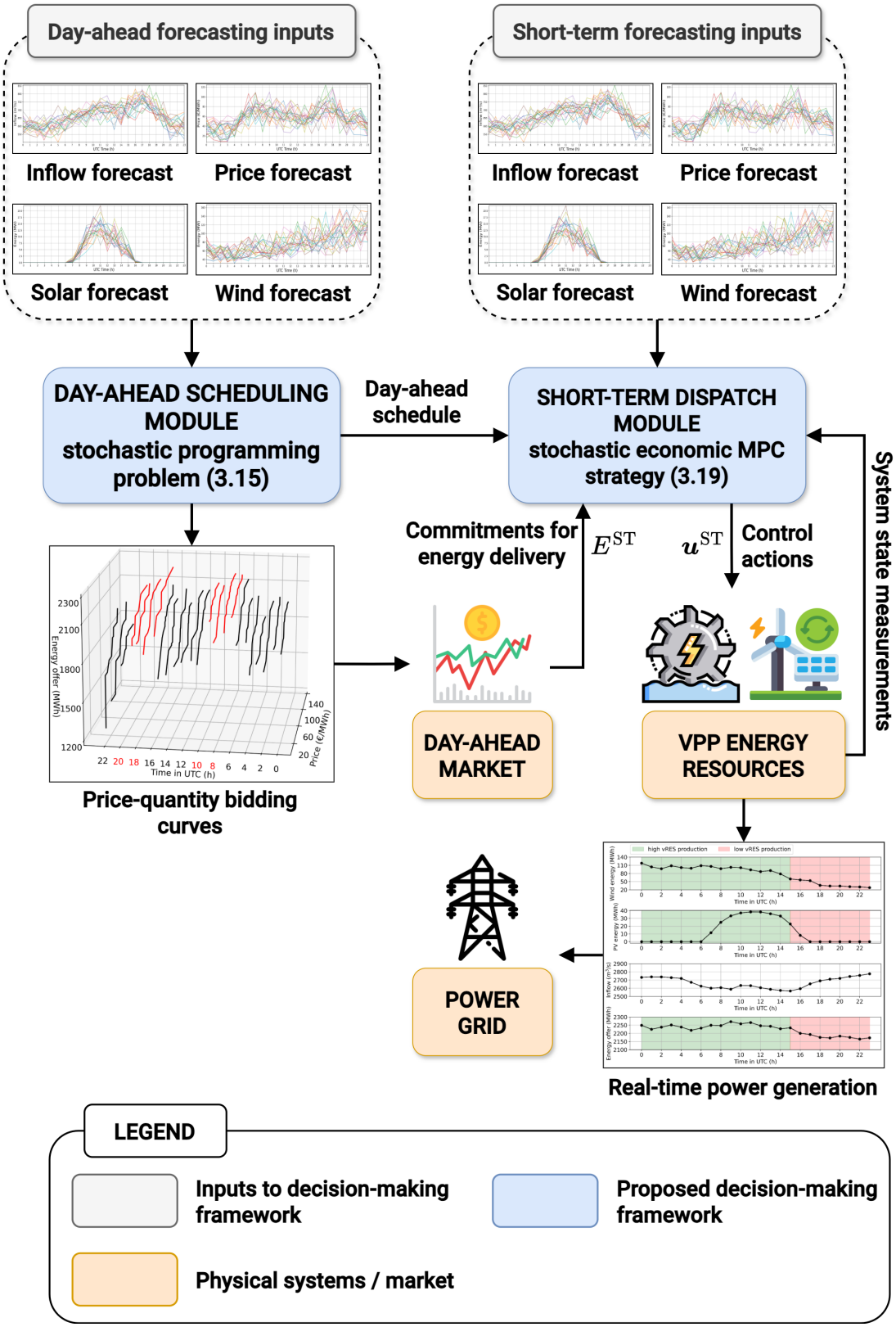

Figure 3.5: The proposed fully stochastic, scenario-based, two-level decision-making framework for optimizing complex VPPs participation in the day-ahead market.

Similar considerations apply to the dispatch module (3.19). Naturally, the spatial and scenario coupling constraints cannot simply be neglected in the original optimization models, as doing so would potentially result in a new solution that could be even infeasible in the feasible space of the original stochastic programs. However, building on this observation about the potential separability of the decision-making framework in both spatial and scenario dimensions, Chapter 4 is dedicated to proposing methods for decomposing the problem and providing a distributed solution for managing the complex VPP.

3.3.4 Evaluating the Proposed Energy Management Strategy for Complex Virtual Power Plants

The proposed energy management strategy for complex VPPs in the energy market consists of a comprehensive two-level stochastic decision-making framework. At the first level, the scheduling module addresses the day-ahead market bidding problem through a scenario-based stochastic programming model. The second level involves a dispatch controller, which refines operational decisions in real time using scenario-based stochastic economic MPC. The effectiveness of this strategy is evaluated using two complementary methods: *out-of-sample validation* and *ex-post evaluation*. Out-of-sample validation is used to determine the number of scenarios to be included in the stochastic programming problems at both the scheduling and dispatch levels of the framework. Ex-post evaluation assesses the performance of the two-level strategy once the uncertainties have materialized and been observed.

In the out-of-sample validation process, multiple sets of scenarios are generated based on the original dataset provided by Compagnie Nationale du Rhône for the primary case study of this thesis. Separate sets of *training scenarios* (also referred to as *in-sample* data) are used to derive the decisions at both the scheduling and dispatch stages. After deriving these decisions, additional testing scenarios (also referred to as *out-of-sample* data) are generated to evaluate their effectiveness under unforeseen outcomes of uncertainty. This process can be repeated iteratively with different sets of training scenarios, each containing varying numbers of scenarios, to analyze the sensitivity of the strategy to the number of scenarios used in the stochastic programming models.

Following out-of-sample validation, ex-post evaluation is conducted to assess the quality of the solutions against actual observed data. This step provides a retrospective analysis of how the decisions made through the stochastic models performed in real-world conditions, including market outcomes and system behavior.

A visual representation of the evaluation process is presented in Fig. 3.6. Further details on these procedures are outlined below.

3.3.4.1 Out-of-Sample Validation

Out-of-sample validation is a key component of evaluating the robustness of scenario-based stochastic optimization strategies. In a stochastic decision-making framework, decisions are made based on scenarios representing uncertain variables such as vRES power generation, market

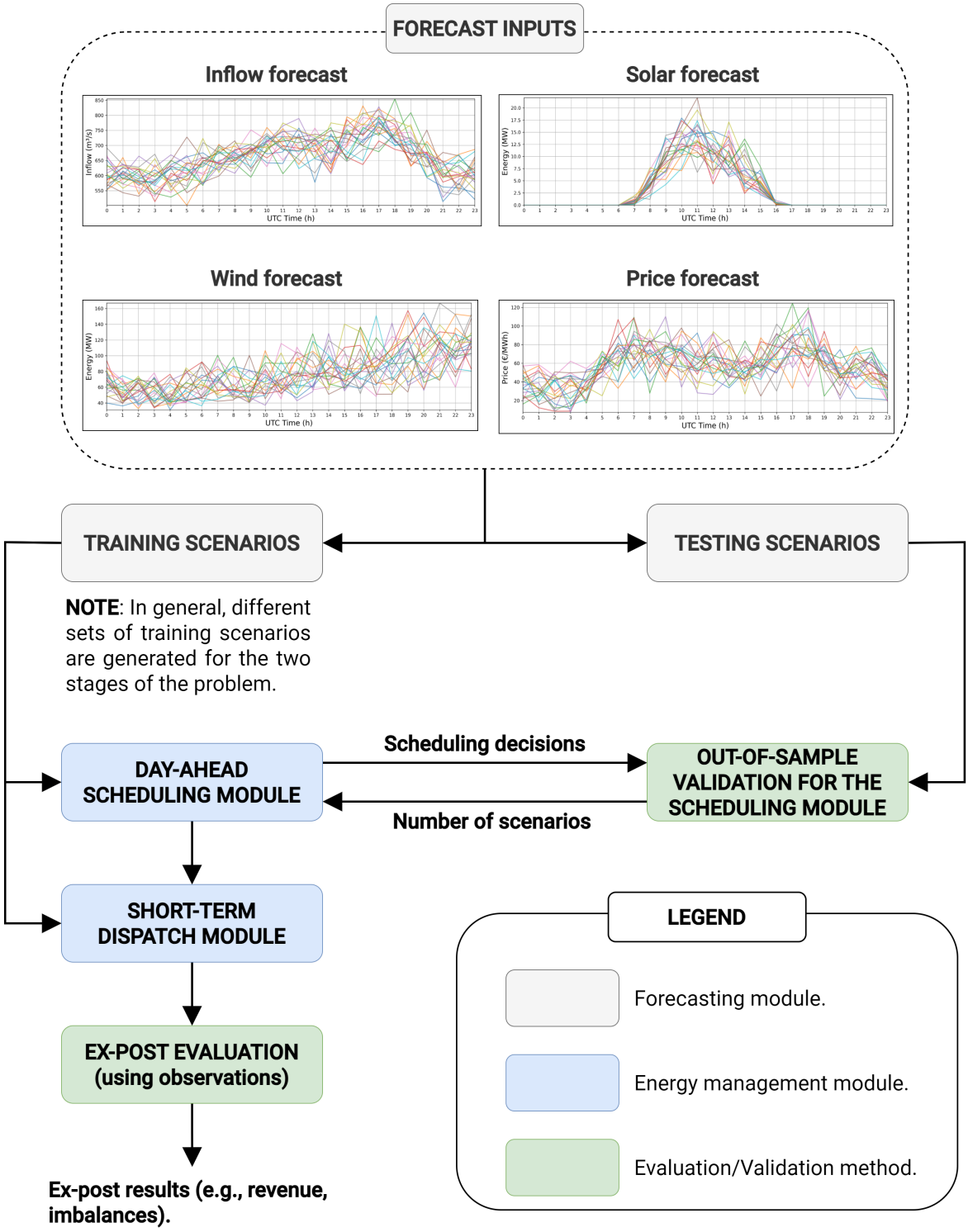

Figure 3.6: A visual representation of the evaluation process adopted in this chapter.

prices, and hydrological conditions. While these scenarios are derived from historical data or forecasts, the validation process ensures that the strategy performs well not only on the data used for scenario generation but also on unseen data.

The primary objective of out-of-sample validation in this context is to assess the sensitivity

of the proposed energy management strategy to the number of scenarios used in the stochastic scheduling and dispatch modules. Scenarios are crucial in capturing the uncertainty inherent in the problem at hand. However, increasing the number of scenarios improves accuracy at the cost of higher computational complexity. Hence, a balance must be struck between solution quality and computational feasibility.

For out-of-sample validation, the stochastic programming model is initially trained on a set of training scenarios (*in-sample scenarios*). The training process involves deriving optimal decisions at both the scheduling and dispatch levels using these training scenarios. Once the model is trained, additional sets of scenarios, not used during training, are generated to serve as testing scenarios (*out-of-sample scenarios*). These testing scenarios are then used to assess the performance of the optimization strategies. This evaluation is done by computing the error between the training and testing solutions. This error is compute by measuring the difference between training objective function value, i.e., the objective function value obtained when using training scenarios and optimal decisions from the training process, and testing objective, i.e., the objective function value obtained when using testing scenarios and optimal decisions from the training process. The method not only measures the robustness of the scheduling and dispatch strategies under unseen conditions but also determines the number of scenarios required to adequately capture uncertainty for reliable decision-making.

The following steps outline the **out-of-sample validation procedure** employed in this thesis to assess the proposed scheduling and dispatch strategies for solving various instances of the integrated bidding problem. Considering the generic formulation of a two-stage stochastic programming problem presented in (3.4), the out-of-sample validation is structured as follows:

1. From the original set of scenarios, define a *training set of scenarios*, denoted by $\boldsymbol{\Omega}^{\mathbf{tra}}$, and a *testing set of scenarios*, denoted by $\boldsymbol{\Omega}^{\mathbf{test}}$, with associated probabilities $\{P_{\omega}^{\mathrm{tra}}\}_{\omega\in\boldsymbol{\Omega}^{\mathbf{tra}}}$, and $\{P_{\omega}^{\mathrm{test}}\}_{\omega\in\boldsymbol{\Omega}^{\mathbf{test}}}$, respectively. Typically, the cardinality of the testing set is significantly larger than that of the training set, i.e., $\left|\boldsymbol{\Omega}^{\mathbf{test}}\right| \gg \left|\boldsymbol{\Omega}^{\mathbf{tra}}\right|$.

2. Solve the optimization problem (3.4) using the training set of scenarios. The optimal first-stage and second-stage decisions obtained from training are denoted by $\boldsymbol{x}^{\mathbf{tra}}$ and $\boldsymbol{y}_{\omega}^{\mathbf{tra}}$, respectively. The optimal objective function value derived from the training procedure, denoted by J^{tra}, is computed as:

$$J^{\mathrm{tra}}\left(\boldsymbol{x}^{\mathbf{tra}}\right) := f^{\mathrm{F}}\left(\boldsymbol{x}^{\mathbf{tra}}\right) + \sum_{\omega\in\boldsymbol{\Omega}^{\mathbf{tra}}} P_{\omega}^{\mathrm{tra}} f^{\mathrm{S}}\left(\boldsymbol{x}^{\mathbf{tra}}, \boldsymbol{y}_{\omega}^{\mathbf{tra}}, \hat{\boldsymbol{\xi}}_{\omega}\right). \tag{3.25}$$

3. To assess the quality of J^{tra}, this objective function value is compared with that of the testing, denoted by J^{test}, and defined as follows:

$$J^{\mathrm{test}}\left(\boldsymbol{x}^{\mathbf{tra}}\right) := f^{\mathrm{F}}\left(\boldsymbol{x}^{\mathbf{tra}}\right) + \sum_{\omega\in\boldsymbol{\Omega}^{\mathbf{test}}} P_{\omega}^{\mathrm{test}} f^{\mathrm{S}}\left(\boldsymbol{x}^{\mathbf{tra}}, \boldsymbol{y}_{\omega}^{\mathbf{test}}, \hat{\boldsymbol{\xi}}_{\omega}\right), \tag{3.26}$$

where $\boldsymbol{y}_{\omega}^{\mathbf{test}}$ represents the second-stage decisions derived by solving the original problem (3.4) with fixed first-stage variables $\boldsymbol{x}^{\mathbf{tra}}$, and considering the testing set of scenarios $\boldsymbol{\Omega}^{\mathbf{test}}$.

4. If $J^{\text{test}} \approx J^{\text{tra}}$, confidence is increased that $\boldsymbol{x}^{\mathbf{tra}} \approx \boldsymbol{x}^{\star}$, where $\boldsymbol{x}^{\star}$ denotes the first-stage decisions obtained by solving (3.4) for an infinite set of scenarios, i.e., a set that represents all possible outcomes of the uncertainty.

5. Else, the selected training set of scenarios is unable to adequately represent the possible outcomes of the uncertainty. This discrepancy may arise for several reasons, particularly if the number of training scenarios is too low, or if the method used to select the training scenarios from the original set of scenarios is inadequate. As the focus of this thesis is on the optimization and control methods for managing complex VPPs, only the former case is analyzed, without relying on *scenario reduction methods* [179] that could be implemented to improve the performance of the training procedure. In other words, $\left|\boldsymbol{\Omega}^{\mathbf{tra}}\right|$ is increased and the out-of-sample validation procedure is repeated.

For example, in a case study involving a simple VPP comprising vRES and storage systems, out-of-sample validation helps to quantify how variations in solar and wind forecasts impact the dispatch of the storage systems. The goal is to ensure that the energy management strategy remains flexible and responsive to fluctuations in renewable output even when presented with forecast errors not encountered during the initial scenario generation phase.

In the more complex case of cascaded hydropower plants integrated into a VPP, out-of-sample validation gains particular importance. Hydrological uncertainties, such as inflow forecasts and water storage levels, are critical to the decision-making process. Validation against out-of-sample scenarios serves to assess the strategy's robustness in managing hydropower flexibility and coordinating the interaction between renewable energy sources (e.g., wind or solar) and hydropower. The results of this process inform the determination of the desired number of scenarios required for both the day-ahead bidding phase and real-time dispatch, ensuring the strategy performs effectively under diverse future conditions. For the cascaded hydropower system, this involves evaluating whether water flows can be efficiently managed to maintain profitability and system stability amidst fluctuating renewable generation and market prices.

Out-of-sample validation also plays a key role in identifying the trade-offs between accuracy and computational burden. As the number of scenarios increases, the solution typically becomes more resilient to uncertainty but entails higher computational costs and complexity. By analyzing the system's performance across different scenario sets, it becomes possible to identify the point at which additional scenarios yield diminishing returns in terms of performance improvement. For both simple and complex VPP configurations, this analysis is critical for balancing decision quality with practical feasibility in real-world applications.

3.3.4.2 Ex-post Evaluation

Ex-post evaluation serves as the second critical evaluation method and provides a retrospective analysis of how the energy management strategy performs under real market and operational conditions. This method is particularly focused on analyzing key performance indicators such as profit, imbalances, and operational behavior, providing valuable insights into the practical efficiency of the proposed strategy after market settlement and system operation.

The ex-post evaluation method involves first solving the energy management problem using forecasts. Once the actual uncertainty is realized and observed, these observations are then used to recompute and simulate the system's ex-post behavior. Key performance indicators are subsequently evaluated based on this simulation. This process allows for a comprehensive assessment of the decision-making framework, examining both the forecasting quality and the efficiency of the proposed scheduling and dispatch methods.

A key metric in the ex-post evaluation conducted in this thesis is market profit. The VPP's profit generation performance is closely tied to the alignment between its bidding strategy and actual market conditions. In the day-ahead market, bids are placed based on forecasted scenarios, and any discrepancies between forecasted and realized prices can result in financial imbalances.

For example, in the case of complex cascaded hydropower systems, ex-post evaluation is used to assess how hydropower flexibility was utilized in practice. The hydropower plants must coordinate with vRES to meet market commitments while considering water storage levels and environmental constraints. Any imbalance between forecasted hydrological conditions and actual inflows, for example, could lead to over- or under-utilization of water resources, impacting both profit and system stability. Ex-post evaluation quantifies these imbalances and helps identify strategies for reducing financial penalties or operational inefficiencies due to forecast errors.

In addition to profit and imbalance metrics, ex-post evaluation examines system behavior, focusing on how effectively the system responded to real-time conditions that deviated from forecasted scenarios. For instance, the analysis may assess whether the storage system was dispatched efficiently in response to unforeseen fluctuations in vRES power generation. In the hydropower system, the evaluation considers whether water flows and power output adhered to operational constraints while optimizing market participation. These insights are crucial for refining the energy management strategy, enabling adaptation to the dynamic nature of renewable energy generation and market conditions.

Ex-post evaluation is indispensable for validating the operational efficiency of the proposed strategy in real-world market environments. The feedback from this evaluation process informs iterative improvements to the bidding and dispatch modules, ensuring the energy management system remains responsive and profitable under varying market and system conditions.

3.4 The Case Study of Compagnie Nationale du Rhône

This section focuses on applying the modeling and decision-making methods introduced in Section 3.3 to the case study of Compagnie Nationale du Rhône, detailed in Section 2.3. It begins by exploring the application of the generic modeling approach presented in Section 3.3.2 to the Compagnie Nationale du Rhône case study. Next, it discusses how the general optimization problem addressed by Compagnie Nationale du Rhône for managing its complex VPP can be reformulated in the form of the generic scheduling and dispatch problems outlined in Section 3.3.3. The section concludes by providing examples of the simulated outcomes when applying the proposed methods, including an ex-post evaluation to assess the aggregator's performance in the market, out-of-sample validation to determine the minimum number of scenarios necessary to

effectively model underlying uncertainties, and sensitivity analysis to assess the robustness of the proposed method to variations in the VPP portfolio and market prices.

The primary aims of the proposed simulations are twofold. First, they seek to validate the proposed modeling approach and decision-making framework, as defined by (3.15) and (3.19), within the context of the real-world complex VPP operated by Compagnie Nationale du Rhône. Second, they address the first research question of this thesis (referred to as **research question Q1** in Chapter 1), which focuses on evaluating the benefits of a combined operation of Compagnie Nationale du Rhône's assets compared to their current uncoordinated participation in the market.

3.4.1 Application of the Proposed Modeling and Energy Management Strategies to the Case Study of Compagnie Nationale du Rhône

As discussed in Section 2.3, Compagnie Nationale du Rhône currently operates its portfolio of energy resources, which includes wind and solar farms alongside run-of-the-river cascaded hydropower, independently. In other words, vRES are managed separately from the hydropower assets. The aim of the simulations presented here, based on the modeling and decision-making approaches described in Section 3.3, is to show the potential benefits of jointly operating these resources in the energy market. A comparison between the current state (**uncoordinated operation** of vRES and hydropower) and the proposed approach (**coordinated operation**) is illustrated in Fig. 3.7. As shown in the figure, the proposed generic modeling framework for complex VPPs can be effectively applied to the Compagnie Nationale du Rhône case study. In this case, as the energy resources are connected to the upstream grid at separate points of common coupling, two distinct clusters can be identified for wind and solar units, alongside a set of clusters corresponding to the hydropower plants integrated into the VPP (three hydropower assets in the example shown).

As thoroughly discussed in Section 3.3, identifying the coupling constraints in the optimization problems addressed in this thesis is particularly relevant. Specifically, the coordinated operation of Compagnie Nationale du Rhône's energy units in the day-ahead market involves three sources of coupling, detailed in the figure:

- *Spatial coupling* due to the hydraulic links between the hydropower assets in the cascade.
- *Spatial coupling* related to power balancing within the VPP.
- *Scenario coupling* to ensure consistency among the scenarios representing the uncertainty in market prices, water inflows, and vRES generation.

It is important to note that the set of coupling constraints differs significantly between the two energy management structures depicted in Fig. 3.7. In the uncoordinated operation of Compagnie Nationale du Rhône's assets, only the hydraulic coupling among the cascaded hydropower plants is considered, while the other coupling constraints are limited to the management of the cascaded hydropower system. However, under the coordinated approach, while accounting for

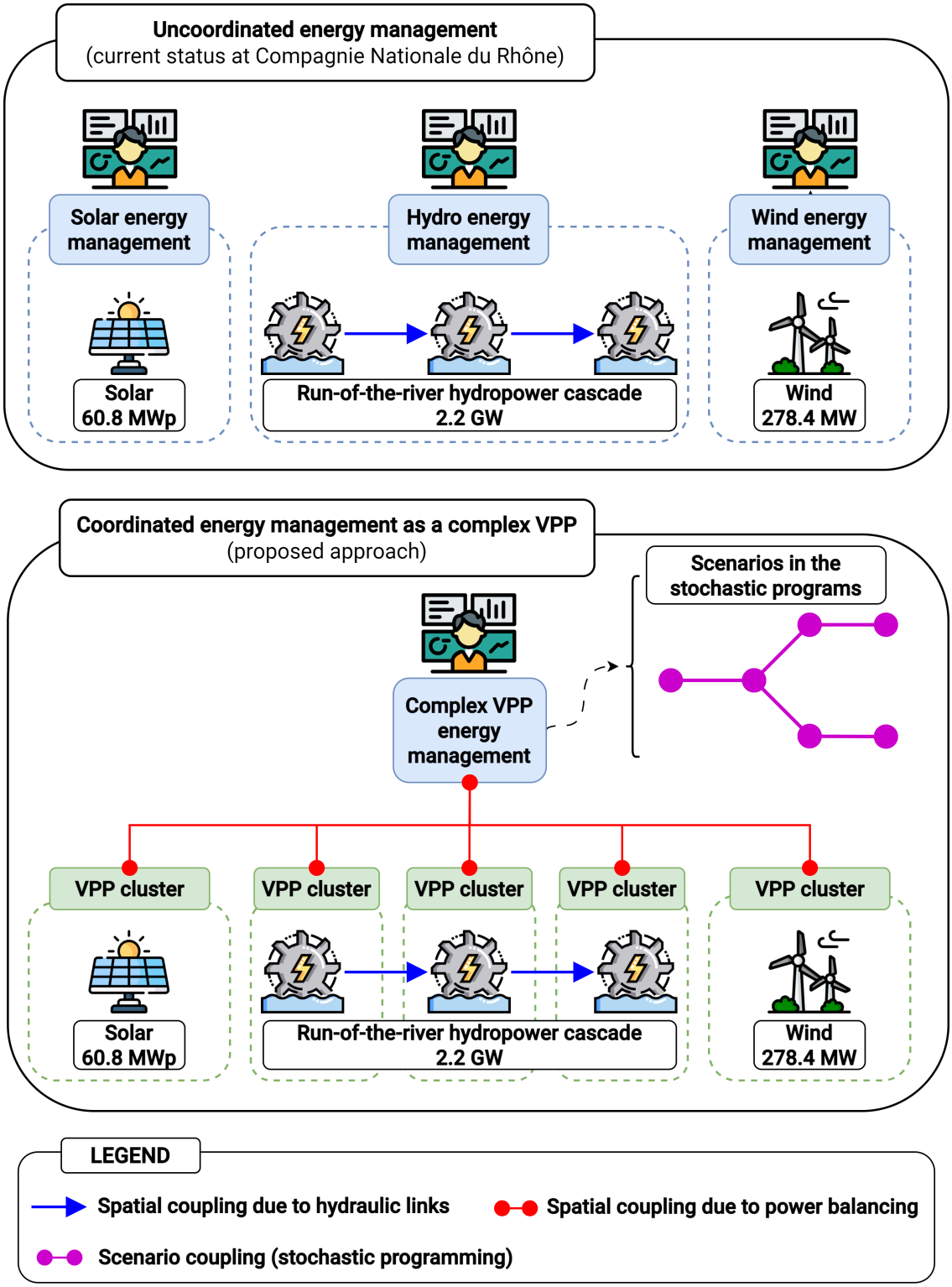

Figure 3.7: Comparison between the current strategy of Compagnie Nationale du Rhône, characterized by uncoordinated energy management (top part of the figure), and the proposed coordinated energy management strategy (bottom part of the figure). Following to the proposed modeling approach, detailed in Section 3.3, the VPP is organized into distinct clusters while clearly identifying the coupling constraints of the coordinated energy management problem.

the hydraulic coupling remains essential, the scenario coupling and the spatial coupling associated with the power balancing extend to a broader and more complex aggregation of energy units, now including both vRES and hydropower plants. This increases the complexity of the optimization problem significantly. The need for scalable solutions to address this complexity justifies the investigation of distributed methods in the following chapter.

The coordinated operation of the vRES (wind and solar units) and the cascaded hydropower system managed by Compagnie Nationale du Rhône can be formulated as a MILP problem, utilizing scenario-based stochastic programming to handle uncertainties (market prices, vRES power generation and water inflows in the cascaded system):

$$\underset{\boldsymbol{z}}{\text{argmin}} \quad J \tag{3.27a}$$

$$\text{subject to} \quad \left(\sum_{n\in\boldsymbol{N}} p^{\mathrm{H}}_{n,\omega,t} + \hat{P}^{\mathrm{W}}_{\omega,t} + \hat{P}^{\mathrm{S}}_{\omega,t}\right)\Delta_T - e_{\omega,t} - \delta^{\mathrm{E}\downarrow}_{\omega,t} + \delta^{\mathrm{E}\uparrow}_{\omega,t} = 0,\ \forall\omega,\forall t, \tag{3.27b}$$

$$\left(\hat{\pi}^{\mathrm{E}}_{\omega,t} - \hat{\pi}^{\mathrm{E}}_{\omega',t}\right)\left(e_{\omega,t} - e_{\omega',t}\right) \geq 0,\ \forall\omega' \in \boldsymbol{\Omega}\setminus\{\omega\},\ \forall\omega,\forall t, \tag{3.27c}$$

$$z^{\mathrm{fbl}}_{n,\omega,t} = z^{\mathrm{fbl}}_{n,\omega,t-1} + \frac{\left(q^{\mathrm{in}}_{n,\omega,t} - q^{\mathrm{out}}_{n,\omega,t}\right)\Delta_T}{S_{n,\omega,t}},\ \forall n,\forall\omega,\forall t, \tag{3.27d}$$

$$z^{\mathrm{fbl}}_{n,\omega,0} = z^{\mathrm{fbl}}_{n,\omega,|\boldsymbol{T}|} = Z^{\mathrm{fbl},0}_{n},\ \forall n,\forall\omega, \tag{3.27e}$$

$$q^{\mathrm{in}}_{n,\omega,t} = q^{\mathrm{br}}_{n-1,\omega,t-\tau^{\mathrm{br}}_{n-1,n}} + q^{\mathrm{tr}}_{n-1,\omega,t-\tau^{\mathrm{tr}}_{n-1,n}} + \hat{Q}^{\mathrm{ext}}_{n,\omega,t},\ \forall n,\forall\omega,\forall t, \tag{3.27f}$$

$$q^{\mathrm{out}}_{n,\omega,t} = q^{\mathrm{br}}_{n,\omega,t} + q^{\mathrm{tr}}_{n,\omega,t},\ \forall n,\forall\omega,\forall t, \tag{3.27g}$$

$$q^{\mathrm{in}}_{n,\omega,t} \geq b^{\mathrm{oc}}_{n,\omega,t,s} Q^{\mathrm{in}}_{n,s},\ \forall s \in \boldsymbol{S}^{\mathbf{oc}}_{n},\forall n,\forall\omega,\forall t, \tag{3.27h}$$

$$q^{\mathrm{in}}_{n,\omega,t} < b^{\mathrm{oc}}_{n,\omega,t,s} Q^{\mathrm{in}}_{n,s+1} + \left(1 - b^{\mathrm{oc}}_{n,\omega,t,s}\right) M_1,\ \forall s \in \boldsymbol{S}^{\mathbf{oc}}_{n},\forall n,\forall\omega,\forall t, \tag{3.27i}$$

$$\sum_{s\in\boldsymbol{S}^{\mathbf{oc}}_{n}} b^{\mathrm{oc}}_{n,\omega,t,s} = 1,\ \forall n,\forall\omega,\forall t, \tag{3.27j}$$

$$\sum_{s\in\boldsymbol{S}^{\mathbf{oc}}_{n}} \underline{Z}^{\mathrm{fbl}}_{n,s} b^{\mathrm{oc}}_{n,\omega,t,s} \leq z^{\mathrm{fbl}}_{n,\omega,t} \leq \sum_{s\in\boldsymbol{S}^{\mathbf{oc}}_{n}} \overline{Z}^{\mathrm{fbl}}_{n,s} b^{\mathrm{oc}}_{n,\omega,t,s},\ \forall n,\forall\omega,\forall t, \tag{3.27k}$$

$$q^{\mathrm{tr}}_{n,\omega,t} - q^{\mathrm{tr}}_{n,\omega,t-1} \leq \Delta q^{\mathrm{tr}}_{n},\ \forall n,\forall\omega,\forall t, \tag{3.27l}$$

$$q^{\mathrm{tr}}_{n,\omega,t-1} - q^{\mathrm{tr}}_{n,\omega,t} \leq \Delta q^{\mathrm{tr}}_{n},\ \forall n,\forall\omega,\forall t, \tag{3.27m}$$

$$b^{\mathrm{br}}_{n,\omega,t}\underline{Q}^{\mathrm{br}}_{n} \leq q^{\mathrm{br}}_{n,\omega,t} \leq b^{\mathrm{br}}_{n,\omega,t} M_2,\ \forall n,\forall\omega,\forall t, \tag{3.27n}$$

$$b^{\mathrm{br}}_{n,\omega,t} \leq 1 - \frac{\sum_{s\in\boldsymbol{S}^{\mathbf{oc}}_{n}} \overline{Z}^{\mathrm{fbl}}_{n,s} b^{\mathrm{oc}}_{n,\omega,t,s} - z^{\mathrm{fbl}}_{n,\omega,t}}{\max\left(\left\{\overline{Z}^{\mathrm{fbl}}_{n,s}\right\}_{s\in\boldsymbol{S}^{\mathbf{oc}}_{n}}\right)},\ \forall n,\forall\omega,\forall t, \tag{3.27o}$$

$$\underline{Q}^{\mathrm{tr}}_{n} \leq q^{\mathrm{tr}}_{n,\omega,t} \leq \overline{Q}^{\mathrm{tr}}_{n},\ \forall n,\forall\omega,\forall t, \tag{3.27p}$$

$$p^{\mathrm{H}}_{n,\omega,t} \geq 10^{-6} w\, g\, \eta^{\mathrm{tr}}_{n}\left(\underline{Q}^{\mathrm{tr}}_{n} h_{n,\omega,t} + \underline{H}_{n} q^{\mathrm{tr}}_{n,\omega,t} - \underline{Q}^{\mathrm{tr}}_{n}\underline{H}_{n}\right),\ \forall n,\forall\omega,\forall t, \tag{3.27q}$$

$$p^{\mathrm{H}}_{n,\omega,t} \geq 10^{-6} w\, g\, \eta^{\mathrm{tr}}_{n}\left(\overline{Q}^{\mathrm{tr}}_{n} h_{n,\omega,t} + \overline{H}_{n} q^{\mathrm{tr}}_{n,\omega,t} - \overline{Q}^{\mathrm{tr}}_{n}\overline{H}_{n}\right),\ \forall n,\forall\omega,\forall t, \tag{3.27r}$$

$$p^{\mathrm{H}}_{n,\omega,t} \leq 10^{-6} w\, g\, \eta^{\mathrm{tr}}_{n}\left(\underline{Q}^{\mathrm{tr}}_{n} h_{n,\omega,t} + \overline{H}_{n} q^{\mathrm{tr}}_{n,\omega,t} - \underline{Q}^{\mathrm{tr}}_{n}\overline{H}_{n}\right),\ \forall n,\forall\omega,\forall t, \tag{3.27s}$$

$$p^{\mathrm{H}}_{n,\omega,t} \leq 10^{-6} w\, g\, \eta^{\mathrm{tr}}_{n}\left(\overline{Q}^{\mathrm{tr}}_{n} h_{n,\omega,t} + \underline{H}_{n} q^{\mathrm{tr}}_{n,\omega,t} - \overline{Q}^{tr}_{n}\underline{H}_{n}\right),\ \forall n,\forall\omega,\forall t, \tag{3.27t}$$

$$h_{n,\omega,t} = z^{\text{fbl}}_{n,\omega,t} - Z^{\text{tlr}}_{n},\ \forall n, \forall \omega, \forall t, \tag{3.27u}$$

$$0 \leq p^{\text{H}}_{n,\omega,t} \leq \overline{P}^{\text{H}}_{n,\omega,t},\ \forall n, \forall \omega, \forall t. \tag{3.27v}$$

Here, J represents the objective function, and the set of decision variables, $\boldsymbol{z}$, is defined as:

$$\boldsymbol{z} := \left\{ e_{\omega,t}, \delta^{\text{E}\uparrow}_{\omega,t}, \delta^{\text{E}\downarrow}_{\omega,t}, q^{\text{tr}}_{n,\omega,t}, q^{\text{br}}_{n,\omega,t}, z^{\text{fbl}}_{n,\omega,t}, p^{\text{H}}_{n,\omega,t}, b^{\text{br}}_{n,\omega,t}, b^{\text{oc}}_{n,\omega,t,s} \right\}_{s \in \boldsymbol{S}^{\text{oc}}_{n}, n \in \boldsymbol{N}, \omega \in \boldsymbol{\Omega}, t \in \boldsymbol{T}}. \tag{3.28}$$

A detailed explanation of all constraints in the optimization model (3.27) is provided in Section 2.3.4.

Clearly, the model (3.27) can be directly reformulated within the generic optimization models (3.15) and (3.19), provided for the scheduling and dispatch of a complex VPP. Specifically, the power balancing constraint in (3.27b) translates into the generic formulations of the power balancing constraints represented by (3.15b) in the scheduling problem and (3.19b) in the dispatch problem. Similarly, the scenario coupling constraints in (3.27c) align with those in the generic formulation of the complex VPP scheduling, described by (3.15c). When solving the MPC optimization problem during the dispatch stage, the scenario coupling constraints of the scheduling problem (3.27c) are replaced by (3.19c), ensuring consistency in the first control action of the control problem (3.19). Additionally, the hydraulic coupling among hydropower assets, given by (3.27d)-(3.27e), along with the individual dynamics of each hydropower plant in (3.27f)-(3.27v) correspond to the set of constraints (3.15d) and (3.19d) in the proposed generic optimization models. The objective function J of (3.27) corresponds to (3.18) when solving the scheduling problem (3.15) and to (3.23) when addressing the dispatch problem (3.19). For this case study, operational cost terms are neglected in the objective function of both scheduling and dispatch phases.

Once the problem is reformulated according to the generic formulations outlined in Section 3.3.3, the optimal operation of the complex VPP operated by Compagnie Nationale du Rhône can be effectively addressed using the scenario-based stochastic two-level decision-making framework described in Section 3.3.3 and illustrated in Fig. 3.5. The results obtained when applying this approach to the case study under investigation are presented in the following section.

3.4.2 Results from the Case Study of Compagnie Nationale du Rhône

This section presents the results from simulating the application of the proposed scenario-based stochastic two-level decision-making framework, as described in Section 3.3.3 and depicted in Fig. 3.5, to the case study of Compagnie Nationale du Rhône.

The simulations span a three-month period (February–April 2017), covering diverse water inflow conditions. For each day in the simulation, the scheduling problem (3.15) is first solved to compute bids for the day-ahead market, followed by solving the dispatch problem (3.19) to manage VPP operations in near real-time. The scheduling problem is solved with an hourly resolution, while the MPC operates with control intervals of 10 minutes and a prediction horizon of 24 hours. As detailed in Section 2.3, the simulations focus solely on the lower Rhône cascade (see Table 2.3), which includes the final 12 hydropower assets in the cascaded system operated

Uncertain parameter		Average hourly values (standard deviation)		
Name	**Symbol**	**February**	**March**	**April**
Energy price	$\hat{\pi}^{\mathrm{E}}$ (€/MWh)	51.1 (12.4)	35.4 (9.8)	34.7 (8.8)
Price of positive imb.	$\hat{\pi}^{\mathrm{E}\uparrow}$ (€/MWh)	58.1 (13.9)	38.6 (10.7)	38.6 (9.7)
Price of negative imb.	$\hat{\pi}^{\mathrm{E}\downarrow}$ (€/MWh)	49.1 (12.8)	32.3 (8.4)	28.5 (8.3)
External water inflow	$\hat{Q}^{\mathrm{ext}}$ (m^3/s)	1367.8 (456.1)	1932.2 (549.3)	798.68 (219.0)
Solar power output	$\hat{P}^{\mathrm{S}}$ (MWh)	6.2 (10.7)	9.6 (14.1)	13.5 (17.4)
Wind power output	$\hat{P}^{\mathrm{W}}$ (MWh)	91.5 (61.9)	84.6 (57.1)	52.8 (29.5)

Table 3.3: Characterization of day-ahead forecasts generated by Compagnie Nationale du Rhône, used as inputs for the proposed decision-making framework.

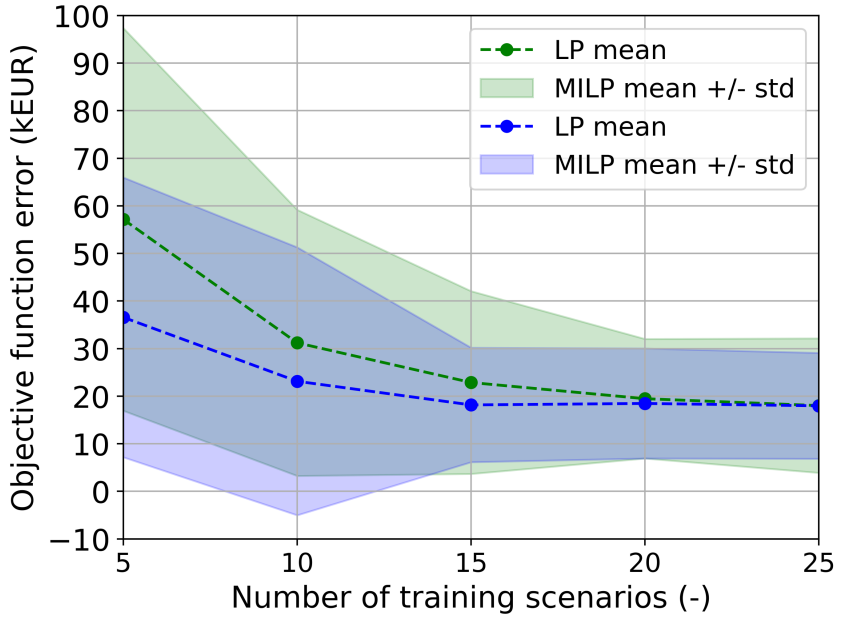

Figure 3.8: Out-of-sample validation results for the scheduling problem, considering 2000 testing scenarios. **MILP**: Mixed-integer programming problem (3.27); **LP**: Linear relaxation of (3.27).

by Compagnie Nationale du Rhône. This selection is due to the fact that only this section of the cascade is utilized for optimizing the aggregator's market participation in real-world operations. In summary, the VPP consists of 12 run-of-the-river hydropower plants with a total installed capacity of 2.2 GW, 6 wind farms (278.4 MW), and 4 solar farms (60.8 MW). A detailed description of the input data, including forecasts provided by the company, is outlined in Section 2.3.6. A characterization of uncertainties in the problem (water inflow, market prices and vRES power generation) is provided in Table 3.3. As detailed in Section 2.3.4, the analysis by Compagnie Nationale du Rhône indicates that uncertainties in vRES, inflows, and prices exhibit minimal correlation and can therefore be treated independently [135]. Thus, separate sets of scenarios are generated for each uncertainty source, randomly combined, and assigned equal probabilities. The simulations use historical French day-ahead market prices, with the algorithms running on an Intel i7 processor and Gurobi 9.5.0 as the solver.

Fig. 3.8 presents the ex-post out-of-sample validation results for the scheduling problem

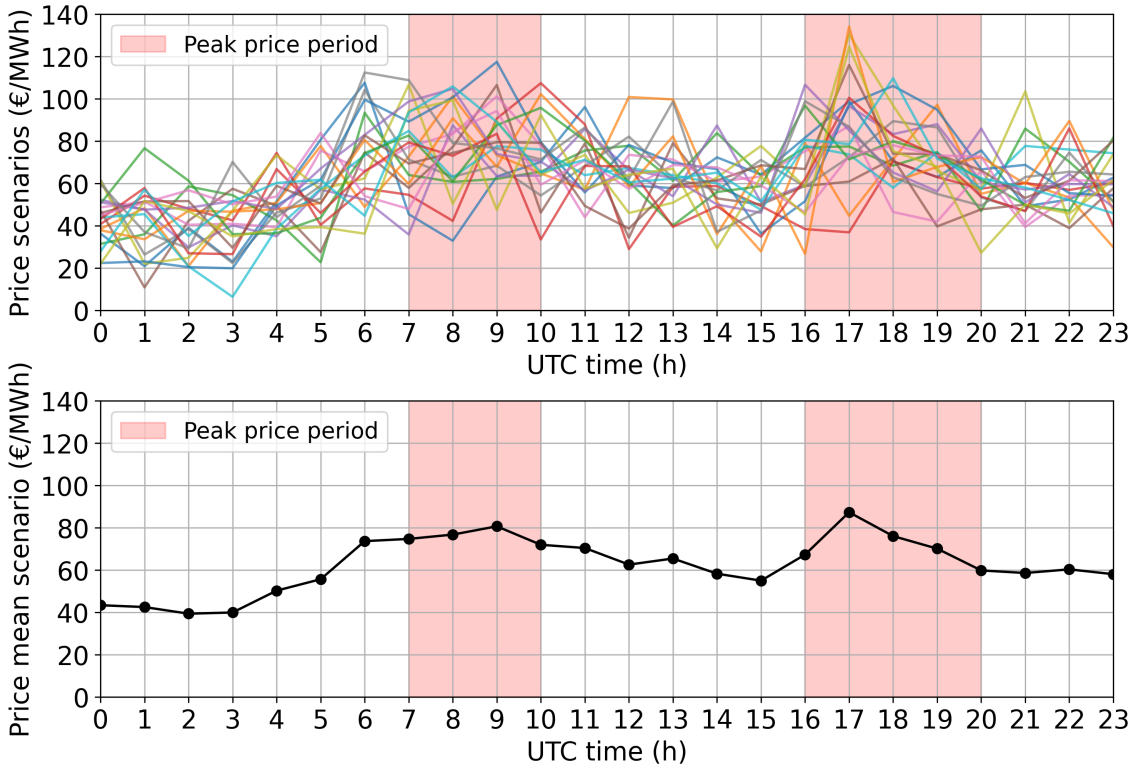

Figure 3.9: Example of day-ahead market energy price forecasting scenarios generated by Compagnie Nationale du Rhône and used as inputs for the proposed day-ahead scheduling strategy (3.15).

(3.15). This standard approach evaluates the performance of the stochastic optimization tool, as detailed in Section 3.3.4.1. The figure shows results obtained using a testing set of 2000 scenarios. The difference between the objective function values from the training and testing sets is referred to as the *objective function error*. Since the problem is solved iteratively over several days, the results are averaged. Fig. 3.8 reports both the average and standard deviation (std) of the error. The findings suggest that 20 scenarios are sufficient to minimize the error for both the mixed-integer problem (3.27) and its linear relaxation. Increasing the number of scenarios beyond 20 raises computational complexity without significantly improving accuracy.

The objective of the first level of the proposed decision-making framework is to minimize the day-ahead objective function J^{DA}, as defined in (3.18). In essence, the goal is to maximize the expected profit of the aggregator in the day-ahead market. Since this case study does not account for any operational costs associated with the energy units in the VPP portfolio, the aggregator's profit maximization relies on leveraging the flexibility of the hydropower cascade to shift the VPP's output to periods with higher expected energy prices, while managing the risk of incurring penalties due to energy imbalances. To achieve this, the aggregator employs the proposed day-ahead scheduling approach to generate price-quantity bidding curves, allowing them to take advantage of favorable market conditions. This behavior is illustrated in Figs. 3.9 and 3.10. As shown in Fig. 3.9, a typical forecast anticipates two distinct energy peak price periods—one in the morning and one in the afternoon. By applying the proposed decision-

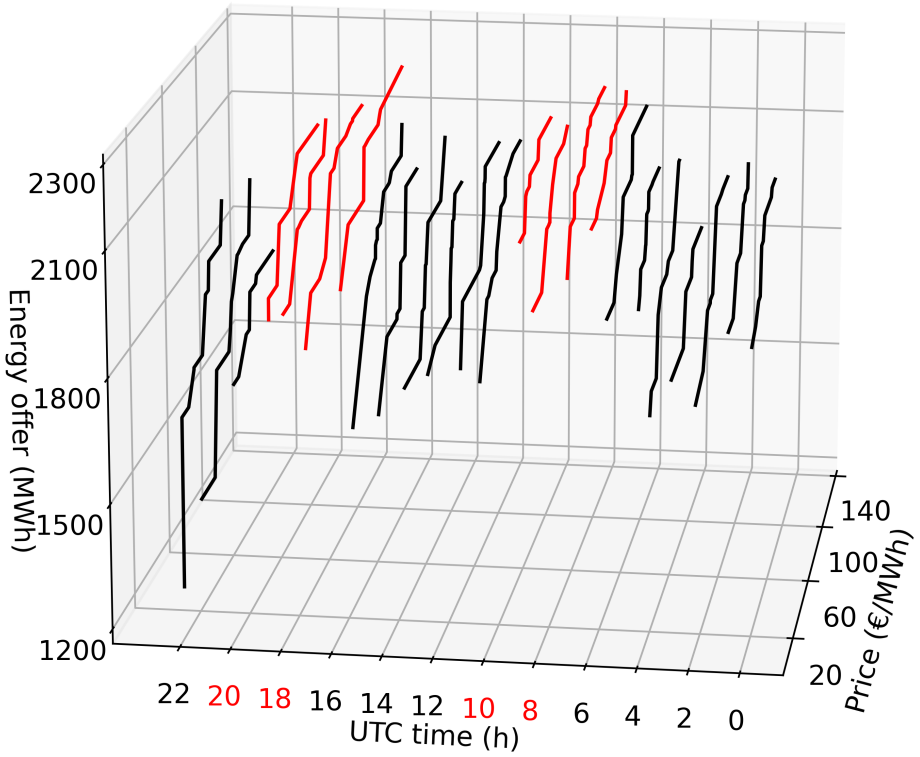

Figure 3.10: Example of price-quantity bidding curves derived via the proposed day-ahead scheduling strategy (3.15). Peak price periods are highlighted in red.

Number of scenarios	Profit per MWh of energy produced (€)	
	Fixed bids	Price-quantity bidding curves
5	33.63	34.38 (+**2.2%**)
10	35.74	36.80 (+**3.0%**)
15	37.82	39.22 (+**3.7%**)
20	39.45	41.22 (+**4.5%**)
25	39.89	41.36 (+**3.7%**)

Table 3.4: Comparison between ex-post profit with fixed hourly bids and price-quantity bidding curves. In brackets, the relative difference with respect to fixed hourly bids.

making framework to these input scenarios, the resulting price-quantity bidding curves typically capitalize on these peak price periods. Fig. 3.10 shows that the scheduling approach effectively coordinates both vRES and hydropower resources to optimize energy bids during these peak price periods. This illustrates not only the proposed strategy's ability to identify and exploit favorable market conditions, but also the potential of the cascaded system, despite the limited storage capacity of run-of-the-river hydropower, to enhance the market value of the VPP. These findings are further generalized in Table 3.4, which indicates that utilizing the proposed bidding optimization method with price-quantity bidding curves can increase the average ex-post market profit of the VPP by up to 4.5% compared to a conventional bidding strategy that employs fixed hourly bids. For a discussion on price-quantity bidding curves in comparison to fixed hourly bids for the day-ahead market, the reader is referred to Section 3.3.2.2.

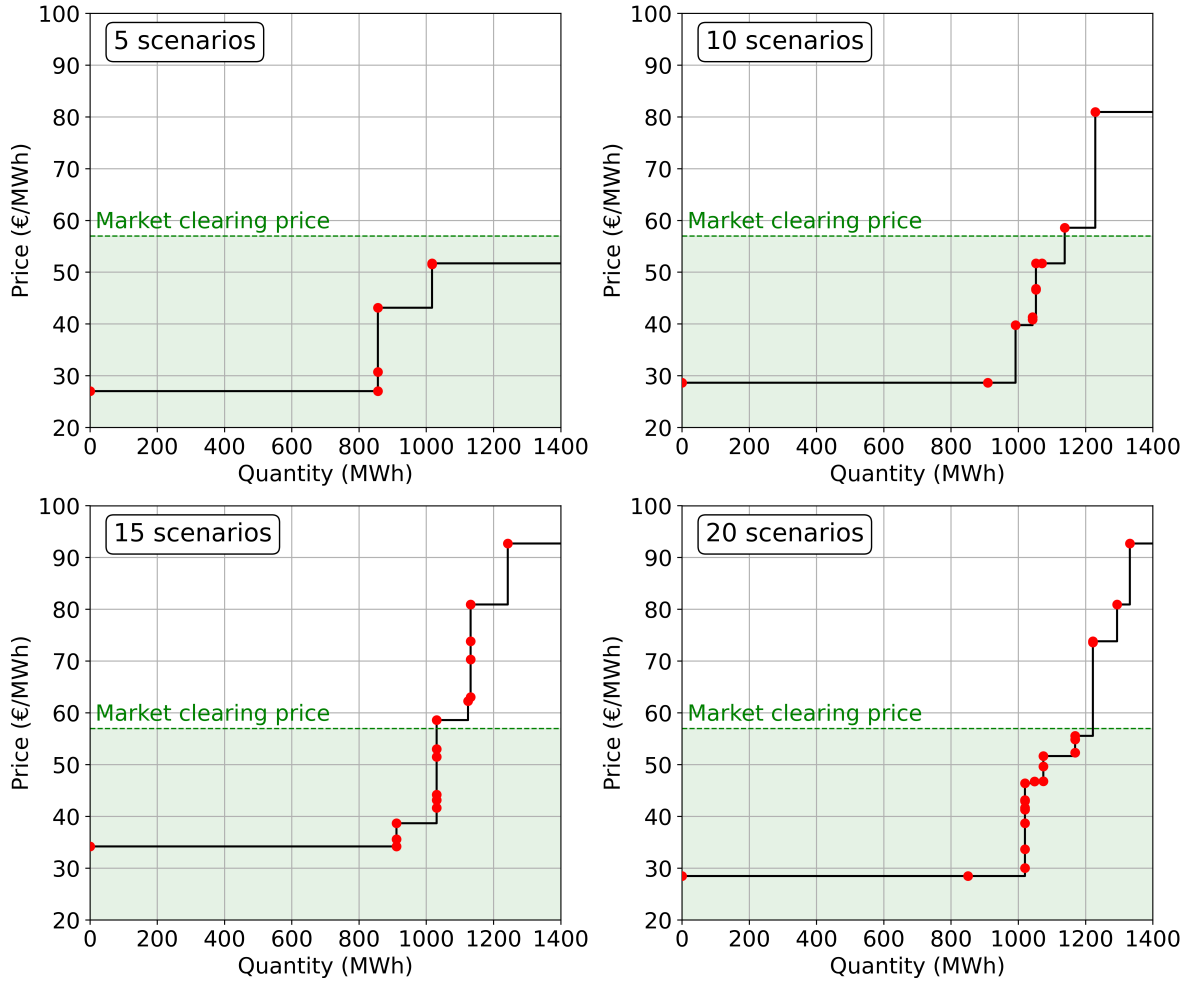

Figure 3.11: Examples of price-quantity bidding curves for one hour when varying numbers of scenarios. This is equivalent to projecting the 3D price-quantity bidding curve from Fig. 3.10 onto the time domain. The breaking points of the curves are highlighted by red dots.

Examples of price-quantity bidding curves for one hour with varying numbers of day-ahead scenarios, i.e., varying $|\mathbf{\Omega^{DA}}|$ in (3.15) , are illustrated in Fig. 3.11. This is equivalent to projecting the 3D price-quantity bidding curve from Fig. 3.10 onto the time domain. The figure highlights the advantage of calculating the energy quantity to be sold in the day-ahead market as a function of forecasted prices, rather than fixing a single quantity for all price levels, as in the fixed hourly bids approach. Specifically, the figure shows that increasing the number of breaking points in the price-quantity curves, corresponding to an increase of the set of day-ahead scenarios, provides the aggregator with greater flexibility. This enables a more adaptive shaping of the offering curve, enhancing its ability to exploit a more detailed representation of uncertainty by incorporating a higher number of potential outcomes. While increasing the number of scenarios enhances the operator's visibility on potential uncertainty outcomes and enables more flexible bidding curves that can improve the aggregator's profit, a larger scenario set inevitably leads to a higher computational burden for the scheduling optimization problem. To preserve the benefits of using a large scenario set while controlling the computational complexity

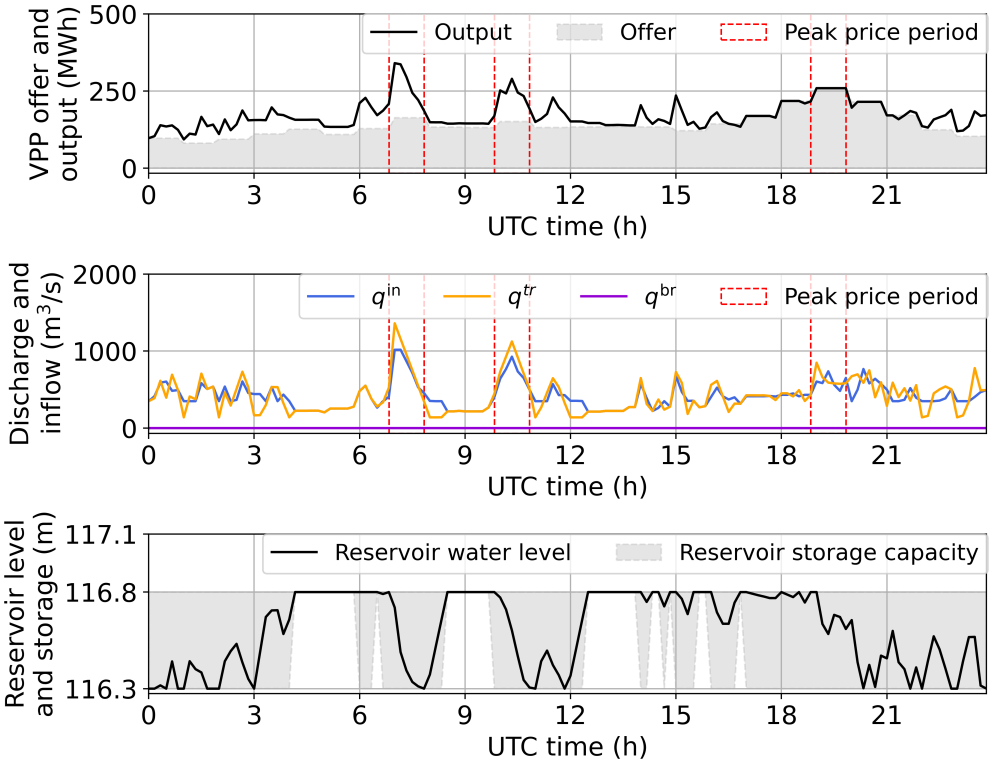

Figure 3.12: Example of real-time operation of a hydropower plant in the cascaded system.

of the decision-making framework, the next chapter focuses on exploring distributed algorithms and decomposition methods for the centralized scheduling and dispatch problems discussed here.

Once the VPP's day-ahead schedule is fixed, with bids submitted to the market operator, the second level of the proposed decision-making framework, namely the MPC algorithm (3.19), is activated to optimize the short-term dispatch of the VPP, aiming to minimize the cost incurred by the aggregator for energy imbalances. Fig. 3.12 illustrates the real-time daily operation of the final hydropower system in the cascade, showcasing the application of the two-level energy management strategy. During peak price periods, the reservoir is strategically depleted to capitalize on these favorable market conditions, reflecting the scheduling output that prioritizes energy provision during profitable times. Notably, the reservoir's storage capacity is constrained by the water inflow, as shown in Fig. 2.9, which in turn depend on the outflow from upstream hydropower developments. Hence, the proposed control approach effectively coordinates the upstream developments to ensure full storage availability during peak price periods. Fig. 3.12 also highlights the integration of economic performance indicators into the control strategy. For instance, when the water level reaches its maximum, the barrage is allowed to open, but this operation proves inefficient from an economic perspective, as the turbines have not yet reached full capacity. Consequently, the barrage remains closed. This behavior is a direct result of the objective function J^{ST} in (3.23), which prioritizes the aggregator's economic objectives through economic MPC, as opposed to the traditional reference-tracking MPC, which focuses solely on minimizing the mismatch between a predefined set-point and the actual real-time output.

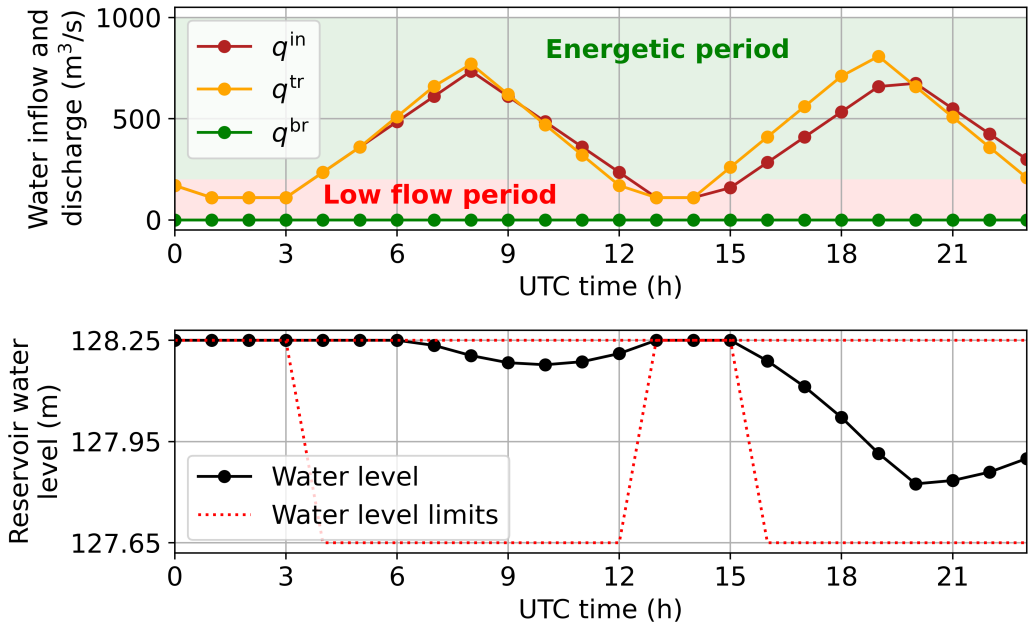

Figure 3.13: Illustration of real-time operation of a hydropower plant within the cascaded system during low flow and energetic periods.

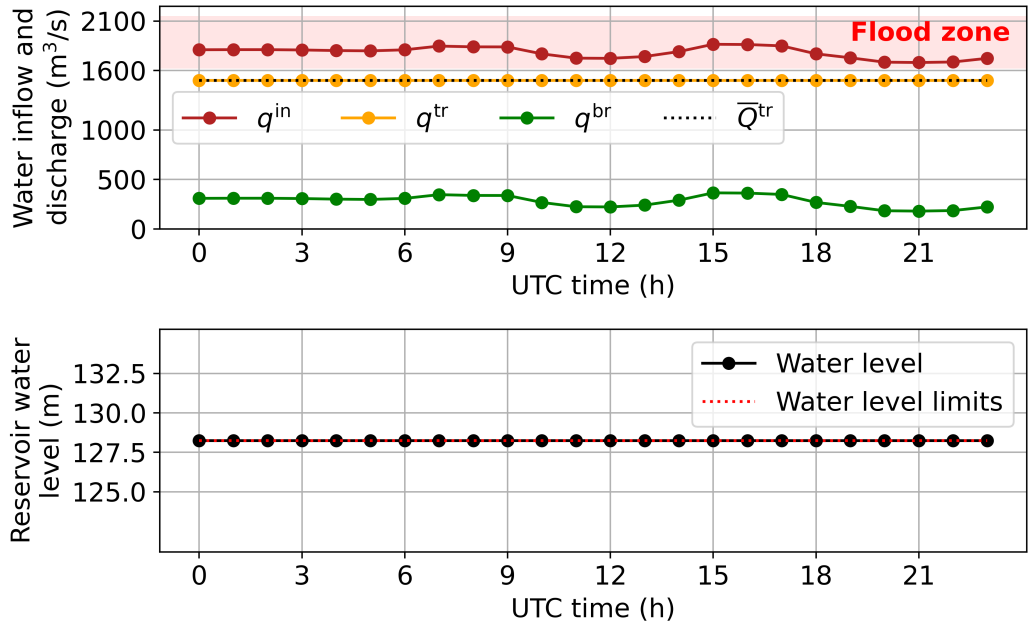

Figure 3.14: Illustration of real-time operation of a hydropower plant within the cascaded system during flood periods.

To show the influence of water inflow conditions on the real-time operation of the cascaded hydropower assets managed by Compagnie Nationale du Rhône, Figs. 3.13 and 3.14 illustrate the real-time operation of a hydropower plant within the cascaded system during low flow, energetic, and flood periods. Due to the operational curves (see Fig. 2.9) employed by the aggregator, the

operation of these plants is closely linked to the observed inflows. Fig. 3.13 illustrates the typical operation during low-flow periods, where the observed inflow q^{in} falls below a minimum threshold and the plant operates in a pure run-of-the-river mode, with no storage capacity available. Similarly, as shown in Fig. 3.14, during floods, the hydropower assets are forced to operate in run-of-the-river mode, using the barrage to ensure a smooth and safe discharge through the hydraulic system. Only during energetic periods the hydropower plants can exploit their storage capacity, offering flexibility to enhance the market value of the VPP, as shown in Fig. 3.13. This indicates that the proposed strategy must not only optimize individual plant operations to maximize output when most advantageous but also account for the cumulative operation of all assets. The hydraulic links between the plants mean that upstream developments significantly impact the storage capacity and flexibility of downstream assets within the cascade.

For a comprehensive assessment of the proposed stochastic economic MPC strategy for energy dispatch detailed in (3.19), a comparative analysis is presented in terms of ex-post profit and imbalances with the following alternative approaches:

- *Reference-tracking MPC*: This approach entails solving the scheduling problem (3.15) for the combined operation of hydropower units and vRES to determine market bids, which subsequently serve as reference set points during the dispatch phase. In contrast to the proposed stochastic economic MPC, this type of controller disregards market price forecasts, focusing on non-economic objectives. While this form of MPC is the most widely used, it is deemed inefficient for addressing economic optimization problems such as the one under consideration. An overview of the fundamental principles behind this control technique is presented in Section 3.2.4.1.

- *Uncoordinated economic MPC*: This method utilizes the proposed two-level decision-making framework but operates the cascaded hydropower independently from vRES, emulating the current operational strategy of Compagnie Nationale du Rhône. Although the mathematical optimization methods align with those of the proposed approach, this method differs by not integrating the hydropower cascade with vRES, resulting in a decoupled management of the available energy resources.

- *Deterministic economic MPC*: This method applies the proposed two-level decision-making framework to solve the VPP scheduling problem. However, instead of utilizing the stochastic economic MPC approach as formulated in (3.19), it employs a deterministic version of (3.19). As a result, fixed hourly bids are generated rather than price-quantity bidding curves. An overview of the fundamental principles behind economic MPC is presented in Section 3.2.4.2.

- *Ideal control*: This method employs the two-level decision framework to jointly optimize the operation of cascaded hydropower and vRES, as in the proposed scheme, but with the assumption that future market prices are known rather than forecasted. This idealized controller represents a benchmark scenario, as in reality, the aggregator cannot have access to market prices before clearing.

Dispatch strategy	**Positive imbalance (MWh/MWh)**	**Negative imbalance (MWh/MWh)**	**Profit (€/MWh)**
RTMPC	0.23	0.30	33.22
UEMPC	0.13 (-43.47%)	0.10 (-66.67%)	38.88 (+17.04%)
DEMPC	0.06 (-73.91%)	0.11 (-63.33%)	39.45 (+18.75%)
SEMPC	0.05 (**-78.26%**)	0.07 (**-76.67%**)	41.22 (**+24.08%**)
Ideal control	0.03 (-86.96%)	0.06 (-80.00%)	42.03 (+26.52%)

Table 3.5: Ex-post energy imbalances and profit for various dispatch strategies in the reference case (20 scenarios). Hourly average values normalized by VPP power generation. In brackets, the relative difference with respect to reference-tracking MPC. **DEMPC**: Deterministic economic MPC; **RTMPC**: Reference-tracking MPC; **SEMPC**: Stochastic economic MPC (proposed method); **UEMPC**: Uncoordinated economic MPC.

Table 3.5 offers a comparative analysis of the control approaches in terms of ex-post profit and imbalances. The differences observed in the results arise solely from the varying utilization strategies of the reservoirs. Since the total energy generation by the VPP is determined by uncontrollable wind power and inflows to the hydropower plants, it remains unaffected by the dispatch strategy. All analyzed economic controllers significantly outperform the traditional reference-tracking MPC in terms of market performance, notably by enhancing the aggregator's profit. The most substantial improvement is achieved by the proposed stochastic economic MPC, which yields a 24.08% profit increase compared to the reference-tracking MPC. This underscores the advantages of incorporating economic key performance indicators not only in the scheduling stage of the decision-making framework but also in the dispatch optimization strategy. Among the economic approaches, the coordinated methods (both deterministic and stochastic economic MPC) clearly outperform the uncoordinated management of VPP resources. This highlights the value of coordinated control of heterogeneous energy resources, yielding an improvement in market value of approximately 6%. The results further validate that combining economic control with stochastic programming, as done in the proposed stochastic economic MPC, is the most suitable solution for managing complex aggregations of resources under significant uncertainty in economic-oriented problems. The proposed stochastic economic MPC shows superior performance compared to both non-economic controllers (such as reference-tracking MPC) and its deterministic counterpart (deterministic economic MPC). When compared to the ideal control case, where the unrealistic assumption is made that the aggregator has prior knowledge of market prices, the proposed controller exhibits less than 2% performance gap.

The profit increase achieved when combining cascaded hydropower with vRES power generation is due to the flexibility of hydropower plants. However, unlike batteries, the storage capacity of the cascaded hydropower system is variable and reliant on the external inflow from the river and its tributaries. As shown in Fig. 3.15 the available storage capacity of the cascaded hydropower plants can be estimated by considering the external inflow. The results in the figure are provided for a smaller section of the cascaded system composed three assets, namely PR, SV and BV (refer to Table 2.3).

Table 3.6 illustrates the influence of inflow seasonality on the aggregator's profit. Under nor-

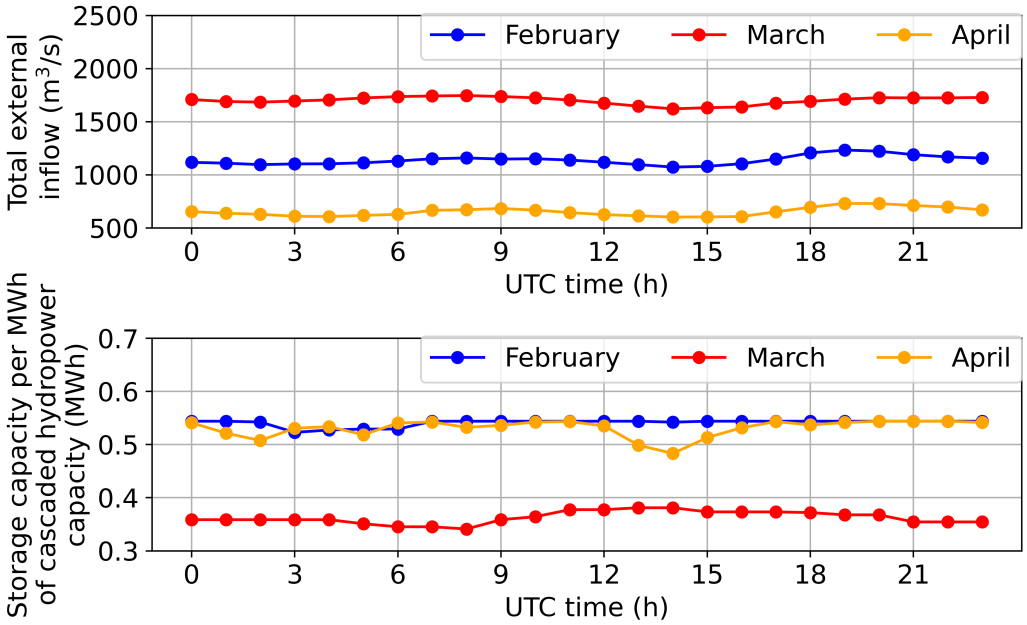

Figure 3.15: Average daily external water inflow and corresponding storage capacity of the hydropower cascade throughout the simulation period, calculated for a smaller cascaded system consisting only of the PR, SV, and BV assets in the lower Rhône cascade (refer to Table 2.3).

Strategy	**Profit (€/MWh)**		
	February	**March**	**April**
Uncoordinated	47.63	33.41	31.52
Coordinated	48.54 (**+1.9%**)	33.70 (**+0.9%**)	32.32 (**+2.5%**)

Table 3.6: Ex-post profit for uncoordinated and coordinated operation of cascaded hydropower and wind farms. These results are calculated for a smaller cascaded system consisting solely of the PR, SV, and BV assets in the lower Rhône (refer to Table 2.3). Hourly average values are normalized by the VPP power generation, with the relative difference compared to the uncoordinated approach indicated in brackets.

mal inflow conditions in February and April, the coordinated dispatch strategy results in notable profit increases of +1.9% and +2.5%, respectively, compared to the uncoordinated dispatch approach. In contrast, during flood periods in March, the cascaded system is largely restricted to operating in a pure run-of-the-river mode, with no available storage capacity. Consequently, the disparity between coordinated and uncoordinated dispatch diminishes significantly. This observation underscores that the run-of-the-river capability to mitigate fluctuations in vRES is inherently tied to inflow seasonality, which directly impacts the storage capacity of the reservoirs.

The results presented in Tables 3.5 and 3.6 clearly show that the coordinated operation of vRES and cascaded hydropower enhances the market value the VPP resources compared to their uncoordinated operation in the energy market. This finding addresses the first research question of this thesis, highlighting the benefits of aggregating heterogeneous and sparse resources within a complex VPP to increase their economic value.

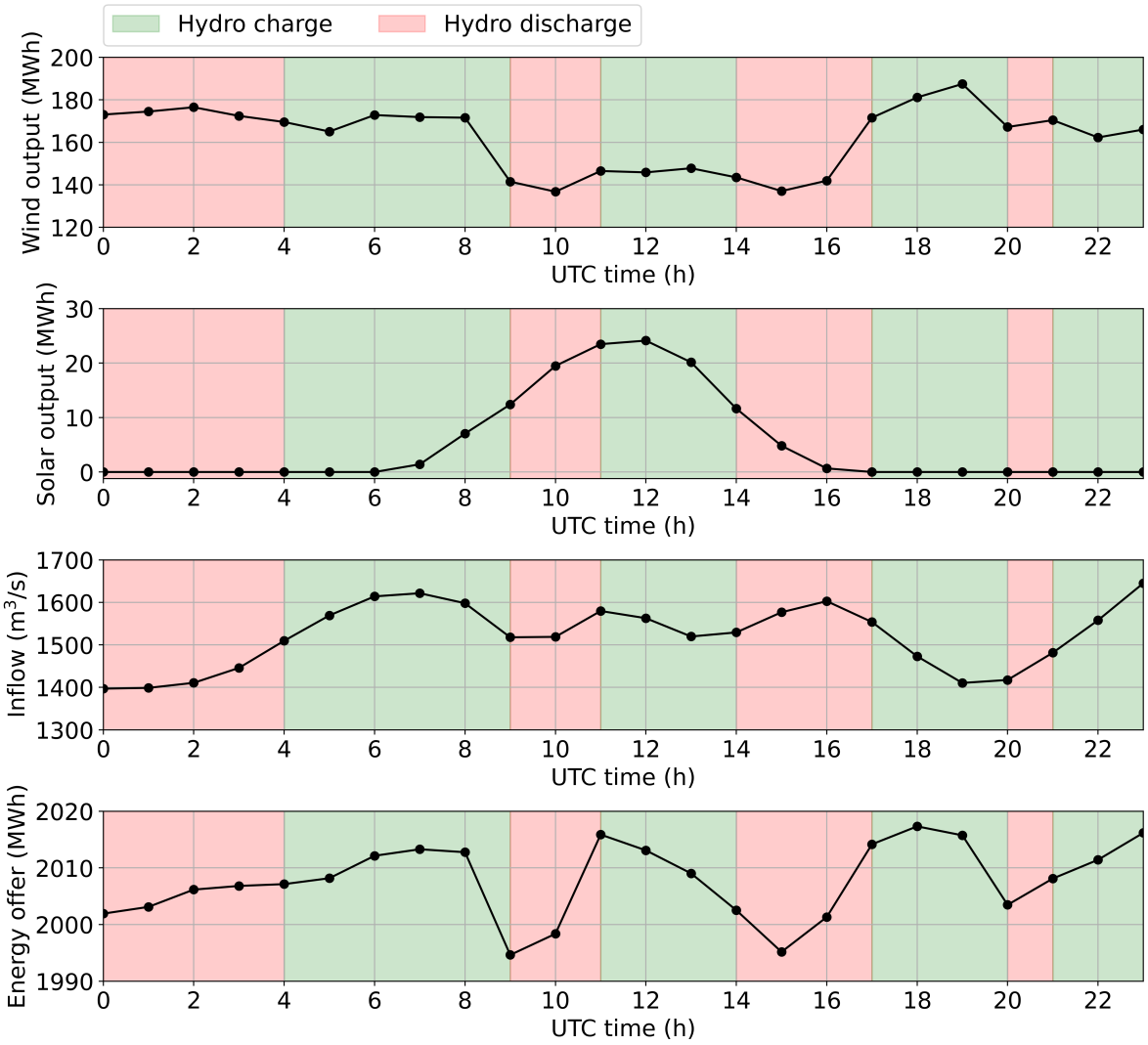

Figure 3.16: Example of energy volumes offered in the day-ahead market during energetic periods when operating cascaded hydropower and vRES in a coordinated manner. The results shown are based on 20 scenarios and fixed price levels maintained throughout each hour of the day.

To provide further insights and characterize the flexibility potential of the cascaded system operated by Compagnie Nationale du Rhône, as well as its capacity to mitigate the stochasticity of vRES, Fig. 3.16 illustrates an example of the bidding curve generated when jointly operating vRES energy, namely wind and solar units, and cascaded hydropower units. As previously detailed, the flexibility of cascaded hydropower is closely linked to inflow conditions, influenced by the strict operational curves employed by Compagnie Nationale du Rhône for asset management. In Fig. 3.16, the VPP is in an energetic period (refer to Fig. 2.9), during which the storage capacity of the cascade is available for exploitation. The results depicted in the figure are derived by fixing the price scenarios in the stochastic scheduling problem (3.15), thereby eliminating the impact of price uncertainty. This approach allows for an assessment of the hydropower cascade's ability to mitigate uncertainty arising from vRES power generation. According to these findings, the reservoirs in the hydropower cascade are charged during periods of high wa-

ter inflow (04:00-09:00, 21:00-23:00) or when vRES power generation is elevated (11:00-14:00, 17:00-20:00). Conversely, they are discharged when there is a drop in vRES energy production (09:00-11:00, 20:00-21:00) or during periods of low vRES energy generation (14:00-17:00). In essence, the cascade operates to compensate for drops in vRES energy during scarcity periods by discharging its reservoirs and recharging them when vRES energy is abundant and inflow is high. This behavior is expected, as the fixed market price scenarios throughout the simulated day encourage the VPP to stabilize energy supply across all hours analyzed. It is important to note that, in addition to the storage capacity of cascaded hydropower, the analysis of the flexibility potential of Compagnie Nationale du Rhône's VPP should also consider the inherent temporal correlation between wind and solar outputs. For instance, while Fig. 3.16 indicates low wind output between 11:00 and 14:00, it is not necessary to rely on the cascaded hydropower system to compensate for this underproduction. The solar power generation ramps up during this period, effectively offsetting the drop in wind power without requiring additional flexibility from the hydropower system.

Conversely, as shown also in previous results, during flood periods the cascaded hydropower plants are constrained to operate as pure run-of-the-river assets, completely losing their ability to enhance vRES integration. For example, Fig. 3.17 presents an analysis similar to that of Fig. 3.16, but now illustrating the scheduling strategy during flood periods when no storage capacity is available. In these conditions, the hydropower cascade operates strictly in run-of-the-river mode, which means it cannot mitigate the variability of vRES. As a result, the bidding curve from the scheduling module closely follows the combined output of wind, and solar units. During periods of high vRES power generation, the energy offered is higher (00:00-15:00) than when vRES generation is low (15:00-23:00). In other words, during flood periods, the aggregation of cascaded hydropower with wind and solar units provides minimal, if any, benefit to enhancing the market value of the system, since no storage capacity can be exploited to mitigate the stochasticity of vRES. This is further confirmed by the analysis in Table 3.6 (see results for March). In this case, the coordinated operation of these assets merely complicates the bidding process without delivering significant advantages.

To conclude the evaluation of the flexibility potential of cascaded hydropower, Fig. 3.18 presents a sensitivity analysis of the VPP's observed profit as wind energy integration increases. The profit is normalized against the ex-post profit when no wind is integrated, where 100% represents the VPP's profit without wind. Wind capacities are expressed as a percentage of the total capacity of the hydropower cascade, with 100% indicating that the wind farm capacity matches that of the cascaded hydropower system. No solar units are included in this aggregation. As shown in the figure, when the total wind capacity integrated into the VPP equals that of the hydropower system (i.e., a normalized wind capacity of 100%), the observed normalized profit drops by more than 20% compared to the case where no wind is integrated. This indicates that the flexibility of the hydropower cascade is significantly "consumed" by the integration of wind energy, as it is heavily utilized to mitigate the stochasticity of vRES. While the consumption of flexibility increases as more wind units are integrated (i.e., as the normalized wind capacity increases), the rate at which this flexibility is consumed decreases progressively. For instance,

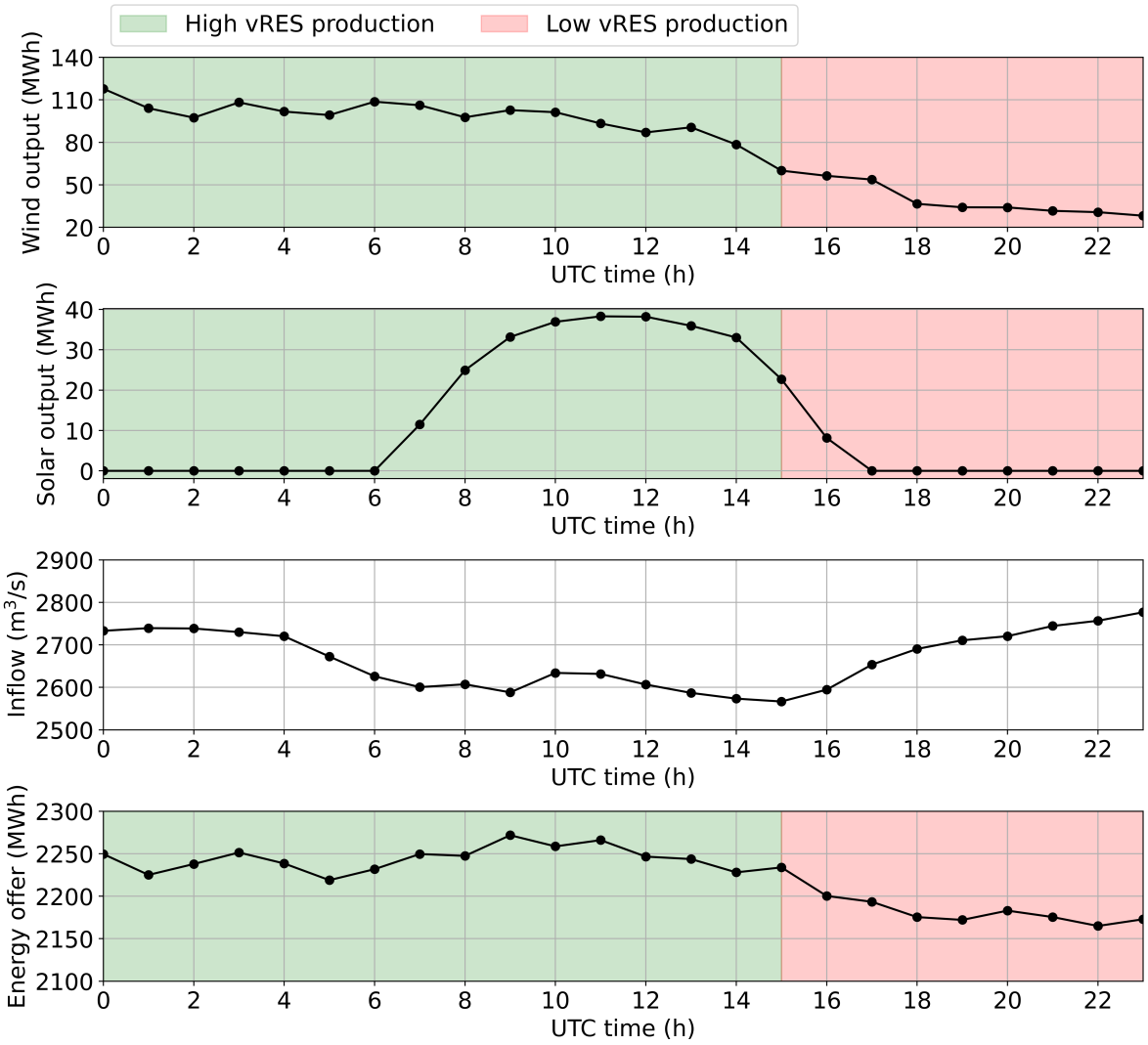

Figure 3.17: Example of energy volumes offered in the day-ahead market during flood periods when operating cascaded hydropower and vRES in a coordinated manner. The results shown are based on 20 scenarios and fixed price levels maintained throughout each hour of the day.

the profit drop observed when increasing the normalized wind capacity from 0% (no wind integration) to 200% (double the capacity of the hydropower cascade) is smaller than the drop when moving from 200% to 1400% (14 times the capacity of the cascade). Notably, despite the decreasing normalized profit as wind penetration grows, the net profit of the aggregator increases. This aligns with the results shown in the figure, as it presents profit per MWh of energy capacity within the VPP. In summary, Fig. 3.18 shows that the flexibility of the cascaded hydropower system is fully utilized when a vRES capacity approximately 14 times greater than that of the cascaded system is integrated into the VPP. This highlights the considerable potential of leveraging the flexibility of the cascaded hydropower system for coordinated operation with vRES, as opposed to the current uncoordinated approach employed by Compagnie Nationale du Rhône.

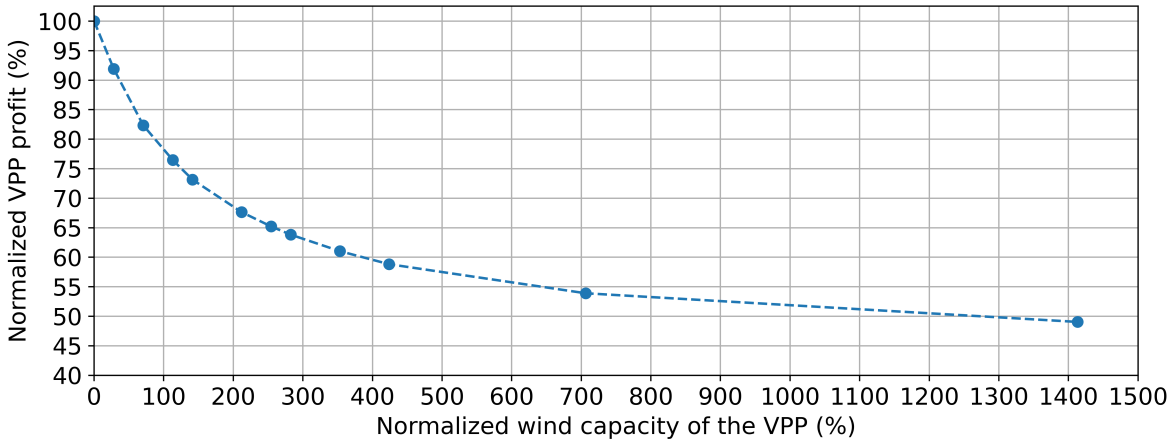

Figure 3.18: Sensitivity of VPP profit to the integration of wind units. The reported profit per MWh of VPP energy capacity is normalized to the ex-post profit when no wind is integrated, with 100% representing the profit of the VPP without wind. Wind capacities are shown as a percentage of the total capacity of the hydropower cascade, where 100% indicates that the wind capacity within the VPP is equal to that of the cascaded hydropower system. No solar units are included in this aggregation.

Chapter 4

Decomposition Methods for the Optimal Bidding of a Complex Virtual Power Plant

Résumé en Français

Ce chapitre se consacre à l'optimisation des centrales électriques virtuelles complexes, en mettant particulièrement l'accent sur leur planification et leur gestion dans le cadre du marché de l'électricité de la veille pour le lendemain. Si la stratégie de décision stochastique à deux niveaux précédemment introduite se révèle performante dans une structure centralisée, son application à grande échelle se heurte toutefois à d'importantes limitations, notamment en raison de la présence de dynamiques non linéaires, d'incertitudes multiples et de contraintes de couplage complexes entre les différentes unités du système. Afin de surmonter ces défis, le chapitre explore des méthodes avancées de décomposition mathématique, qui permettent de diviser le problème global en sous-problèmes plus simples et mieux adaptés à une résolution efficace, améliorant ainsi la scalabilité et la rapidité des calculs. Parmi ces approches, les méthodologies décentralisées, hiérarchiques et distribuées sont examinées pour leur capacité à accroître la flexibilité opérationnelle et à faciliter l'intégration de ressources hétérogènes. En particulier, une méthode de résolution distribuée avancée est introduite, assurant des performances optimales grâce à l'établissement de bornes sur l'optimum global, ce qui permet d'évaluer rigoureusement la qualité des solutions obtenues. Enfin, le chapitre s'achève par une démonstration mathématique de la validité de cette approche, mettant en évidence son potentiel pour améliorer significativement la gestion et l'exploitation des centrales électriques virtuelles complexes.

4.1 Introduction

The stochastic two-level decision-making strategy introduced in Chapter 3 provides a practical, robust solution for scheduling VPP resources in the day-ahead market, while enabling responsive dispatch control to optimize the VPP profitability. This strategy, however, operates under a traditional *centralized* structure, wherein data from all VPP assets and uncertainties are aggregated at each stage by a central controller, which computes optimal decisions and dispatches instructions to each resource individually. While this centralized approach is effective for smaller systems, such as microgrids [170] or hybrid systems [52], it becomes computationally burdensome for large-scale, *complex* VPPs [54].

As previously noted, managing complex VPPs introduces three primary layers of complexity: nonlinear dynamics of individual assets, numerous and heterogeneous uncertainty sources, and intricate coupling constraints among VPP units. The nonlinear characteristics of each asset introduce significant challenges in centralized optimization, as these often require MINLP models, which lack efficient, off-the-shelf solvers. Even when simplified to MILP models, the numerous integer variables needed to accurately represent complex VPP dynamics, especially under strict safety constraints, add substantial difficulty to centralized approaches. Additionally, the involvement of various, heterogeneous uncertainties typically necessitates incorporating a large number of scenarios in stochastic programming, which significantly expands the dimensionality and complexity of the model. Coupling constraints between units and scenarios further complicate this, as coordinated decision-making across all assets is required, effectively limiting the feasibility of straightforward decentralization approaches.

To address these multiple layers of complexity, one potential approach involves moving away from traditional mathematical optimization toward alternative methods that may offer improved scalability. These alternatives include heuristic methods [180], and data-driven approaches such as machine learning [181]. However, both machine learning and heuristic methods, while potentially faster and more adaptable, frequently face issues with limited interpretability and lack convergence guarantees, which can be critical drawbacks in optimization settings requiring both reliability and accuracy.

To address the **research question Q2** from Chapter 1, a method is required that can manage the inherent complexity of the problems under investigation, ensure *performance guarantees*, and minimize disruptions to the company's existing tools. In this regard, *mathematical decomposition methods* [182] have proven highly effective. These methods offer significant advantages over traditional centralized approaches. By enabling parallelization, decomposition methods can surpass centralized strategies in terms of solution speed and scalability. Additionally, while centralized approaches are vulnerable to single-point failures, decomposition enhances the robustness and resilience of the optimization process and can uphold data privacy. Furthermore, the modular and flexible structure of decomposition methods aligns well with the dynamic nature of complex VPPs, facilitating seamless integration with existing decision-making tools in most cases.

Decomposition methods can be implemented in various configurations [38], ranging from

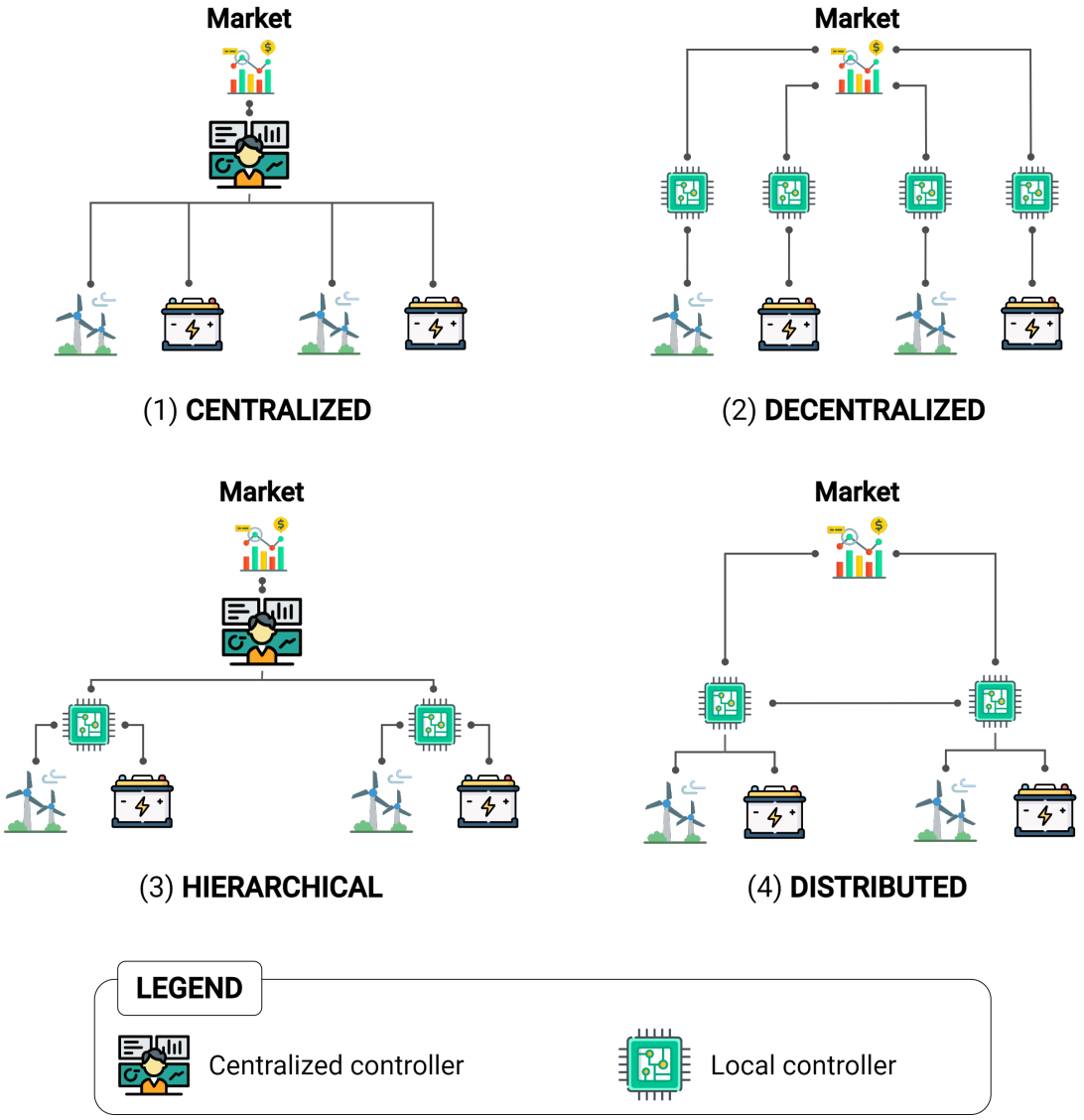

Figure 4.1: Centralized, decentralized, hierarchical, and distributed structures of the VPP decision-making tool, based on the terminology of [38].

purely *decentralized* approaches—where local agents independently optimize each subproblem with no information exchange—to *hierarchical* and *distributed* methods, which do involve information exchange. In hierarchical methods, a central controller coordinates the optimization of subproblems by collecting information from lower-level agents in a structured hierarchy. In contrast, distributed methods achieve coordination without a centralized controller, relying instead on information exchange between neighboring agents. An overview of decomposition methods compared to centralized approaches is shown in Fig. 4.1, while Table 4.1 contrasts these methods in terms of scalability, accuracy, privacy, and robustness against single-point communication failures.

Beyond the choice of decomposition configuration, scenario-based stochastic optimization for complex VPPs allows for decomposition along the *spatial and scenario dimensions* of the problem, corresponding to the *spatial and scenario coupling constraints* identified in Chapter 3.

Property	Centralized	Decentralized	Hierarchical	Distributed
Accuracy	⋆⋆⋆	⋆	⋆⋆	⋆⋆
Scalability	⋆	⋆⋆⋆	⋆⋆	⋆⋆⋆
Privacy	⋆	⋆⋆⋆	⋆⋆	⋆⋆
Robustness	⋆	⋆⋆⋆	⋆⋆	⋆⋆⋆

Table 4.1: Comparison between centralized, decentralized, hierarchical, and distributed structures of the VPP decision-making tool in terms of scalability, accuracy, and robustness against single-point communication failures. **Legend**: ⋆ → poor; ⋆⋆ → medium; ⋆⋆⋆ → good.

In spatial decomposition, the original centralized model is decomposed by assets or groups of assets by decoupling spatial constraints (e.g., power balancing among units or hydraulic coupling in a cascaded hydropower system). In scenario decomposition, the model is decomposed by scenario, with the decision variables for each scenario optimized independently; information exchange among subproblems (one per scenario) then ensures convergence to the global optimum of the original problem. To maximize scalability and convergence potential, a **combined scenario-spatial decomposition approach** (**contribution C3** in Chapter 1) is investigated here. Based on the proposed combined scenario-spatial decomposition method, a distributed solution for addressing convex VPP scheduling and dispatch models is provided (**contribution C4** in Chapter 1).

However, for nonconvex problems, commonly used distributed optimization techniques—such as ADMM and other augmented Lagrangian relaxation-based methods—generally cannot guarantee convergence to the global optimum [183]. Even in MILP models, these methods typically provide heuristic solutions [184]. To address this limitation, **this chapter proposes a novel ADMM-based distributed method for solving MILP models of complex VPPs while enforcing a performance guarantee** (**contribution C5** in Chapter 1). This is achieved by calculating upper and lower bounds on the global optimum of the original centralized problem based on the distributed solution at each iteration of the algorithm. Then, the VPP operator can continuously measure the accuracy of the distributed solution by monitoring the "distance" between upper and lower bounds. A mathematical proof is provided to establish the existence and validity of these bounds (**contribution C6** in Chapter 1). In this sense, **the proposed distributed method is trustworthy**, providing a solution that the VPP operator can confidently evaluate and trust.

It is worth noting that while the following discussion centers on a specific complex VPP, namely the one operated by Compagnie Nationale du Rhône, whose main complexity arises from managing an intricate cascaded hydropower system, the methods presented here are designed to generalize the original centralized optimization problems into a versatile form that can readily apply to other complex VPPs. As detailed below, the proposed decomposition approach is built on identifying common coupling constraints in complex VPPs and provides a generalized framework for decoupling these constraints, enabling the use of trustworthy distributed methods even in complex mixed-integer cases.

The methods and results presented here expand upon the discussions in two papers that are outcomes of this thesis, namely [185] and [186].

4.1.1 Positioning Within the Related Literature

Comprehensive physical or operational models for complex VPPs typically result in challenging MINLP problems [187], for which efficient off-the-shelf solvers remain unavailable. To address the inherent complexity, the original model is often simplified using three primary methods: aggregation, optimization/heuristics, and decomposition approaches [188].

Aggregation methods are frequently applied in complex VPPs that integrate multiple assets with similar dynamics, such as fleets of electric vehicles [189] or cascaded hydropower systems with comparable reservoir and inflow profiles [190]. While aggregation offers a straightforward means to simplify model complexity, its accuracy depends heavily on the similarity of asset dynamics. When stringent operational constraints and complex dynamics are involved—as in cascaded hydropower systems—simple aggregation often falls short, failing to provide the performance guarantees required by complex VPP operators.

Alternative approaches maintain detailed representations of individual asset dynamics while simplifying the original MINLP model. A common method is outer approximation [187], which decomposes the problem into separate MILP and NLP components, albeit often at the cost of optimality. Another widely used simplification involves approximating the original model, converting the problem into LP [191], MILP [192], quadratic programming (QP) [193], mixed-integer quadratic programming (MIQP) [194], or NLP [195] formulations. A comprehensive review of over 120 articles on VPP optimization found that MILP models were employed in about 60% of cases, underscoring a trend toward MILP for balancing tractability and precision [28]. Various solution techniques are then used for these simplified models, including classical centralized mathematical optimization methods [196], dynamic programming [122], rule-based approaches [197], and heuristic methods [198]. However, centralized classical optimization and dynamic programming approaches often lack the scalability required for complex VPP problems, while rule-based methods may oversimplify the problem, and heuristics rarely provide the robust performance guarantees needed for reliable VPP operation.

To address these limitations, researchers have turned to *mathematical decomposition methods*. In these frameworks, large-scale power systems are divided into sub-regions, enabling efficient subproblem solutions that can be coordinated to address the overall problem. Decomposition methods also facilitate parallel processing of local subproblems, thereby enhancing computational efficiency [36]. A key benefit of these approaches is the reduced need for data exchange, as only essential information is shared between sub-regions or with a central coordinator. Furthermore, these methods offer adaptability, which is critical for complex VPPs as their structure and topology grow increasingly dynamic.

Several classifications exist for decomposition methods, particularly in power system applications. One classification distinguishes between *static* and *dynamic* decomposition algorithms (often referred to as *offline* and *online* methods, respectively) [199]. In static methods, agents communicate iteratively to generate control setpoints that are applied after convergence. In contrast, a dynamic method allows immediate implementation of computed control setpoints, enabling real-time feedback and adjustment on the grid. For the proposed two-level stochastic decision-making framework in this thesis, static methods suit the first-level scheduling phase de-

tailed in 3.15, while dynamic methods fit the near-real-time control required in the second-level dispatch phase detailed in 3.19.

Another key distinction in decomposition methods lies in the decoupling strategy used for the original centralized problem [36]. Some approaches apply *generator-based decomposition*, which facilitates coordination by exchanging cost or price information specific to individual generators. In contrast, *geography-based decomposition* divides the system into multiple geographic regions connected by tie-lines, where coordination occurs through the exchange of voltage data and power flow information at boundary buses and tie-lines. In the context of scenario-based stochastic programming problems, decomposition is often classified into scenario and spatial approaches. *Spatial decomposition* divides the problem by asset or groups of assets [200], whereas *scenario decomposition* partitions the original stochastic problem by scenario [201]. The combined scenario-spatial decomposition approach adopted here advances beyond conventional methods, which generally handle only one of these dimensions. This combined approach enables efficient, full-scale parallelization for optimizing VPP operations.

Once the problem is decomposed, an algorithm is required to coordinate subproblems toward an optimal solution. Two primary categories exist for such coordination methods [38]. The first, based on *augmented Lagrangian decomposition*, includes techniques such as dual decomposition, ADMM, analytical target cascading (ATC), and the auxiliary problem principle (APP) [202]. The second involves decentralized Karush-Kuhn-Tucker condition-based methods, such as optimality condition decomposition and consensus+innovation [203]. This thesis focuses on augmented Lagrangian-based methods, specifically ADMM and APP, which have proven highly adaptable to a wide range of optimization problems and have demonstrated effectiveness across diverse applications [37].

In this context, ADMM has attracted considerable interest due to its flexibility, relatively straightforward parameterization, and strong performance across a wide range of problem types. Additionally, ADMM subproblems often admit closed-form solutions, reducing per-iteration computational complexity [182]. Originally developed by [204] and [205] in the 1970s, ADMM has evolved significantly, with numerous variants now available [40]. For this thesis, two key ADMM characteristics are relevant:

- Classical ADMM's hierarchical structure, requiring a central coordinator for dual variables updates, limits scalability and robustness in settings like complex VPP dispatch, where fast, decentralized solutions are essential. APP, in contrast, avoids this limitation by linearizing cross-terms, enabling fully distributed solutions without a central coordinator [38]. For this reason, this chapter proposes an APP-based decomposition approach for the centralized MPC dispatch problem presented in Section 3.3.3, achieving faster, scalable solutions compared to classical ADMM.

- A critical limitation of ADMM and related augmented Lagrangian methods is their convergence guarantee, which generally applies strictly to convex problems [206]. This constraint is problematic for complex VPPs, as these problems are often inherently nonconvex. To address this, the chapter extends the ADMM by incorporating upper and lower bounds

Ref.	Comput. strategy	Uncertainty modeled?	Problem	Decomposition	Trustworthy
[190]	AGG	×	MILP	×	✓
[188]	AGG	✓(SP)	NLP	×	✓
[192]	OPTIM	×	MILP	×	✓
[195]	OPTIM	×	NLP	×	✓
[159]	OPTIM	✓(RO)	LP	×	✓
[196]	OPTIM	✓(IP)	MILP	×	✓
[161]	OPTIM	✓(CCO)	LP	×	✓
[197]	OPTIM	✓(SP)	LP	×	✓
[186]⋆	DECOM	×	MILP	Spatial	×
[194]⋆	DECOM	×	MIQP	Spatial	×
[200]	DECOM	✓(SP)	MILP	Spatial	×
[187]	DECOM	✓(SP)	MINLP	Scenario	×
[201]⋆	DECOM	✓(SP)	MIQP	Scenario	×
This chapter⋆	DECOM	✓(SP)	MILP	Scenario&spatial	✓

Table 4.2: Comparison of the proposed trustworthy distributed algorithm with the relevant related literature, focusing specifically on the optimal operation of cascaded hydropower systems, which form the primary case study of this thesis. The studies employing augmented Lagrangian relaxation-based algorithms are denoted by the ⋆ symbol. **AGG**: Aggregation; **CCO**: Chance constrained optimization; **DECOM**: Decomposition; **IP**: Interval programming; **OPTIM**: Optimization; **RO**: Robust optimization; **SP**: Stochastic programming.

on the global optimum, calculated at each iteration of the distributed algorithm. By assessing the "distance" between these bounds, the VPP operator can reliably evaluate the quality of the distributed solution. In this sense, the resulting distributed algorithms is *trustworthy*. Furthermore, the following discussion presents a mathematical proof of the bounds' validity, establishing a strong performance guarantee for the proposed distributed method in the mixed-integer case.

Table 4.2 provides a comparison of the proposed method with the relevant related literature, focusing specifically on the optimal operation of cascaded hydropower systems, which form the primary case study of this thesis.

4.1.2 Chapter Outline

The remainder of this chapter is structured as follows. Section 4.2 introduces the mathematical foundations relevant to this chapter. Section 4.3 describes the proposed decomposition methods applied to the centralized two-level decision-making framework introduced in Section 3.3. Lastly, Sections 4.4 and 4.5 present the results for a small-scale illustrative example and the Compagnie Nationale du Rhône case study, respectively.

4.2 Mathematical Background

This section aims to provide an overview of the primary optimization tools used in the following section to formulate the proposed distributed solutions for decision-making in complex VPP problems. The foundational concepts covered include the ADMM and APP algorithms, as well as general consensus optimization. A comprehensive description of these concepts is beyond the scope of this section; however, readers are referred to the following contributions for detailed analyses: [39] offers an in-depth discussion of the ADMM algorithm, [40] reviews various ADMM extensions and their applications, [207] explores the APP algorithm, and [208] provides a thorough treatment of ADMM applied to consensus optimization problems.

Consider an optimization problem of the form:

$$\min_{\boldsymbol{x}} \quad \sum_{n\in\boldsymbol{N}} f_n\left(\boldsymbol{x}_n\right) \tag{4.1a}$$

$$\text{subject to} \quad \sum_{n\in\boldsymbol{N}} \mathbf{A}_n\boldsymbol{x}_n = \boldsymbol{b}, \tag{4.1b}$$

where $f_n(\cdot)$ is a cost function, $\boldsymbol{x}_n \in \mathbb{R}^{p_n}$ denotes the vector of decision variables associated with f_n, $\boldsymbol{x} := \{\boldsymbol{x}_n\}_{n\in\boldsymbol{N}}$, $\mathbf{A} \in \mathbb{R}^{m\times p_n}$, and $\boldsymbol{b} \in \mathbb{R}^m$. The optimization problem (4.1) clearly exhibits a decomposable structure, which can be leveraged to derive a distributed solution for this centralized problem. In particular, the Lagrangian function of (4.1) can be exploited using *dual decomposition techniques* [209]. The *Lagrangian* for (4.1) is:

$$L(\boldsymbol{x},\boldsymbol{\lambda}) := \sum_{n\in\boldsymbol{N}} L_n(\boldsymbol{x}_n,\boldsymbol{\lambda}), \tag{4.2}$$

where

$$L_n(\boldsymbol{x}_n,\boldsymbol{\lambda}) := f_n\left(\boldsymbol{x}_n\right) + \boldsymbol{\lambda}^\top\mathbf{A}_n\boldsymbol{x}_n - \frac{1}{|\boldsymbol{N}|}\boldsymbol{\lambda}^\top\boldsymbol{b},\ \forall n\in\boldsymbol{N}, \tag{4.3}$$

and $\boldsymbol{\lambda} \in \mathbb{R}^m$ denotes the vector of dual variables. Dual decomposition methods use an iterative process known as the *dual ascent method* [210] to decompose the original centralized problem (4.1):

$$\boldsymbol{x}_n^{i+1} := \underset{\boldsymbol{x}_n}{\operatorname{argmin}}\, L_n\left(\boldsymbol{x}_n,\boldsymbol{\lambda}^i\right),\ \forall n\in\boldsymbol{N}, \tag{4.4a}$$

$$\boldsymbol{\lambda}^{i+1} := \boldsymbol{\lambda}^i + \alpha^i\left(\sum_{n\in\boldsymbol{N}}\mathbf{A}_n\boldsymbol{x}_n^{i+1} - \boldsymbol{b}\right). \tag{4.4b}$$

Here, i denotes the iteration of the algorithm, and α^i denotes the step size at iteration i. Since (4.4a), referred to as the *minimization step* of the algorithm, can be solved in parallel for each $n \in \boldsymbol{N}$, (4.4) enables a decomposition of the original centralized problem (4.1). However, the algorithm requires gathering all information from the subproblems to execute step (4.4b), referred to as the *dual variable update* step, resulting in a *hierarchical* rather than fully distributed structure. Additionally, the convergence of dual decomposition techniques is not always guaranteed, even for convex problems, and depends critically on the choice of the step size α^i [38].

The ADMM first originated in the 1970s with the works of Glowinski-Marocco [204] and Mercier-Gabay [205], aiming to enhance the robustness of the dual ascent method and, notably, to achieve convergence without requiring assumptions such as strict convexity [39]. Like dual decomposition, ADMM includes minimization and dual variable update steps, but it utilizes an *augmented* Lagrangian function [39]. The ADMM applies to optimization problems of the following form:

$$\min_{\boldsymbol{x},\boldsymbol{z}} \quad f(\boldsymbol{x}) + g(\boldsymbol{z}) \tag{4.5a}$$

$$\text{subject to} \quad \mathbf{A}\boldsymbol{x} + \mathbf{B}\boldsymbol{z} = \boldsymbol{c}, \tag{4.5b}$$

where $\boldsymbol{x}$ and $\boldsymbol{z}$ are decision variable vectors, $\mathbf{A}$ and $\mathbf{B}$ are specified matrices, $\boldsymbol{c}$ is a specified vector, and $f(\cdot)$ and $g(\cdot)$ are specified cost functions. The *augmented Lagrangian* for (4.5) is

$$L_\rho := f(\boldsymbol{x}) + g(\boldsymbol{z}) + \boldsymbol{\lambda}^\top (\mathbf{A}\boldsymbol{x} + \mathbf{B}\boldsymbol{z} - \boldsymbol{c}) + \frac{\rho}{2} \|\mathbf{A}\boldsymbol{x} + \mathbf{B}\boldsymbol{z} - \boldsymbol{c}\|_2^2, \tag{4.6}$$

where $\rho > 0$ is the penalty parameter of the algorithm and $\|\cdot\|_2$ denotes the two-norm. The ADMM algorithm minimizes the augmented Lagrangian iteratively through the following updates:

$$\boldsymbol{x}^{i+1} := \operatorname*{argmin}_{\boldsymbol{x}} L_\rho \left(\boldsymbol{x}, \boldsymbol{z}^i, \boldsymbol{\lambda}^i\right), \tag{4.7a}$$

$$\boldsymbol{z}^{i+1} := \operatorname*{argmin}_{\boldsymbol{z}} L_\rho \left(\boldsymbol{x}^{i+1}, \boldsymbol{z}, \boldsymbol{\lambda}^i\right), \tag{4.7b}$$

$$\boldsymbol{\lambda}^{i+1} := \boldsymbol{\lambda}^i + \rho \left(\mathbf{A}\boldsymbol{x}^{i+1} + \mathbf{B}\boldsymbol{z}^{i+1} - \boldsymbol{c}\right). \tag{4.7c}$$

Similar to the dual ascent method, classical ADMM (4.7) also exhibits a *hierarchical* structure due to the dual variable update step (4.7c).

If the functions $f(\boldsymbol{x})$ and $g(\boldsymbol{z})$ are convex, the constraint residual under ADMM is guaranteed to converge to zero, and the objective value will approach the minimum of the original centralized problem (4.5). The convergence rate depends on the choice of ρ and various strategies have been proposed for adaptively selecting this parameter [39]. While the ADMM algorithm can be applied to nonconvex problems and often provides effective heuristics in such cases, there is no guarantee of convergence.

Like the previous methods, the APP decomposes an optimization problem into subproblems with shared variables [207]. Similar to ADMM, an augmented Lagrangian approach is used to ensure consistency across subproblems. The key difference between APP and ADMM is that the cross-terms in the two-norm term of the augmented Lagrangian (4.6) are linearized, rather than treated directly. This linearization decouples the subproblems, removing the need for a central coordinator. As a result, APP is a *distributed* approach, unlike classical ADMM and dual ascent methods. Convergence of the APP method is guaranteed if all subproblems are convex [38].

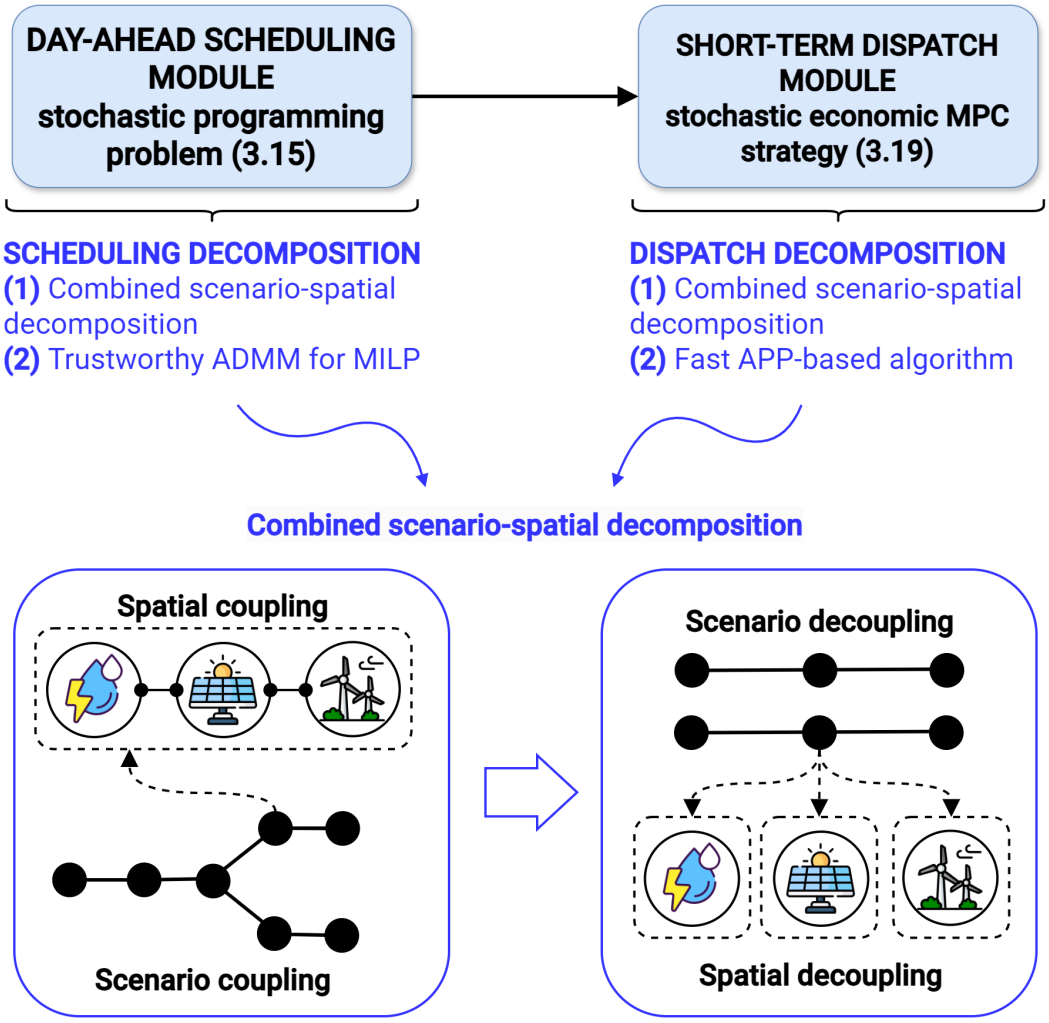

Figure 4.2: Decomposition of the proposed fully stochastic, scenario-based, two-level decision-making framework illustrated in Fig. 3.5.

4.3 Methodology

This section describes the methods proposed to decompose the stochastic two-level energy management strategy provided in Chapter 3 for optimizing complex VPPs participation in the day-ahead market (see Fig. 3.5). As outlined in the previous chapter, the two-level approach includes a *scheduling phase*, where an optimization problem is solved to position VPP resources in the market, and a *dispatch phase*, where a control problem is solved to maximize VPP profit in real-time. Since these phases can be addressed independently, separate decomposition methods are proposed for each. Section 4.3.1 introduces an ADMM-based decomposition method for the scheduling phase. For convex scheduling problems, a straightforward application of the ADMM algorithm guarantees convergence to the global optimum of the original problem. In the case of MILP problems, a modified ADMM approach is introduced to ensure a performance guarantee. Both methods decompose the original scheduling problem along scenario and spatial dimensions to allow full parallelization.

While accuracy is the main focus in the scheduling phase, the second-level dispatch con-

trol problem prioritizes speed due to the need for rapid real-time decision-making. Therefore, Section 4.3.2 introduces an APP-based control method to decompose the economic MPC of Chapter 3, creating a distributed controller capable of fast responses even for complex VPPs. A schematic of the proposed decomposition approaches for the original two-level decision-making strategy is shown in Fig. 4.2. The decomposition methods are then directly applied to the Compagnie Nationale du Rhône case study, to illustrate their application. Nonetheless, the reformulations presented can be adapted to general complex VPPs, establishing a broad approach for decomposing VPP optimization and control problems. Notation for decision variables and parameters specific to cascaded hydropower systems operated by Compagnie Nationale du Rhône is outlined in Section 2.3, while symbols, vectors and matrices previously defined in Chapter 3 are consistently used here for coherence with prior discussions.

4.3.1 A Scenario-Spatial Decomposition with a Performance Guarantee for Scheduling in Complex Virtual Power Plants

This section presents the proposed decomposition method for the scheduling phase, as formulated in (3.15), of the two-level decision-making framework outlined in Chapter 3 (i.e., the first level shown in Fig. 4.2). In Section 4.3.1.1, the centralized scheduling problem is reformulated as a consensus problem to enable full decoupling along the spatial and scenario dimensions. Section 4.3.1.2 then offers a distributed solution for the reformulated problem in the convex case, while Section 4.3.1.3 provides a trustworthy distributed solution in the mixed-integer case.

In this section, all variables refer to the day-ahead stage of the complex VPP decision-making problem discussed in the previous chapter. However, to streamline the notation, the superscript DA is omitted in the following.

4.3.1.1 Scheduling Problem Reformulation and Decoupling

The first step of the proposed decomposition method consists of reformulating the scheduling problem (3.15) into a *general consensus problem*, which takes the following form:

$$\min_{\{x_n, z_n\}_{n \in \boldsymbol{N}}} \quad \sum_{n \in \boldsymbol{N}} f_n(x_n) \tag{4.8a}$$

$$\text{subject to} \quad x_n - z_n = 0, \ \forall n \in \boldsymbol{N}, \tag{4.8b}$$

with decision variables $\{x_n\}_{n \in \boldsymbol{N}}$ and $\{z_n\}_{n \in \boldsymbol{N}}$, and cost functions $f_n(\cdot)$. This reformulation, as detailed below, enables the application of the distributed optimization methods presented in the following sections.

Consider the scheduling optimization problem (3.27) addressed by Compagnie Nationale du Rhône for operating its complex VPP. As outlined in Chapter 3, three sets of coupling constraints are identified in this problem (see Fig. 3.7):

- **Hydraulic coupling** among hydropower assets within the cascade, defined by constraints (3.27d)-(3.27e) (*spatial coupling*).

- **Electrical coupling** between non-dispatchable vRES and dispatchable hydropower plants, defined by constraints (3.27b) (*spatial coupling*).
- **Scenario coupling** among decision variables across different scenarios in the stochastic programming scheduling problem, defined by constraints (3.27c) (*scenario coupling*).

All sets of coupling constraints (3.27b)-(3.27e) involve three groups of **global variables**: the hydropower turbine outflow variables,

$$\boldsymbol{q}^{\mathbf{tr}}_{n,\omega} := \left[q^{\mathrm{tr}}_{n,\omega,1}, ..., q^{\mathrm{tr}}_{n,\omega,t}, ..., q^{\mathrm{tr}}_{n,\omega,|\boldsymbol{T}|}\right]^{\top}, \ \forall n, \forall \omega, \tag{4.9}$$

the hydropower barrage outflow variables,

$$\boldsymbol{q}^{\mathbf{br}}_{n,\omega} := \left[q^{\mathrm{br}}_{n,\omega,1}, ..., q^{\mathrm{br}}_{n,\omega,t}, ..., q^{\mathrm{br}}_{n,\omega,|\boldsymbol{T}|}\right]^{\top}, \ \forall n, \forall \omega, \tag{4.10}$$

and the hydropower generation variables,

$$\boldsymbol{p}^{\mathbf{H}}_{n,\omega} := \left[p^{\mathrm{H}}_{n,\omega,1}, ..., p^{\mathrm{H}}_{n,\omega,t}, ..., p^{\mathrm{H}}_{n,\omega,|\boldsymbol{T}|}\right]^{\top}, \ \forall n, \forall \omega. \tag{4.11}$$

By duplicating the global variables of the problem, the following **local copies** are defined:

$$\tilde{\boldsymbol{q}}^{\mathbf{tr}}_{n,\omega} := \left[\tilde{q}^{\mathrm{tr}}_{n,\omega,1}, ..., \tilde{q}^{\mathrm{tr}}_{n,\omega,t}, ..., \tilde{q}^{\mathrm{tr}}_{n,\omega,|\boldsymbol{T}|}\right]^{\top}, \ \forall n, \forall \omega, \tag{4.12}$$

$$\bar{\boldsymbol{q}}^{\mathbf{tr}}_{n,\omega} := \left[\bar{q}^{\mathrm{tr}}_{n,\omega,1}, ..., \bar{q}^{\mathrm{tr}}_{n,\omega,t}, ..., \bar{q}^{\mathrm{tr}}_{n,\omega,|\boldsymbol{T}|}\right]^{\top}, \ \forall n, \forall \omega, \tag{4.13}$$

$$\tilde{\boldsymbol{q}}^{\mathbf{br}}_{n,\omega} := \left[\tilde{q}^{\mathrm{br}}_{n,\omega,1}, ..., \tilde{q}^{\mathrm{br}}_{n,\omega,t}, ..., \tilde{q}^{\mathrm{br}}_{n,\omega,|\boldsymbol{T}|}\right]^{\top}, \ \forall n, \forall \omega, \tag{4.14}$$

$$\bar{\boldsymbol{q}}^{\mathbf{br}}_{n,\omega} := \left[\bar{q}^{\mathrm{br}}_{n,\omega,1}, ..., \bar{q}^{\mathrm{br}}_{n,\omega,t}, ..., \bar{q}^{\mathrm{br}}_{n,\omega,|\boldsymbol{T}|}\right]^{\top}, \ \forall n, \forall \omega, \tag{4.15}$$

$$\tilde{\boldsymbol{p}}^{\mathbf{H}}_{n,\omega} := \left[\tilde{p}^{\mathrm{H}}_{n,\omega,1}, ..., \tilde{p}^{\mathrm{H}}_{n,\omega,t}, ..., \tilde{p}^{\mathrm{H}}_{n,\omega,|\boldsymbol{T}|}\right]^{\top}, \ \forall n, \forall \omega, \tag{4.16}$$

$$\bar{\boldsymbol{p}}^{\mathbf{H}}_{n,\omega} := \left[\bar{p}^{\mathrm{H}}_{n,\omega,1}, ..., \bar{p}^{\mathrm{H}}_{n,\omega,t}, ..., \bar{p}^{\mathrm{H}}_{n,\omega,|\boldsymbol{T}|}\right]^{\top}, \ \forall n, \forall \omega. \tag{4.17}$$

Achieving consensus between the global variables and their local copies requires ensuring that

$$\tilde{\boldsymbol{q}}^{\mathbf{tr}}_{n,\omega} = \boldsymbol{q}^{\mathbf{tr}}_{n,\omega}, \ \forall n, \forall \omega, \tag{4.18}$$

$$\bar{\boldsymbol{q}}^{\mathbf{tr}}_{n,\omega} = \boldsymbol{q}^{\mathbf{tr}}_{n,\omega}, \ \forall n, \forall \omega, \tag{4.19}$$

$$\tilde{\boldsymbol{q}}^{\mathbf{br}}_{n,\omega} = \boldsymbol{q}^{\mathbf{br}}_{n,\omega}, \ \forall n, \forall \omega, \tag{4.20}$$

$$\bar{\boldsymbol{q}}^{\mathbf{br}}_{n,\omega} = \boldsymbol{q}^{\mathbf{br}}_{n,\omega}, \ \forall n, \forall \omega, \tag{4.21}$$

$$\tilde{\boldsymbol{p}}^{\mathbf{H}}_{n,\omega} = \boldsymbol{p}^{\mathbf{H}}_{n,\omega}, \ \forall n, \forall \omega, \tag{4.22}$$

$$\bar{\boldsymbol{p}}^{\mathbf{H}}_{n,\omega} = \boldsymbol{p}^{\mathbf{H}}_{n,\omega}, \ \forall n, \forall \omega. \tag{4.23}$$

By introducing the local copies (4.12)-(4.17) and the consensus constraints (4.18)-(4.23), the original centralized problem (3.27) is reformulated as the following consensus optimization problem:

$$\underset{\left\{\boldsymbol{z}^{\mathbf{B}},\left\{\boldsymbol{z}^{\mathbf{H}}_{n,\omega}\right\}_{n\in\boldsymbol{N},\omega\in\boldsymbol{\Omega}}\right\}}{\operatorname{argmin}} \quad J \tag{4.24a}$$

$$\text{subject to} \quad \boldsymbol{z}^{\mathbf{B}} \in \boldsymbol{\Xi}\left(\boldsymbol{\beta}\right), \tag{4.24b}$$

$$\boldsymbol{z}^{\mathbf{H}}_{n,\omega} \in \boldsymbol{\Gamma}_{n,\omega}\left(\boldsymbol{\theta}_{n,\omega}\right), \ \forall n, \forall \omega, \tag{4.24c}$$

$$\boldsymbol{z}^{\mathbf{B,H}}_{n,\omega} = \bar{\boldsymbol{z}}^{\mathbf{B,H}}_{n,\omega} \ : \ \boldsymbol{\lambda}_{n,\omega}, \ \forall n, \forall \omega. \tag{4.24d}$$

Here, $\boldsymbol{z}^{\mathbf{B}}$ encompasses the decision variables related to the power balancing of the VPP, as specified by

$$\boldsymbol{z}^{\mathbf{B}} := \left\{e_{\omega,t}, \delta^{\mathrm{E}\uparrow}_{\omega,t}, \delta^{\mathrm{E}\downarrow}_{\omega,t}, \bar{\boldsymbol{p}}^{\mathbf{H}}_{n,\omega}\right\}_{n\in\boldsymbol{N},\omega\in\boldsymbol{\Omega},t\in\boldsymbol{T}}. \tag{4.25}$$

The decision variables representing the dynamics of each hydropower plant are gathered in $\boldsymbol{z}^{\mathbf{H}}_{n,\omega}$, as defined by

$$\boldsymbol{z}^{\mathbf{H}}_{n,\omega} := \left\{b^{\mathrm{br}}_{n,\omega,t}, b^{\mathrm{oc}}_{n,\omega,t}, h_{n,\omega,t}, z^{\mathrm{fbl}}_{n,\omega,t}, \bar{\boldsymbol{q}}^{\mathbf{tr}}_{n,\omega}, \tilde{\boldsymbol{q}}^{\mathbf{tr}}_{n,\omega}, \bar{\boldsymbol{q}}^{\mathbf{br}}_{n,\omega}, \tilde{\boldsymbol{q}}^{\mathbf{br}}_{n,\omega}, \tilde{\boldsymbol{p}}^{\mathbf{H}}_{n,\omega}\right\}_{t\in\boldsymbol{T}}, \ \forall n, \forall \omega. \tag{4.26}$$

The feasible sets of $\boldsymbol{z}^{\mathbf{B}}$ and $\boldsymbol{z}^{\mathbf{H}}_{n,\omega}$ are denoted by $\boldsymbol{\Xi}\left(\boldsymbol{\beta}\right)$ and $\boldsymbol{\Gamma}_{n,\omega}\left(\boldsymbol{\theta}_{n,\omega}\right)$, respectively. The former is defined by (3.27b), (3.27c), and (3.27v). The latter is defined by (3.27d)-(3.27v). Vectors $\boldsymbol{\beta}$ and $\boldsymbol{\theta}_{n,\omega}$ collect the parameters associated with the constraints defining the feasible sets $\boldsymbol{\Xi}$ and $\boldsymbol{\Gamma}_{n,\omega}$, respectively. In words, $\boldsymbol{\Xi}\left(\boldsymbol{\beta}\right)$ encompasses all constraints related to power balancing within the VPP. Meanwhile, the sets $\boldsymbol{\Gamma}_{n,\omega}\left(\boldsymbol{\theta}_{n,\omega}\right)$ contain the individual constraints for each hydropower asset in the cascaded system, with one subproblem defined per asset and scenario.

Moreover, the vector $\boldsymbol{z}^{\mathbf{B,H}}_{n,\omega} \in \mathbb{R}^{6\times|\boldsymbol{T}|}$ collects the global variables of the problem, as defined by

$$\boldsymbol{z}^{\mathbf{B,H}}_{n,\omega} := \left[\boldsymbol{q}^{\mathbf{tr}}_{n-1,\omega}, \boldsymbol{q}^{\mathbf{br}}_{n-1,\omega}, \boldsymbol{q}^{\mathbf{tr}}_{n,\omega}, \boldsymbol{q}^{\mathbf{br}}_{n,\omega}, \boldsymbol{p}^{\mathbf{H}}_{n,\omega}, \boldsymbol{p}^{\mathbf{H}}_{n,\omega}\right]^{\top}, \ \forall n, \forall \omega. \tag{4.27}$$

The vector $\bar{\boldsymbol{z}}^{\mathbf{B,H}}_{n,\omega} \in \mathbb{R}^{6\times|\boldsymbol{T}|}$ collects the *local copies* of the global variables in $\boldsymbol{z}^{\mathbf{B,H}}_{n,\omega}$, as defined by

$$\bar{\boldsymbol{z}}^{\mathbf{B,H}}_{n,\omega} := \left[\tilde{\boldsymbol{q}}^{\mathbf{tr}}_{n-1,\omega}, \tilde{\boldsymbol{q}}^{\mathbf{br}}_{n-1,\omega}, \bar{\boldsymbol{q}}^{\mathbf{tr}}_{n,\omega}, \bar{\boldsymbol{q}}^{\mathbf{br}}_{n,\omega}, \tilde{\boldsymbol{p}}^{\mathbf{H}}_{n,\omega}, \bar{\boldsymbol{p}}^{\mathbf{H}}_{n,\omega}\right]^{\top}, \ \forall n, \forall \omega. \tag{4.28}$$

The **consensus constraints** in (4.24d) enforce consistency between the global variables and their local copies. The associated vector of dual variables, $\boldsymbol{\lambda}_{n,\omega} \in \mathbb{R}^{6\times|\boldsymbol{T}|}$, is defined as

$$\boldsymbol{\lambda}_{n,\omega} := \left[\tilde{\boldsymbol{\lambda}}^{\mathbf{tr}}_{n-1,\omega}, \tilde{\boldsymbol{\lambda}}^{\mathbf{br}}_{n-1,\omega}, \bar{\boldsymbol{\lambda}}^{\mathbf{tr}}_{n,\omega}, \bar{\boldsymbol{\lambda}}^{\mathbf{br}}_{n,\omega}, \tilde{\boldsymbol{\lambda}}^{\mathbf{p}}_{n,\omega}, \bar{\boldsymbol{\lambda}}^{\mathbf{p}}_{n,\omega}\right]^{\top}, \ \forall n, \forall \omega. \tag{4.29}$$

Clearly, problem (4.24) exhibits a decomposable structure. Subproblem (4.24b) pertains to the VPP power balancing and is referred to as the *power balancing subproblem*. Subproblems (4.24c) address the hydropower plants individual dynamics and are referred to as the *local hydropower scheduling subproblems*. An example of the resulting decomposed structure is shown in Fig. 4.3 for $|\boldsymbol{N}| = 3$ and $|\boldsymbol{\Omega}| = 1$. The computational advantage of this decomposition is that the original stochastic MILP problem, solved for all n and ω, is now broken down into $|\boldsymbol{N}| \times |\boldsymbol{\Omega}|$

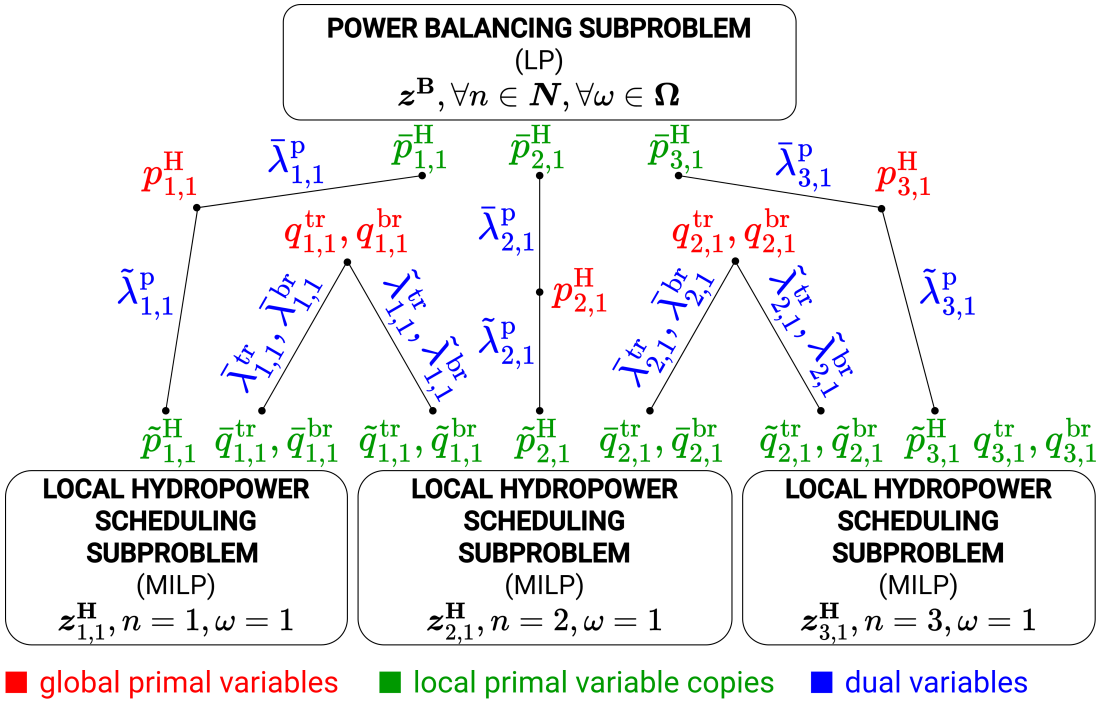

Figure 4.3: Example of decomposed structure of problem (3.27) when reformulated as the consensus problem (4.24) (**combined scenario-spatial decomposition**). The edges in the bipartite graph represent the consistency constraint linking global variables with their local copies.

deterministic MILP subproblems, and one stochastic LP subproblem, solved for all n and ω. While problem (4.24) is solved in a centralized manner, the subproblems (4.24b) and (4.24c), which have reduced dimensions compared to the original problem, can be solved in parallel using the distributed methods outlined in the following sections. This approach enables a faster and more scalable solution to the complex VPP scheduling problem by decomposing the problem along both the spatial and scenario dimensions simultaneously. Thus, it is referred to here as a **combined scenario-spatial decomposition** approach.

Additionally, Fig. 4.3 illustrates the necessity of using two distinct sets of decision variable copies, as detailed in (4.12)-(4.17), for the proposed reformulation. For the hydropower generation variables, one set of copies is assigned to the power balancing subproblem (4.24b) (denoted by the bar symbol in Fig. 4.3), while separate copies are allocated to the hydropower scheduling subproblems (4.24c) (denoted by the tilde symbol in Fig. 4.3). On the other hand, for the hydropower turbine and barrage outflows, two distinct sets of copies are introduced to account for the hydraulic connections within the cascaded system. For each hydropower plant, the first set of local copies, indicated by the bar symbol, represents the outflows of the given asset, while the second set, marked by the tilde symbol, represents the outflows of the neighboring (upstream) hydropower plant. Through this duplication mechanism, the problem is reformulated to enable decomposition while maintaining consistency in water flow propagation throughout the cascaded system.

The proposed consensus optimization-based reformulation method is applied to the case study of Compagnie Nationale du Rhône; however, it can be easily extended to handle generic

complex VPPs. This approach identifies the coupling constraints in the stochastic VPP problem, which typically involve multiple clusters of spatial coupling constraints and scenario coupling in scenario-based stochastic programming. By duplicating the decision variables associated with these coupling constraints and ensuring consistency between the original variables and their duplicates, the complex VPP problem can be reformulated in consensus form. Specifically, the decision variables related to the power balancing of the complex VPP are decoupled from those governing the local dynamics of the individual VPP assets. If additional spatial constraints exist among the VPP resources, such as the hydraulic links within the cascaded hydropower system in the Compagnie Nationale du Rhône case study, these coupling constraints are identified, and local copies are created and assigned to each asset's subproblem, recursively decoupling these constraints. Then, if the resulting power balancing subproblem involves only linear dynamics—typically the case due to the linear nature of the power balancing constraint—while the individual asset dynamics are complex (and potentially nonconvex), this mechanism provides a straightforward approach to separate the complex dynamics of each asset from both the other assets and the global power balancing of the VPP. It is important to note that the decomposition approach is applied only to dispatchable units, such as the hydropower systems in the Compagnie Nationale du Rhône case study. Decomposing non-dispatchable units would not be beneficial (from a scalability perspective), as they do not contribute to the computational complexity of the problem.

Although (4.24) now clearly exhibits a decomposable structure, it remains a *centralized* problem. To obtain a distributed solution, a dedicated algorithm must be developed that can exploit the decomposable structure of this reformulation. This is done in Section 4.3.1.2 for the convex case and in Section 4.3.1.3 for the mixed-integer case.

4.3.1.2 A Distributed Solution for the Convex Case

The reformulation provided in (4.24) allows for the use of various distributed optimization algorithms based on augmented Lagrangian relaxation. Among others, the consensus ADMM algorithm has proven to be highly effective in this context [39]. Let i denote the current iteration of the distributed algorithm, and ρ^i denote the penalty parameter of the algorithm at iteration i, which is adjusted dynamically according to the procedure outlined in [39]. For ease of presentation, define the matrix $\mathbf{M} \in \mathbb{R}^{6|\boldsymbol{T}|\times 6|\boldsymbol{T}|}$ as a diagonal matrix with a $5|\boldsymbol{T}|\times 5|\boldsymbol{T}|$ identity matrix in the top-left block and the last $|\boldsymbol{T}|$ diagonal elements set to zero:

$$\mathbf{M} = \begin{pmatrix} \mathbf{I}_{5|\boldsymbol{T}|} & \mathbf{0} \\ \mathbf{0} & \mathbf{0}_{|\boldsymbol{T}|} \end{pmatrix}. \tag{4.30}$$

Here, $\mathbf{I}_{5|\boldsymbol{T}|}$ is a $5|\boldsymbol{T}| \times 5|\boldsymbol{T}|$ identity matrix, and $\mathbf{0}_{|\boldsymbol{T}|}$ is a $|\boldsymbol{T}| \times |\boldsymbol{T}|$ zero matrix.

The iterative steps below are obtained by applying the consensus ADMM algorithm to (4.24).

Step I. *Local primal variables update* (4.31a)-(4.31b):

$$\boldsymbol{z}_{n,\omega}^{\mathbf{H}\ i+1} = \underset{\boldsymbol{z}_{n,\omega}^{\mathbf{H}} \in \boldsymbol{\Gamma}_{n,\omega}}{\operatorname{argmin}} \left\{ \left(\mathbf{M}\boldsymbol{\lambda}_{n,\omega}{}^{i}\right)^{\top} \bar{\boldsymbol{z}}_{n,\omega}^{\mathbf{B},\mathbf{H}} + \frac{\rho^i}{2} \left\| \mathbf{M}\left(\bar{\boldsymbol{z}}_{n,\omega}^{\mathbf{B},\mathbf{H}} - \boldsymbol{z}_{n,\omega}^{\mathbf{B},\mathbf{H}^i}\right) \right\|_2^2 \right\}, \ \forall n, \forall \omega, \tag{4.31a}$$

$$\boldsymbol{z}^{\mathbf{B}\,i+1} = \underset{z^{\mathbf{B}}\in\boldsymbol{\Xi}}{\operatorname{argmin}}\left\{ J + \sum_{n\in\boldsymbol{N}}\sum_{\omega\in\boldsymbol{\Omega}}\left(\left(\bar{\boldsymbol{\lambda}}^{\mathbf{p}}_{n,\omega}{}^{i}\right)^{\top}\bar{\boldsymbol{p}}^{\mathbf{H}}_{n,\omega} + \frac{\rho^{i}}{2}\left\|\bar{\boldsymbol{p}}^{\mathbf{H}}_{n,\omega} - \boldsymbol{p}^{\mathbf{H}}_{n,\omega}{}^{i}\right\|_2^2\right)\right\}. \tag{4.31b}$$

Step II. *Global primal variables update* in (4.32):

$$\boldsymbol{q}^{\mathbf{tr}}_{n,\omega}{}^{i+1} = \frac{1}{2}\left(\bar{\boldsymbol{q}}^{\mathbf{tr}}_{n,\omega}{}^{i+1} + \tilde{\boldsymbol{q}}^{\mathbf{tr}}_{n,\omega}{}^{i+1}\right),\ \forall n, \forall\omega, \tag{4.32a}$$

$$\boldsymbol{q}^{\mathbf{br}}_{n,\omega}{}^{i+1} = \frac{1}{2}\left(\bar{\boldsymbol{q}}^{\mathbf{br}}_{n,\omega}{}^{i+1} + \tilde{\boldsymbol{q}}^{\mathbf{br}}_{n,\omega}{}^{i+1}\right),\ \forall n, \forall\omega, \tag{4.32b}$$

$$\boldsymbol{p}^{\mathbf{H}}_{n,\omega}{}^{i+1} = \frac{1}{2}\left(\bar{\boldsymbol{p}}^{\mathbf{H}}_{n,\omega}{}^{i+1} + \tilde{\boldsymbol{p}}^{\mathbf{H}}_{n,\omega}{}^{i+1}\right),\ \forall n, \forall\omega. \tag{4.32c}$$

Step III. *Dual variables update* in (4.33):

$$\boldsymbol{\lambda}_{n,\omega}{}^{i+1} = \boldsymbol{\lambda}_{n,\omega}{}^{i} + \rho^{i}\left(\bar{\boldsymbol{z}}^{\mathbf{B},\mathbf{H}}_{n,\omega}{}^{i+1} - \boldsymbol{z}^{\mathbf{B},\mathbf{H}}_{n,\omega}{}^{i+1}\right),\ \forall n, \forall\omega. \tag{4.33}$$

Through the application of the consensus ADMM steps (4.31a)-(4.33) to the decomposed problem (4.24), a fully distributed solution to the original centralized problem (3.27) can be derived. Algorithm 1 outlines the consensus ADMM algorithm with adaptive penalty parameters from [39] applied to the proposed decomposed problem (4.24). While Algorithm 1 is essentially an adaptation of the original consensus ADMM algorithm, this adaptation is made possible by the decomposition detailed in the previous section. This decomposition enables the use of several augmented Lagrangian relaxation-based methods. The approach combines decomposition in both the scenario and spatial dimensions, making Algorithm 1 a *fully distributed method*. This is a significant departure from the *hierarchical* nature of the classical ADMM approach and facilitates full parallelization across both the spatial and scenario dimensions in complex VPP scheduling optimization.

In general, Algorithm 1 guarantees convergence to the global optimum of the original problem (3.27) **only** in the convex case, as it inherits the theoretical convergence properties of the classical ADMM method. To ensure a scalable distributed solution for complex VPP optimal scheduling problems, including for MILP models (which are typically used for such problems, as shown in Fig. 1.2), the next section provides an extension of Algorithm 1.

4.3.1.3 A Distributed Solution for the Mixed-Integer Case

In the previous section, Algorithm 1 was introduced as a direct application of the consensus ADMM method to address the complex VPP scheduling problem (3.27), reformulated as problem (4.24) to allow full decomposition along both the scenario and spatial dimensions. When the subproblems (4.24b) and (4.24c), derived from decomposing the original problem (3.27), are convex, Algorithm 1 converges to the global optimum (if it exists) of the original centralized problem [211]. Although convergence is theoretically assured in these convex cases, practical performance and convergence rate can vary significantly depending on algorithmic parameter tuning [212], especially the choice of the penalty parameter ρ [213], which in turn depends on the step-size parameter τ used in Algorithm 1 for dynamic penalty parameter updates as outlined in [39]. For nonconvex cases, however, Algorithm 1 functions as a **heuristic**, inheriting the

Algorithm 1 Consensus ADMM

Input: Parameter vectors $\{\boldsymbol{\theta}_{n,\omega}\}_{n\in\boldsymbol{N},\omega\in\boldsymbol{\Omega}}$ and $\boldsymbol{\beta}$.

Output: Optimal price-quantity bidding curves and power generation $\boldsymbol{z}^{\mathbf{B}\star}$.

1: Initialize primal and dual variables $\left\{\boldsymbol{q}_{n,\omega}^{\mathbf{tr}\ 0}, \boldsymbol{q}_{n,\omega}^{\mathbf{br}\ 0}, \boldsymbol{p}_{n,\omega}^{\mathbf{H}\ 0}, \boldsymbol{\lambda}_{n,\omega}{}^{0}\right\}_{n\in\boldsymbol{N},\omega\in\boldsymbol{\Omega}}$, primal residual $\boldsymbol{r}^0$, dual residual $\boldsymbol{s}^0$, penalty parameter $\rho^0 \leftarrow 2$, tolerance parameter $\epsilon \leftarrow 10^{-4}$, maximum number of algorithm's iterations $\overline{I} \leftarrow 1000$, $\tau \leftarrow 2$, $\mu \leftarrow 10$;

2: $i \leftarrow 0$;

3: **while** $\min\left(\left\|\boldsymbol{r}^i\right\|_2, \left\|\boldsymbol{s}^i\right\|_2\right) > \epsilon$ and $i < \overline{I}$ **do**

4: *Local primal variables update*: $\left\{\boldsymbol{z}_{n,\omega}^{\mathbf{H}\ i+1}\right\}_{n\in\boldsymbol{N},\omega\in\boldsymbol{\Omega}} \leftarrow$ (4.31a), $\boldsymbol{z}^{\mathbf{B}i+1} \leftarrow$ (4.31b);

5: *Global primal variables update*: $\left\{\boldsymbol{q}_{n,\omega}^{\mathbf{tr}\ i+1}, \boldsymbol{q}_{n,\omega}^{\mathbf{br}\ i+1}, \boldsymbol{p}_{n,\omega}^{\mathbf{H}\ i+1}\right\}_{n\in\boldsymbol{N},\omega\in\boldsymbol{\Omega}} \leftarrow$ (4.32);

6: *Dual variables update*: $\left\{\boldsymbol{\lambda}_{n,\omega}{}^{i+1}\right\}_{n\in\boldsymbol{N},\omega\in\boldsymbol{\Omega}} \leftarrow$ (4.33);

7: *Primal residual update*:

$$\begin{aligned}\boldsymbol{r}_{n,\omega}^{i+1} \leftarrow \Big[&\bar{\boldsymbol{q}}_{n,\omega}^{\mathbf{tr}\ i+1} - \boldsymbol{q}_{n,\omega}^{\mathbf{tr}\ i+1}, \tilde{\boldsymbol{q}}_{n,\omega}^{\mathbf{tr}\ i+1} - \boldsymbol{q}_{n,\omega}^{\mathbf{tr}\ i+1}, \bar{\boldsymbol{q}}_{n,\omega}^{\mathbf{br}\ i+1} - \boldsymbol{q}_{n,\omega}^{\mathbf{br}\ i+1},\\ &\tilde{\boldsymbol{q}}_{n,\omega}^{\mathbf{br}\ i+1} - \boldsymbol{q}_{n,\omega}^{\mathbf{br}\ i+1}, \bar{\boldsymbol{p}}_{n,\omega}^{\mathbf{H}\ i+1} - \boldsymbol{p}_{n,\omega}^{\mathbf{H}\ i+1}, \tilde{\boldsymbol{p}}_{n,\omega}^{\mathbf{H}\ i+1} - \boldsymbol{p}_{n,\omega}^{\mathbf{H}\ i+1}\Big]^\top, \forall n, \forall\omega;\end{aligned} \tag{4.34}$$

8: *Dual residual update*:

$$\boldsymbol{s}_{n,\omega}^{i+1} \leftarrow -\rho^i \left[\boldsymbol{q}_{n,\omega}^{\mathbf{tr}\ i+1} - \boldsymbol{q}_{n,\omega}^{\mathbf{tr}\ i}, \boldsymbol{q}_{n,\omega}^{\mathbf{br}\ i+1} - \boldsymbol{q}_{n,\omega}^{\mathbf{br}\ i}, \boldsymbol{p}_{n,\omega}^{\mathbf{H}\ i+1} - \boldsymbol{p}_{n,\omega}^{\mathbf{H}\ i}\right]^\top, \ \forall n, \forall\omega; \tag{4.35}$$

9: *Collect residuals*:

$$\boldsymbol{r}^{i+1} := \left[\boldsymbol{r}_{1,1}^{i+1}, ..., \boldsymbol{r}_{1,|\boldsymbol{\Omega}|}^{i+1}, ..., \boldsymbol{r}_{|\boldsymbol{N}|,1}^{i+1}, ..., \boldsymbol{r}_{|\boldsymbol{N}|,|\boldsymbol{\Omega}|}^{i+1}\right]^\top, \tag{4.36}$$

$$\boldsymbol{s}^{i+1} := \left[\boldsymbol{s}_{1,1}^{i+1}, ..., \boldsymbol{s}_{1,|\boldsymbol{\Omega}|}^{i+1}, ..., \boldsymbol{s}_{|\boldsymbol{N}|,1}^{i+1}, ..., \boldsymbol{s}_{|\boldsymbol{N}|,|\boldsymbol{\Omega}|}^{i+1}\right]^\top; \tag{4.37}$$

10: **if** $\left\|\boldsymbol{r}^{i+1}\right\|_2 > \mu \left\|\boldsymbol{s}^{i+1}\right\|_2$ **then** ▷ Penalty parameter update

11: $\rho^{i+1} = \tau\rho^i$;

12: **else if** $\left\|\boldsymbol{s}^{i+1}\right\|_2 > \mu \left\|\boldsymbol{r}^{i+1}\right\|_2$ **then**

13: $\rho^{i+1} = \frac{\rho^i}{\tau}$;

14: **else**

15: $\rho^{i+1} = \rho^i$;

16: **end if**

17: $i \leftarrow i + 1$;

18: **end while**

19: $\boldsymbol{z}^{\mathbf{B}\star} \leftarrow \boldsymbol{z}^{\mathbf{B}i}$;

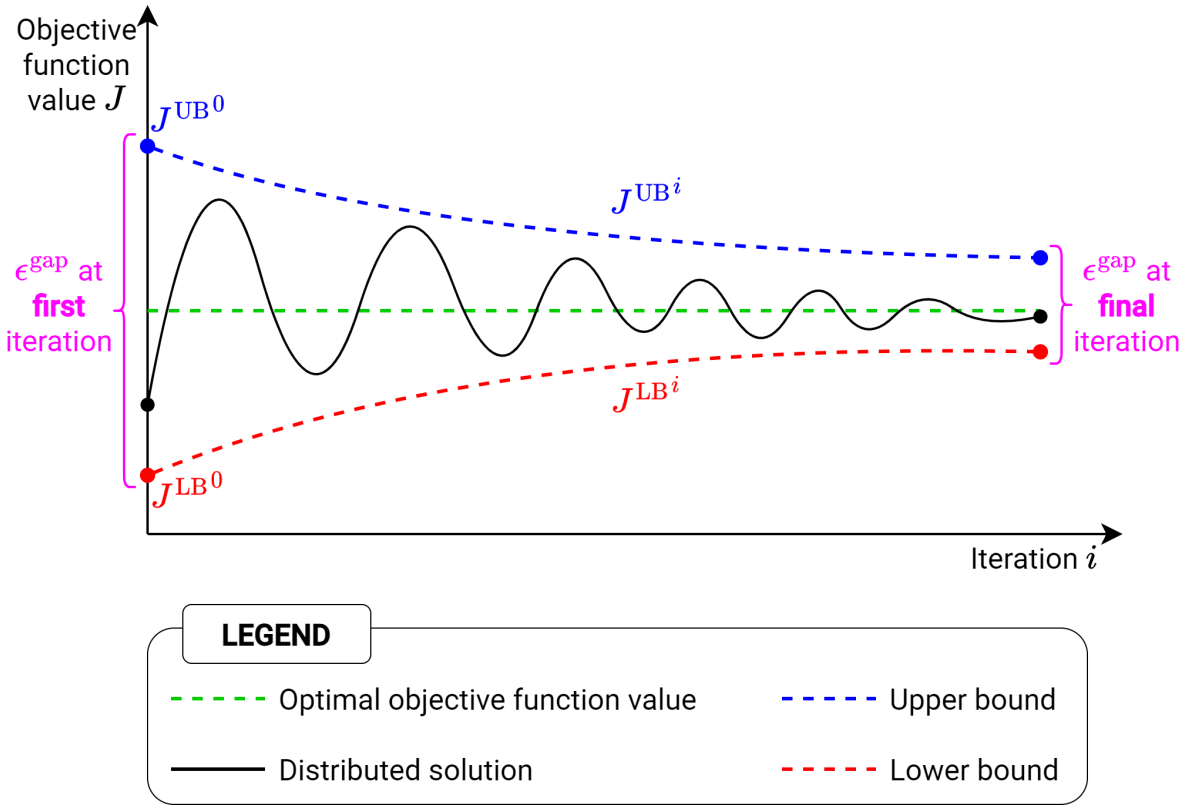

Figure 4.4: Illustration of the functioning of the proposed novel, trustworthy ADMM-based distributed algorithm.

convergence limitations of classical ADMM [44].

To address this limitation, Algorithm 1 is extended here to handle nonconvex problems while retaining a performance guarantee on the optimality of the final solution. The focus is on MILP scheduling models, the most widely used models in VPP operations [28]. Even for MILP problems, ADMM does not always converge, and when it does, it may not reach an optimal point, functioning essentially as a local optimization method. While numerous studies highlight the potential of ADMM in complex mixed-integer problems as an effective heuristic [214], the practical deployment of such a distributed approach in real-world engineering applications—where solution accuracy is paramount—requires robust *performance guarantees*. Without such guarantees, adoption remains limited. This work contributes to this ongoing research [215] by presenting an extension to Algorithm 1, which previously assured convergence only for convex models, to provide a quality guarantee on the final distributed solution for MILP models as well. In this sense, the novel distributed algorithm, developed based on Algorithm 1 and detailed below, is *trustworthy*, as it offers a distributed solution that the VPP operator can confidently evaluate and trust.

Inspired by popular methods for solving MILP models, such as Branch and Bound methods [216], the proposed trustworthy distributed algorithm leverages upper and lower bounds on the optimal objective function value of (3.27), denoted by $J^{\star}$, which are derived from the distributed solution provided at each iteration of Algorithm 1. Here, the lower bound calculated at the i-th

iteration of the distributed algorithm is denoted by J^{LB^i}, and the upper bound by J^{UB^i}. The "distance" between these bounds is used to assess the quality of the distributed solution at each iteration of the algorithm. Initially, the upper and lower bounds are set by the algorithm, with values J^{UB^0} and J^{LB^0}, respectively. As the distributed algorithm proceeds, two separate mechanisms are employed at each iteration to update the upper and lower bounds. When the "distance" between the upper and lower bounds falls below a specified threshold, denoted by ϵ^{gap} and set by the VPP operator, the algorithm terminates. The final solution obtained is guaranteed to be within an ϵ^{gap}-neighborhood of the global optimum of the original centralized problem, meaning that the maximum error of the final distributed solution is guaranteed to be no greater than ϵ^{gap} (e.g., 0.01%). A mathematical proof is provided below to establish the existence and validity of the bounds. Fig. 4.4 illustrates the functioning of the proposed novel, trustworthy ADMM-based distributed algorithm.

The proposed novel, trustworthy consensus ADMM-based distributed algorithm, hereafter referred to as the **Consensus ADMM with Bounds** (**CADMMB**), involves the following **key steps**:

- **Initialization of upper and lower bounds**: The *initial lower bound*, denoted by J^{LB^0}, is derived by solving the linear relaxation of the original centralized problem (3.27), which expands the feasible set and thereby produces an optimal value less than or equal to $J^\star$. This linear relaxation is obtained by allowing the binary variables in the original problem (3.27) to take fractional values. Conversely, the *initial upper bound*, denoted by J^{UB^0}, is obtained by tightening the feasible space of (3.27). Identical upper and lower limits are set on the forebay water levels for each hydropower plant, effectively treating the cascaded hydropower system as having no storage capacity and operating as a series of pure run-of-the-river plants. This approach is implemented by fixing the binary variables in (3.27k). Calculating both J^{LB^0} and J^{UB^0} requires solving two LP problems, which incurs minimal computational cost before the distributed algorithm is started. As the consensus ADMM Algorithm 1 progresses, these bounds are iteratively refined following two distinct strategies outlined below.

- **Upper bound update** (**quasi-projection step**): At each iteration i, the upper bound J^{UB^i} is refined through a quasi-projection step. Let $\boldsymbol{z}^i$ represents the primal variable value obtained from consensus ADMM. This value is projected onto a new LP formed by fixing the binary variables in the original centralized problem (3.27) to the values in $\boldsymbol{z}^i$. Clearly, this projection, denoted by $\boldsymbol{z}^{\mathrm{prj}^i}$, remains feasible within the feasible space of (3.27), resulting in a new bound defined as $J^{\mathrm{UB}^i} := J\left(\boldsymbol{z}^{\mathrm{prj}^i}\right)$ where $J^\star \leq J^{\mathrm{UB}^i}$.

- **Lower bound update**: To obtain a lower bound on the global optimum, duality theory provides a useful foundation [217]. However, deriving a straightforward solution for the dual of (3.27), especially for a complex VPP optimization problem, is often challenging and may lack scalability. Instead, the dual variables iteratively computed by the consensus ADMM Algorithm 1 can be leveraged to build an efficient approach for computing a new lower bound at each iteration of the distributed algorithm. The method is built

upon the theoretical results detailed in Proposition 1 and utilizes the dual variables tied to the consensus constraints in (4.24). The proposed approach extends the theoretical findings from [218] provided for consensus ADMM in scenario decomposition, to the case of combined scenario-spatial decomposition of a MILP problem.

Proposition 1. *Let* $\boldsymbol{\lambda} := \{\boldsymbol{\lambda}_{n,\omega}\}_{n\in\boldsymbol{N},\omega\in\boldsymbol{\Omega}}$ *satisfy the following conditions (component-wise):*

$$\sum_{n\in\boldsymbol{N}}\sum_{\omega\in\boldsymbol{\Omega}} P_\omega\left(\bar{\boldsymbol{\lambda}}^{\boldsymbol{p}}_{n,\omega}+\tilde{\boldsymbol{\lambda}}^{\boldsymbol{p}}_{n,\omega}\right)=0, \tag{4.38}$$

$$\sum_{n\in\boldsymbol{N}}\sum_{\omega\in\boldsymbol{\Omega}} P_\omega\left(\bar{\boldsymbol{\lambda}}^{\mathbf{tr}}_{n,\omega}+\tilde{\boldsymbol{\lambda}}^{\mathbf{tr}}_{n,\omega}\right)=0, \tag{4.39}$$

$$\sum_{n\in\boldsymbol{N}}\sum_{\omega\in\boldsymbol{\Omega}} P_\omega\left(\bar{\boldsymbol{\lambda}}^{\mathbf{br}}_{n,\omega}+\tilde{\boldsymbol{\lambda}}^{\mathbf{br}}_{n,\omega}\right)=0. \tag{4.40}$$

Let

$$D^{\mathrm{B}}(\boldsymbol{\lambda}) := \min_{\boldsymbol{z}^{B}\in\boldsymbol{\Xi}}\left\{J+\sum_{n\in\boldsymbol{N}}\sum_{\omega\in\boldsymbol{\Omega}} P_\omega\left(\bar{\boldsymbol{\lambda}}^{\mathbf{p}}_{n,\omega}\right)^\top \boldsymbol{p}^{\mathbf{H}}_{n,\omega}\right\}, \tag{4.41}$$

and

$$D^{\mathrm{H}}_{n,\omega}(\boldsymbol{\lambda}_{n,\omega}) := \min_{\boldsymbol{z}^{\mathbf{H}}_{n,\omega}\in\boldsymbol{\Gamma}_{n,\omega}}\left\{(\mathbf{M}\boldsymbol{\lambda}_{n,\omega})^\top \boldsymbol{z}^{\mathbf{B},\mathbf{H}}_{n,\omega}\right\}, \forall n, \forall\omega. \tag{4.42}$$

Then

$$D(\boldsymbol{\lambda}) := D^{\mathrm{B}}(\boldsymbol{\lambda}) + \sum_{n\in\boldsymbol{N}}\sum_{\omega\in\boldsymbol{\Omega}} P_\omega D^{\mathrm{H}}_{n,\omega}(\boldsymbol{\lambda}_{n,\omega}) \le J^\star. \tag{4.43}$$

Proof. Let $\left\{\boldsymbol{b}^{\mathbf{br}^\star}, \boldsymbol{b}^{\mathbf{oc}^\star}\boldsymbol{e}^\star, \boldsymbol{\delta}^{\mathbf{E}^\star}, \boldsymbol{p}^{\mathbf{H}^\star}, \boldsymbol{q}^{\mathbf{tr}^\star}, \boldsymbol{q}^{\mathbf{br}^\star}, \boldsymbol{z}^{\mathbf{fbl}^\star}\right\}$ be an optimal solution of the original problem (3.27). Feasibility implies that this optimal solution is also feasible within the relaxed feasible spaces of the subproblems (4.24b) and (4.24c), i.e., it is feasible in $\boldsymbol{\Xi}$ and $\boldsymbol{\Gamma}_{n,\omega}, \forall n, \forall\omega$, respectively. Thus:

$$D^{\mathrm{B}}(\boldsymbol{\lambda}) \le J(\boldsymbol{e}^\star, \boldsymbol{\delta}^{\mathbf{E}^\star}) + \sum_{n\in\boldsymbol{N}}\sum_{\omega\in\boldsymbol{\Omega}} P_\omega\left(\bar{\boldsymbol{\lambda}}^{\mathbf{p}}_{n,\omega}\right)^\top \boldsymbol{p}^{\mathbf{H}^\star}_{n,\omega}, \tag{4.44}$$

and

$$\begin{aligned} D^{\mathrm{H}}(\boldsymbol{\lambda}_{n,\omega}) \le &\left(\tilde{\boldsymbol{\lambda}}^{\mathbf{p}}_{n,\omega}\right)^\top \boldsymbol{p}^{\mathbf{H}^\star}_{n,\omega} + \left(\tilde{\boldsymbol{\lambda}}^{\mathbf{tr}}_{n-1,\omega}\right)^\top \boldsymbol{q}^{\mathbf{tr}^\star}_{n-1,\omega} + \left(\tilde{\boldsymbol{\lambda}}^{\mathbf{br}}_{n-1,\omega}\right)^\top \boldsymbol{q}^{\mathbf{br}^\star}_{n-1,\omega} + \left(\bar{\boldsymbol{\lambda}}^{\mathbf{tr}}_{n,\omega}\right)^\top \boldsymbol{q}^{\mathbf{tr}^\star}_{n,\omega} \\ &+ \left(\bar{\boldsymbol{\lambda}}^{\mathbf{br}}_{n,\omega}\right)^\top \boldsymbol{q}^{\mathbf{br}^\star}_{n,\omega}\ , \ \forall n, \forall\omega. \end{aligned} \tag{4.45}$$

Then

$$\begin{aligned} D(\boldsymbol{\lambda}) \le &\sum_{n\in\boldsymbol{N}}\sum_{\omega\in\boldsymbol{\Omega}} P_\omega\left(\bar{\boldsymbol{\lambda}}^{\mathbf{p}}_{n,\omega}+\tilde{\boldsymbol{\lambda}}^{\mathbf{p}}_{n,\omega}\right)^\top \boldsymbol{p}^{\mathbf{H}^\star}_{n,\omega} + \sum_{n\in\boldsymbol{N}}\sum_{\omega\in\boldsymbol{\Omega}} P_\omega\left(\bar{\boldsymbol{\lambda}}^{\mathbf{tr}}_{n,\omega}+\tilde{\boldsymbol{\lambda}}^{\mathbf{tr}}_{n,\omega}\right)^\top \boldsymbol{q}^{\mathbf{tr}^\star}_{n,\omega} \\ &+ \sum_{n\in\boldsymbol{N}}\sum_{\omega\in\boldsymbol{\Omega}} P_\omega\left(\bar{\boldsymbol{\lambda}}^{\mathbf{br}}_{n,\omega}+\tilde{\boldsymbol{\lambda}}^{\mathbf{br}}_{n,\omega}\right)^\top \boldsymbol{q}^{\mathbf{br}^\star}_{n,\omega} + J(\boldsymbol{e}^\star, \boldsymbol{\delta}^{\mathbf{E}^\star}) \\ =&J(\boldsymbol{e}^\star, \boldsymbol{\delta}^{\mathbf{E}^\star}) = J^\star. \end{aligned} \tag{4.46}$$

The second last equality follows from (4.38)-(4.40), which are inherently satisfied by the ADMM, as shown in [39]. □

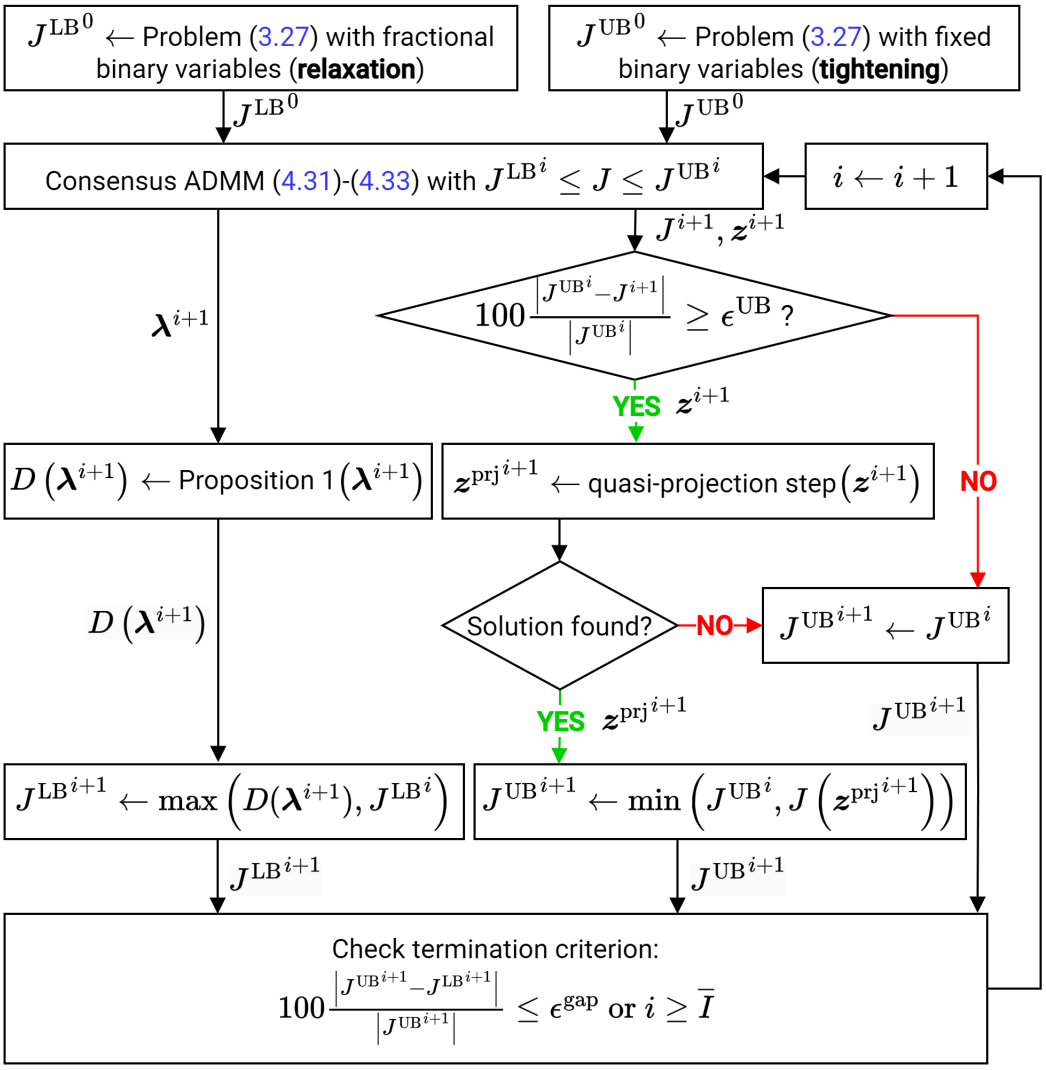

Figure 4.5: Illustration of the proposed trustworthy CADMMB Algorithm 2.

According to Proposition 1, the lower bound can be updated from (4.43) as $J^{\mathrm{LB}^i} \leftarrow D\left(\boldsymbol{\lambda}^i\right)$. Since each iteration of Algorithm 1 calculates a new update for the dual variables $\boldsymbol{\lambda}$, this simple algebraic step for updating the lower bound can be incorporated into an extended version of the algorithm with negligible additional computational effort. If the new lower bound from (4.43) provides a tighter bound than the algorithm's current lower bound, the lower bound is updated accordingly. In contrast, the quasi-projection step needed to compute a new upper bound requires solving a LP optimization problem. Although solving this straightforward problem requires minimal computation, it may still be advantageous to limit the execution of this step to enhance the algorithm's computational efficiency. For this purpose, the proposed distributed method includes a check to determine whether to update the upper bound at iteration i, based on a tolerance parameter ϵ^{UB}:

$$100\frac{\left|J^{\mathrm{UB}^i} - J^{i+1}\right|}{\left|J^{\mathrm{UB}^i}\right|} \geq \epsilon^{\mathrm{UB}}. \tag{4.47}$$

The termination criterion of the proposed distributed algorithm is given by:

$$J^{\text{gap}i} := 100\frac{\left|J^{\text{UB}^i} - J^{\text{LB}^i}\right|}{\left|J^{\text{UB}^i}\right|} \leq \epsilon^{\text{gap}} \text{ or } i \geq \overline{I}. \tag{4.48}$$

The proposed trustworthy CADMMB is detailed in Algorithm 2, with a schematic overview of its main steps shown in Fig. 4.5.

Algorithm 2 Consensus ADMM with Bounds (CADMMB)

Input: Parameter vectors $\{\boldsymbol{\theta}_{n,\omega}\}_{n\in\boldsymbol{N},\omega\in\boldsymbol{\Omega}}$ and $\boldsymbol{\beta}$.

Output: Optimal price-quantity bidding curves and power generation $\boldsymbol{z}^{\mathbf{B}\star}$, lower bound $J^{\mathrm{LB}\star}$, and upper bound $J^{\mathrm{UB}\star}$.

Initialize primal and dual variables $\left\{\boldsymbol{q}^{\mathbf{tr}}_{n,\omega}{}^{0}, \boldsymbol{q}^{\mathbf{br}}_{n,\omega}{}^{0}, \boldsymbol{p}^{\mathbf{H}}_{n,\omega}{}^{0}, \boldsymbol{\lambda}_{n,\omega}{}^{0}\right\}_{n\in\boldsymbol{N},\omega\in\boldsymbol{\Omega}}$, primal residual $\boldsymbol{r}^0$, dual residual $\boldsymbol{s}^0$, penalty parameter $\rho^0 \leftarrow 2$, tolerance parameter $\epsilon \leftarrow 10^{-4}$, maximum number of algorithm's iterations $\overline{I} \leftarrow 1000$, $\tau \leftarrow 2$, $\mu \leftarrow 10$, $\epsilon^{\mathrm{UB}} \leftarrow 0.01\%$, $\epsilon^{\mathrm{gap}} \leftarrow 0.01\%$;

Lower bound initialization: $J^{\mathrm{LB}^0} \leftarrow$ Optimal objective function value of (3.27) with fractional binary variables (*relaxation*);

Upper bound initialization: $J^{\mathrm{UB}^0} \leftarrow$ Optimal objective function value of (3.27) with fixed binary variables (*tightening*);

$i \leftarrow 0$;

while $J^{\mathrm{gap}^i} \geq \epsilon^{\mathrm{gap}}$ or $i < \overline{I}$ **do**

Local primal variables update: $\left\{\boldsymbol{z}^{\mathbf{H}}_{n,\omega}{}^{i+1}\right\}_{n\in\boldsymbol{N},\omega\in\boldsymbol{\Omega}} \leftarrow$ (4.31a), $\left\{J^{i+1}, \boldsymbol{z}^{\mathbf{B}^{i+1}}\right\} \leftarrow$ (4.31b) with additional constraints $J^{\mathrm{LB}^i} \leq J \leq J^{\mathrm{UB}^i}$;

Global primal variables update: $\left\{\boldsymbol{q}^{\mathbf{tr}}_{n,\omega}{}^{i+1}, \boldsymbol{q}^{\mathbf{br}}_{n,\omega}{}^{i+1}, \boldsymbol{p}^{\mathbf{H}}_{n,\omega}{}^{i+1}\right\}_{n\in\boldsymbol{N},\omega\in\boldsymbol{\Omega}} \leftarrow$ (4.32);

Dual variables update: $\boldsymbol{\lambda}^{i+1} = \left\{\boldsymbol{\lambda}_{n,\omega}{}^{i+1}\right\}_{n\in\boldsymbol{N},\omega\in\boldsymbol{\Omega}} \leftarrow$ (4.33);

$D\left(\boldsymbol{\lambda}^{i+1}\right) \leftarrow$ Proposition 1$\left(\boldsymbol{\lambda}^{i+1}\right)$;

Lower bound update: $J^{\mathrm{LB}^{i+1}} \leftarrow \max\left(J^{\mathrm{LB}^{i+1}}, D\left(\boldsymbol{\lambda}^{i+1}\right)\right)$;

if $100\frac{\left|J^{\mathrm{UB}^i} - J^{i+1}\right|}{\left|J^{\mathrm{UB}^i}\right|} \geq \epsilon^{\mathrm{UB}}$ **then**

$\boldsymbol{z}^{i+1} \leftarrow \left\{\boldsymbol{z}^{\mathbf{B}^{i+1}} \cup \left\{\boldsymbol{z}^{\mathbf{H}}_{n,\omega}{}^{i+1}\right\}_{n\in\boldsymbol{N},\omega\in\boldsymbol{\Omega}}\right\}$;

$\boldsymbol{z}^{\mathrm{prj}^{i+1}} \leftarrow$ quasi-projection step$(\boldsymbol{z}^{i+1})$;

if If a solution is obtained from the quasi-projection step **then**

Upper bound update: $J^{\mathrm{UB}^{i+1}} \leftarrow \min\left(J^{\mathrm{UB}^i}, J\left(\boldsymbol{z}^{\mathrm{prj}^{i+1}}\right)\right)$;

else

Upper bound update: $J^{\mathrm{UB}^{i+1}} \leftarrow J^{\mathrm{UB}^i}$;

end if

end if

Primal residual update:

$$\begin{aligned}\boldsymbol{r}^{i+1}_{n,\omega} \leftarrow \Big[&\bar{\boldsymbol{q}}^{\mathbf{tr}}_{n,\omega}{}^{i+1} - \boldsymbol{q}^{\mathbf{tr}}_{n,\omega}{}^{i+1}, \tilde{\boldsymbol{q}}^{\mathbf{tr}}_{n,\omega}{}^{i+1} - \boldsymbol{q}^{\mathbf{tr}}_{n,\omega}{}^{i+1}, \bar{\boldsymbol{q}}^{\mathbf{br}}_{n,\omega}{}^{i+1} - \boldsymbol{q}^{\mathbf{br}}_{n,\omega}{}^{i+1},\\ &\tilde{\boldsymbol{q}}^{\mathbf{br}}_{n,\omega}{}^{i+1} - \boldsymbol{q}^{\mathbf{br}}_{n,\omega}{}^{i+1}, \bar{\boldsymbol{p}}^{\mathbf{H}}_{n,\omega}{}^{i+1} - \boldsymbol{p}^{\mathbf{H}}_{n,\omega}{}^{i+1}, \tilde{\boldsymbol{p}}^{\mathbf{H}}_{n,\omega}{}^{i+1} - \boldsymbol{p}^{\mathbf{H}}_{n,\omega}{}^{i+1}\Big]^\top, \forall n, \forall\omega;\end{aligned} \tag{4.49}$$

Dual residual update:

$$\boldsymbol{s}^{i+1}_{n,\omega} \leftarrow -\rho^i\left[\boldsymbol{q}^{\mathbf{tr}}_{n,\omega}{}^{i+1} - \boldsymbol{q}^{\mathbf{tr}}_{n,\omega}{}^{i}, \boldsymbol{q}^{\mathbf{br}}_{n,\omega}{}^{i+1} - \boldsymbol{q}^{\mathbf{br}}_{n,\omega}{}^{i}, \boldsymbol{p}^{\mathbf{H}}_{n,\omega}{}^{i+1} - \boldsymbol{p}^{\mathbf{H}}_{n,\omega}{}^{i}\right]^\top, \ \forall n, \forall\omega; \tag{4.50}$$

Collect residuals:

$$\boldsymbol{r}^{i+1} := \left[\boldsymbol{r}^{i+1}_{1,1}, ..., \boldsymbol{r}^{i+1}_{1,|\boldsymbol{\Omega}|}, ..., \boldsymbol{r}^{i+1}_{|\boldsymbol{N}|,1}, ..., \boldsymbol{r}^{i+1}_{|\boldsymbol{N}|,|\boldsymbol{\Omega}|}\right]^\top, \tag{4.51}$$

$$\boldsymbol{s}^{i+1} := \left[\boldsymbol{s}^{i+1}_{1,1}, ..., \boldsymbol{s}^{i+1}_{1,|\boldsymbol{\Omega}|}, ..., \boldsymbol{s}^{i+1}_{|\boldsymbol{N}|,1}, ..., \boldsymbol{s}^{i+1}_{|\boldsymbol{N}|,|\boldsymbol{\Omega}|}\right]^\top; \tag{4.52}$$

if $\left\|\boldsymbol{r}^{i+1}\right\|_2 > \mu \left\|\boldsymbol{s}^{i+1}\right\|_2$ **then** ▷ Penalty parameter update
  $\rho^{i+1} = \tau\rho^i$;
else if $\left\|\boldsymbol{s}^{i+1}\right\|_2 > \mu \left\|\boldsymbol{r}^{i+1}\right\|_2$ **then**
  $\rho^{i+1} = \frac{\rho^i}{\tau}$;
else
  $\rho^{i+1} = \rho^i$;
end if
$i \leftarrow i + 1$;
end while
$\boldsymbol{z}^{\mathbf{B}^\star} \leftarrow \boldsymbol{z}^{\mathbf{B}^i}$, $J^{\mathrm{LB}^\star} \leftarrow J^{\mathrm{LB}^i}$, $J^{\mathrm{UB}^\star} \leftarrow J^{\mathrm{UB}^i}$;

4.3.2 Distributed Economic Model Predictive Control for Dispatch in Complex Virtual Power Plants

This section presents the proposed decomposition method for the dispatch phase, as formulated in (3.19), of the two-level decision-making framework outlined in Chapter 3 (i.e., the second level shown in Fig. 4.2). The objective here is to provide a distributed solution for the economic MPC strategy developed in the previous chapter to address the short-term dispatch of a complex VPP. While the method is specifically applied to the case study of Compagnie Nationale du Rhône, detailed in (3.27), it can be readily extended to a generic complex VPP, following the same considerations of the previous section. To introduce the decomposition approach, a **deterministic version** of the control problem (3.19) is considered (i.e., $|\Omega| = t+1|t$) to simplify the presentation of the scenario-spatial decomposition technique. Therefore, the subscript ω is omitted in the following equations. The distributed method outlined here addresses the spatial scaling of the original centralized control problem, but it can easily be extended to include multiple scenarios of the uncertainty representation following the procedure detailed in Section 4.3.1.1. Since the following equations pertain to the short-term phase of the complex VPP decision-making process, the superscript ST is used to ensure consistency with the notation employed in Chapter 3.

In the dispatch MPC problem, as in the scheduling phase, two types of spatial coupling constraints exist: hydraulic and electrical coupling. Additionally, scenario coupling arises if scenario-based stochastic programming is applied also in this stage of the decision-making process. Similar to the scheduling phase, each set of coupling constraints is linked to three groups of **global variables**: the hydropower turbine outflow variables,

$$\boldsymbol{q}_n^{\mathbf{tr,ST}} := \left[q^{\mathrm{tr,ST}}_{n,t+1|t}, ..., q^{\mathrm{tr,ST}}_{n,t+k|t}, ..., q^{\mathrm{tr,ST}}_{n,t+|\boldsymbol{K}||t}\right]^\top, \ \forall n, \tag{4.53}$$

the hydropower barrage outflow variables,

$$\boldsymbol{q}_n^{\mathbf{br,ST}} := \left[q^{\mathrm{br,ST}}_{n,t+1|t}, ..., q^{\mathrm{br,ST}}_{n,t+k|t}, ..., q^{\mathrm{br,ST}}_{n,t+|\boldsymbol{K}||t}\right]^\top, \ \forall n, \tag{4.54}$$

and the hydropower generation variables,

$$\boldsymbol{p}_n^{\mathbf{H,ST}} := \left[p_{n,t+1|t}^{\mathrm{H,ST}}, ..., p_{n,t+k|t}^{\mathrm{H,ST}}, ..., p_{n,t+|\boldsymbol{K}||t}^{\mathrm{H,ST}}\right]^\top, \ \forall n. \tag{4.55}$$

By duplicating the global variables of the problem, the following **local copies** are defined:

$$\tilde{\boldsymbol{q}}_n^{\mathbf{tr,ST}} := \left[\tilde{q}_{n,t+1|t}^{\mathrm{tr,ST}}, ..., \tilde{q}_{n,t+k|t}^{\mathrm{tr,ST}}, ..., \tilde{q}_{n,t+|\boldsymbol{K}||t}^{\mathrm{tr,ST}}\right]^\top, \ \forall n, \tag{4.56}$$

$$\bar{\boldsymbol{q}}_n^{\mathbf{tr,ST}} := \left[\bar{q}_{n,t+1|t}^{\mathrm{tr,ST}}, ..., \bar{q}_{n,t+k|t}^{\mathrm{tr,ST}}, ..., \bar{q}_{n,t+|\boldsymbol{K}||t}^{\mathrm{tr,ST}}\right]^\top, \ \forall n, \tag{4.57}$$

$$\tilde{\boldsymbol{q}}_n^{\mathbf{br,ST}} := \left[\tilde{q}_{n,t+1|t}^{\mathrm{br,ST}}, ..., \tilde{q}_{n,t+k|t}^{\mathrm{br,ST}}, ..., \tilde{q}_{n,t+|\boldsymbol{K}||t}^{\mathrm{br,ST}}\right]^\top, \ \forall n, \tag{4.58}$$

$$\bar{\boldsymbol{q}}_n^{\mathbf{br,ST}} := \left[\bar{q}_{n,t+1|t}^{\mathrm{br,ST}}, ..., \bar{q}_{n,t+k|t}^{\mathrm{br,ST}}, ..., \bar{q}_{n,t+|\boldsymbol{K}||t}^{\mathrm{br,ST}}\right]^\top, \ \forall n, \tag{4.59}$$

$$\tilde{\boldsymbol{p}}_n^{\mathbf{H,ST}} := \left[\tilde{p}_{n,t+1|t}^{\mathrm{H,ST}}, ..., \tilde{p}_{n,t+k|t}^{\mathrm{H,ST}}, ..., \tilde{p}_{n,t+|\boldsymbol{K}||t}^{\mathrm{H,ST}}\right]^\top, \ \forall n, \tag{4.60}$$

$$\bar{\boldsymbol{p}}_n^{\mathbf{H,ST}} := \left[\bar{p}_{n,t+1|t}^{\mathrm{H,ST}}, ..., \bar{p}_{n,t+k|t}^{\mathrm{H,ST}}, ..., \bar{p}_{n,t+|\boldsymbol{K}||t}^{\mathrm{H,ST}}\right]^\top, \ \forall n. \tag{4.61}$$

Analogous to the proposed reformulation (4.24) of the scheduling problem, the original centralized dispatch model (3.19) can be restructured as the following consensus optimization problem, when applied to the Compagnie Nationale du Rhône optimization model (3.27):

$$\underset{\left\{\boldsymbol{z}^{\mathbf{B,ST}}, \left\{\boldsymbol{z}_n^{\mathbf{H,ST}}\right\}_{n\in\boldsymbol{N}}\right\}}{\operatorname{argmin}} \quad J^{\mathrm{ST}} \tag{4.62a}$$

$$\text{subject to} \quad \boldsymbol{z}^{\mathbf{B,ST}} \in \boldsymbol{\Xi}^{\mathbf{ST}}\left(\boldsymbol{\beta}^{\mathbf{ST}}\right), \tag{4.62b}$$

$$\boldsymbol{z}_n^{\mathbf{H,ST}} \in \boldsymbol{\Gamma}_n^{\mathbf{ST}}\left(\boldsymbol{\theta}_n^{\mathbf{ST}}\right), \ \forall n, \tag{4.62c}$$

$$\boldsymbol{z}_n^{\mathbf{B,H,ST}} = \bar{\boldsymbol{z}}_n^{\mathbf{B,H,ST}} \ : \ \boldsymbol{\lambda}_n^{\mathbf{ST}}, \ \forall n. \tag{4.62d}$$

Here, $\boldsymbol{z}^{\mathbf{B,ST}}$ encompasses the decision variables related to the power balancing of the VPP, as specified by

$$\boldsymbol{z}^{\mathbf{B,ST}} := \left\{\delta_{t+k|t}^{\mathrm{E}\uparrow,\mathrm{ST}}, \delta_{t+k|t}^{\mathrm{E}\downarrow,\mathrm{ST}}, \bar{\boldsymbol{p}}_n^{\mathbf{H,ST}}\right\}_{n\in\boldsymbol{N},k\in\boldsymbol{K}}. \tag{4.63}$$

Observe that, unlike $\boldsymbol{z}^{\mathbf{B}}$ in (4.25), $\boldsymbol{z}^{\mathbf{B,ST}}$ does not contain the day-ahead decision variable e^{DA}, which is fixed in the dispatch phase as a result of the scheduling optimization (4.24). Similarly to (4.26), the decision variables representing the dynamics of each hydropower plant are gathered in $\boldsymbol{z}_n^{\mathbf{H,ST}}$, as defined by

$$\boldsymbol{z}_n^{\mathbf{H,ST}} := \left\{b_{n,t+k|t}^{\mathrm{br,ST}}, b_{n,t+k|t}^{\mathrm{oc,ST}}, h_{n,t+k|t}^{\mathrm{ST}}, z_{n,t+k|t}^{\mathrm{fbl,ST}}, \bar{\boldsymbol{q}}_n^{\mathbf{tr,ST}}, \tilde{\boldsymbol{q}}_n^{\mathbf{tr,ST}}, \bar{\boldsymbol{q}}_n^{\mathbf{br,ST}}, \tilde{\boldsymbol{q}}_n^{\mathbf{br,ST}}, \tilde{\boldsymbol{p}}_n^{\mathbf{H,ST}}\right\}_{k\in\boldsymbol{K}}, \quad \forall n. \tag{4.64}$$

The feasible sets of $\boldsymbol{z}^{\mathbf{B,ST}}$ and $\boldsymbol{z}_n^{\mathbf{H,ST}}$ are denoted by $\boldsymbol{\Xi}^{\mathbf{ST}}\left(\boldsymbol{\beta}^{\mathbf{ST}}\right)$ and $\boldsymbol{\Gamma}_n^{\mathbf{ST}}\left(\boldsymbol{\theta}_n^{\mathbf{ST}}\right)$, respectively.

The former is defined by (3.27v), and the short-term power balancing constraint:

$$\left(\sum_{n\in\boldsymbol{N}} p^{\mathrm{H,ST}}_{n,t+k|t} + \hat{P}^{\mathrm{W,ST}}_{t+k} + \hat{P}^{\mathrm{S,ST}}_{t+k}\right)\Delta_K - E^{\mathrm{ST}}_{t+k} - \delta^{\mathrm{E}\downarrow,\mathrm{ST}}_{t+k|t} + \delta^{\mathrm{E}\uparrow,\mathrm{ST}}_{t+k|t} = 0,\ \forall k. \tag{4.65}$$

The latter is defined by (3.27d)-(3.27v). Vectors $\boldsymbol{\beta}^{\mathbf{ST}}$ and $\boldsymbol{\theta}^{\mathbf{ST}}_n$ collect the parameters associated with the constraints defining the feasible sets $\boldsymbol{\Xi}^{\mathbf{ST}}$ and $\boldsymbol{\Gamma}^{\mathbf{ST}}_n$, respectively.

Moreover, the vector $\boldsymbol{z}^{\mathbf{B,H,ST}}_n \in \mathbb{R}^{6\times|\boldsymbol{K}|}$ collects the global variables of the problem, as defined by

$$\boldsymbol{z}^{\mathbf{B,H,ST}}_n := \left[\boldsymbol{q}^{\mathbf{tr,ST}}_{n-1}, \boldsymbol{q}^{\mathbf{br,ST}}_{n-1}, \boldsymbol{q}^{\mathbf{tr,ST}}_{n}, \boldsymbol{q}^{\mathbf{br,ST}}_{n}, \boldsymbol{p}^{\mathbf{H,ST}}_{n}, \boldsymbol{p}^{\mathbf{H,ST}}_{n}\right]^\top,\ \forall n. \tag{4.66}$$

The vector $\bar{\boldsymbol{z}}^{\mathbf{B,H,ST}}_n \in \mathbb{R}^{6\times|\boldsymbol{K}|}$ collects the *local copies* of the global variables in $\boldsymbol{z}^{\mathbf{B,H,ST}}_n$, as defined by

$$\bar{\boldsymbol{z}}^{\mathbf{B,H,ST}}_n := \left[\tilde{\boldsymbol{q}}^{\mathbf{tr,ST}}_{n-1}, \tilde{\boldsymbol{q}}^{\mathbf{br,ST}}_{n-1}, \bar{\boldsymbol{q}}^{\mathbf{tr,ST}}_{n}, \bar{\boldsymbol{q}}^{\mathbf{br,ST}}_{n}, \tilde{\boldsymbol{p}}^{\mathbf{H,ST}}_{n}, \bar{\boldsymbol{p}}^{\mathbf{H,ST}}_{n}\right]^\top,\ \forall n. \tag{4.67}$$

The **consensus constraints** in (4.24d) enforce consistency between the global variables and their local copies. The associated vector of dual variables, $\boldsymbol{\lambda}^{\mathbf{ST}}_n \in \mathbb{R}^{6\times|\boldsymbol{K}|}$, is defined as

$$\boldsymbol{\lambda}^{\mathbf{ST}}_n := \left[\tilde{\boldsymbol{\lambda}}^{\mathbf{tr,ST}}_{n-1}, \tilde{\boldsymbol{\lambda}}^{\mathbf{br,ST}}_{n-1}, \bar{\boldsymbol{\lambda}}^{\mathbf{tr,ST}}_{n}, \bar{\boldsymbol{\lambda}}^{\mathbf{br,ST}}_{n}, \tilde{\boldsymbol{\lambda}}^{\mathbf{p,ST}}_{n}, \bar{\boldsymbol{\lambda}}^{\mathbf{p,ST}}_{n}\right]^\top,\ \forall n. \tag{4.68}$$

In (4.62), the objective function J^{ST} is defined as follows:

$$J^{\mathrm{ST}} := \sum_{k\in\boldsymbol{K}} \left(\hat{\pi}^{\mathrm{E}\uparrow,\mathrm{ST}}_{t+k}\delta^{\mathrm{E}\uparrow,\mathrm{ST}}_{t+k|t} - \hat{\pi}^{\mathrm{E}\downarrow,\mathrm{ST}}_{t+k}\delta^{\mathrm{E}\downarrow,\mathrm{ST}}_{t+k|t}\right). \tag{4.69}$$

As with the decomposition method proposed in Section 4.3.1.1, also the proposed reformulation (4.62) enables the use of several augmented Lagrangian relaxation-based distributed algorithms.

In Section 4.3.1.1 a key objective was to ensure a performance guarantee for the proposed distributed algorithm, even in the MILP case. In contrast, the focus here shifts to developing a distributed algorithm that not only allows parallelization of the original centralized optimization problem (3.19) but also achieves better scalability than the classical ADMM method, due to the need for rapid, near-real-time decisions in the dispatch phase. To this end, consider the steps of the classical ADMM method outlined in (4.7a)-(4.7c). The main limitation to scalability lies in its sequential updates of the primal and dual variables. Specifically, (4.7a) must be completed *before* (4.7b), and (4.7c) must be completed *before* both (4.7a) and (4.7b). Clearly, a straightforward application of the classical ADMM method to (4.62) does not allow a full parallelization of the problem due to the algorithm's inherent sequential structure.

While a consensus ADMM-based solution to (4.62) can be obtained through the proposed Algorithm 2, following the same steps outlined in the previous section, an alternative approach is introduced here, which leverages the APP method. This involves linearizing the augmented terms in (4.7a) and (4.7b) at the current iterate and adding quadratic separable terms [219]. This approach leads to the iterative steps outlined below.

Step I. *Local primal variables update* (4.70a)-(4.70b):

$$\begin{aligned}\boldsymbol{z}_n^{\mathbf{H,ST}^{i+1}} = \underset{\boldsymbol{z}_n^{\mathbf{H,ST}} \in \boldsymbol{\Gamma}_n^{\mathbf{ST}}}{\operatorname{argmin}} \Bigg\{ & \left(\mathbf{M}\boldsymbol{\lambda}_n^{\mathbf{ST}^i}\right)^\top \bar{\boldsymbol{z}}_n^{\mathbf{B,H,ST}} \\ & + \underbrace{\rho^i \left(\mathbf{M}\left(\bar{\boldsymbol{z}}_n^{\mathbf{B,H,ST}^i} - \boldsymbol{z}_n^{\mathbf{B,H,ST}^i}\right)\right)^\top \bar{\boldsymbol{z}}_n^{\mathbf{B,H,ST}}}_{\text{Augmented term linearization}} \\ & + \underbrace{\rho^i \left\|\mathbf{M}\left(\bar{\boldsymbol{z}}_n^{\mathbf{B,H,ST}} - \bar{\boldsymbol{z}}_n^{\mathbf{B,H,ST}^i}\right)\right\|_2^2}_{\text{Quadratic separable term}} \Bigg\}, \ \forall n, \end{aligned} \tag{4.70a}$$

$$\begin{aligned}\boldsymbol{z}^{\mathbf{B,ST}^{i+1}} = \underset{\boldsymbol{z}^{\mathbf{B,ST}} \in \boldsymbol{\Xi}^{\mathbf{ST}}}{\operatorname{argmin}} \Bigg\{ J^{\mathrm{ST}} + \sum_{n \in \boldsymbol{N}} \Bigg(& \left(\bar{\boldsymbol{\lambda}}_n^{\mathbf{p,ST}^i}\right)^\top \bar{\boldsymbol{p}}_n^{\mathbf{H,ST}} \\ & + \underbrace{\rho^i \left(\bar{\boldsymbol{p}}_n^{\mathbf{H,ST}^i} - \boldsymbol{p}_n^{\mathbf{H,ST}^i}\right)^\top \bar{\boldsymbol{p}}_n^{\mathbf{H,ST}}}_{\text{Augmented term linearization}} \\ & + \underbrace{\rho^i \left\|\bar{\boldsymbol{p}}_n^{\mathbf{H,ST}} - \bar{\boldsymbol{p}}_n^{\mathbf{H,ST}^i}\right\|_2^2}_{\text{Quadratic separable term}} \Bigg) \Bigg\}. \end{aligned} \tag{4.70b}$$

Step II. *Global primal variables update* in (4.71):

$$\begin{aligned}\boldsymbol{z}_n^{\mathbf{B,H,ST}^{i+1}} = \underset{\boldsymbol{z}_n^{\mathbf{B,H,ST}} \in \boldsymbol{\Gamma}_n^{\mathbf{ST}}}{\operatorname{argmin}} \Bigg\{ & - \left(\boldsymbol{\lambda}_n^{\mathbf{ST}^i}\right)^\top \boldsymbol{z}_n^{\mathbf{B,H,ST}} \\ & - \underbrace{\rho^i \left(\bar{\boldsymbol{z}}_n^{\mathbf{B,H,ST}^i} - \boldsymbol{z}_n^{\mathbf{B,H,ST}^i}\right)^\top \boldsymbol{z}_n^{\mathbf{B,H,ST}}}_{\text{Augmented term linearization}} \\ & + \underbrace{\rho^i \left\|\boldsymbol{z}_n^{\mathbf{B,H,ST}} - \boldsymbol{z}_n^{\mathbf{B,H,ST}^i}\right\|_2^2}_{\text{Quadratic separable term}} \Bigg\}, \ \forall n. \end{aligned} \tag{4.71}$$

Step III. *Dual variables update* in (4.72):

$$\boldsymbol{\lambda}_n^{\mathbf{ST}^{i+1}} = \boldsymbol{\lambda}_n^{\mathbf{ST}^i} + \rho^i \left(\bar{\boldsymbol{z}}_n^{\mathbf{B,H,ST}^{i+1}} - \boldsymbol{z}_n^{\mathbf{B,H,ST}^{i+1}}\right), \ \forall n. \tag{4.72}$$

The key advantage of this method over the consensus ADMM approach in (4.31a)-(4.33) lies in the ability to perform updates of both local and global variables **in parallel**. This is possible because the linearization of the augmented Lagrangian terms of (4.70a)-(4.71) results in a new algorithm where the $i+1$-th update of these variables only requires their values from the previous iteration, i. In contrast, the consensus ADMM method described in the previous section requires sequential updating: the global primal variable update (4.32) must wait for the local primal variable update (4.31a)-(4.31b) to complete first. This sequential dependency in consensus ADMM is inherent to the classical ADMM method's sequential structure, as discussed above. It is worth noting, however, that the improved scalability of APP typically comes at the

cost of reduced accuracy of this method compared to the ADMM, since the linearization of the augmented terms diminishes the algorithm's effectiveness in steering the distributed solution toward the global optimum of the problem.

Algorithm 3 APP-Based Distributed Economic MPC

Input: Parameter vectors $\left\{\boldsymbol{\theta}_n^{\mathbf{ST}}\right\}_{n\in\boldsymbol{N}}$ and $\boldsymbol{\beta}^{\mathbf{ST}}$.

Output: Optimal power generation, turbine outflows and barrage outflows $\boldsymbol{z}^{\mathbf{B,H,ST}^\star}$.

1: Initialize primal and dual variables $\left\{\boldsymbol{q}_n^{\mathbf{tr,ST}^0}, \boldsymbol{q}_n^{\mathbf{br,ST}^0}, \boldsymbol{p}_n^{\mathbf{H,ST}^0}, \boldsymbol{\lambda}_n^{\mathbf{ST}^0}\right\}_{n\in\boldsymbol{N}}$, primal residual $\boldsymbol{r}^{\mathbf{ST}^0}$, dual residual $\boldsymbol{s}^{\mathbf{ST}^0}$, penalty parameter $\rho^0 \leftarrow 2$, tolerance parameter $\epsilon \leftarrow 10^{-4}$, maximum number of algorithm's iterations $\overline{I} \leftarrow 1000$, $\tau \leftarrow 2$, $\mu \leftarrow 10$;

2: $i \leftarrow 0$;

3: **while** $\min\left(\left\|\boldsymbol{r}^{\mathbf{ST}^i}\right\|_2, \left\|\boldsymbol{s}^{\mathbf{ST}^i}\right\|_2\right) > \epsilon$ and $i < \overline{I}$ **do**

4: *Local primal variables update*: $\left\{\boldsymbol{z}_n^{\mathbf{H,ST}^{i+1}}\right\}_{n\in\boldsymbol{N}} \leftarrow$ (4.70a), $\boldsymbol{z}^{\mathbf{B,ST}^{i+1}} \leftarrow$ (4.70b);

5: *Global primal variables update*: $\left\{\boldsymbol{z}_n^{\mathbf{B,H,ST}^{i+1}}\right\}_{n\in\boldsymbol{N}} \leftarrow$ (4.71);

6: *Dual variables update*: $\left\{\boldsymbol{\lambda}_n^{\mathbf{ST}^{i+1}}\right\}_{n\in\boldsymbol{N}} \leftarrow$ (4.72);

7: *Primal residual update*:

$$\begin{aligned}\boldsymbol{r}_n^{\mathbf{ST}^{i+1}} \leftarrow \Big[&\bar{\boldsymbol{q}}_n^{\mathbf{tr,ST}^{i+1}} - \boldsymbol{q}_n^{\mathbf{tr,ST}^{i+1}}, \tilde{\boldsymbol{q}}_n^{\mathbf{tr,ST}^{i+1}} - \boldsymbol{q}_n^{\mathbf{tr,ST}^{i+1}}, \bar{\boldsymbol{q}}_n^{\mathbf{br,ST}^{i+1}} - \boldsymbol{q}_n^{\mathbf{br,ST}^{i+1}},\\ &\tilde{\boldsymbol{q}}_n^{\mathbf{br,ST}^{i+1}} - \boldsymbol{q}_n^{\mathbf{br,ST}^{i+1}}, \bar{\boldsymbol{p}}_n^{\mathbf{H,ST}^{i+1}} - \boldsymbol{p}_n^{\mathbf{H,ST}^{i+1}},\\ &\tilde{\boldsymbol{p}}_n^{\mathbf{H,ST}^{i+1}} - \boldsymbol{p}_n^{\mathbf{H,ST}^{i+1}}\Big]^\top, \forall n;\end{aligned} \tag{4.73}$$

8: *Dual residual update*:

$$\boldsymbol{s}_n^{\mathbf{ST}^{i+1}} \leftarrow -\rho^i \left[\boldsymbol{q}_n^{\mathbf{tr,ST}^{i+1}} - \boldsymbol{q}_n^{\mathbf{tr,ST}^{i}}, \boldsymbol{q}_n^{\mathbf{br,ST}^{i+1}} - \boldsymbol{q}_n^{\mathbf{br,ST}^{i}}, \boldsymbol{p}_n^{\mathbf{H,ST}^{i+1}} - \boldsymbol{p}_n^{\mathbf{H,ST}^{i}}\right]^\top, \ \forall n; \tag{4.74}$$

9: *Collect residuals*:

$$\boldsymbol{r}^{\mathbf{ST}^{i+1}} := \left[\boldsymbol{r}_1^{\mathbf{ST}^{i+1}}, ..., \boldsymbol{r}_n^{\mathbf{ST}^{i+1}}, ..., \boldsymbol{r}_{|\boldsymbol{N}|}^{\mathbf{ST}^{i+1}}\right]^\top, \tag{4.75}$$

$$\boldsymbol{s}^{\mathbf{ST}^{i+1}} := \left[\boldsymbol{s}_1^{\mathbf{ST}^{i+1}}, ..., \boldsymbol{s}_n^{\mathbf{ST}^{i+1}}, ..., \boldsymbol{s}_{|\boldsymbol{N}|}^{\mathbf{ST}^{i+1}}\right]^\top; \tag{4.76}$$

10: **if** $\left\|\boldsymbol{r}^{\mathbf{ST}^{i+1}}\right\|_2 > \mu \left\|\boldsymbol{s}^{\mathbf{ST}^{i+1}}\right\|_2$ **then** ▷ Penalty parameter update

11: $\rho^{i+1} = \tau\rho^i$;

12: **else if** $\left\|\boldsymbol{s}^{\mathbf{ST}^{i+1}}\right\|_2 > \mu \left\|\boldsymbol{r}^{\mathbf{ST}^{i+1}}\right\|_2$ **then**

13: $\rho^{i+1} = \frac{\rho^i}{\tau}$;

14: **else**

15: $\rho^{i+1} = \rho^i$;

16: **end if**

17: $i \leftarrow i + 1$;

18: **end while**

19: $\boldsymbol{z}^{\mathbf{B,H,ST}^\star} \leftarrow \boldsymbol{z}^{\mathbf{B,H,ST}^i}$;

The **distributed economic MPC method** proposed here, based on applying the APP

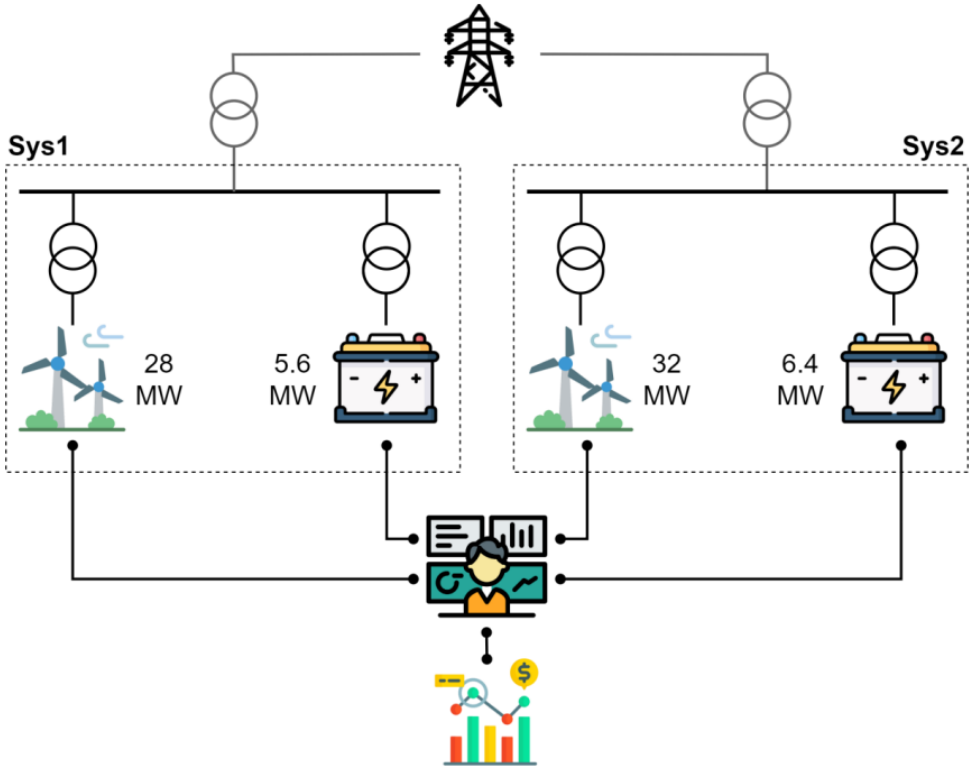

Figure 4.6: Diagram of the hybrid system for this illustrative case study.

steps (4.70a)-(4.72) to the decomposed problem (4.62), is presented in Algorithm 3.

4.4 A Small Illustrative Example

To familiarize the reader with augmented Lagrangian relaxation-based distributed optimization methods [38], a simple use case is presented [220], where three distinct methods are applied: the consensus ADMM method detailed in Algorithm 1, the APP method described in Algorithm 3, and the ATC method [221]. Section 4.4.1 provides an overview of this illustrative example, while Section 4.4.2 presents the results of the case study.

4.4.1 A Small Illustrative Example: Case Study Description

Consider the optimal scheduling problem for a wind-based commercial hybrid system that incorporates battery energy storage systems (BESSs). The setup of this system is depicted in Fig. 4.6. The goal of the scheduling strategy is to optimize the hybrid system's participation in the day-ahead market while minimizing BESS degradation.

This problem can be modeled as a deterministic optimization problem over discrete time intervals $t \in \boldsymbol{T}$, with a sampling time Δ_T. At each time t, the state of charge of each BESS $j \in \boldsymbol{N}^{\mathbf{BESS}}$ is denoted by $x_{j,t}^{\mathrm{BESS}}$, and the power charged and discharged to and from the BESS are denoted by $p_{j,t}^{\mathrm{BESS,C}}$ and $p_{j,t}^{\mathrm{BESS,D}}$, respectively. Charging and discharging efficiencies are represented by $\eta^{\mathrm{BESS,C}}$ and $\eta^{\mathrm{BESS,D}}$, respectively, with maximum charging and discharging power

limits denoted by $\overline{P}^{\text{BESS,C}}$ and $\overline{P}^{\text{BESS,D}}$, respectively. The vRES power generation of the hybrid system at time t is denoted by P_t^{vRES}, while the vRES capacity and BESS capacity for each unit j are denoted by $\overline{P}^{\text{vRES}}$ and $\overline{X}_j^{\text{BESS}}$, respectively. Additionally, two sets of binary variables, $b^{\text{BESS,C}}$ and $b^{\text{BESS,D}}$, are introduced to prevent each BESS from charging and discharging at the same time.

This scheduling problem can be formulated as the following MILP problem:

$$\underset{\boldsymbol{z}^{\mathbf{BESS}}}{\text{argmin}} \quad J^{\text{BESS}} \tag{4.77a}$$

$$\text{subject to} \quad P_t^{\text{vRES}}\Delta_T + \sum_{j\in\boldsymbol{N}^{\mathbf{BESS}}} \left(p_{j,t}^{\text{BESS,D}} - p_{j,t}^{\text{BESS,C}}\right)\Delta_T = e_t - \delta_t^{\text{E}\uparrow} + \delta_t^{\text{E}\downarrow},\ \forall t, \tag{4.77b}$$

$$x_{j,t+1}^{\text{BESS}} = x_{j,t}^{\text{BESS}} + \eta_j^{\text{BESS,C}} p_{j,t}^{\text{BESS,C}}\Delta_T - \eta_j^{\text{BESS,D}} p_{j,t}^{\text{BESS,D}}\Delta_T,\ \forall j, \forall t, \tag{4.77c}$$

$$x_{j,0}^{\text{BESS}} = X_j^{\text{BESS},0},\ \forall t, \tag{4.77d}$$

$$e_t \le \overline{P}^{\text{vRES}}\Delta_T + \sum_{j\in\boldsymbol{N}^{\mathbf{BESS}}} \overline{X}_j^{\text{BESS}}\Delta_T,\ \forall t, \tag{4.77e}$$

$$0 \le p_{j,t}^{\text{BESS,C}} \le b_{j,t}^{\text{BESS,C}}\overline{P}_j^{\text{BESS,C}},\ \forall j, \forall t, \tag{4.77f}$$

$$0 \le p_{j,t}^{\text{BESS,D}} \le b_{j,t}^{\text{BESS,D}}\overline{P}_j^{\text{BESS,D}},\ \forall j, \forall t, \tag{4.77g}$$

$$b_{j,t}^{\text{BESS,C}} + b_{j,t}^{\text{BESS,D}} \le 1,\ \forall j, \forall t, \tag{4.77h}$$

$$0 \le x_{j,t}^{\text{BESS}} \le \overline{X}_j^{\text{BESS}}\Delta_T,\ \forall j, \forall t. \tag{4.77i}$$

Here, the set of decision variables $\boldsymbol{z}^{\mathbf{BESS}}$ is defined as:

$$\boldsymbol{z}^{\mathbf{BESS}} := \left\{e_t, \delta_t^{\text{E}\uparrow}, \delta_t^{\text{E}\downarrow}, p_{j,t}^{\text{BESS,C}}, p_{j,t}^{\text{BESS,D}}, x_{j,t}^{\text{BESS}}, b_{j,t}^{\text{BESS,C}}, b_{j,t}^{\text{BESS,D}}\right\}_{j\in\boldsymbol{N}^{\mathbf{BESS}}, t\in\boldsymbol{T}}, \tag{4.78}$$

while the objective function J^{BESS} is defined as:

$$J^{\text{BESS}} := \sum_{t\in\boldsymbol{T}} \left(\underbrace{-\pi_t^{\text{E}} e_t + \pi^{\text{E}\uparrow}\delta_t^{\text{E}\uparrow} - \pi^{\text{E}\downarrow}\delta_t^{\text{E}\downarrow}}_{\text{Market profit}} + \underbrace{\sum_{j\in\boldsymbol{N}^{\mathbf{BESS}}} \pi_{j,t}^{\text{BESS}}(p_{j,t}^{\text{BESS,C}} + p_{j,t}^{\text{BESS,D}})\Delta_T}_{\text{Storage degradation}} \right). \tag{4.79}$$

The objective function includes two terms: the first captures the system's profit in the day-ahead market, and the second represents a simplified model of BESS degradation, weighted by the degradation cost π^{BESS}.

In (4.77), (4.77b) represents the power balance within the hybrid system, (4.77c)-(4.77d) describe the dynamics governing the BESS units, and (4.77e)-(4.77i) define the limits on the decision variables in the problem.

Clearly, (4.77) can be reformulated into the general structure of complex VPP scheduling problems, as shown in (3.15) in Chapter 3. Then, by following the steps of the decomposition method outlined in this chapter, (4.77) can be reformulated as a consensus problem to enable the application of augmented Lagrangian-relaxation-based distributed methods, such as the

Parameter	Value
$\eta_1^{\text{BESS,C}}; \eta_2^{\text{BESS,C}}$	0.95; 0.95
$\eta_1^{\text{BESS,D}}; \eta_2^{\text{BESS,D}}$	$\frac{1}{0.95}; \frac{1}{0.95}$
$\overline{X}_1^{\text{BESS}}; \overline{X}_2^{\text{BESS}}$	5.6 MW; 6.4 MW
$X_1^{\text{BESS,0}}; X_2^{\text{BESS,0}}$	2.5 MWh; 2.5 MWh
$\overline{P}_1^{\text{BESS,C}}; \overline{P}_2^{\text{BESS,C}}$	1.12 MW; 1.28 MW
$\overline{P}_1^{\text{BESS,D}}; \overline{P}_2^{\text{BESS,D}}$	1.12 MW; 1.28 MW

Table 4.3: Parameter values used in the simulation.

		Moderate accuracy ($\epsilon = 10^{-2}$)			**High accuracy** ($\epsilon = 10^{-4}$)		
	CO	**ATC**	**ADMM**	**APP**	**ATC**	**ADMM**	**APP**
Obj. relative error (%)	-	0.24	**0.18**	0.84	0.24	**0**	0.14
No. iterations	-	11	**6**	25	**11**	14	30
Time (sequential) (s)	**3**	67	25	489	67	62	540
Time (parallel) (s)		38	21	425	38	50	495

Table 4.4: Comparison between the proposed decomposition coordination algorithms in terms of relative error with respect to the optimal objective function value of the centralized (CO) approach (obj. relative error), number of iterations and time (when the algorithm is implemented in a sequential or parallel mode) required to meet the desired accuracy ϵ or reach the allowed maximum number of iterations ($\overline{I}$=30).

proposed Algorithms 1 and 2.

4.4.2 A Small Illustrative Example: Results

This section presents the results obtained by applying augmented Lagrangian-relaxation-based distributed methods to the illustrative example described in Section 4.4.1. Specifically, three methods are considered: the consensus ADMM Algorithm 1, the APP Algorithm 3, and the ATC [221]. The results are derived from a simulation period of 5 months (January 2017 to May 2017), using historical market prices in France. Table 4.3 provides the parameter values used in the simulation.

Table 4.4 reports a comparison between the proposed algorithms in terms of their relative error with respect to the optimal objective function value of the centralized approach, i.e., a centralized solution to (4.77), number of iterations and time required to meet the desired accuracy ϵ, or reach the allowed maximum number of iterations.

All methods converge to the optimal objective function value of the problem with less than 1% error. Among the proposed decomposition coordination algorithms, the ADMM-based approach in Algorithm 1 achieves the lowest error in the final solution and it results to be the fastest decomposition approach both in terms of number of iterations and time needed to converge, when moderated accuracy is required. On the other hand, ATC is insensitive to changes

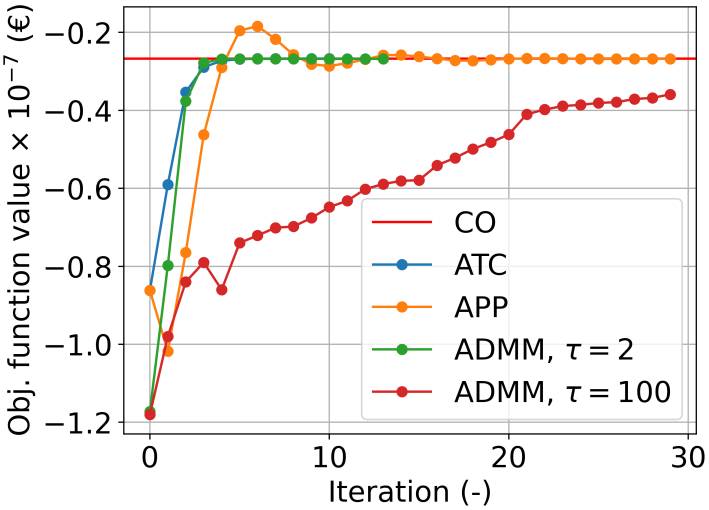

Figure 4.7: Convergence of the proposed decomposition coordination algorithms (ATC, ADMM and APP) to the optimal objective function value of the centralized optimization (CO) approach.

in the parameter ϵ. This is due to the simple nature of the problem, which allows for a fast accurate convergence of the algorithm even when a small value of ϵ is considered. The distributed optimization-based approach, namely APP, shows less attractive performances in terms of time and number of iterations required to converge. However, for more complex problems, employing fully distributed approaches such as APP is expected to bring significant advantages in terms of scalability of the scheduling strategy, as shown in the following section. An increase in the problem complexity may arise either from the integration of additional assets in the system, resulting in a large-scale portfolio of energy resources, or from the integration of several heterogeneous resources, which require specific complex constraints to model their dynamics and technical limits. While a parallel implementation of the decomposition coordination algorithms significantly accelerates solution times compared to a sequential approach, the centralized method still provides a faster solution for this simple scheduling problem. This clearly highlights that the advantages of decomposition methods, in terms of solution speed, are most evident in large-scale, complex VPPs rather than in simpler hybrid systems.

Fig. 4.7 illustrates the convergence of the proposed hierarchical and distributed optimization-based methods to the optimal objective function value of the centralized optimization approach. In this simple problem, all algorithms converge within 30 iterations. As shown, improper tuning of algorithm parameters, particularly the step size τ used to update the penalty parameter ρ in Algorithm 1, can significantly impact the convergence rate of these distributed algorithms.

For a further investigation of the impact of parameters tuning in these decomposition coordination algorithms, Figs. 4.8 and 4.9 report a sensitivity analysis on the choice of the step-size parameter τ in the ADMM and ATC methods, respectively. These algorithms iteratively converge, under some assumptions, to the global optimum by taking steps in the direction of the optimal solution. The size of these steps depends on the value of τ. For both ADMM-based and ATC-based methods it is possible to identify an optimal value of the step-size parameter, denoted by τ^*, which minimizes the number of iterations required to converge. This optimal value,

not only depends on the considered method, but also on the tuning of the other parameters in the algorithm (e.g., ϵ).

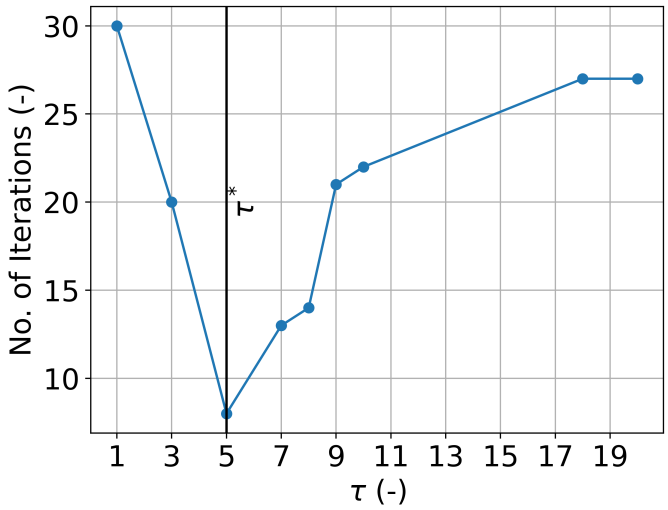

Figure 4.8: Sensitivity of ADMM Algorithm 1 to the choice of the step-size parameter τ. The optimal value of the step-size parameter is denoted by τ^*.

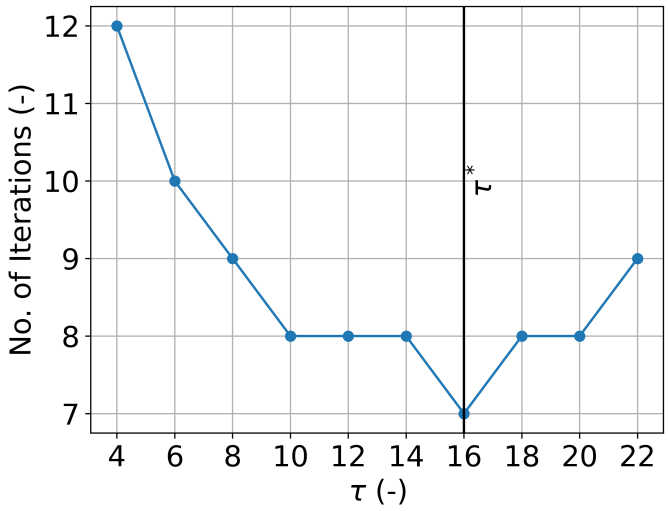

Figure 4.9: Sensitivity of ATC [221] to the choice of the step-size parameter τ. The optimal value of the step-size parameter is denoted by τ^*.

4.5 The Case Study of Compagnie Nationale du Rhône

The results from the simple illustrative example presented in the previous section highlight two key aspects regarding the performance of the augmented Lagrangian relaxation-based decomposition coordination algorithms under investigation. First, when applied to small-scale aggregated systems, the time required to solve the decomposed problem is generally longer than that for the original centralized problem, indicating that a distributed solution does not offer time ad-

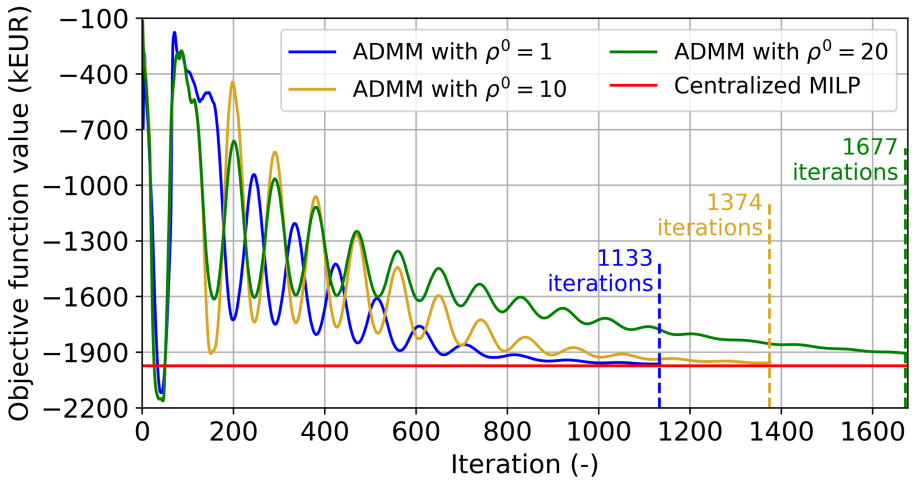

Figure 4.10: Example of convergence of the standard consensus ADMM Algorithm 1 for various initial penalty parameter values, when considering 5 scenarios.

vantages in this case. Second, the performance of these decomposition coordination algorithms is highly sensitive to the tuning of their parameters.

To show the efficacy of a distributed solution in large-scale, complex VPPs decision-making problem rather than simple small-scale hybrid systems optimization, and to further explore the impact of algorithm parameter tuning in complex problems, Sections 4.5.1 and 4.5.2 present the results of applying the consensus ADMM Algorithm 1 and the proposed novel trustworthy CADMMB Algorithm 2 to the scheduling problem of the complex VPP managed by Compagnie Nationale du Rhône. Additionally, Section 4.5.3 shows the results obtained from the application of the proposed novel APP-based distributed economic MPC Algorithm 3 to the dispatch problem of the complex VPP managed by Compagnie Nationale du Rhône.

The simulations span a three-month period (February–April 2017), covering diverse water inflow conditions. As detailed in Section 2.3, the simulations focus solely on the lower Rhône cascade (see Table 2.3), which includes the final 12 hydropower assets in the cascaded system operated by Compagnie Nationale du Rhône. The results for the distributed scheduling take into account the entire set of 12 hydropower plants in the cascade, whereas the results for the distributed dispatch focus on only 3 assets, namely PR, SV and BV (see Table 2.3). A characterization of uncertainties in the problem (water inflow, market prices and vRES power generation) is provided in Table 3.3. As detailed in Section 2.3.4, the analysis by Compagnie Nationale du Rhône indicates that uncertainties in vRES, inflows, and prices exhibit minimal correlation and can therefore be treated independently [135]. Thus, separate sets of scenarios are generated for each uncertainty source, randomly combined, and assigned equal probabilities. The simulations use historical day-ahead market prices in France, with the algorithms running on an Intel i7 processor and Gurobi 9.5.0 as the solver.

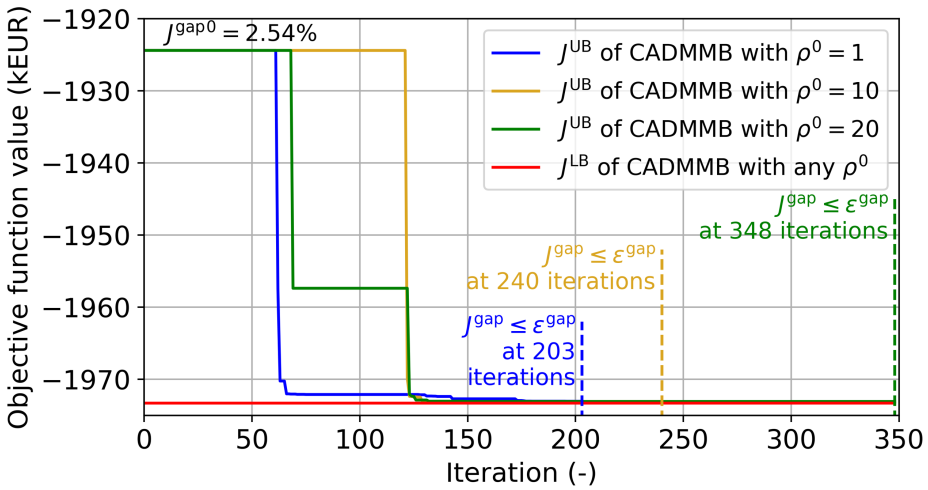

Figure 4.11: Example of convergence of the proposed trustworthy CADMMB Algorithm 2 for various initial penalty parameter values, when considering 5 scenarios.

4.5.1 Distributed Scheduling Results: A Stylized Illustrative Example

The out-of-sample validation illustrated in Fig. 3.8 for the scenario-based stochastic scheduling strategy applied to this case study suggests that 20 scenarios are adequate to represent the underlying sources of uncertainty. Increasing the number of scenarios beyond 20 increases computational complexity without significantly enhancing accuracy. Therefore, in the full case study, 20 scenarios are used to model the sources of uncertainty involved in this case study.

However, before presenting the full case study, results from a simplified example using 5 scenarios are provided. Figs. 4.10 and 4.11 show the convergence rates of the consensus ADMM and the proposed CADMMB, respectively, under varying initial values of the penalty parameter ρ. The results indicate that the standard ADMM converges in fewer than 1140 iterations at best but exhibits undesirable oscillations. In contrast, the CADMMB, not only eliminates these oscillations but also achieves bounds convergence with 99.99% accuracy in a maximum of 203 iterations. The initial lower bound estimate is already close to the global optimum and remains stable throughout the iterations. The initial gap between bounds is relatively small (2.54%), highlighting the advantages of warm-starting the algorithm with initial bounds, as shown in Fig. 4.5. While the consensus ADMM shows satisfactory performance, the accuracy of its solutions remains indeterminate without explicitly calculating the global optimum through centralized optimization. In contrast, the trustworthy CADMMB provides bounds that quantify the "distance" from the global optimum and enables precise control over the desired accuracy by tuning the ϵ^{gap} parameter.

4.5.2 Distributed Scheduling Results: Full Scale Case Study

Figs. 4.12 and 4.13 show the performance of both the standard consensus ADMM and the proposed trustworthy CADMMB, respectively, when applied to the full-scale case study involving 20 scenarios. As shown in Fig. 4.12, the ADMM struggles to handle the complexity of

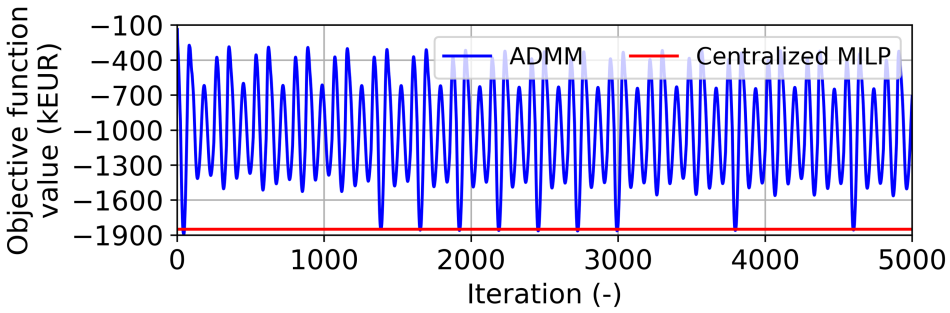

Figure 4.12: Example of ADMM Algorithm 1 performance when considering 20 scenarios.

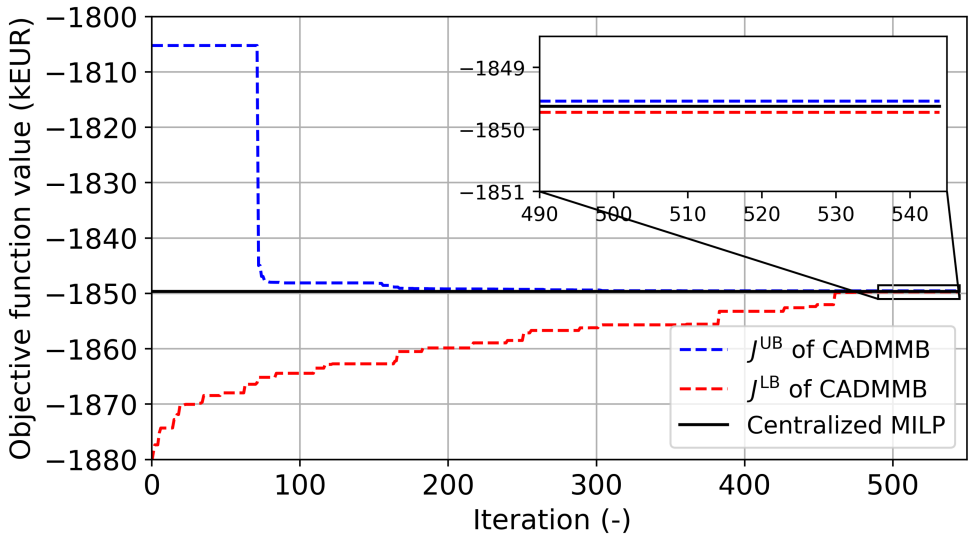

Figure 4.13: Example of trustworthy CADMMB Algorithm 2 performance when considering 20 scenarios.

the problem. In contrast, Fig. 4.13 shows that the CADMMB exhibits robust performance, converging efficiently with 99.99% accuracy in approximately 550 iterations. In this case, the initial lower bound estimate is significantly far from the optimum, requiring iterative updates to refine J^{LB}. Notably, the evolution of J^{LB} and J^{UB} throughout the iterations follows distinct patterns. While J^{LB} is updated continuously based on the progression of dual variables, J^{UB} is determined through a projection step into a new feasible space, leading to the large jump observed in Fig. 4.13.

Fig. 4.14 further shows the average runtime for solving the daily bidding problems and the number of failures—defined as instances where the algorithm fails to provide a solution within the 4-hour optimization window—for different algorithms, as a function of the number of scenarios. In the reference case (20 scenarios), CADMMB reduces the average runtime by approximately 35% compared to consensus ADMM and by 57% compared to traditional centralized optimization. Additionally, while both the ADMM and centralized algorithms experience a significant increase in intractable instances as the number of scenarios grows, the CADMMB consistently delivers a distributed solution with over 99.99% accuracy ($\epsilon^{\text{gap}} = 0.01\%$).

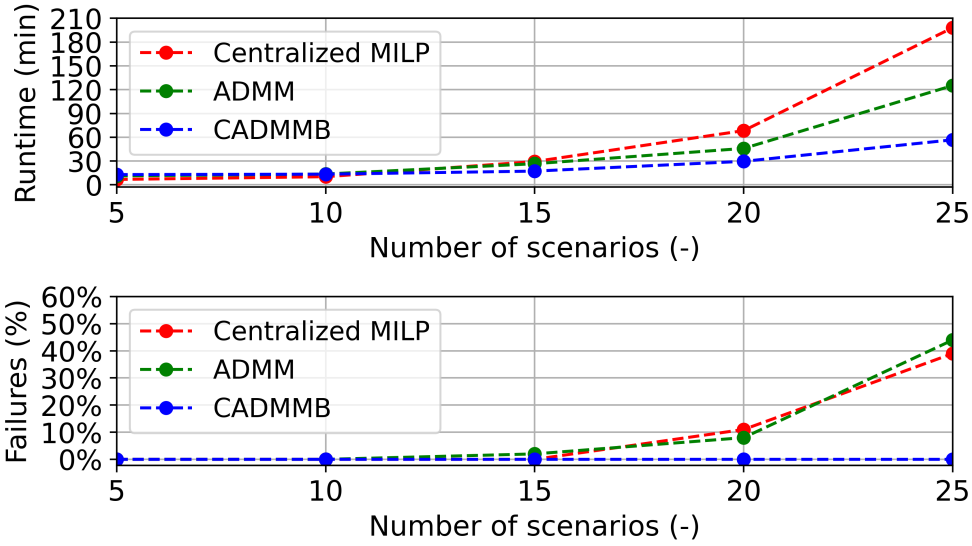

Figure 4.14: Comparison between centralized MILP, consensus ADMM Algorithm 1, and the proposed trustworthy CADMMB Algorithm 2 based on average runtime per scheduling period and failure rates (% of total simulation days), as a function of the number of scenarios.

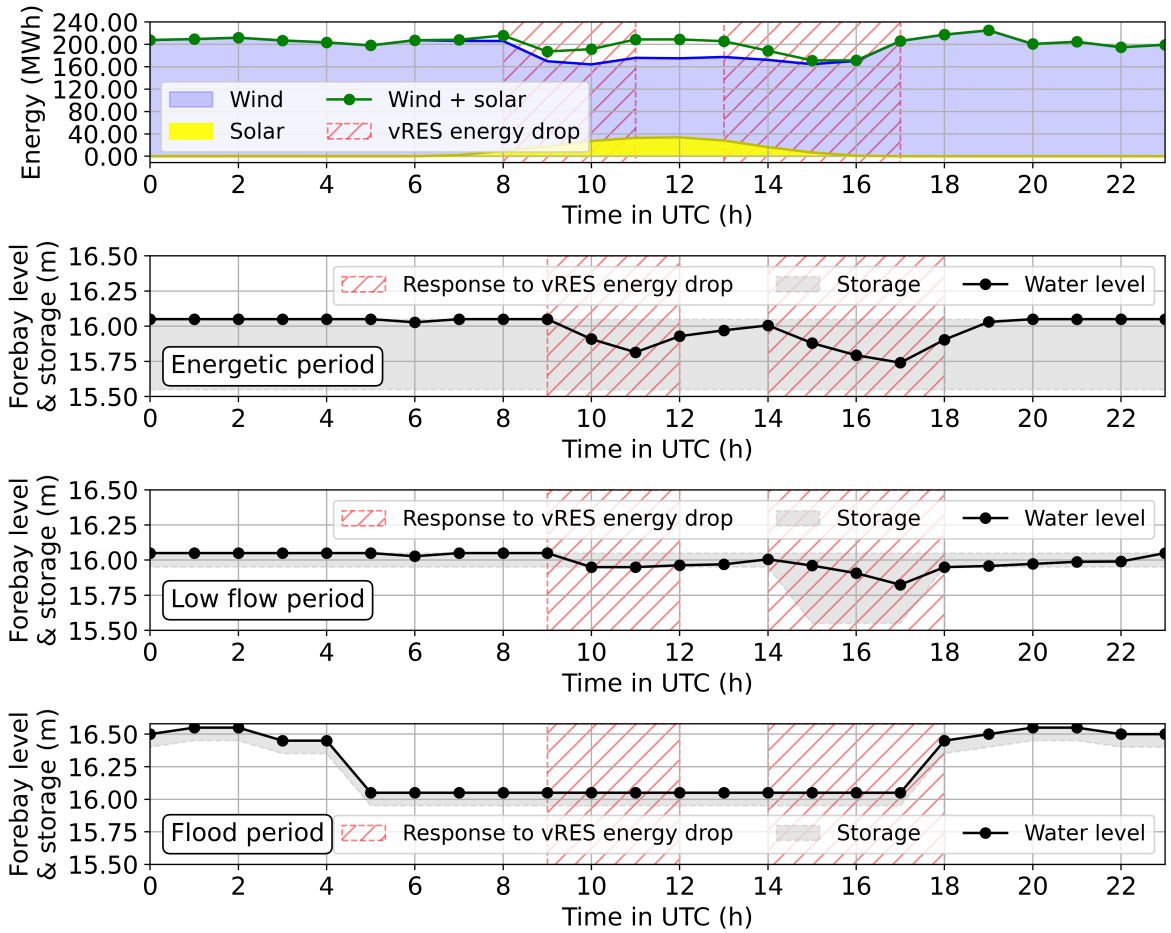

Figure 4.15: Example of coordination between the hydropower cascade and vRES under various inflow conditions when the proposed trustworthy CADMMB Algorithm 2 is employed.

Quantity	Centralized MPC			Distributed MPC		
	Mean	**Std**	**Max**	**Mean**	**Std**	**Max**
Relative error (%)	-	-	-	0.48	0.91	1.96
Iteration time (s)	-	-	-	0.41	0.36	1.56
Iterations count (-)	-	-	-	23.21	3.81	30
MPC step time (s)	10.58	6.58	27.31	9.51	5.67	26.86

Table 4.5: Comparison of computational performance between the classical centralized economic MPC (3.19) and the proposed APP-based distributed economic MPC Algorithm 3. The error is measured relative to the objective function value of the centralized MPC.

Finally, Fig. 4.15 shows a typical daily operation of the last hydropower asset in the cascade when using CADMMB to tackle the scheduling of this complex VPP. The figure presents three distinct inflow scenarios: high-flow, low-flow, and flood conditions. Due to constraints set by the operational curves for hydropower (see Fig. 2.9), the plant is able to fully respond to vRES energy shortfalls by releasing water from the reservoir only during high-flow periods, when ample storage capacity is available. During low-flow periods the storage capacity is reduced, but CADMMB still allows the plant to address the largest vRES drop. In flood conditions, the plant is limited to pure run-of-the-river operation, with no storage capacity available, making it unable to compensate for any unexpected vRES drops.

4.5.3 Distributed Dispatch Results

This section discusses the outcomes of applying the proposed APP-based distributed economic MPC Algorithm 3 to manage the dispatch of Compagnie Nationale du Rhône's complex VPP. Table 4.5 provides numerical comparisons of computational performance between the classical centralized economic MPC (3.19) and the proposed APP-based distributed economic MPC Algorithm 3. The distributed MPC achieves over 99% accuracy while reducing the average computation time per control step by approximately 10% compared to the centralized MPC approach. This contrasts with the results from the simple illustrative case study in Table 4.4, where the centralized method proved faster than decomposition methods. These differing results indicate that while a centralized approach may be more efficient and deliver a faster solution in small-scale case studies, distributed methods can significantly outperform traditional centralized control in large-scale, complex VPPs problems. This advantage applies not only on average but also in worst-case scenarios, as detailed in Table 4.5.

As discussed above, one of the challenges in implementing distributed algorithms is their sensitivity to parameter tuning, which can significantly impact both computational efficiency and solution quality. Fig. 4.16 examines the computational performance of the proposed APP-based distributed economic MPC Algorithm 3 under varying values of the penalty parameter τ and tolerance parameter ϵ, shedding light on the critical role of parameter selection in achieving optimal performance. When τ is set at relatively low levels, the proposed APP-based distributed economic MPC Algorithm 3 shows faster computation times for solving the complex VPP dispatch

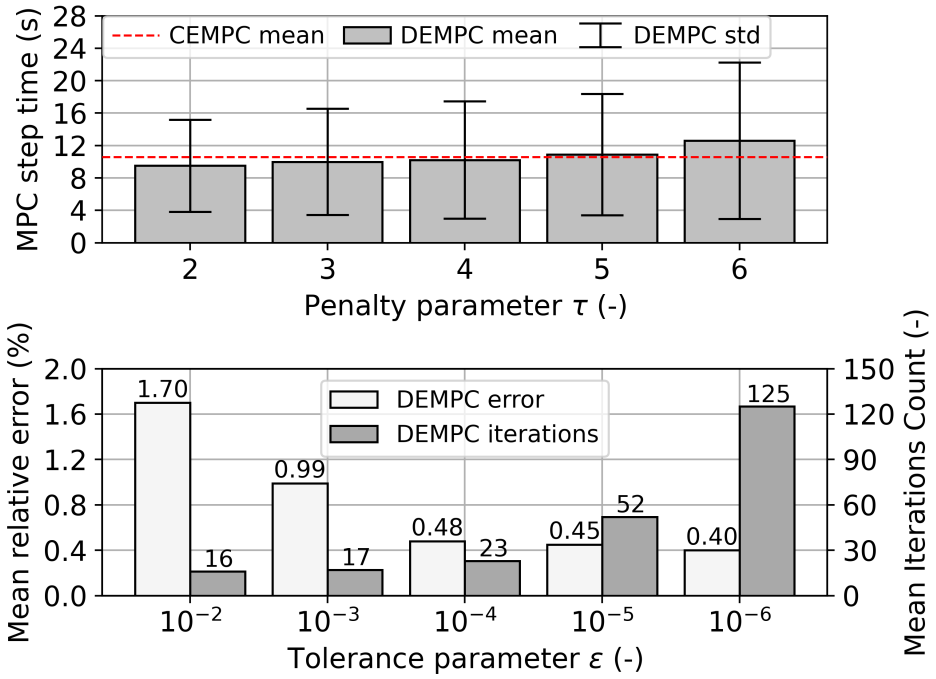

Figure 4.16: Sensitivity to parameters tuning of the proposed APP-based distributed economic MPC Algorithm 3. **CEMPC**: Centralized Economic MPC (3.19); **DEMPC**: APP-based Distributed Economic MPC Algorithm 3.

problem, outperforming the centralized MPC approach in terms of execution speed. However, if τ is not well-tuned, execution time may increase substantially, thus offsetting the computational advantages gained through the distributed structure of the algorithm. This sensitivity underscores the importance of careful parameter adjustment to fully leverage the decomposition strategy.

Moreover, Fig. 4.16 reveals a nuanced trade-off between controller execution time and accuracy. Lower values of ϵ generally result in a higher number of iterations required for convergence of the proposed APP-based distributed economic MPC Algorithm 3, which enhances the precision of the solution but at the cost of increased computation time. Once ϵ falls below a certain threshold (specifically $\epsilon = 10^{-4}$ in this analysis), the computational burden begins to grow exponentially while yielding only minor improvements in accuracy. This exponential rise illustrates a practical limit beyond which further precision gains become computationally prohibitive. Established guidelines, such as those found in [39], provide insights into effective parameter tuning strategies, helping to optimize the balance between execution time and solution quality for practical applications.

Chapter 5

Extension to Multi-Market Trading

Résumé en Français

Ce chapitre explore l'extension du cadre décisionnel stochastique à deux niveaux afin de permettre la participation des centrales électriques virtuelles à plusieurs marchés de l'électricité, notamment le marché de la régulation de la fréquence. Dans un contexte de transformation des marchés européens de l'énergie, avec l'intégration croissante des énergies renouvelables variables dans le réseau, il devient nécessaire de repenser la gestion des ressources énergétiques. Cela inclut non seulement la gestion de la production d'électricité à court terme, mais aussi la fourniture de services de régulation du réseau, tels que le contrôle de la fréquence, essentiels pour maintenir la stabilité du réseau électrique. Le chapitre se concentre spécifiquement sur la régulation de la fréquence, qui inclut des services comme la régulation primaire et secondaire, utilisés pour ajuster la fréquence du réseau en réponse aux fluctuations de la demande et de la production. En explorant la participation des centrales électriques virtuelles à ces services, ce travail met en évidence les défis associés à la coordination des ressources diversifiées, notamment les énergies renouvelables et les systèmes de stockage d'énergie. L'étude de cas présentée, portant sur l'utilisation combinée d'unités éoliennes et de systèmes de stockage d'énergie, démontre comment le cadre décisionnel développé peut être appliqué pour optimiser la participation simultanée à plusieurs marchés. Cette approche permet non seulement de répondre aux exigences techniques des services de régulation, mais aussi d'assurer une gestion efficace des incertitudes, tout en améliorant la flexibilité et la rentabilité des centrales électriques virtuelles dans un système énergétique de plus en plus décentralisé.

5.1 Introduction

The previous chapters have focused on developing a stochastic two-level decision-making framework designed to optimize the management of resources within complex VPPs for day-ahead market participation and near-real-time VPP portfolio control. In Chapter 3, this framework is introduced as a centralized decision-making tool, while Chapter 4 presents a decomposition of the framework, enabling a distributed solution to the sequential scheduling and dispatch of complex VPPs. These chapters aim at developing flexible, generic methods capable of handling the diverse configurations, uncertainties, internal dynamics, and objectives inherent to complex VPPs, all while ensuring that the solutions remain scalable and efficient. However, one aspect remains unexplored: the participation of such complex VPPs in multiple electricity markets.

In recent years, European electricity markets have experienced significant regulatory transformations aligned with the overarching goals of decarbonization, decentralization, and digitalization [175]. Section 2.2.5 offers an overview of this transition. Key initiatives, such as the European Green Deal [222] and updates to the Clean Energy Package [223], reflect the commitment of the European Union to these objectives, fostering the integration of renewables, promoting demand-side flexibility, and supporting innovation in market design. The shift from centralized, large-scale energy provision to decentralized energy systems aligns with the increasing integration of vRES into power systems. This transition requires a fundamental rethinking of market design to enhance the visibility and active participation of vRES in multiple electricity markets. In this context, VPPs improve the visibility of vRES and enable their market integration. The optimal scheduling and dispatch of a VPP across multiple electricity markets is referred to here as the *multi-market trading* problem.

The challenges of multi-market participation are substantial. These include managing market-specific requirements, reconciling short-term operational needs with long-term objectives, and efficiently coordinating a diverse portfolio of resources within a VPP to meet the varying timescales and performance obligations across markets [224]. While an in-depth analysis of the performance of complex VPPs across all existing markets is beyond the scope of this thesis, the goal of this chapter is to show how the decision-making tools developed in Chapters 3 and 4 can be extended to address the VPP's participation in markets beyond the day-ahead electricity market (**contribution C7** in Chapter 1).

Although various markets could be considered to demonstrate the applicability of the proposed decision-making tools in a multi-market context, this work focuses on participation in the **ancillary services market** for several reasons. Ancillary services encompass all operations required by system operators to ensure the reliable and secure functioning of the power grid. Traditionally, these services have been provided exclusively by large-scale conventional thermal and hydropower plants. However, the increasing integration of vRES into modern power systems necessitates a shift towards their active involvement in providing ancillary services. Despite the challenges posed by the stochastic nature of vRES, their aggregation with dispatchable units enables the resulting system to effectively participate in delivering these services [225]. This chapter emphasizes the market-based provision of ancillary services, recognizing that the partic-

ipation of renewable units in this domain remains an emerging area of research [28]. Although many studies focus on simultaneous trading in day-ahead and intraday markets (see Fig. 1.3), contributions addressing multi-market trading involving market-based ancillary services provision are still limited, as outlined in the literature review in Section 3.1.1.1 and summarized in Table 3.1. More importantly, participation in market-based ancillary services provision presents a challenging case study for VPPs [226]. The complexity of the problem increases as it involves not only day-ahead market prices and vRES power generation, but also the prices and real-time activation of ancillary services, all of which introduce additional uncertainties into the multi-market trading problem [227]. Furthermore, the necessity for fast, real-time provision of these services underscores the urgency of addressing the dispatch control phase of the complex VPP [228], in conjunction with bid placement during the scheduling phase. This highlights the critical need for a comprehensive sequential decision-making framework that enables the joint optimization of both the scheduling and dispatch phases of the VPP, as proposed in Chapter 3.

Among the various ancillary services, ranging from standard voltage control to emergency black start recovery, this chapter focuses on the provision of **frequency control services** through renewable-based aggregated systems [229]. The modeling and integration of these services into the proposed scheduling and dispatch methods for complex VPPs are detailed in the subsequent sections.

Ancillary services are generally divided into *frequency ancillary services* and *non-frequency ancillary services* (such as voltage control) [230]. This distinction underscores the essential role of frequency control—commonly referred to as electricity balancing—in ensuring grid stability. For a detailed review of the categories of frequency-related ancillary services, the reader is directed to [231]. These services are typically organized into *primary*, *secondary*, and *tertiary frequency control*. In the European context, the standard balancing products include [232]:

- *Frequency Containment Reserve* (FCR) for primary frequency control: A fast-response service activated within seconds to stabilize grid frequency deviations immediately after disturbances.
- *Automatic Frequency Restoration Reserve* (aFRR) for secondary frequency control: Automatically activated by transmission system operators to restore frequency and release FCR capacity, typically within a few minutes.
- *Manual Frequency Restoration Reserve* (mFRR) for tertiary frequency control: Manually activated to further restore system balance and replace aFRR over a slightly longer time frame.
- *Replacement Reserve* (RR) for tertiary frequency control: Activated for long-term imbalances, ensuring grid stability over extended periods.

These services are integral to the European frequency control scheme, which aims to contain frequency deviations and restore the grid frequency to its nominal value (50 Hz in continental Europe), as shown in Fig. 5.1. The coordination of these reserves follows a hierarchical activation

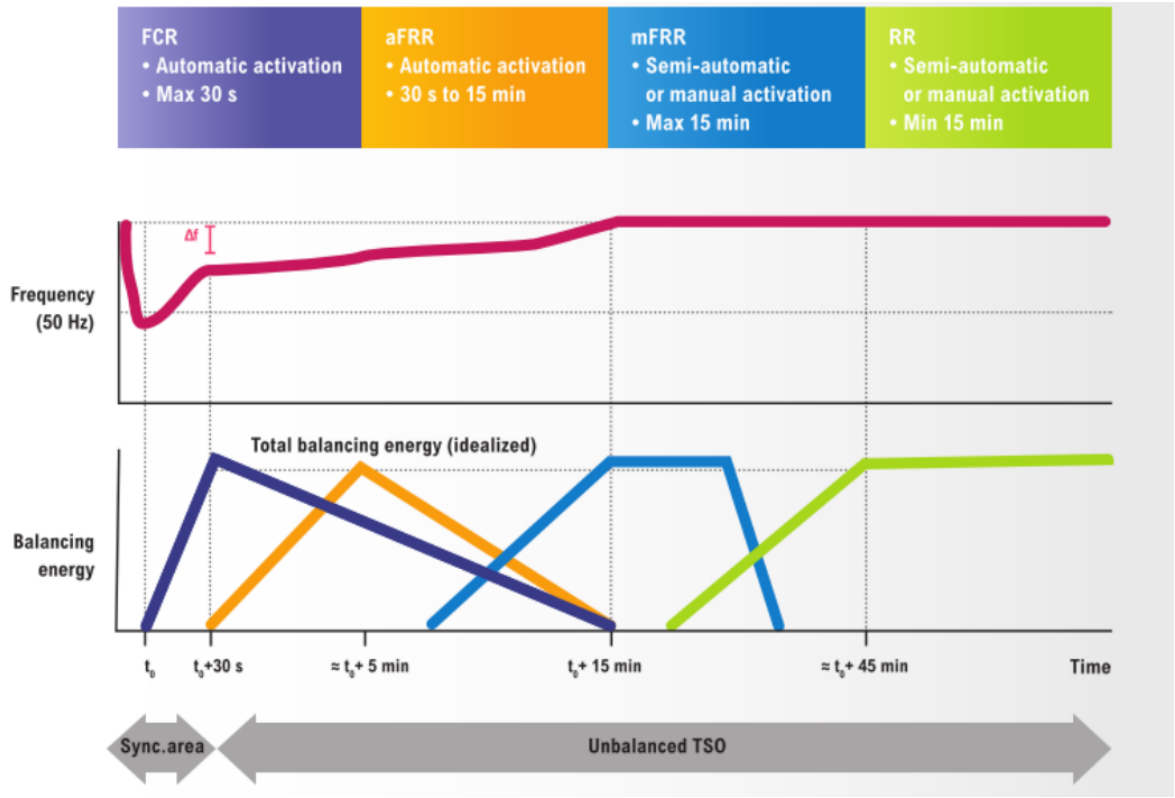

Figure 5.1: Frequency control scheme implemented in Europe [232].

scheme: FCR addresses immediate disturbances, aFRR provides automatic support to maintain balance, and mFRR and RR ensure stability over longer horizons.

This chapter specifically explores how the proposed two-level stochastic decision-making framework—implemented in both centralized and distributed forms in the previous chapter—can be tailored for the simultaneous participation of complex VPPs in both day-ahead energy markets and ancillary services markets. Particular attention is given to the market-based procurement of FCR and aFRR products. A case study examining the coordinated operation of wind units and BESS is investigated to show the adaptability of the proposed decision-making framework in addressing multi-market trading problems.

The methods and results presented here expand upon the discussions in two papers that are outcomes of this thesis, namely [233] and [234].

5.1.1 Chapter Outline

The remainder of the chapter is organized as follows. Section 5.2 details the extension of the two-level stochastic decision-making framework, developed for complex VPPs participating in the day-ahead market in Chapter 3, to the multi-market trading case. Specifically, Section 5.2.1 formulates the multi-market trading problem. Then, Section 5.2.2 addresses both the adaptation of the proposed scheduling optimization model (3.15) to the multi-market trading case, and the extension of the proposed dispatch MPC strategy (3.19) to this context, while offering insights into the impact of integrating additional markets into the complex VPP scheduling and dispatch

tools when using the proposed decomposition methods outlined in Chapter 4. Finally, Section 5.3 describes the proposed case study and presents the observed results.

5.2 Methodology

This section presents an extension of the two-level stochastic decision-making framework for operating complex VPPs, introduced in Chapter 4, to the context of multi-market trading. Specifically, simultaneous participation in the day-ahead and ancillary services markets for the market-based procurement of frequency regulation services is considered as an illustrative example, highlighting the adaptability of the proposed decision-making tool to accommodate multi-market trading scenarios.

5.2.1 Formulating the Complex Virtual Power Plant Participation in Day-Ahead and Ancillary Services Markets

This section builds upon the discussion in Section 3.3.1, which focuses on formulating the bidding problem for a VPP participating exclusively in the day-ahead market, by extending it to the case where the VPP engages in both the day-ahead and ancillary services markets, addressing a multi-market trading problem. It is important to note that the landscape of ancillary services markets, and market-based procurement of such services more broadly, remains dynamic and evolving within the European context [235]. As a detailed representation of ancillary services markets lies beyond the scope of this research, a simplified modeling approach is adopted, drawing primarily on mechanisms employed in the coupled market area of Germany, Austria, Switzerland, the Netherlands, France, and Belgium, where frequency services are procured through daily tenders [236].

As detailed in Section 3.3.1, when a VPP participates in the day-ahead market, it assumes the role of a BRP, becoming accountable for imbalances—real-time deviations from the submitted power generation schedule. From a system-wide perspective, imbalances arise when some BRPs generate a surplus (producing more energy than scheduled) while others experience deficits (producing less than scheduled). These individual imbalances partially offset one another, leaving a residual imbalance that must be corrected to maintain system stability. This correction occurs through the frequency control process, which leverages balancing energy to restore the nominal system frequency. Balancing energy is procured by system operators through various products, typically traded in ancillary services markets [237].

The European Network of Transmission System Operators for Electricity (ENTSO-E) Electricity Balancing Guidelines [232] define both standard and specific products for frequency services, summarized in Fig. 5.2. Here, it is assumed that the gate closure time for the ancillary services market coincides with that of the day-ahead market—24 hours before delivery. Thus, the VPP places bids simultaneously in both markets. While small-scale energy resources are generally not permitted to participate individually in ancillary services markets, the aggregation of these resources within a large-scale VPP enables their participation. This is increasingly common in European markets [238].

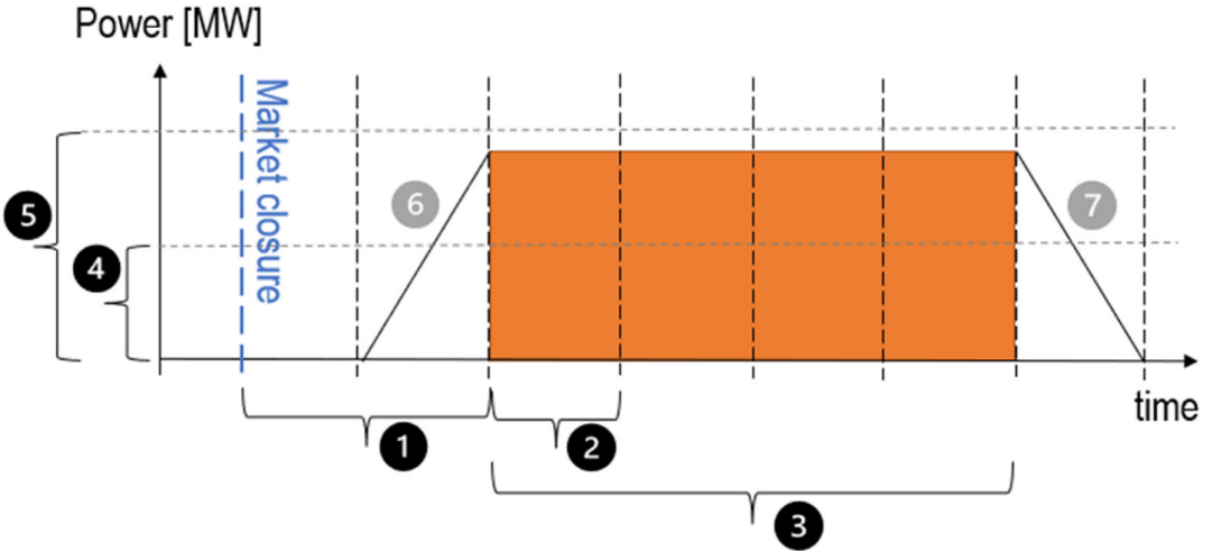

Figure 5.2: Schematic representation of a balancing product, highlighting 1) gate closure distance to delivery, 2) minimum and 3) maximum time definitions, and 4) minimum and 5) maximum bid sizes. Further requirements can be set for 6) ramping and 7) de-ramping rates [235].

Electricity balancing practices differ across markets, primarily based on the dispatching model employed. Two main models exist: the *self-dispatch model* (decentralized coordination) and the *central-dispatch model*. According to ENTSO-E guidelines [232], the self-dispatch model allows BRPs to independently determine generation and consumption schedules, as well as the dispatching of their assets. Conversely, the central-dispatch model grants the system operator control over scheduling and dispatching within an integrated framework. Here, a self-dispatching scheme is assumed for the market-based procurement of frequency control services, aligning with European guidelines that mandate self-dispatch as the standard model for generation and consumption scheduling [232]. For a detailed comparison of the advantages and disadvantages of these dispatching models, see [239].

When a VPP participates in ancillary services markets to provide frequency control services, it assumes the role of a *balancing service provider* (BSP). A BSP offers upward and downward balancing capacities, or *reserves*, to the system operator. In real-time, the system operator activates these reserves as needed to restore the system's nominal frequency. Frequency control processes involve several stages—primary, secondary, and tertiary control—each utilizing distinct balancing products (see Fig. 5.1). Here, the VPP is assumed to trade in both FCR for primary frequency control and aFRR for secondary frequency control.

In the balancing ancillary services market, the VPP participates by offering two types of reserves: *upward reserve*, which entails providing energy capacity to increase the injection of energy into the grid, and *downward reserve*, which involves offering energy capacity to absorb energy from the grid. For primary frequency control, the VPP offers FCR, denoted by r^{FCR}. For secondary frequency control, the VPP provides upward and downward aFRR, denoted by $r^{\mathrm{aFRR}\uparrow}$ and $r^{\mathrm{aFRR}\downarrow}$, respectively. FCR is modeled as a single variable since it is assumed to be *symmetric*, meaning the upward reserve offered equals the downward reserve, as is the case in

many European balancing AS markets (e.g., Germany) [235].

Balancing energy remuneration occurs through two mechanisms [177]: *capacity remuneration*, also known as availability remuneration, and *energy remuneration*, referred to as activation remuneration. In the former, the VPP is compensated for maintaining balancing capacity available for frequency control, whereas in the latter, payment is made for the actual activation of balancing energy. While both FCR and aFRR products receive capacity remuneration, energy remuneration is applicable only to aFRR products. The price for FCR capacity is denoted by π^{FCR}, while the prices for upward and downward aFRR capacity are represented by $\pi^{\text{aFRR}\uparrow}$ and $\pi^{\text{aFRR}\downarrow}$, respectively. Additionally, aFRR energy activation is remunerated at prices $\pi^{\text{aFRR,bal}\uparrow}$ for upward activation and $\pi^{\text{aFRR,bal}\downarrow}$ for downward activation.

Balancing capacity procured in the market can be activated in real-time during the frequency control process. FCR activation is governed by the FCR activation signal $\alpha^{\text{FCR}} \in [-1, 1]$, where positive values ($\alpha^{\text{FCR}} > 0$) indicate upward activation, with full activation occurring at $\alpha^{\text{FCR}} = 1$. Conversely, negative values ($\alpha^{\text{FCR}} < 0$) represent downward activation, with full activation at $\alpha^{\text{FCR}} = -1$. Similarly, aFRR activation is guided by two separate activation signals to distinguish between upward and downward activation, denoted by $\alpha^{\text{aFRR},\uparrow} \in [0, 1]$ and $\alpha^{\text{aFRR},\downarrow} \in [0, 1]$, respectively. When $\alpha^{\text{aFRR},\uparrow} > 0$, upward aFRR is activated, reaching full activation at $\alpha^{\text{aFRR},\uparrow} = 1$. Likewise, downward aFRR is activated when $\alpha^{\text{aFRR},\downarrow} > 0$, with full activation occurring at $\alpha^{\text{aFRR},\downarrow} = 1$. These activation signals are assumed to be transmitted to the VPP by the system operator.

In light of the previous discussion, the total compensation obtained by the VPP from the market-based provision of FCR and aFRR, referred to here as *balancing ancillary services market remuneration* (BASMR), is given by:

$$\begin{aligned}\text{BASMR}_t = &\underbrace{\pi_t^{\text{FCR}} r_t^{\text{FCR}} + \pi_t^{\text{aFRR}\uparrow} r_t^{\text{aFRR}\uparrow} + \pi_t^{\text{aFRR}\downarrow} r_t^{\text{aFRR}\downarrow}}_{\text{Capacity remuneration}} \\ &+ \underbrace{\alpha_t^{\text{aFRR}\uparrow} \pi_t^{\text{aFRR,bal}\uparrow} r_t^{\text{aFRR}\uparrow} \Delta_T + \alpha_t^{\text{aFRR}\downarrow} \pi_t^{\text{aFRR,bal}\downarrow} r_t^{\text{aFRR}\downarrow} \Delta_T}_{\text{Energy remuneration}}, \ \forall t. \end{aligned} \tag{5.1}$$

A compact representation of (5.1) is provided in (5.2), utilizing the composite unitary prices for upward and downward aFRR, denoted as $\pi^{\text{aFRR,comp}\uparrow}$ and $\pi^{\text{aFRR,comp}\downarrow}$, respectively:

$$\text{BASMR}_t = \pi_t^{\text{FCR}} r_t^{\text{FCR}} + \pi_t^{\text{aFRR,comp}\uparrow} r_t^{\text{aFRR}\uparrow} + \pi_t^{\text{aFRR,comp}\downarrow} r_t^{\text{aFRR}\downarrow}, \ \forall t. \tag{5.2}$$

Here, composite unitary prices encapsulate the total remuneration per unit of aFRR capacity, accounting for both capacity and energy remuneration mechanisms:

$$\pi_t^{\text{aFRR,comp}\uparrow} = \pi_t^{\text{aFRR}\uparrow} + \alpha_t^{\text{aFRR}\uparrow} \pi_t^{\text{aFRR,bal}\uparrow} \Delta_T, \ \forall t, \tag{5.3}$$

$$\pi_t^{\text{aFRR,comp}\downarrow} = \pi_t^{\text{aFRR}\downarrow} + \alpha_t^{\text{aFRR}\downarrow} \pi_t^{\text{aFRR,bal}\downarrow} \Delta_T, \ \forall t. \tag{5.4}$$

The BSP may deviate from its reserve offers, leading to *deficits*. Similar to the BRP's management of energy imbalances, the BSP incurs economic penalties for these deviations.

Here, the deficits for FCR, upward aFRR, and downward aFRR are denoted by δ^{FCR}, $\delta^{\text{aFRR}\uparrow}$, and $\delta^{\text{aFRR}\downarrow}$, respectively. The penalty prices associated with these deficits are denoted as $\pi^{\delta\text{FCR}}$, $\pi^{\delta\text{aFRR}\uparrow}$, and $\pi^{\delta\text{aFRR}\downarrow}$.

Following the rationale used to derive (5.2), the cumulative penalty incurred by the BSP due to deficits can be straightforwardly determined. This penalty, termed the *balancing ancillary services market penalty* (BASMP), is defined as follows:

$$\text{BASMP}_t = \pi_t^{\delta\text{FCR}}\delta_t^{\text{FCR}} + \pi_t^{\delta\text{aFRR,comp}\uparrow}\delta_t^{\text{aFRR}\uparrow} + \pi_t^{\delta\text{aFRR,comp}\downarrow}\delta_t^{\text{aFRR}\downarrow},\ \forall t, \tag{5.5}$$

where the composite unitary penalty prices for upward and downward aFRR deficits, denoted by $\pi^{\delta\text{aFRR,comp}\uparrow}$ and $\pi^{\delta\text{aFRR,comp}\downarrow}$, respectively, are defined as

$$\pi_t^{\delta\text{aFRR,comp}\uparrow} = \pi_t^{\delta\text{aFRR}\uparrow} + \alpha_t^{\text{aFRR}\uparrow}\pi_t^{\text{aFRR,bal}\uparrow}\Delta_T, \forall t, \tag{5.6}$$

$$\pi_t^{\delta\text{aFRR,comp}\downarrow} = \pi_t^{\delta\text{aFRR}\downarrow} + \alpha_t^{\text{aFRR}\downarrow}\pi_t^{\text{aFRR,bal}\downarrow}\Delta_T, \forall t. \tag{5.7}$$

A detailed description of the assumptions made regarding the ancillary services market and the formulation briefly outlined above is provided in one of the articles resulting from this thesis, namely [234].

5.2.2 A Fully Stochastic Two-Level Decision-Making Framework for Optimizing Complex Virtual Power Plant Participation in the Day-Ahead and Ancillary Services Markets

This section examines the adaptability of the fully stochastic two-level decision-making framework presented in Section 3.3, originally designed for the optimal operation of complex VPPs in the day-ahead market, to the multi-market trading problem. As an illustrative example, the case of simultaneous participation in the day-ahead and ancillary services markets is considered. The considerations presented can, however, be generalized to broader multi-market trading problems. As detailed in Section 3.3, the proposed framework consists of a first layer (scheduling module) for optimizing the bidding strategy in electricity markets and a second layer (dispatch module) that optimizes the short-term operation of the complex VPP based on the schedule provided by the first layer. The separability of these two phases in the proposed model allows the extension to multi-market trading to be addressed independently within each layer.

In the **scheduling layer**, the generic stochastic optimization problem (3.15) optimizes the day-ahead objective J^{DA}, detailed in (3.18), subject to the following constraints: (3.15b) describes the power balancing within the VPP, (3.15c) describes the bids formulation for the day-ahead market, and (3.15d) details the individual dynamics of the VPP clusters in which the proposed generic complex VPP model is structured (see Section 3.3). The impact of integrating an additional market is limited to a modification of the objective function J^{DA} and the power balancing constraints.

Specifically, the objective function J^{DA}, defined in (3.18) for the single-market trading case,

is rewritten as follows:

$$J^{\mathrm{DA}} := \sum_{\omega \in \mathbf{\Omega^{DA}}} \sum_{t \in \boldsymbol{T}} P_{\omega}^{\mathrm{DA}} \Bigg(\underbrace{\left(\hat{\boldsymbol{\pi}}_{\omega,t}^{\boldsymbol{\delta}\mathbf{E,DA}}\right)^{\top} \boldsymbol{\delta}_{\omega,t}^{\mathbf{E,DA}} - \hat{\pi}_{\omega,t}^{\mathrm{E,DA}} e_{\omega,t}^{\mathrm{DA}}}_{\text{Revenue in the day-ahead energy market}} + \underbrace{\left(\hat{\boldsymbol{\pi}}_{\omega,t}^{\boldsymbol{\delta}\mathbf{R,DA}}\right)^{\top} \boldsymbol{\delta}_{\omega,t}^{\mathbf{R,DA}} - \left(\hat{\boldsymbol{\pi}}_{\omega,t}^{\mathbf{R,DA}}\right)^{\top} \boldsymbol{r}_{t}^{\mathbf{DA}}}_{\text{Revenue in the ancillary services market}} + \frac{1}{\left|\boldsymbol{N}^{\mathbf{VPPBR}}\right|} \sum_{b \in \boldsymbol{N}^{\mathbf{VPPBR}}} \frac{1}{\left|\boldsymbol{N}_{b}^{\mathbf{VPPCL}}\right|} \sum_{c \in \boldsymbol{N}_{b}^{\mathbf{VPPCL}}} C_{c,b,\omega,t}^{\mathrm{VPPCL,DA}} \Bigg). \quad (5.8)$$

Here, the vector of day-ahead reserve offers, denoted by $\boldsymbol{r}_{t}^{\mathbf{DA}}$, is defined as

$$\boldsymbol{r}_{t}^{\mathbf{DA}} := \left[r_{t}^{\mathrm{FCR,DA}}, r_{t}^{\mathrm{aFRR}\uparrow\mathrm{,DA}}, r_{t}^{\mathrm{aFRR}\downarrow\mathrm{,DA}}\right]^{\top}, \ \forall t. \quad (5.9)$$

The vector of day-ahead reserve deficits, denoted by $\boldsymbol{\delta}_{\omega,t}^{\mathbf{R,DA}}$, is defined as

$$\boldsymbol{\delta}_{\omega,t}^{\mathbf{R,DA}} := \left[\delta_{\omega,t}^{\mathrm{FCR,DA}}, \delta_{\omega,t}^{\mathrm{aFRR}\uparrow\mathrm{,DA}}, \delta_{\omega,t}^{\mathrm{aFRR}\downarrow\mathrm{,DA}}\right]^{\top}, \ \forall \omega, \forall t. \quad (5.10)$$

Moreover, the vectors of day-ahead reserve prices, denoted by $\boldsymbol{\pi}_{\omega,t}^{\mathbf{R,DA}}$, day-ahead energy imbalances penalty prices, denoted by $\boldsymbol{\pi}_{\omega,t}^{\boldsymbol{\delta}\mathbf{E,DA}}$, and day-ahead reserve deficits penalty prices, denoted by $\boldsymbol{\pi}_{\omega,t}^{\boldsymbol{\delta}\mathbf{R,DA}}$, are defined as

$$\boldsymbol{\pi}_{\omega,t}^{\mathbf{R,DA}} := \left[\pi_{\omega,t}^{\mathrm{FCR,DA}}, \pi_{\omega,t}^{\mathrm{aFRR,comp}\uparrow\mathrm{,DA}}, \pi_{\omega,t}^{\mathrm{aFRR,comp}\downarrow\mathrm{,DA}}\right]^{\top}, \ \forall \omega, \forall t, \quad (5.11)$$

$$\boldsymbol{\pi}_{\omega,t}^{\boldsymbol{\delta}\mathbf{E,DA}} := \left[\pi_{\omega,t}^{\mathrm{E}\uparrow\mathrm{,DA}}, -\pi_{\omega,t}^{\mathrm{E}\downarrow\mathrm{,DA}}\right]^{\top}, \ \forall \omega, \forall t, \quad (5.12)$$

$$\boldsymbol{\pi}_{\omega,t}^{\boldsymbol{\delta}\mathbf{R,DA}} := \left[\pi_{\omega,t}^{\delta\mathrm{FCR,DA}}, \pi_{\omega,t}^{\delta\mathrm{aFRR,comp}\uparrow\mathrm{,DA}}, \pi_{\omega,t}^{\delta\mathrm{aFRR,comp}\downarrow\mathrm{,DA}}\right]^{\top}, \ \forall \omega, \forall t. \quad (5.13)$$

Moreover, the power balancing constraints, defined in (3.15b) for the single-market trading case, is rewritten as follows:

$$\sum_{b \in \boldsymbol{N}^{\mathbf{VPPBR}}} \sum_{c \in \boldsymbol{N}^{\mathbf{VPPCL}}} p_{c,b,\omega,t}^{\mathrm{VPPCL,DA}} \Delta_T - e_{\omega,t}^{\mathrm{DA}} + [1,-1]^{\top} \boldsymbol{\delta}_{\omega,t}^{\mathbf{E,DA}} + \left(\hat{\boldsymbol{\alpha}}_{\omega,t}^{\mathbf{DA}}\right)^{\top} \left(\boldsymbol{r}_{t}^{\mathbf{DA}} - \boldsymbol{\delta}_{\omega,t}^{\mathbf{R,DA}}\right) \Delta_T = 0, \ \forall \omega, \forall t. \quad (5.14)$$

Here, the vector of day-ahead frequency control activation signals, denoted by $\boldsymbol{\alpha}_{\omega,t}^{\mathbf{DA}}$, is defined as:

$$\boldsymbol{\alpha}_{\omega,t}^{\mathbf{DA}} = \left[-\alpha_{\omega,t}^{\mathrm{FCR,DA}}, -\alpha_{\omega,t}^{\mathrm{aFRR}\uparrow\mathrm{,DA}}, \alpha_{\omega,t}^{\mathrm{aFRR}\downarrow\mathrm{,DA}}\right]^{\top}, \ \forall \omega, \forall t. \quad (5.15)$$

The constraints (3.15c) that model the formulation of price-quantity bidding curves for the day-ahead market remain unchanged, as they pertain solely to the interaction with the day-ahead market. It is assumed here that the VPP submits fixed hourly bids to the ancillary services market. However, to extend this to formulating price-quantity bidding curves for the ancillary

services market, the problem can be slightly reformulated, as detailed in Section 3.3 for the day-ahead energy market. In the multi-market trading problem, the constraints (3.15d) representing the individual dynamics of the energy resource clusters integrated within the complex VPP also remain unaffected, as they are independent of the external dynamics of the VPP, such as its interactions with electricity markets and system operators.

The generic model proposed in (3.15) thus distinguishes the VPP's objective, represented by the objective function J^{DA}, and the constraints governing the interaction among energy resources within the VPP, represented by the power balancing constraints (3.15d), from the individual internal dynamics of the VPP resources, which remain unchanged when extending the framework to the multi-market trading problem. In other words, **the generic formulation presented in (3.15) for complex VPP scheduling problems allows for a straightforward extension to the multi-market trading case through localized adjustments to the original optimization problem**. This represents a clear advantage over case-study-specific models for VPP optimization problems.

Similar considerations apply to the **dispatch layer**, where the stochastic economic MPC strategy outlined in (3.19) is employed. Here, the objective function J^{ST}, defined in (3.23) for the single-market trading case, is rewritten as follows:

$$J^{\mathrm{ST}} := \sum_{\omega \in \boldsymbol{\Omega}^{\mathbf{ST}}} \sum_{k \in \boldsymbol{K}} P_{\omega}^{\mathrm{ST}} \Bigg(\underbrace{\left(\hat{\boldsymbol{\pi}}_{\omega,t+k}^{\boldsymbol{\delta}\mathbf{E},\mathbf{ST}}\right)^{\top} \boldsymbol{\delta}_{\omega,t+k|t}^{\mathbf{E},\mathbf{ST}}}_{\substack{\text{Penalty in the} \\ \text{day-ahead energy market}}} + \underbrace{\left(\hat{\boldsymbol{\pi}}_{\omega,t+k}^{\boldsymbol{\delta}\mathbf{R},\mathbf{ST}}\right)^{\top} \boldsymbol{\delta}_{\omega,t+k|t}^{\mathbf{R},\mathbf{ST}}}_{\substack{\text{Penalty in the} \\ \text{ancillary services market}}}$$
$$+ \frac{1}{|\boldsymbol{N}^{\mathbf{VPPBR}}|} \sum_{b \in \boldsymbol{N}^{\mathbf{VPPBR}}} \frac{1}{\left|\boldsymbol{N}_b^{\mathbf{VPPCL}}\right|} \sum_{c \in \boldsymbol{N}_b^{\mathbf{VPPCL}}} C_{c,b,\omega,t+k|t}^{\mathrm{VPPCL,ST}} \Bigg). \quad (5.16)$$

Here, the vector of short-term reserve deficits, denoted by $\boldsymbol{\delta}_{\omega,t+k|t}^{\mathbf{R},\mathbf{ST}}$, is defined as

$$\boldsymbol{\delta}_{\omega,t+k|t}^{\mathbf{R},\mathbf{ST}} := \left[\delta_{\omega,t+k|t}^{\mathrm{FCR,ST}}, \delta_{\omega,t+k|t}^{\mathrm{aFRR}\uparrow,\mathrm{ST}}, \delta_{\omega,t+k|t}^{\mathrm{aFRR}\downarrow,\mathrm{ST}}\right]^{\top}, \ \forall \omega, \forall k. \quad (5.17)$$

Moreover, the vectors of short-term energy imbalances penalty prices, denoted by $\boldsymbol{\pi}_{\omega,t+k}^{\boldsymbol{\delta}\mathbf{E},\mathbf{ST}}$, and short-term reserve deficits penalty prices, denoted by $\boldsymbol{\pi}_{\omega,t+k}^{\boldsymbol{\delta}\mathbf{R},\mathbf{ST}}$, are defined as

$$\boldsymbol{\pi}_{\omega,t+k}^{\boldsymbol{\delta}\mathbf{E},\mathbf{ST}} := \left[\pi_{\omega,t+k}^{\mathrm{E}\uparrow,\mathrm{ST}}, -\pi_{\omega,t+k}^{\mathrm{E}\downarrow,\mathrm{ST}}\right]^{\top}, \ \forall \omega, \forall k, \quad (5.18)$$

$$\boldsymbol{\pi}_{\omega,t+k}^{\boldsymbol{\delta}\mathbf{R},\mathbf{ST}} := \left[\pi_{\omega,t+k}^{\delta\mathrm{FCR,ST}}, \pi_{\omega,t+k}^{\delta\mathrm{aFRR,comp}\uparrow,\mathrm{ST}}, \pi_{\omega,t+k}^{\delta\mathrm{aFRR,comp}\downarrow,\mathrm{ST}}\right]^{\top}, \ \forall \omega, \forall k. \quad (5.19)$$

After the aggregator submits its bids, the energy and ancillary services markets clear, assigning the aggregator specific energy delivery volumes E_{t+k}^{ST}, FCR $R_{t+k}^{\mathrm{FCR,ST}}$, upward aFRR $R_{t+k}^{\mathrm{aFRR}\uparrow,\mathrm{ST}}$, and downward aFRR $R_{t+k}^{\mathrm{aFRR}\downarrow,\mathrm{ST}}$. Then, the power balancing constraints, defined in (3.19b) for the single-market trading case, is rewritten as follows:

$$\sum_{b \in \boldsymbol{N}^{\mathbf{VPPBR}}} \sum_{c \in \boldsymbol{N}^{\mathbf{VPPCL}}} p_{c,b,\omega,t+k|t}^{\mathrm{VPPCL,ST}} \Delta_K - E_{\omega,t+k}^{\mathrm{ST}} + [1,-1]^{\top} \boldsymbol{\delta}_{\omega,t+k|t}^{\mathbf{E},\mathbf{ST}}$$

$$+ (\hat{\boldsymbol{\alpha}}_{\omega,t+k})^{\top} \left(\boldsymbol{R}^{\mathbf{ST}}_{t+k} - \boldsymbol{\delta}^{\mathbf{R,ST}}_{\omega,t+k|t} \right) \Delta_K = 0, \ \forall \omega, \forall k. \quad (5.20)$$

Here, the vector of short-term reserves, denoted by $\boldsymbol{R}^{\mathbf{ST}}_{t+k}$, is defined as

$$\boldsymbol{R}^{\mathbf{ST}}_{t+k} := \left[R^{\mathrm{FCR,ST}}_{t+k}, R^{\mathrm{aFRR}\uparrow,\mathrm{ST}}_{t+k}, R^{\mathrm{aFRR}\downarrow,\mathrm{ST}}_{t+k} \right]^{\top}, \ \forall k. \quad (5.21)$$

The vector of short-term frequency control activation signals, denoted by $\boldsymbol{\alpha}^{\mathbf{ST}}_{\omega,t+k}$, is defined as:

$$\boldsymbol{\alpha}^{\mathbf{ST}}_{\omega,t+k} = \left[-\alpha^{\mathrm{FCR,ST}}_{\omega,t+k}, -\alpha^{\mathrm{aFRR}\uparrow,\mathrm{ST}}_{\omega,t+k}, \alpha^{\mathrm{aFRR}\downarrow,\mathrm{ST}}_{\omega,t+k} \right]^{\top}, \ \forall \omega, \forall k. \quad (5.22)$$

Finally, the vector of control actions, defined in (3.19c) for the single-market trading case, is rewritten as follows:

$$\boldsymbol{u}^{\mathbf{ST}}_{t|t} := \left[\boldsymbol{u}^{\mathbf{VPP,ST}}_{\omega,t|t}, \boldsymbol{\delta}^{\mathbf{E,ST}}_{\omega,t|t}, \boldsymbol{\delta}^{\mathbf{R,ST}}_{\omega,t|t} \right]^{\top}, \ \forall \omega. \quad (5.23)$$

Similarly to the scheduling strategy, **the generic formulation presented in (3.19) for complex VPP short-term dispatch control problems allows for a straightforward extension to the multi-market trading case through localized adjustments to the original MPC strategy**.

The enhanced modularity and adaptability of the proposed generic modeling approach for complex VPP optimization problems, compared to conventional case-study-specific models, extends naturally to the decomposition methods described in Chapter 4. For instance, consider the problem decomposition depicted in Fig. 4.3, applied to the case study of the Compagnie Nationale du Rhône. The proposed combined scenario-spatial decomposition method fully decouples the original centralized optimization model in both the spatial and scenario dimensions. Consequently, the problem is divided into subproblems, with one subproblem assigned to each dispatchable unit in the VPP and an additional subproblem managing the global VPP objectives and power balancing.

As discussed in this section, when the VPP participates in new markets, as in this case study, the proposed generic modeling approach requires adjustments only to the objective function and power balancing constraint. Thus, in the decomposition method outlined in Chapter 4, these modifications affect only the power balancing subproblem, while the subproblems associated with the individual dynamics of each VPP resource (namely the *local hydropower scheduling subproblems* in Fig. 4.3) remain unaffected. For instance, Fig. 5.3 illustrates the adjustments to the proposed decomposition of the Compagnie Nationale du Rhône scheduling problem when transitioning from single-market trading (day-ahead energy market only) to multi-market trading (day-ahead energy and ancillary services markets). As illustrated in the figure, extending the bidding strategy of the VPP operator to include an additional market requires modifications solely to a specific subproblem within the distributed scheduling framework. This approach minimizes disruptions to the existing decision-making tools implemented prior to the integration of a new market.

Furthermore, the proposed decomposition method also facilitates the seamless integration of additional dispatchable assets into the VPP. This is achieved by introducing a new subproblem

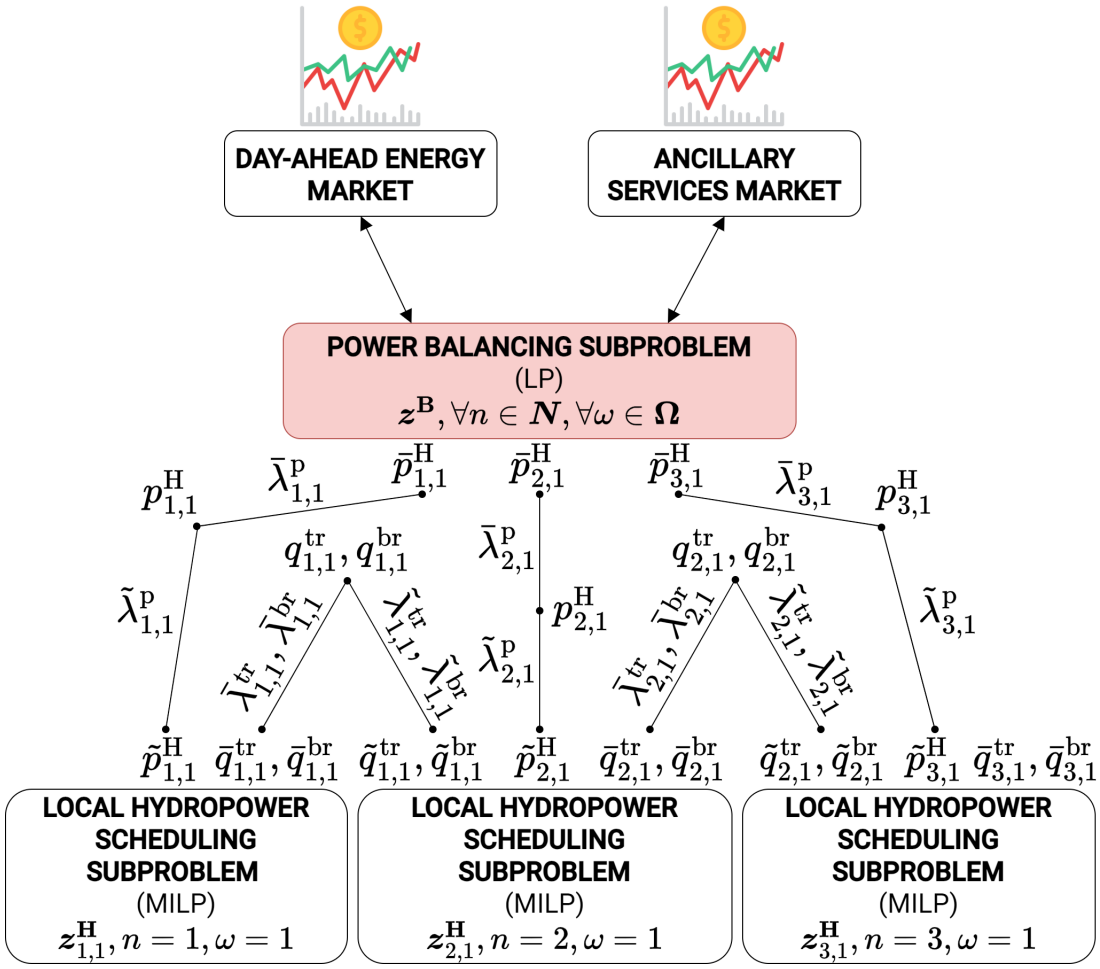

Figure 5.3: Illustration of the impact of integrating an additional market (ancillary services market) into the distributed VPP decision-making strategy depicted in Fig. 4.3. The subproblems of the proposed distributed structure influenced by this modification are highlighted in red.

to represent the individual dynamics of the added asset and adjusting the coupling constraints within the power balancing subproblem, all with minimal impact on the existing control architecture. Fig. 5.4 illustrates this adaptability. As depicted, the subproblems corresponding to the individual dynamics of the assets previously integrated in the VPP remain unaffected by this addition.

In essence, **by enabling a full decoupling of all coupling constraints in the original optimization problem (including both spatial and scenario dimensions), the proposed decomposition method not only maximizes the scalability potential of the resulting distributed algorithms but also ensures efficient adaptation to the dynamic nature of complex VPPs**. This adaptability facilitates the seamless integration of new assets and additional markets into the bidding strategy with minimal disruption to the existing decision-making framework.

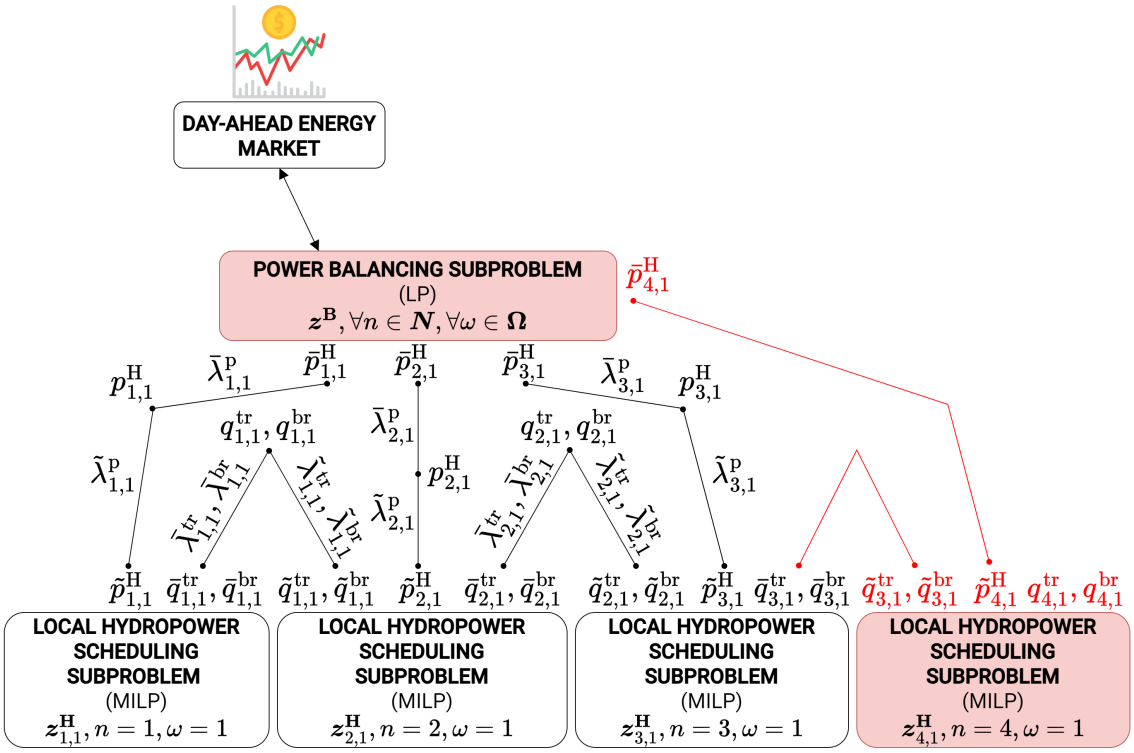

Figure 5.4: Illustration of the impact of integrating an additional dispatchable unit (hydropower system $n = 4$) into the distributed VPP decision-making strategy depicted in Fig. 4.3. The subproblems of the proposed distributed structure influenced by this modification are highlighted in red.

5.3 Case Study Description and Results

To show the adaptability of the proposed stochastic two-level decision-making framework of Section 3.3 in addressing the multi-market trading problem, this section presents a case study involving a real hybrid power plant composed of an onshore wind farm and a stationary BESS sharing the same grid connection point. Historical time series of wind power production, available in the framework of the Smart4RES EU Project [240], are utilized. The VPP model builds upon that of Section 4.4, extending it to enable simultaneous participation in the day-ahead energy market and the ancillary services market for market-based procurement of FCR and aFRR. A comprehensive characterization of the problem and a detailed description of the input data are provided in one of the papers resulting from this thesis, namely [234]. In particular, reference is made to the Romanian energy and balancing ancillary services markets; consequently, all prices are expressed in the Romanian currency (RON).

Similarly to the analysis presented in Section 3.4.2 for the optimal bidding of the complex VPP in the day-ahead energy market, this section considers three distinct methods:

- **Stochastic Day-Ahead + Stochastic Economic MPC (SDA+SEMPC)**: This is the proposed fully stochastic two-level decision-making framework (see Section 3.3), extended in Section 5.2 to address the multi-market trading problem. In the first level, the approach utilizes scenario-based stochastic programming to derive market bids, as formulated in

Strategy	Economic-oriented predictive control	Stochastic model
DDA+DRTMPC	-	-
DDA+DEMPC	✓	-
SDA+SEMPC	✓	✓

Table 5.1: Comparison between the proposed SDA+SEMPC and the benchmark approaches.

Strategy	Market revenue (RON/MW/h)	BESS degradation (RON/MW/h)
Market modeling: Perfect prices, Persistent ancillary services activation		
DDA+DRTMPC	264.8 (99.35)	1.3 (1.4)
DDA+DEMPC	301.43 (86.27)	0.97 (1.4)
SDA+SEMPC	**303.76 (83.4)**	**1 (1.2)**
Market modeling: Persistent prices, Persistent ancillary services activation		
DDA+DEMPC	222.4 (169.6)	1 (1.4)
Market modeling: Perfect prices, Perfect ancillary services activation		
DDA+DEMPC	301.49 (86.15)	1 (1.4)

Table 5.2: Normalized revenue and BESS degradation when participating in the energy and balancing ancillary services markets. Hourly mean value and standard deviation (in brackets). Values are in RON/MW/h since the energy generation is normalized by both the nominal capacity of the aggregated system and the number of hours in the simulation period.

(3.15). In the second level, stochastic economic MPC is employed to optimize the VPP dispatch in near-real-time, as formulated in (3.19).

- **Deterministic Day-Ahead + Deterministic Reference-Tracking MPC (DDA + RTMPC)**: This serves as the first benchmark for evaluating the proposed SDA+SEMPC strategy. In this approach, the first level uses a deterministic version of (3.15) to formulate market bids, while the second level applies traditional deterministic reference-tracking (non-economic) MPC (see Section 3.2.4.1) to optimize the VPP dispatch in near-real-time.
- **Deterministic Day-Ahead + Deterministic Economic MPC (DDA+DEMPC)**: This serves as the second benchmark for evaluating the proposed SDA+SEMPC strategy. In this approach, the first level uses a deterministic version of (3.15) to formulate market bids, while the second level applies deterministic economic MPC (see Section 3.2.4.2) to optimize the VPP dispatch in near-real-time.

A comparison between the proposed SDA+SEMPC and the aforementioned benchmark approaches is detailed in Table 5.1.

Table 5.2 presents a comparison of the proposed SDA+SEMPC method with the benchmark strategies when participating in the day-ahead energy market and balancing ancillary services market. Consistent with the results for the energy-only case (see Section 3.4.2), the economic-oriented approaches (DDA+DEMPC and SDA+SEMPC) significantly outperform the traditional reference-tracking DDA+DRTMPC strategy. The proposed fully stochastic

Strategy	Energy imbalances (MWh/MW/h)		Reserve deficits (MWh/MW/h)		
	$\delta^{\mathrm{E}\uparrow}$	$\delta^{\mathrm{E}\downarrow}$	$\delta^{\mathrm{FCR}}\Delta_T$	$\delta^{\mathrm{aFRR}\uparrow}\Delta_T$	$\delta^{\mathrm{aFRR}\downarrow}\Delta_T$
DDA+DRTMPC	0.04 (0.1)	0.43 (0.39)	0.003 (0.01)	0.03 (0.08)	0.12 (0.15)
DDA+DEMPC	0.04 (0.11)	0.48 (0.44)	0 (0)	0 (0)	0 (0)
SDA+SEMPC	**0.04 (0.1)**	**0.5 (0.44)**	**0 (0)**	**0 (0)**	**0 (0)**

Table 5.3: Normalized energy imbalances, FCR deficit and aFRR deficits, when participating in the day-ahead energy and balancing ancillary services markets. Hourly mean value and standard deviation (in brackets). Values are in MWh/MW/h since imbalances and deficits are normalized by both the nominal capacity of the system and the number of hours in the simulation period.

SDA+SEMPC method achieves a 15% increase in revenue and a 23% reduction in BESS degradation compared to the DDA+DRTMPC approach, along with a lower standard deviation. As observed in Section 3.4.2 for day-ahead market trading alone, incorporating economic key performance indicators into both levels of the decision-making framework significantly enhances its economic performance.

When compared to the most effective deterministic approach, DDA+DEMPC, the proposed fully stochastic SDA+SEMPC further increases market revenue and reduces storage degradation. This demonstrates that the stochastic method provides better hedging against the various uncertainties inherent in complex VPP problems, as highlighted in the results of the Compagnie Nationale du Rhône case study (see Section 3.4.2).

To evaluate the impact of uncertainty sources, Table 5.2 also examines two cases using the DDA+DEMPC benchmark: (1) unknown market prices (persistent prices) and (2) an idealized case with perfect knowledge of market prices and ancillary service activation signals (perfect prices, perfect ancillary services activation). In the first case, a significant reduction in ex-post market revenue is observed, highlighting the substantial effect of price uncertainty on decision-making performance. In the second case, perfect knowledge of ancillary service activation signals results in only a minor increase in market revenue compared to using persistent ancillary service activation, while ex-post storage degradation remains largely unchanged in both cases.

Table 5.3 presents the ex-post energy imbalances and reserve deficits. On average, the economic-oriented approaches successfully avoid reserve deficits, showing greater reliability in providing ancillary services compared to the traditional control approach using standard reference-tracking for dispatch (DDA+DRTMPC benchmark). To achieve this without significantly increasing storage degradation, both the DDA+DEMPC and SDA+SEMPC strategies experience, on average, larger deviations from the energy offer than DDA+DRTMPC. This is primarily driven by the observed market prices, which penalize reserve deficits more heavily than energy imbalances [234].

Clearly, high penalty prices tend to have a minimal impact on the traditional DDA+DRTMPC approach, whose control strategy is insensitive to prices. In contrast, the economic-oriented approaches, which are price-driven, are more significantly affected. A traditional reference-tracking approach typically distributes deviations across all services, while an economic-oriented strat-

egy focuses them on the less profitable markets. Therefore, when choosing DDA+DEMPC or SDA+SEMPC over DDA+DRTMPC, a reduction in energy market revenue is expected in exchange for increased revenue from the balancing ancillary services market and reduced storage degradation.

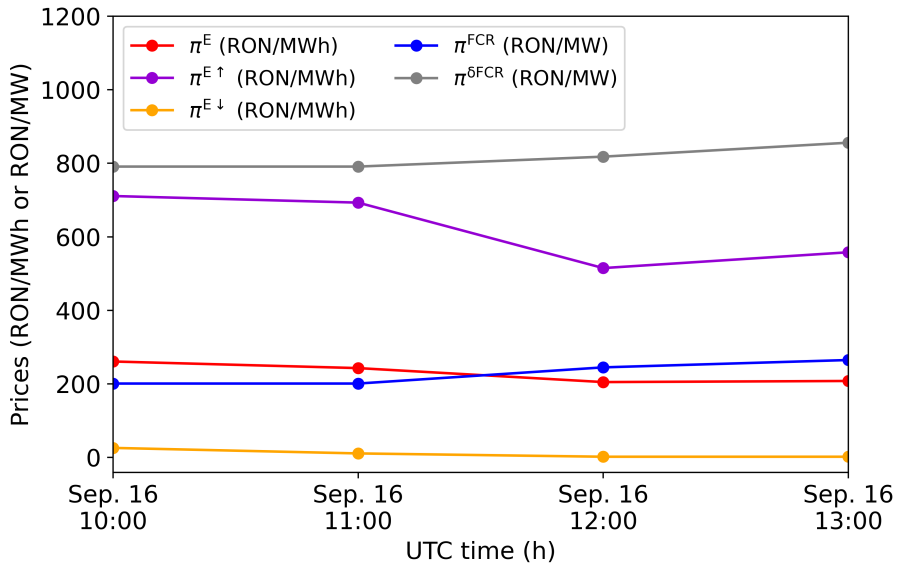

(a) Hourly prices of energy market and balancing ancillary services market.

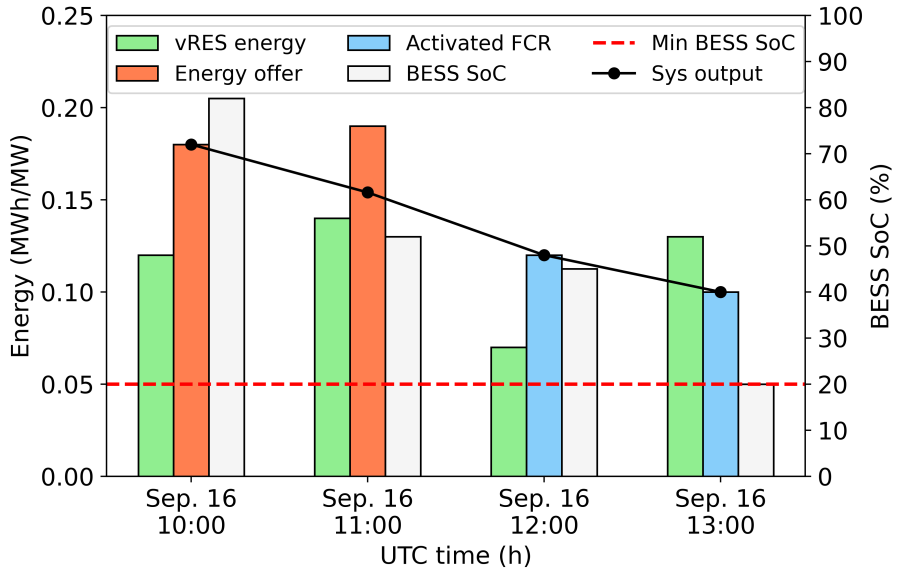

(b) BESS SoC, market offers, vRES energy and hybrid system output.

Figure 5.5: Example of BESS State of Charge (SoC) variations with the proposed SDA+SEMPC when providing energy and FCR. For each hour, the figure provides market prices, the initial BESS SoC, the energy offer, activated FCR balancing energy, and the total output of the aggregated system. Energy values are normalized by the nominal capacity of the aggregated system.

For a more comprehensive understanding of the benefits of an economically oriented control strategy, Fig. 5.5 illustrates an example of BESS State of Charge variations with the proposed SDA+SEMPC method when delivering both energy and FCR. During this period, aFRR is not

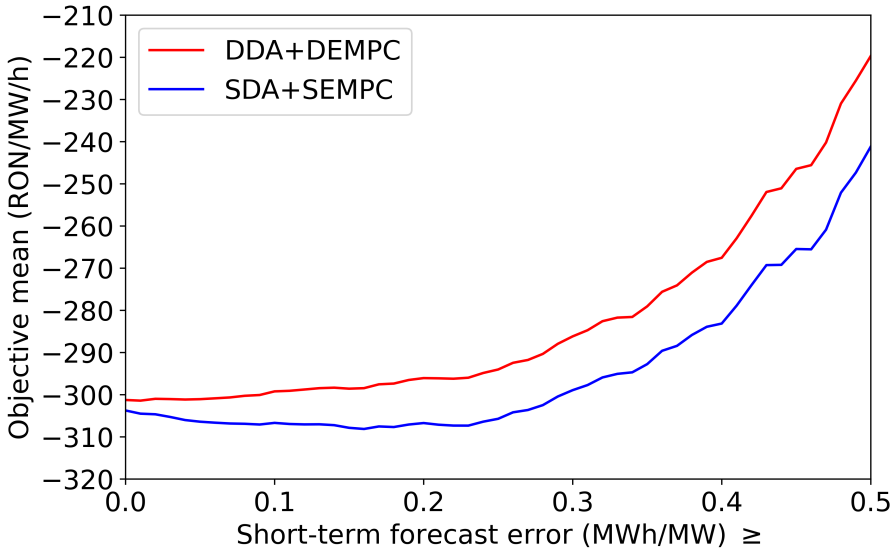

(a) Normalized ex-post mean of the objective function J^{DA}.

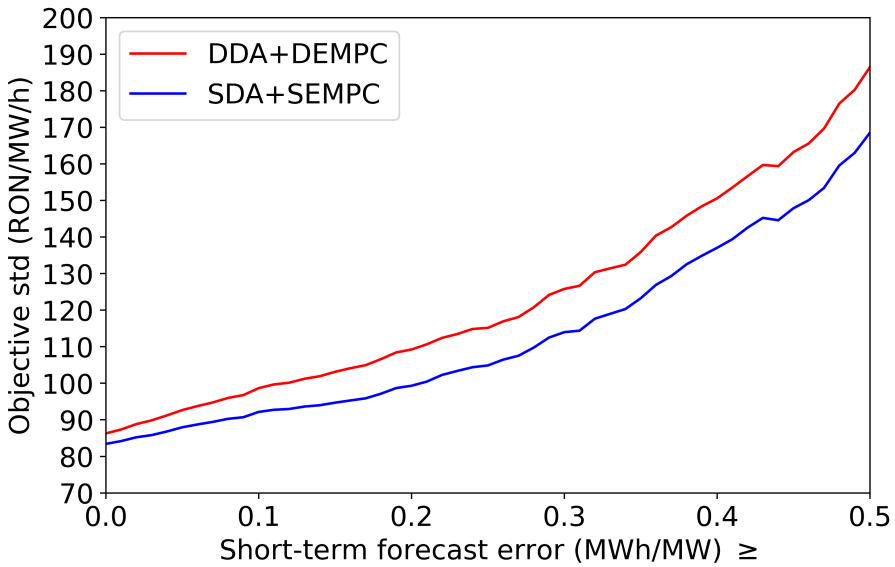

(b) Normalized ex-post standard deviation of the objective function J^{DA}.

Figure 5.6: Impact of the short-term vRES energy forecast error on the mean and standard deviation of the normalized ex-post day-ahead objective function value, i.e., ex-post value of J^{DA} defined in (5.8). Values are in RON/MW/h since J^{DA} is normalized by the nominal capacity of the aggregated system.

activated by the system operator. When the energy price exceeds the FCR price (at 10:00 and 11:00), the aggregator solely provides energy. However, when the FCR price surpasses the energy price, the aggregator focuses entirely on delivering FCR. At both 11:00 and 12:00, unforeseen deficiencies in vRES generation occur. Since the BESS does not have sufficient capacity to cover the shortages in both hours, a decision must be made on how to allocate deviations between the two markets. Given that the proposed controller accounts for market prices, the BESS is operated to minimize the FCR deficit at 12:00, even if it means incurring penalties for the

energy imbalance at 11:00. In contrast, a traditional reference-tracking control strategy would distribute deviations equally between the two markets, resulting in a less profitable outcome compared to the SDA+SEMPC, as shown in the results presented in Table 5.2.

For a more comprehensive understanding of the benefits of a fully stochastic decision-making framework, Fig. 5.6 presents the mean and standard deviation of the normalized ex-post day-ahead objective function values obtained with SDA+SEMPC and DDA+DEMPC, as a function of the short-term vRES energy forecast error. The SDA+SEMPC method reduces both the mean and standard deviation of the objective function J^{DA}, detailed in (5.8), compared to DDA+DEMPC, achieving up to a 9% decrease in the mean value and a 13% reduction in the standard deviation. These results show that a fully stochastic approach integrating scenario-based stochastic programming in both scheduling and dispatch levels (SDA+SEMPC) significantly mitigates sensitivity to forecast errors, in contrast to a decision framework that relies on deterministic models to handle uncertainty.

Overall, this analysis shows how the decision-making framework presented in Section 3.3 for day-ahead energy market trading can be seamlessly extended to the multi-market trading scenario, thanks to the high generality, modularity, and adaptability of the proposed scheduling and dispatch models.

Chapter 6

Conclusions and Future Directions

Résumé en Français

La transition énergétique mondiale exige une réduction substantielle des émissions du secteur énergétique, impliquant un basculement des infrastructures à forte intensité carbone vers des systèmes reposant sur des énergies renouvelables variables. Toutefois, l'intégration de ces ressources pose des défis majeurs en raison de leur intermittence et de leur imprévisibilité. Les centrales électriques virtuelles, en agrégeant des actifs énergétiques distribués et hétérogènes, constituent une solution prometteuse pour accroître la flexibilité du système électrique et améliorer sa résilience. Cette thèse développe un cadre d'optimisation décisionnelle pour la gestion des centrales électriques virtuelles complexes, intégrant des dynamiques non linéaires, des incertitudes et des contraintes multi-échelles. L'approche repose sur une optimisation distribuée, permettant de réduire le temps de calcul tout en préservant la précision des solutions, et offre une modularité facilitant l'adaptation aux évolutions du marché et aux nouveaux actifs énergétiques. Des perspectives de recherche incluent l'extension aux opérations en temps réel et à long terme, l'intégration de ressources thermiques et l'application de l'optimisation distribuée à des systèmes énergétiques de plus grande échelle. Ce travail vise ainsi à favoriser l'adoption des centrales électriques virtuelles complexes, contribuant à la transition énergétique et à la durabilité des systèmes électriques.

Addressing emissions in the energy sector is critical for mitigating global warming and meeting climate targets. The ongoing energy transition involves a global shift from fossil fuel-based systems to sustainable, low-carbon infrastructures, with the large-scale integration of vRES playing a key role. As vRES are deployed at scale, their active involvement in energy production and grid services, which are vital for ensuring the safe and reliable operation of power systems, becomes increasingly essential. However, the inherent intermittency and variability of vRES present significant challenges to their integration. In this context, VPPs have emerged as a promising solution. By aggregating geographically distributed and heterogeneous energy resources, VPPs enhance system flexibility, allowing for the effective management of stochastic resources such as vRES through the coordinated operation of dispatchable units. Although VPPs have received considerable attention in both research and industry, their development is still an evolving field.

In this context, Chapter 2 has provided an overview of the current state of VPPs. This analysis has revealed that existing studies and projects on VPPs primarily rely on case-specific modeling approaches, with few efforts at generalization, which only address the growing dimensionality of modern VPPs. However, increasing dimensionality is only one facet of their complexity, which also encompasses hard nonlinear dynamics, multiple sources of uncertainty, and intricate coupling constraints between the aggregated units. To fully capture the complexity of modern VPPs, a new paradigm has been introduced: the complex VPP, defined as a large-scale VPP with complex dynamics. The chapter concludes by presenting a real-world case study of a complex VPP operated by the French aggregator Compagnie Nationale du Rhône, which integrates 19 cascaded hydropower plants alongside wind and solar units. As the company's current operations involve uncoordinated management of wind, solar, and cascaded hydropower, the first research question arises: Does the aggregated operation of these resources within a complex VPP result in economic benefits?

To address this research question, Chapter 3 has introduced the modeling and decision-making tools that form the foundation for the proposed complex VPP energy management strategy. The goal is to address both day-ahead scheduling and short-term dispatch for a complex VPP participating in the day-ahead energy market. First, a modular modeling approach has been presented, organizing the complex VPP into generic clusters of energy resources, whose interconnection is represented through coupling constraints. A characterization of common coupling constraints in VPP models has been provided, ranging from electrical coupling to scenario coupling constraints. Building upon the generic modeling framework for complex VPPs, a two-level, scenario-based, fully stochastic decision-making tool has been proposed to address the VPP bidding problem. The first level employs scenario-based stochastic programming to derive price-quantity bidding curves, while the second level utilizes stochastic economic MPC for the short-term optimization of VPP imbalances in the market.

When applied to the case study of Compagnie Nationale du Rhône, the proposed stochastic economic MPC has shown superior performance compared to both non-economic controllers (with a 24% profit increase compared to the traditional non-economic reference-tracking MPC strategy) and its deterministic counterpart (with a 5% profit increase compared to the determin-

istic economic MPC strategy). Additionally, the coordinated operation of cascaded hydropower, wind, and solar units has been shown to be significantly influenced by inflow seasonality. During normal flow periods, the hydropower systems of Compagnie Nationale du Rhône have been shown to provide sufficient capacity to mitigate the stochasticity of vRES, thereby enhancing the market value of the aggregation. In contrast, during flood periods, these assets are constrained to operate as pure run-of-the-river systems with no storage capacity, causing the gap between coordinated and uncoordinated management to narrow significantly. Moreover, to assess the flexibility potential of the cascaded system, a sensitivity analysis was conducted by simulating a gradual increase in the wind capacity within the complex VPP. The results showed that the storage capacity of the hydropower cascade was "consumed" by this integration, up to a point (when wind capacity equaled 14 times the cascaded hydropower capacity, according to the simulations) where the flexibility of the hydropower systems was fully utilized. Beyond this threshold, the combined operation of wind and cascaded hydropower systems offered no economic advantage to the aggregator over their uncoordinated operation, as the stochasticity introduced by the large number of wind units in the VPP could not be effectively managed by the limited flexibility of the cascaded hydropower system.

As the scope of these aggregations expands and more assets with complex dynamics are integrated (e.g., the cascaded hydropower system integrated with wind and solar units, as in the case study of Compagnie Nationale du Rhône), the complexity of the associated VPP energy management strategy increases significantly, posing substantial challenges to conventional centralized solution methods. To address these challenges, Chapter 4 introduced a consensus-based optimization approach for decomposing the original two-level decision-making framework. A comprehensive decomposition strategy was proposed, which decoupled the problem across both spatial and scenario dimensions, thus maximizing scalability. Then, augmented Lagrangian relaxation-based methods were shown to provide the tools for deriving a fully distributed solution to the original centralized decision-making framework.

To ensure a performance guarantee for the proposed distributed strategy, especially for mixed-integer problems where a direct application of the ADMM would result in a heuristic approach, upper and lower bounds on the optimality gap relative to the original centralized problem were derived. By measuring the distance between these bounds, the proposed trustworthy distributed method enables a systematic evaluation of the quality of the distributed solution at each iteration. A mathematical proof was also provided to demonstrate the existence and validity of these bounds. The results showed the scalability and efficiency of the proposed distributed methods in comparison to centralized approaches, with significant reductions in both algorithm runtime and complexity. Specifically, when the proposed trustworthy CADMMB Algorithm 2 was applied to the MILP scheduling problem of the Compagnie Nationale du Rhône, the average runtime was observed to reduce by approximately 35% compared to consensus ADMM and by 57% compared to traditional centralized optimization. Moreover, while both the ADMM and centralized algorithms faced a significant increase in intractable instances as the number of scenarios employed in the stochastic programming problem increased, the CADMMB consistently provided a distributed solution with over 99.99% accuracy.

Finally, Chapter 5 extended the analysis to multi-market trading, exemplified by VPP participation in both day-ahead energy and ancillary services markets. The modularity of the proposed two-level decision-making framework was shown to facilitate seamless integration of new markets and assets into the VPP architecture, with minimal disruption to existing components. This modularity was retained in the distributed version of the framework, ensuring that the introduction of new market opportunities or assets affected only localized subproblems, leaving other components of the distributed decision-making framework unchanged. Results further validated the effectiveness of the stochastic economic methods for simultaneous participation in energy and ancillary services markets, particularly in the trading of frequency control services.

This thesis has examined several promising research directions, but numerous significant challenges and opportunities for **future investigation** remain.

The two-level decision-making framework presented in Chapter 3 can be extended in several directions. Firstly, a comprehensive approach for modern VPPs must also address the long-term planning phase of VPP operations, which could be incorporated into the proposed decision-making strategy rather than treated as a separate input phase. Similarly, the VPP may integrate resources requiring real-time operation, for which the proposed dispatch module might have too broad a time frame. Moreover, the generic modeling approach for complex VPPs provided in Chapter 3 introduces the potential to generalize the concepts of clusters and branches in the VPP model structure to include thermal components. However, the practical use and benefits of integrating such components are not explored here. Additionally, leveraging the proposed method for the seamless integration of new revenue streams, such as adding new markets to the VPP's scope, represents a promising area for further research, reinforcing the generalizability of the proposed approach.

As for the decomposition methods detailed in Chapter 4, several areas for further exploration remain. Building on the mathematical proof proposed in Chapter 4, the distributed methods provided for the mixed-integer case can be extended to other classes of nonconvex problems while maintaining a theoretical performance guarantee. Specifically, for the trustworthy CADMMB Algorithm 2, the warm-starting of the upper and lower bounds remains case-study specific and could be generalized for a broader class of complex VPPs. Further investigation is also needed regarding the convergence rate of the proposed distributed methods, particularly in relation to parameters tuning. More generally, while here the primary focus is on the development of distributed methods for providing fast, scalable solutions to complex VPP optimization and control problems, distributed approaches also contribute to two other relevant research directions: privacy-preserving methods, as the proposed decomposed structure ensures local agents share only part of their local information, and robustness to single-point failures, as the intelligence of the decision-making tool is distributed across multiple agents. These directions offer interesting avenues for further research, particularly in the application of asynchronous methods for exchanging information among agents of distributed algorithms, which can enhance robustness to communication failures.

In the broader context of **alternative approaches to the decomposition techniques presented here**, Reinforcement Learning is a widely discussed option. However, as explored in

previous chapters, Reinforcement Learning algorithms generally offer weaker convergence guarantees than the mathematical optimization methods employed in this work. Additionally, they lack the interpretability required in decision-making, which poses a significant challenge when dealing with delicate physical systems, like those considered in this study. Alternatively, simpler artificial intelligence techniques, such as decision trees, could provide data-driven solutions with improved interpretability. Yet, these methods are believed to have limited scalability and may not be as effective in handling large-scale, complex systems, such as those addressed in this research, compared to the proposed mathematical decomposition algorithms. Online control could serve as a viable alternative to the distributed MPC strategy proposed in Algorithm 3, potentially reducing the computational complexity of the dispatch module. On the other hand, online control relies solely on current information for decision-making, which typically limits its long-term effectiveness compared to MPC.

Overall, this thesis acknowledges the critical role of modern VPPs in enabling the rapid and secure integration of vRES into modern power systems. At the same time, it recognizes that the increasing complexity of these aggregated systems presents significant challenges to their broader adoption. The main objectives of this work have been to generalize the models and methods used for managing modern VPPs, enabling fast and scalable solutions to address their growing complexity, while retaining a theoretical performance guarantee on the decision-making process. It is believed that the methods presented here contribute to achieving these objectives, while laying a foundation for further development that could facilitate the wider adoption of the VPP concept and, ultimately, help address the critical challenges of the energy transition.

Bibliography

[1] J. Hansen, R. Ruedy, J. Glascoe, and M. Sato. "GISS analysis of surface temperature change". *Journal of Geophysical Research: Atmospheres* 104.D24 (1999), pp. 30997–31022 (cit. on p. 2).

[2] FR IEA. "Global methane tracker 2022". *iea Publications* (2022) (cit. on p. 2).

[3] S. Chu and A. Majumdar. "Opportunities and challenges for a sustainable energy future". *nature* 488.7411 (2012), pp. 294–303 (cit. on p. 2).

[4] J. Zhao, T. Zheng, and E. Litvinov. "A Unified Framework for Defining and Measuring Flexibility in Power System". *IEEE Transactions on Power Systems* 31.1 (2016), pp. 339–347 (cit. on p. 3).

[5] S. Kerscher and P. Arboleya. "The key role of aggregators in the energy transition under the latest European regulatory framework". *International Journal of Electrical Power Energy Systems* 134 (2022), p. 107361 (cit. on p. 3).

[6] P. Asmus. "Microgrids, virtual power plants and our distributed energy future". *The Electricity Journal* 23.10 (2010), pp. 72–82 (cit. on p. 3).

[7] A. Hussain, V. H. Bui, and H. M. Kim. "Microgrids as a resilience resource and strategies used by microgrids for enhancing resilience". *Applied Energy* 240 (2019), pp. 56–72 (cit. on p. 3).

[8] J.F. Manwell et al. "Hybrid energy systems". *Encyclopedia of energy* 3.2004 (2004), pp. 215–229 (cit. on p. 3).

[9] M. Sangaré, L. Brotcorne, H. Le Cadre, and M. Poss. "Cooperative game theory and cost allocation in energy communities". 2024 (cit. on p. 3).

[10] E. Cutore, R. Volpe, R. Sgroi, and A. Fichera. "Energy management and sustainability assessment of renewable energy communities: The Italian context". *Energy Conversion and Management* 278 (2023), p. 116713 (cit. on p. 3).

[11] X. Wang, Z. Liu, H. Zhang, Y. Zhao, J. Shi, and H. Ding. "A review on virtual power plant concept, application and challenges". *2019 IEEE Innovative Smart Grid Technologies-Asia (ISGT Asia)* (2019), pp. 4328–4333 (cit. on p. 3).

[12] H. M. Rouzbahani, H. Karimipour, and L. Lei. "A review on virtual power plant for energy management". *Sustainable energy technologies and assessments* 47 (2021), p. 101370 (cit. on pp. 4, 12).

[13] S. Panda, Sa. Mohanty, P. K. Rout, and B. K. Sahu. "A conceptual review on transformation of micro-grid to virtual power plant: Issues, modeling, solutions, and future prospects". *International journal of energy research* 46.6 (2022), pp. 7021–7054 (cit. on p. 4).

[14] J. F. Venegas-Zarama, J. I. Muñoz-Hernandez, L. Baringo, P. Diaz-Cachinero, and I. De Domingo-Mondejar. "A review of the evolution and main roles of virtual power plants as key stakeholders in power systems". *IEEE Access* 10 (2022), pp. 47937–47964 (cit. on pp. 4, 64).

[15] S. M. Nosratabadi, R.-A. Hooshmand, and E. Gholipour. "A comprehensive review on microgrid and virtual power plant concepts employed for distributed energy resources scheduling in power systems". *Renewable and Sustainable Energy Reviews* 67 (2017), pp. 341–363 (cit. on pp. 4, 12).

[16] S. Sierla, M. Pourakbari-Kasmaei, and V. Vyatkin. "A taxonomy of machine learning applications for virtual power plants and home/building energy management systems". *Automation in Construction* 136 (2022), p. 104174 (cit. on p. 4).

[17] E. A. Bhuiyan, M. Z. Hossain, S.M. Muyeen, S. R. Fahim, S. K. Sarker, and S. K. Das. "Towards next generation virtual power plant: Technology review and frameworks". *Renewable and Sustainable Energy Reviews* 150 (2021), p. 111358 (cit. on p. 5).

[18] Z. Liu, W. Zheng, F. Qi, L. Wang, B. Zou, F. Wen, et al. "Optimal dispatch of a virtual power plant considering demand response and carbon trading". *Energies* 11.6 (2018), p. 1488 (cit. on pp. 5, 11, 64, 65).

[19] M. Giuntoli and D. Poli. "Optimized thermal and electrical scheduling of a large scale virtual power plant in the presence of energy storages". *IEEE Transactions on Smart Grid* 4.2 (2013), pp. 942–955 (cit. on pp. 5, 11, 65, 66, 78).

[20] M. Jafari and A. A. Foroud. "A medium/long-term auction-based coalition-forming model for a virtual power plant based on stochastic programming". *International Journal of Electrical Power & Energy Systems* 118 (2020), p. 105784 (cit. on p. 5).

[21] S. Camal, A. Michiorri, and G. Kariniotakis. "Optimal Offer of Automatic Frequency Restoration Reserve From a Combined PV/Wind Virtual Power Plant". *IEEE Transactions on Power Systems* 33.6 (2018), pp. 6155–6170 (cit. on p. 5).

[22] J. Zhu, P. Duan, M. Liu, Y. Xia, Y. Guo, and X. Mo. "Bi-Level Real-Time Economic Dispatch of VPP Considering Uncertainty". *IEEE Access* 7 (2019), pp. 15282–15291 (cit. on p. 6).

[23] L. A. Roald, D. Pozo, A. Papavasiliou, D. K. Molzahn, J. Kazempour, and A. Conejo. "Power systems optimization under uncertainty: A review of methods and applications". *Electric Power Systems Research* 214 (2023), p. 108725 (cit. on pp. 6, 26, 71).

[24] A. Baringo and L. Baringo. "A Stochastic Adaptive Robust Optimization Approach for the Offering Strategy of a Virtual Power Plant". *IEEE Transactions on Power Systems* 32.5 (2017), pp. 3492–3504 (cit. on p. 6).

[25] C. Huang, D. Yue, J. Xie, Y. Li, and K. Wang. "Economic dispatch of power systems with virtual power plant based interval optimization method". *CSEE Journal of Power and Energy Systems* 2.1 (2016), pp. 74–80 (cit. on p. 6).

[26] Y. Zhou, Z. Wei, G. Sun, H. Zang, S. Chen, and M. Shahidehpour. "A Linear Chance Constrained Model for a Virtual Power Plant in Day-ahead, Real-time and Spinning Reserve Markets". *2019 IEEE Power Energy Society General Meeting (PESGM)*. 2019, pp. 1–14 (cit. on p. 6).

[27] H. Pandžić, J. M. Morales, A. J. Conejo, and I. Kuzle. "Offering model for a virtual power plant based on stochastic programming". *Applied Energy* 105 (2013), pp. 282–292 (cit. on p. 6).

[28] N. Naval and J. M. Yusta. "Virtual power plant models and electricity markets - A review". *Renewable and Sustainable Energy Reviews* 149 (2021), p. 111393 (cit. on pp. 7, 9, 10, 12, 19, 21, 25, 28, 30, 31, 59, 75, 76, 116, 129, 153).

[29] Y. Zhang, F. Liu, Z. Wang, Y. Su, W. Wang, and S. Feng. "Robust Scheduling of Virtual Power Plant Under Exogenous and Endogenous Uncertainties". *IEEE Transactions on Power Systems* 37.2 (2022), pp. 1311–1325 (cit. on p. 6).

[30] G. Mohy-ud-din, K. M. Muttaqi, and D. Sutanto. "Adaptive and Predictive Energy Management Strategy for Online Optimal Power Dispatch from VPPs with Renewable Energy and Energy Storage". *2020 IEEE Industry Applications Society Annual Meeting*. 2020, pp. 1–8 (cit. on p. 6).

[31] J. Naughton, H. Wang, M. Cantoni, and P. Mancarella. "Co-Optimizing Virtual Power Plant Services Under Uncertainty: A Robust Scheduling and Receding Horizon Dispatch Approach". *IEEE Transactions on Power Systems* 36.5 (2021), pp. 3960–3972 (cit. on p. 7).

[32] A. J. Conejo, E. Castillo, R. Minguez, and R. Garcia-Bertrand. *Decomposition techniques in mathematical programming: engineering and science applications*. Springer Science & Business Media, 2006 (cit. on p. 8).

[33] M. R. Scuzziato, E. C. Finardi, and A. Frangioni. "Comparing Spatial and Scenario Decomposition for Stochastic Hydrothermal Unit Commitment Problems". *IEEE Transactions on Sustainable Energy* 9.3 (2018), pp. 1307–1317 (cit. on pp. 8, 12).

[34] C. Wu, W. Gu, S. Zhou, and X. Chen. "Coordinated Optimal Power Flow for Integrated Active Distribution Network and Virtual Power Plants Using Decentralized Algorithm". *IEEE Transactions on Power Systems* 36.4 (2021), pp. 3541–3551 (cit. on p. 8).

[35] G. Chen and J. Li. "A fully distributed ADMM-based dispatch approach for virtual power plant problems". *Applied Mathematical Modelling* 58 (2018), pp. 300–312 (cit. on p. 8).

[36] Y. Wang, S. Wang, and L. Wu. "Distributed optimization approaches for emerging power systems operation: A review". *Electric Power Systems Research* 144 (2017), pp. 127–135 (cit. on pp. 8, 116, 117).

[37] B. H. Kim and R. Baldick. "A comparison of distributed optimal power flow algorithms". *IEEE Transactions on Power Systems* 15.2 (2000), pp. 599–604 (cit. on pp. 8, 117).

[38] D. K. Molzahn, F. Dörfler, H. Sandberg, S. H. Low, S. Chakrabarti, R. Baldick, et al. "A survey of distributed optimization and control algorithms for electric power systems". *IEEE Transactions on Smart Grid* 8.6 (2017), pp. 2941–2962 (cit. on pp. 8, 9, 113, 114, 117, 119, 120, 140).

[39] S. Boyd, N. Parikh, E. Chu, B. Peleato, J. Eckstein, et al. "Distributed optimization and statistical learning via the alternating direction method of multipliers". *Foundations and Trends® in Machine learning* 3.1 (2011), pp. 1–122 (cit. on pp. 8, 119, 120, 126, 127, 131, 150).

[40] Y. Yang, X. Guan, Q.-S. Jia, L. Yu, B. Xu, and C. J. Spanos. "A survey of admm variants for distributed optimization: Problems, algorithms and features". *arXiv preprint arXiv:2208.03700* (2022) (cit. on pp. 8, 12, 117, 119).

[41] M. Kraning, E. Chu, J. Lavaei, S. Boyd, et al. "Dynamic network energy management via proximal message passing". *Foundations and Trends® in Optimization* 1.2 (2013), pp. 73–126 (cit. on p. 8).

[42] T.-H. Chang, M. Hong, and X. Wang. "Multi-agent distributed optimization via inexact consensus ADMM". *IEEE Transactions on Signal Processing* 63.2 (2014), pp. 482–497 (cit. on p. 8).

[43] J. Christiansen, B. Dandurand, A. Eberhard, and F. Oliveira. "A study of progressive hedging for stochastic integer programming". *Computational Optimization and Applications* 86.3 (2023), pp. 989–1034 (cit. on pp. 8, 12, 13).

[44] J. P. Watson and D. L. Woodruff. "Progressive hedging innovations for a class of stochastic mixed-integer resource allocation problems". *Computational Management Science* 8 (2011), pp. 355–370 (cit. on pp. 8, 129).

[45] P. D. Cameron and M. Brothwood. *Competition in energy markets: law and regulation in the European Union*. Oxford University Press, USA, 2002 (cit. on p. 9).

[46] G. Pepermans. "European energy market liberalization: Experiences and challenges". *International Journal of Economic Policy Studies* 13.1 (2019), pp. 3–26 (cit. on p. 9).

[47] F. R. Aune, R. Golombek, S. A.C. Kittelsen, and K. E. Rosendahl. "Liberalizing European energy markets". *An Economic Analysis* (2008) (cit. on p. 9).

[48] C. Liu, R. J. Yang, X. Yu, C. Sun, P. S.P. Wong, and H. Zhao. "Virtual power plants for a sustainable urban future". *Sustainable cities and society* 65 (2021), p. 102640 (cit. on p. 10).

[49] V. Piron, G. Bontron, and M. Pochat. "Operating a hydropower cascade to optimize energy management". *Hydropower & Dams* 22.5 (2015), pp. 2–6 (cit. on pp. 10, 19, 41).

[50] M. Y. Ramandi, N. Bigdeli, and K. Afshar. "Stochastic economic model predictive control for real-time scheduling of balance responsible parties". *International Journal of Electrical Power & Energy Systems* 118 (2020), p. 105800 (cit. on pp. 11, 68, 69).

[51] T. Borsche, F. Oldewurtel, and G. Andersson. "Scenario-based MPC for energy schedule compliance with demand response". *IFAC Proceedings Volumes* 47.3 (2014), pp. 10299–10304 (cit. on pp. 11, 69).

[52] A. González-Garrido, H. Gaztañaga, A. Saez-de-Ibarra, A. Milo, and P. Eguia. "Electricity and reserve market bidding strategy including sizing evaluation and a novel renewable complementarity-based centralized control for storage lifetime enhancement". *Applied Energy* 262 (2020), p. 114591 (cit. on pp. 11, 68, 69, 113).

[53] M. Esfahani, A. Alizadeh, N. Amjady, and I. Kamwa. "A distributed VPP-integrated co-optimization framework for energy scheduling, frequency regulation, and voltage support using data-driven distributionally robust optimization with Wasserstein metric". *Applied Energy* 361 (2024), p. 122883 (cit. on p. 12).

[54] A. Gligor, P. Cofta, T. Marciniak, and C.-D. Dumitru. "Challenges for the Large-Scale Integration of Distributed Renewable Energy Resources in the Next Generation Virtual Power Plants". *Proceedings*. Vol. 63. 1. 2020, p. 20 (cit. on pp. 12, 113).

[55] J. Zhang. "The concept, project and current status of virtual power plant: a review". *Journal of Physics: Conference Series*. Vol. 2152. 1. 2022, p. 012059 (cit. on pp. 12, 31).

[56] T. Yang, X. Yi, J. Wu, Y. Yuan, D. Wu, Z. Meng, et al. "A survey of distributed optimization". *Annual Reviews in Control* 47 (2019), pp. 278–305 (cit. on p. 12).

[57] A. Muhtadi, D. Pandit, N. Nguyen, and J. Mitra. "Distributed energy resources based microgrid: Review of architecture, control, and reliability". *IEEE Transactions on Industry Applications* 57.3 (2021), pp. 2223–2235 (cit. on p. 19).

[58] H. Gao, T. Jin, C. Feng, C. Li, Q. Chen, and C. Kang. "Review of virtual power plant operations: Resource coordination and multidimensional interaction". *Applied Energy* 357 (2024), p. 122284 (cit. on p. 19).

[59] H. Xie, T. Ahmad, D. Zhang, H. H. Goh, and T. Wu. "Community-based virtual power plants' technology and circular economy models in the energy sector: a techno-economy study". *Renewable and Sustainable Energy Reviews* 192 (2024), p. 114189 (cit. on p. 19).

[60] A. F. Minai, A. A. Khan, K. Bahn, M. Falilou Ndiaye, T. Alam, R. Khargotra, et al. "Evolution and role of virtual power plants: Market strategy with integration of renewable based microgrids". *Energy Strategy Reviews* 53 (2024), p. 101390 (cit. on p. 19).

[61] S. Yu, F. Fang, Y. Liu, and J. Liu. "Uncertainties of virtual power plant: Problems and countermeasures". *Applied Energy* 239 (2019), pp. 454–470 (cit. on pp. 19, 22, 24, 25).

[62] VPP4Islands team. *About our VPP4Islands project*. https://vpp4islands.eu/ (cit. on p. 19).

[63] A. Piguet, A. Benefice, G. Bontron, C. Helbert, and G. Vial. "Metamodeling the optimal total revenues of the short-term optimization of a hydropower cascade under uncertainty". *Science and Technology for Energy Transition* 78 (2023), p. 31 (cit. on p. 19).

[64] S. Awerbuch and A. Preston. *The virtual utility: Accounting, technology & competitive aspects of the emerging industry*. Springer Science & Business Media, 1997 (cit. on p. 20).

[65] M. Othman, Y.G. Hegazy, and A. Abdelaziz. "A Review of Virtual power plant Definitions, Components, Framework and Optimization". *International Electrical Engineering Journal (IEEJ)* 6 (2015), pp. 2010–2024 (cit. on p. 20).

[66] W. Zhang, C. He, H. Qian, Z. Lin, Y. Li, X. Zhao, et al. "Virtual power plant integration with smart grids: A review". *2022 IEEE 5th International Electrical and Energy Conference (CIEEC)*. 2022, pp. 4755–4759 (cit. on p. 20).

[67] K. El Bakari and W.L. Kling. "Virtual power plants: An answer to increasing distributed generation". *2010 IEEE PES Innovative Smart Grid Technologies Conference Europe (ISGT Europe)*. 2010, pp. 1–6 (cit. on p. 20).

[68] A.Y. Abdelaziz, Y.G. Hegazy, W. El-Khattam, and M.M. Othman. "Virtual power plant: the future of power delivery systems". *European workshop on renewable energy systems*. 2013, pp. 1–2 (cit. on p. 20).

[69] A. Michiorri, S. Camal, and G. Kariniotakis. "Ancillary services from a renewable-sourced virtual power plant: the REstable project". *6th International Conference Energy & Meteorology*. 2019 (cit. on p. 20).

[70] O. M. Babatunde, J. L. Munda, and Y. Hamam. "Power system flexibility: A review". *Energy Reports* 6 (2020), pp. 101–106 (cit. on p. 20).

[71] Z. Ullah, G. Mokryani, F. Campean, and Y. F. Hu. "Comprehensive review of VPPs planning, operation and scheduling considering the uncertainties related to renewable energy sources". *IET Energy Systems Integration* 1 (2019), pp. 147–157 (cit. on p. 21).

[72] E. G. Kardakos, C. K. Simoglou, and A. G. Bakirtzis. "Optimal offering strategy of a virtual power plant: A stochastic bi-level approach". *IEEE Transactions on Smart Grid* 7.2 (2015), pp. 794–806 (cit. on p. 21).

[73] F. Bourry, J. Juban, L. Costa, and G. Kariniotakis. "Advanced strategies for wind power trading in short-term electricity markets". *European Wind Energy Conference & Exhibition EWEC 2008*. 2008, 8–pages (cit. on p. 21).

[74] N. Pourghaderi, M. Fotuhi-Firuzabad, M. Moeini-Aghtaie, and M. Kabirifar. "Commercial demand response programs in bidding of a technical virtual power plant". *IEEE Transactions on Industrial Informatics* 14.11 (2018), pp. 5100–5111 (cit. on p. 22).

[75] G. Kariniotakis and P. Pinson. "Uncertainty of short-term wind power forecasts a methodology for on-line assessment". *2004 International Conference on Probabilistic Methods Applied to Power Systems*. 2004, pp. 729–736 (cit. on p. 22).

[76] S. Camal, G. Kariniotakis, F. Sossan, Q. Libois, R. Legrand, L. Raynaud, et al. "Smart4RES: Next generation solutions for renewable energy forecasting and applications with focus on distribution grids". *IET Conference Proceedings* 2021 (6 2021), pp. 2899–2903 (cit. on p. 22).

[77] J. Zhang, B.-M. Hodge, E. Gomez-Lazaro, A. L. Lovholm, E. Berge, J. Miettinen, et al. *Analysis of variability and uncertainty in wind power forecasting: an international comparison*. Tech. rep. National Renewable Energy Lab.(NREL), Golden, CO (United States), 2013 (cit. on p. 22).

[78] D. Lew, M. Milligan, G. Jordan, and R. Piwko. *Value of wind power forecasting*. Tech. rep. National Renewable Energy Lab.(NREL), Golden, CO (United States), 2011 (cit. on p. 23).

[79] A. Stratigakos, A. Michiorri, and G. Kariniotakis. "A value-oriented price forecasting approach to optimize trading of renewable generation". *2021 IEEE Madrid PowerTech*. 2021, pp. 1–6 (cit. on p. 23).

[80] X. Shang-fe. "Value at risk and price volatility forecasting in electricity market: a literature review". *Power System Protection and Control* 42 (2014), pp. 146–153 (cit. on p. 23).

[81] S. Camal, A. Michiorri, G. Kariniotakis, and A. Liebelt. "Short-term forecast of automatic frequency restoration reserve from a renewable energy based virtual power plant". *2017 IEEE PES Innovative Smart Grid Technologies Conference Europe (ISGT-Europe)*. 2017, pp. 1–6 (cit. on p. 23).

[82] A. Gerossier, R. Girard, G. Kariniotakis, and A. Michiorri. "Probabilistic day-ahead forecasting of household electricity demand". *CIRED 2017-24th International Conference on Electricity Distribution*. Vol. 2017. 1. 2017, pp. 2500–2504 (cit. on p. 23).

[83] K. Clement-Nyns, E. Haesen, and J. Driesen. "The impact of charging plug-in hybrid electric vehicles on a residential distribution grid". *IEEE Transactions on power systems* 25.1 (2009), pp. 371–380 (cit. on p. 23).

[84] L. Hirth. "The market value of variable renewables: The effect of solar wind power variability on their relative price". *Energy economics* 38 (2013), pp. 218–236 (cit. on p. 23).

[85] S. Camal, F. Teng, A. Michiorri, G. Kariniotakis, and L. Badesa. "Scenario generation of aggregated wind, photovoltaics and small hydro production for power systems applications". *Applied Energy* 242 (2019), pp. 1396–1406 (cit. on p. 23).

[86] W. Li. "The Virtual Power Plant Bidding Strategy Model based on Multi-stage Semi-anticipativity Distributionally Robust Optimization". *Electric Power Systems Research* 237 (2024), p. 111015 (cit. on p. 24).

[87] M. M. Roozbehani, E. Heydarian-Forushani, S. Hasanzadeh, and S. B. Elghali. "Virtual power plant operational strategies: Models, markets, optimization, challenges, and opportunities". *Sustainability* 14.19 (2022) (cit. on p. 26).

[88] E. Mashhour and S. M. Moghaddas-Tafreshi. "Bidding strategy of virtual power plant for participating in energy and spinning reserve markets—Part II: Numerical analysis". *IEEE Transactions on Power Systems* 26.2 (2010), pp. 957–964 (cit. on p. 26).

[89] M. Rahimiyan and L. Baringo. "Strategic bidding for a virtual power plant in the day-ahead and real-time markets: A price-taker robust optimization approach". *IEEE Transactions on Power Systems* 31.4 (2015), pp. 2676–2687 (cit. on p. 26).

[90] G. He, Q. Chen, C. Kang, Q. Xia, and K. Poolla. "Cooperation of wind power and battery storage to provide frequency regulation in power markets". *IEEE Transactions on Power Systems* 32.5 (2016), pp. 3559–3568 (cit. on p. 26).

[91] G. Chicco and A. Mazza. "Metaheuristic optimization of power and energy systems: Underlying principles and main issues of the 'rush to heuristics'". *Energies* 13.19 (2020), p. 5097 (cit. on p. 26).

[92] E. Mashhour and S. M. Moghaddas-Tafreshi. "Bidding strategy of virtual power plant for participating in energy and spinning reserve markets—Part I: Problem formulation". *IEEE Transactions on Power Systems* 26.2 (2010), pp. 949–956 (cit. on p. 26).

[93] W. Wang, P. Chen, D. Zeng, and J. Liu. "Electric vehicle fleet integration in a virtual power plant with large-scale wind power". *IEEE Transactions on Industry Applications* 56.5 (2020), pp. 5924–5931 (cit. on p. 26).

[94] Z.-H. Zhou. *Machine learning*. Springer nature, 2021 (cit. on p. 27).

[95] Z. Yi, Y. Xu, and C. Wu. "Model-free economic dispatch for virtual power plants: An adversarial safe reinforcement learning approach". *IEEE Transactions on Power Systems* 39.2 (2023), pp. 3153–3168 (cit. on p. 27).

[96] W. Chen, J. Qiu, J. Zhao, Q. Chai, and Z. Y. Dong. "Customized rebate pricing mechanism for virtual power plants using a hierarchical game and reinforcement learning approach". *IEEE Transactions on Smart Grid* 14.1 (2022), pp. 424–439 (cit. on p. 27).

[97] A. Stratigakos, S. Camal, A. Michiorri, and G. Kariniotakis. "Prescriptive trees for integrated forecasting and optimization applied in trading of renewable energy". *IEEE Transactions on Power Systems* 37.6 (2022), pp. 4696–4708 (cit. on p. 27).

[98] S. M. Shinners. *Modern control system theory and design*. Vol. 1. John Wiley & Sons, 1998 (cit. on p. 27).

[99] A. Bukhari, S. H. Yusoff, M. S. F. M. Yunus, S. N.h M. Sapihie, and N. S. I. Razali. "Virtual Power Plant Management Using PID Controller". *International Conference on Electrical, Control & Computer Engineering*. 2023, pp. 457–470 (cit. on p. 27).

[100] L. C. Evans. "An introduction to mathematical optimal control theory". *Lecture Notes, University of California, Department of Mathematics, Berkeley* 3 (2005), pp. 15–40 (cit. on p. 27).

[101] H. Kwakernaak. "Robust control and H-optimization—tutorial paper". *automatica* 29.2 (1993), pp. 255–273 (cit. on p. 27).

[102] E. F. Camacho, C. Bordons, E. F. Camacho, and C. Bordons. *Constrained model predictive control*. Springer, 2007 (cit. on pp. 27, 72, 73).

[103] H. Ali, B. Francois, L. Brotcorne, Z. Foroozandeh, and J. P. Soares. "Model predictive control for smart grid charging of autonomous electric vehicle fleet using local renewable energy generation". *27th International Conference on Electricity Distribution (CIRED 2023)*. Vol. 2023. 2023, pp. 1889–1893 (cit. on p. 28).

[104] L. Santosuosso, G. Kariniotakis, A. Di Giorgio, F. Liberati, S. Camal, and A. Michiorri. "Advanced Model Predictive Control Strategies for the Provision of Energy and Ancillary Services by Wind Farms Coupled with Storage". *WindEurope Technology Workshop 2022*. 2022 (cit. on p. 28).

[105] T. I. Reigstad and K. Uhlen. "Variable speed hydropower for provision of fast frequency reserves in the nordic grid". *IEEE Transactions on Power Systems* 36.6 (2021), pp. 5476–5485 (cit. on p. 28).

[106] H. Algarvio. "Risk-Sharing Contracts and risk management of bilateral contracting in electricity markets". *International Journal of Electrical Power & Energy Systems* 144 (2023), p. 108579 (cit. on p. 28).

[107] M. Shabanzadeh, M.-K. Sheikh-El-Eslami, and M.-R. Haghifam. "The design of a risk-hedging tool for virtual power plants via robust optimization approach". *Applied Energy* 155 (2015), pp. 766–777 (cit. on p. 28).

[108] M. Shabanzadeh, M.-K. Sheikh-El-Eslami, and M.-R. Haghifam. "Decision making tool for virtual power plants considering midterm bilateral contracts". *Iranian Regulation CIRED Conf. and Exhibition on Electricity Distribution*. 2015, pp. 1–6 (cit. on p. 28).

[109] N. Thie and L. Kloibhofer. "Influence of European market frameworks on market participation and risk management of virtual power plants". *2018 15th International Conference on the European Energy Market (EEM)*. 2018, pp. 1–5 (cit. on p. 28).

[110] J.-F. Toubeau, Z. De Grève, and F. Vallée. "Medium-term multimarket optimization for virtual power plants: A stochastic-based decision environment". *IEEE Transactions on Power Systems* 33.2 (2017), pp. 1399–1410 (cit. on p. 28).

[111] S. Ottesen, A. Tomasgard, and S.-E. Fleten. "Prosumer bidding and scheduling in electricity markets". *Energy* 94 (2016), pp. 828–843 (cit. on p. 29).

[112] J. Kazempour, M. P. Moghaddam, and G. R. Yousefi. "Self-scheduling of a price-taker hydro producer in day-ahead energy and ancillary service markets". *2008 IEEE Canada Electric Power Conference*. 2008, pp. 1–6 (cit. on p. 29).

[113] H. Ding, P. Pinson, Z. Hu, J. Wang, and Y. Song. "Optimal offering and operating strategy for a large wind-storage system as a price maker". *IEEE Transactions on Power Systems* 32.6 (2017), pp. 4904–4913 (cit. on p. 29).

[114] A. Khodadadi, L. Söder, and M. Amelin. "Stochastic adaptive robust approach for day-ahead energy market bidding strategies in hydro dominated sequential electricity markets". *Sustainable Energy, Grids and Networks* 32 (2022), p. 100827 (cit. on p. 29).

[115] P. Mancarella and G. Chicco. "Integrated energy and ancillary services provision in multi-energy systems". *2013 IREP Symposium Bulk Power System Dynamics and Control-IX Optimization, Security and Control of the Emerging Power Grid*. 2013, pp. 1–19 (cit. on p. 29).

[116] S. Bahramara, P. Sheikhahmadi, A. Mazza, and G. Chicco. "Day-ahead self-scheduling from risk-averse microgrid operators to provide reserves and flexible ramping ancillary services". *International journal of electrical power & energy systems* 142 (2022), p. 108381 (cit. on p. 29).

[117] S. Camal, A. Michiorri, and G. Kariniotakis. "Reliable provision of ancillary services from aggregated variable renewable energy sources through forecasting of extreme quantiles". *IEEE Transactions on Power Systems* 38.4 (2022), pp. 3070–3084 (cit. on p. 29).

[118] P. C. Granado, J. Rajasekharan, S. Venkatesh Pandiyan, A. Tomasgard, G. Kara, H. Farahmand, et al. "Flexibility characterization, aggregation, and market design trends with a high share of renewables: a review". *Current Sustainable/Renewable Energy Reports* 10.1 (2023), pp. 12–21 (cit. on p. 29).

[119] E. H. Allen and M. D. Ilic. "Reserve markets for power systems reliability". *IEEE Transactions on Power Systems* 15.1 (2000), pp. 228–233 (cit. on p. 29).

[120] S. R. Dabbagh and M. K. Sheikh-El-Eslami. "Risk assessment of virtual power plants offering in energy and reserve markets". *IEEE Transactions on Power Systems* 31.5 (2015), pp. 3572–3582 (cit. on pp. 29, 30).

[121] P. Shinde and M. Amelin. "A literature review of intraday electricity markets and prices". *2019 IEEE Milan PowerTech* (2019), pp. 1–6 (cit. on p. 30).

[122] D. Wozabal and G. Rameseder. "Optimal bidding of a virtual power plant on the Spanish day-ahead and intraday market for electricity". *European Journal of Operational Research* 280.2 (2020), pp. 639–655 (cit. on pp. 30, 116).

[123] D. Koraki and K. Strunz. "Wind and solar power integration in electricity markets and distribution networks through service-centric virtual power plants". *IEEE Transactions on Power Systems* 33.1 (2017), pp. 473–485 (cit. on p. 30).

[124] Q. Wang, C. Zhang, Y. Ding, G. Xydis, J. Wang, and J. Østergaard. "Review of real-time electricity markets for integrating distributed energy resources and demand response". *Applied Energy* 138 (2015), pp. 695–706 (cit. on p. 30).

[125] M. Olsson and L. Söder. "Modeling real-time balancing power market prices using combined SARIMA and Markov processes". *IEEE Transactions on Power Systems* 23.2 (2008), pp. 443–450 (cit. on p. 30).

[126] T. Morstyn, A. Teytelboym, and M. McCulloch. "Bilateral contract networks for peer-to-peer energy trading". *IEEE Transactions on Smart Grid* 10.2 (2018), pp. 2026–2035 (cit. on p. 31).

[127] J. Jansen, A. van der Welle, C. Kolokathis, C. Madina, and A. Diaz. *Fenix deliverable 3.3: Financial and socio-economic impacts of embracing the Fenix concept*. http://resolver.tudelft.nl/uuid:fdc61ac4-563e-4c5c-9408-bf3aef3298dc (cit. on pp. 31, 32).

[128] Fraunhofer IWES. *Kombikraftwerk2*. https://www.iee.fraunhofer.de/en/research_projects/search/2013/kombikraftwerk2.html (cit. on pp. 31, 32).

[129] K. Levy. "Snapshot of decentralized energy trading platforms in Australia". *Energy News* 35.2 (2017), pp. 13–15 (cit. on p. 32).

[130] M. Zdrilić, H. Pandžić, and I. Kuzle. "The mixed-integer linear optimization model of virtual power plant operation". *2011 8th International Conference on the European Energy Market (EEM)*. 2011, pp. 467–471 (cit. on p. 32).

[131] J. Zapata, J. Vandewalle, and W. D'haeseleer. "A comparative study of imbalance reduction strategies for virtual power plant operation". *Applied Thermal Engineering* 71.2 (2014), pp. 847–857 (cit. on p. 32).

[132] Y. Liu, M. Li, H. Lian, X. Tang, C. Liu, and C. Jiang. "Optimal dispatch of virtual power plant using interval and deterministic combined optimization". *International Journal of Electrical Power & Energy Systems* 102 (2018), pp. 235–244 (cit. on p. 32).

[133] H. Wang, S. Riaz, and P. Mancarella. "Integrated techno-economic modeling, flexibility analysis, and business case assessment of an urban virtual power plant with multi-market co-optimization". *Applied Energy* 259 (2020), p. 114142 (cit. on p. 32).

[134] NordNordWest. *Map of the Rhône River Basin*. Own work using GTOPO-30 Elevation Data by USGS. 2014. URL: https://commons.wikimedia.org/w/index.php?curid=3769538 (cit. on p. 33).

[135] A. Piguet. "Optimisation sous incertitudes par métamodèle pour la planification à court terme de la production conjointe d'une chaine hydroélectrique et d'actifs de production variable". PhD thesis. Université de Lyon, 2022 (cit. on pp. 34, 39, 48, 49, 99, 145).

[136] P. Breeze. *Hydropower*. Academic Press, 2018 (cit. on p. 37).

[137] E.C. Finardi and E.L. da Silva. "Solving the hydro unit commitment problem via dual decomposition and sequential quadratic programming". *IEEE Transactions on Power Systems* 21.2 (2006), pp. 835–844 (cit. on p. 44).

[138] K.V. Santos and E.C. Finardi. "Piecewise linear approximations for hydropower production function applied on the hydrothermal unit commitment problem". *International Journal of Electrical Power & Energy Systems* 135 (2022), p. 107464 (cit. on p. 44).

[139] S. Cerisola, J. M. Latorre, and A. Ramos. "Stochastic dual dynamic programming applied to nonconvex hydrothermal models". *European Journal of Operational Research* 218.3 (2012), pp. 687–697 (cit. on p. 44).

[140] I. T. Jolliffe and D. B. Stephenson. *Forecast verification: a practitioner's guide in atmospheric science*. John Wiley & Sons, 2012 (cit. on p. 51).

[141] T. Gneiting and A. E. Raftery. "Strictly proper scoring rules, prediction, and estimation". *Journal of the American statistical Association* 102.477 (2007), pp. 359–378 (cit. on p. 51).

[142] J. E. Matheson and R. L. Winkler. "Scoring rules for continuous probability distributions". *Management science* 22.10 (1976), pp. 1087–1096 (cit. on p. 51).

[143] T. Gneiting, A. E. Raftery, A. H. Westveld, and T. Goldman. "Calibrated probabilistic forecasting using ensemble model output statistics and minimum CRPS estimation". *Monthly Weather Review* 133.5 (2005), pp. 1098–1118 (cit. on p. 51).

[144] International Energy Agency. *Hydropower Special Market Report*. https://www.iea.org/reports/hydropower-special-market-report. 2021 (cit. on p. 58).

[145] G. Steeger, L. A. Barroso, and S. Rebennack. "Optimal bidding strategies for hydro-electric producers: A literature survey". *IEEE Transactions on Power Systems* 29.4 (2014), pp. 1758–1766 (cit. on pp. 63, 75, 77).

[146] N. Mazzi, A. Trivella, and J. M. Morales. "Enabling active/passive electricity trading in dual-price balancing markets". *IEEE Transactions on Power Systems* 34.3 (2018), pp. 1980–1990 (cit. on pp. 64, 65).

[147] D. Shropshire, A. Purvins, I. Papaioannou, and I. Maschio. "Benefits and cost implications from integrating small flexible nuclear reactors with off-shore wind farms in a virtual power plant". *Energy Policy* 46 (2012), pp. 558–573 (cit. on p. 64).

[148] E. Handschin, F. Neise, H. Neumann, and R. Schultz. "Optimal operation of dispersed generation under uncertainty using mathematical programming". *International Journal of Electrical Power & Energy Systems* 28.9 (2006), pp. 618–626 (cit. on p. 64).

[149] H. Pandžić, I. Kuzle, and T. Capuder. "Virtual power plant mid-term dispatch optimization". *Applied energy* 101 (2013), pp. 134–141 (cit. on p. 64).

[150] A. H. Elgamal, G. Kocher-Oberlehner, V. Robu, and M. Andoni. "Optimization of a multiple-scale renewable energy-based virtual power plant in the UK". *Applied Energy* 256 (2019), p. 113973 (cit. on pp. 64, 65).

[151] A. F. Raab, E. Lauth, K. Strunz, and D. Göhlich. "Implementation schemes for electric bus fleets at depots with optimized energy procurements in virtual power plant operations". *World Electric Vehicle Journal* 10.1 (2019), p. 5 (cit. on p. 64).

[152] D. M. Anand, R. T. de Salis, Y. Cheng, J. Moyne, and D. M. Tilbury. "A hierarchical incentive arbitration scheme for coordinated pev charging stations". *IEEE Transactions on Smart Grid* 6.4 (2015), pp. 1775–1784 (cit. on p. 64).

[153] J. Liu, J. Li, Y. Xiang, X. Zhang, and W. Jiang. "Optimal sizing of cascade hydropower and distributed photovoltaic included virtual power plant considering investments and complementary benefits in electricity markets". *Energies* 12.5 (2019), p. 952 (cit. on pp. 64, 65).

[154] C. Wei, J. Xu, S. Liao, Y. Sun, Y. Jiang, D. Ke, et al. "A bi-level scheduling model for virtual power plants with aggregated thermostatically controlled loads and renewable energy". *Applied Energy* 224 (2018), pp. 659–670 (cit. on pp. 64, 65).

[155] S. Rahmani-Dabbagh and M. K. Sheikh-El-Eslami. "A profit sharing scheme for distributed energy resources integrated into a virtual power plant". *Applied energy* 184 (2016), pp. 313–328 (cit. on pp. 64, 65).

[156] A. Laur, J. Nieto-Martin, D. W. Bunn, and A. Vicente-Pastor. "Optimal procurement of flexibility services within electricity distribution networks". *European Journal of Operational Research* 285.1 (2020), pp. 34–47 (cit. on p. 64).

[157] A. G. Zamani, A. Zakariazadeh, S. Jadid, and A. Kazemi. "Stochastic operational scheduling of distributed energy resources in a large scale virtual power plant". *International Journal of Electrical Power & Energy Systems* 82 (2016), pp. 608–620 (cit. on p. 65).

[158] S. Hadayeghparast, A. SoltaniNejad Farsangi, and H. Shayanfar. "Day-ahead stochastic multi-objective economic/emission operational scheduling of a large scale virtual power plant". *Energy* 172 (2019), pp. 630–646 (cit. on p. 65).

[159] D. Apostolopoulou, Z. De Grève, and M. McCulloch. "Robust optimization for hydroelectric system operation under uncertainty". *IEEE Transactions on Power Systems* 33.3 (2018), pp. 3337–3348 (cit. on pp. 66, 118).

[160] B. Zhou, G. Geng, and Q. Jiang. "Hydro-thermal-wind coordination in day-ahead unit commitment". *IEEE Transactions on Power Systems* 31.6 (2016), pp. 4626–4637 (cit. on p. 66).

[161] Y. Qiu, J. Lin, F. Liu, Y. Song, G. Chen, and L. Ding. "Stochastic Online Generation Control of Cascaded Run-of-the-River Hydropower for Mitigating Solar Power Volatility". *IEEE Transactions on Power Systems* 35.6 (2020) (cit. on pp. 66, 118).

[162] S.-E. Fleten and T. K. Kristoffersen. "Stochastic programming for optimizing bidding strategies of a Nordic hydropower producer". *European Journal of Operational Research* 181.2 (2007), pp. 916–928 (cit. on p. 66).

[163] A. Ben-Tal, A. Nemirovski, and L. El Ghaoui. *Robust optimization*. Princeton university press, 2009 (cit. on p. 66).

[164] A. T. Saric and A. M. Stankovic. "An application of interval analysis and optimization to electric energy markets". *IEEE Transactions on Power Systems* 21.2 (2006), pp. 515–523 (cit. on p. 67).

[165] A. Charnes and W. W. Cooper. "Chance-constrained programming". *Management science* 6.1 (1959), pp. 73–79 (cit. on p. 67).

[166] J. R. Birge and F. Louveaux. *Introduction to stochastic programming*. Springer Science & Business Media, 2011 (cit. on p. 67).

[167] Z. Chen, Z. Liu, and L. Wang. "A modified model predictive control method for frequency regulation of microgrids under status feedback attacks and time-delay attacks". *International Journal of Electrical Power & Energy Systems* 137 (2022), p. 107713 (cit. on pp. 68, 69).

[168] J. R. Nelson and N. G. Johnson. "Model predictive control of microgrids for real-time ancillary service market participation". *Applied Energy* 269 (2020), p. 114963 (cit. on pp. 68, 69).

[169] S. Cai and R. Matsuhashi. "Model predictive control for EV aggregators participating in system frequency regulation market". *IEEE Access* 9 (2021), pp. 80763–80771 (cit. on pp. 68, 69).

[170] F. Garcia-Torres, C. Bordons, J. Tobajas, R. Real-Calvo, I. Santiago, and S. Grieu. "Stochastic optimization of microgrids with hybrid energy storage systems for grid flexibility services considering energy forecast uncertainties". *IEEE Transactions on Power Systems* 36.6 (2021), pp. 5537–5547 (cit. on pp. 68, 69, 113).

[171] D. Van der Meer, G. C. Wang, and J. Munkhammar. "An alternative optimal strategy for stochastic model predictive control of a residential battery energy management system with solar photovoltaic". *Applied Energy* 283 (2021), p. 116289 (cit. on pp. 68, 69, 87).

[172] J. Vasilj, S. Gros, D. Jakus, and M. Zanon. "Day-ahead scheduling and real-time economic MPC of CHP unit in microgrid with smart buildings". *IEEE Transactions on Smart Grid* 10.2 (2017), pp. 1992–2001 (cit. on p. 69).

[173] M. Ellis, H. Durand, and P. Christofides. "A tutorial review of economic model predictive control methods". *Journal of Process Control* 24.8 (2014), pp. 1156–1178 (cit. on p. 74).

[174] A. Mesbah. "Stochastic model predictive control: An overview and perspectives for future research". *IEEE Control Systems Magazine* 36.6 (2016), pp. 30–44 (cit. on p. 75).

[175] L. Meeus. *The evolution of electricity markets in Europe*. Edward Elgar Publishing, 2020 (cit. on pp. 75, 152).

[176] ENTSO-E. *An overview of the European balancing market and electricity balancing guideline*. https://www.entsoe.eu/news/2018/12/12/electricity-balancing-in-europe-entso-e-releases-an-overview-of-the-european-electricity-balancing-market-and-guideline/. 2018 (cit. on p. 76).

[177] S. Camal. "Forecasting and optimization of ancillary services provision by renewable energy sources". PhD thesis. Université Paris sciences et lettres, 2020 (cit. on pp. 76, 157).

[178] N. Mazzi, J. Kazempour, and P. Pinson. "Price-Taker Offering Strategy in Electricity Pay-as-Bid Markets". *IEEE Transactions on Power Systems* 33.2 (2018), pp. 2175–2183 (cit. on pp. 82, 83).

[179] J. Dupačová, N. Gröwe-Kuska, and W. Römisch. "Scenario reduction in stochastic programming". *Mathematical programming* 95 (2003), pp. 493–511 (cit. on p. 93).

[180] W. Jiekang, Z. Jianquan, C. Guotong, and Z. Hongliang. "A hybrid method for optimal scheduling of short-term electric power generation of cascaded hydroelectric plants based on particle swarm optimization and chance-constrained programming". *IEEE Transactions on power systems* 23.4 (2008), pp. 1570–1579 (cit. on p. 113).

[181] Z. Yi, Y. Xu, and C. Wu. "Model-Free Economic Dispatch for Virtual Power Plants: An Adversarial Safe Reinforcement Learning Approach". *IEEE Transactions on Power Systems* 39.2 (2024), pp. 3153–3168 (cit. on p. 113).

[182] A. Maneesha and K. S. Swarup. "A survey on applications of alternating direction method of multipliers in smart power grids". *Renewable and Sustainable Energy Reviews* 152 (2021), p. 111687 (cit. on pp. 113, 117).

[183] D.-R. Han. "A survey on some recent developments of alternating direction method of multipliers". *Journal of the Operations Research Society of China* (2022), pp. 1–52 (cit. on p. 115).

[184] V. Kaisermayer, D. Muschick, M. Horn, and M. Gölles. "Progressive hedging for stochastic energy management systems: The mixed-integer linear case". *Energy Systems* 12.1 (2021), pp. 1–29 (cit. on p. 115).

[185] L. Santosuosso, S. Camal, A. Lett, G. Bontron, J. Kazempour, and G. Kariniotakis. "A Scenario-Spatial Decomposition Approach With a Performance Guarantee for the Combined Bidding of Cascaded Hydropower and Renewables". *HAL* (2024) (cit. on p. 115).

[186] L. Santosuosso, S. Camal, A. Lett, G. Bontron, and G. Kariniotakis. "Distributed economic model predictive control for the joint energy dispatch of wind farms and run-of-the-river hydropower plants". *Electric Power Systems Research* 235 (2024), p. 110805 (cit. on pp. 115, 118).

[187] C. J. López-Salgado, O. Añó, and D. M. Ojeda-Esteybar. "Stochastic unit commitment and optimal allocation of reserves: A hybrid decomposition approach". *IEEE Transactions on Power Systems* 33.5 (2018), pp. 5542–5552 (cit. on pp. 116, 118).

[188] E. Shayesteh, M. Amelin, and L. Söder. "Multi-station equivalents for short-term hydropower scheduling". *IEEE Transactions on Power Systems* 31.6 (2016), pp. 4616–4625 (cit. on pp. 116, 118).

[189] N. Ki. Panda and S. H. Tindemans. "Efficient quantification and representation of aggregate flexibility in Electric Vehicles". *Electric Power Systems Research* 235 (2024), p. 110811 (cit. on p. 116).

[190] L. S.M. Guedes, P. de Mendonça Maia, A. C. Lisboa, D. A. G. Vieira, and R. R. Saldanha. "A unit commitment algorithm and a compact MILP model for short-term hydro-power generation scheduling". *IEEE Transactions on Power Systems* 32.5 (2016), pp. 3381–3390 (cit. on pp. 116, 118).

[191] A. Alahyari, M. Ehsan, and M. Mousavizadeh. "A hybrid storage-wind virtual power plant (VPP) participation in the electricity markets: A self-scheduling optimization considering price, renewable generation, and electric vehicles uncertainties". *Journal of Energy Storage* 25 (2019), p. 100812 (cit. on p. 116).

[192] Z. Zhao, C. Cheng, S. Liao, Y. Li, and Q. Lü. "A MILP based framework for the hydro unit commitment considering irregular forbidden zone related constraints". *IEEE Transactions on Power Systems* 36.3 (2020), pp. 1819–1832 (cit. on pp. 116, 118).

[193] E. C. Finardi, E. L. Silva, and C. Sagastizàbal. "Solving the unit commitment problem of hydropower plants via Lagrangian relaxation and sequential quadratic programming". *Computational & applied mathematics* 24 (2005), pp. 317–342 (cit. on p. 116).

[194] Y. Ma, Y. Huang, G. Wu, J. Liu, Y. Liu, Y. Xiang, et al. "Decentralized monthly generation scheduling of cascade hydropower plants in multiple time scale markets". *International Journal of Electrical Power & Energy Systems* 135 (2022), p. 107420 (cit. on pp. 116, 118).

[195] J. Huang, X. Wu, Z. Zheng, Y. Huang, and W. Li. "Multi-objective optimal operation of combined cascade reservoir and hydrogen system". *IEEE Transactions on Industry Applications* 58.2 (2021), pp. 2836–2847 (cit. on pp. 116, 118).

[196] N. Lu, G. Wang, C. Su, Z. Ren, X. Peng, and Q. Sui. "Medium-and long-term interval optimal scheduling of cascade hydropower-photovoltaic complementary systems considering multiple uncertainties". *Applied Energy* 353 (2024), p. 122085 (cit. on pp. 116, 118).

[197] R. Egging, S.-E. Fleten, I. Grønvik, A. Hadziomerovic, and N. Ingvoldstad. "Linear decision rules for hydropower scheduling under uncertainty". *IEEE Transactions on Power Systems* 32.1 (2016), pp. 103–113 (cit. on pp. 116, 118).

[198] M.A. Hannan, M. G.M. Abdolrasol, M. Faisal, Pin J. Ker, R.A. Begum, and A. Hussain. "Binary particle swarm optimization for scheduling MG integrated virtual power plant toward energy saving". *IEEE Access* 7 (2019), pp. 107937–107951 (cit. on p. 116).

[199] N. Patari, V. Venkataramanan, A. Srivastava, D. K. Molzahn, N. Li, and A. Annaswamy. "Distributed optimization in distribution systems: Use cases, limitations, and research needs". *IEEE Transactions on Power Systems* 37.5 (2021), pp. 3469–3481 (cit. on p. 116).

[200] A. Helseth, S. Jaehnert, and A. L. Diniz. "Convex relaxations of the short-term hydrothermal scheduling problem". *IEEE Transactions on Power Systems* 36.4 (2020), pp. 3293–3304 (cit. on pp. 117, 118).

[201] S. Takriti, J. R. Birge, and E. Long. "A stochastic model for the unit commitment problem". *IEEE Transactions on Power Systems* 11.3 (1996), pp. 1497–1508 (cit. on pp. 117, 118).

[202] A. Kargarian, J. Mohammadi, J. Guo, S. Chakrabarti, M. Barati, G. Hug, et al. "Toward distributed/decentralized DC optimal power flow implementation in future electric power systems". *IEEE Transactions on Smart Grid* 9.4 (2016), pp. 2574–2594 (cit. on p. 117).

[203] J. Nocedal and S. J. Wright. *Numerical optimization*. Springer, 1999 (cit. on p. 117).

[204] R. Glowinski and A. Marroco. "Sur l'approximation, par éléments finis d'ordre un, et la résolution, par pénalisation-dualité d'une classe de problèmes de Dirichlet non linéaires". *Revue française d'automatique, informatique, recherche opérationnelle. Analyse numérique* 9.R2 (1975), pp. 41–76 (cit. on pp. 117, 120).

[205] D. Gabay and B. Mercier. "A dual algorithm for the solution of nonlinear variational problems via finite element approximation". *Computers & mathematics with applications* 2.1 (1976), pp. 17–40 (cit. on pp. 117, 120).

[206] Y. Wang, W. Yin, and J. Zeng. "Global convergence of ADMM in nonconvex nonsmooth optimization". *Journal of Scientific Computing* 78 (2019), pp. 29–63 (cit. on p. 117).

[207] G. Cohen. "Optimization by decomposition and coordination: A unified approach". *IEEE Transactions on automatic control* 23.2 (1978), pp. 222–232 (cit. on pp. 119, 120).

[208] W. Shi, Q. Ling, K. Yuan, G. Wu, and W. Yin. "On the linear convergence of the ADMM in decentralized consensus optimization". *IEEE Transactions on Signal Processing* 62.7 (2014), pp. 1750–1761 (cit. on p. 119).

[209] H. Everett III. "Generalized Lagrange multiplier method for solving problems of optimum allocation of resources". *Operations research* 11.3 (1963), pp. 399–417 (cit. on p. 119).

[210] P. Tseng. "Dual ascent methods for problems with strictly convex costs and linear constraints: A unified approach". *SIAM Journal on Control and Optimization* 28.1 (1990), pp. 214–242 (cit. on p. 119).

[211] M. Fukushima. "Application of the alternating direction method of multipliers to separable convex programming problems". *Computational Optimization and Applications* 1 (1992), pp. 93–111 (cit. on p. 127).

[212] S. Mhanna, G. Verbič, and A. C. Chapman. "Adaptive ADMM for distributed AC optimal power flow". *IEEE Transactions on Power Systems* 34.3 (2018), pp. 2025–2035 (cit. on p. 127).

[213] C. Mavromatis, M. Foti, and Ma. Vavalis. "Auto-tuned weighted-penalty parameter ADMM for distributed optimal power flow". *IEEE Transactions on Power Systems* 36.2 (2020), pp. 970–978 (cit. on p. 127).

[214] R. Takapoui, N. Moehle, S. Boyd, and A. Bemporad. "A simple effective heuristic for embedded mixed-integer quadratic programming". *International journal of control* 93.1 (2020), pp. 2–12 (cit. on p. 129).

[215] Y. Yang, Q.-S. Jia, Z. Xu, X. Guan, and C. J. Spanos. "Proximal admm for nonconvex and nonsmooth optimization". *Automatica* 146 (2022), p. 110551 (cit. on p. 129).

[216] E. L. Lawler and D. E. Wood. "Branch-and-bound methods: A survey". *Operations research* 14.4 (1966), pp. 699–719 (cit. on p. 129).

[217] M. L. Fisher, W. D. Northup, and J. F. Shapiro. "Using duality to solve discrete optimization problems: Theory and computational experience". *Nondifferentiable optimization*. Springer, 2009, pp. 56–94 (cit. on p. 130).

[218] D.r Gade, G. Hackebeil, S. M. Ryan, J.-P. Watson, R. J.-B. Wets, and D. L Woodruff. "Obtaining lower bounds from the progressive hedging algorithm for stochastic mixed-integer programs". *Mathematical Programming* 157 (2016), pp. 47–67 (cit. on p. 131).

[219] S. Zhan, J. Morren, W. van Den Akker, A. van der Molen, N. G. Paterakis, and J. G. Slootweg. "Combined MV-LV power grid operation: Comparing sequential, integrated, and decentralized control architectures". *2022 International Conference on Smart Energy Systems and Technologies (SEST)*. 2022, pp. 1–6 (cit. on p. 137).

[220] L. Santosuosso, S. Camal, A. Lett, G. Bontron, and G. Kariniotakis. "Optimization of large-scale virtual power plants integrating wind farms". *WindEurope Annual Event 2023*. Copenhagen, Denmark, 2023 (cit. on p. 140).

[221] N. Michelena, H. Park, and P. Y. Papalambros. "Convergence properties of analytical target cascading". *AIAA journal* 41.5 (2003), pp. 897–905 (cit. on pp. 140, 142, 144).

[222] C. Fetting. "The European green deal". *ESDN Report, December* 2.9 (2020) (cit. on p. 152).

[223] L. Meeus and A. Nouicer. *The EU clean energy package*. Florence School of Regulation, Energy, Electricity, 2018 (cit. on p. 152).

[224] Z. Ullah, A. Arshad, and A. Nekahi. "Virtual Power Plants: Challenges, Opportunities, and Profitability Assessment in Current Energy Markets". *Electricity* 5.2 (2024), pp. 370–384 (cit. on p. 152).

[225] A. Gonzalez-Garrido, A. Saez-de-Ibarra, H. Gaztanaga, A. Milo, and P. Eguia. "Annual optimized bidding and operation strategy in energy and secondary reserve markets for solar plants with storage systems". *IEEE Transactions on Power Systems* 34.6 (2018), pp. 5115–5124 (cit. on p. 152).

[226] A. Banshwar, N. K. Sharma, Y. R. Sood, and R. Shrivastava. "Market based procurement of energy and ancillary services from Renewable Energy Sources in deregulated environment". *Renewable Energy* 101 (2017), pp. 1390–1400 (cit. on p. 153).

[227] G. Wenzel, M. Negrete-Pincetic, D. E. Olivares, J. MacDonald, and D. S. Callaway. "Real-time charging strategies for an electric vehicle aggregator to provide ancillary services". *IEEE Transactions on Smart Grid* 9.5 (2017), pp. 5141–5151 (cit. on p. 153).

[228] A. Lesage-Landry, H. Wang, I. Shames, P. Mancarella, and J. A. Taylor. "Online convex optimization of multi-energy building-to-grid ancillary services". *IEEE Transactions on Control Systems Technology* 28.6 (2019), pp. 2416–2431 (cit. on p. 153).

[229] S. Camal, A. Michiorri, and G. Kariniotakis. "Optimal offer of automatic frequency restoration reserve from a combined PV/wind virtual power plant". *IEEE Transactions on Power Systems* 33.6 (2018), pp. 6155–6170 (cit. on p. 153).

[230] Europen Union. "Directive (EU) 2019/944 of the European Parliament and of the Council of 5 June 2019 on common rules for the internal market for electricity and amending Directive 2012/27". *Journal of the European Union* 158 (2019), pp. 125–199 (cit. on p. 153).

[231] F. Bovera, G. Rancilio, D. Falabretti, and M. Merlo. "Data-driven evaluation of secondary-and tertiary-reserve needs with high renewables penetration: The italian case". *Energies* 14.8 (2021), p. 2157 (cit. on p. 153).

[232] ENTSO-E. *Electricity Balancing in Europe – ENTSO-E releases an overview of the European electricity balancing market and guideline*. https://www.entsoe.eu/news/2018/12/12/electricity-balancing-in-europe-entso-e-releases-an-overview-of-the-european-electricity-balancing-market-and-guideline/ (cit. on pp. 153–156).

[233] L. Santosuosso, S. Camal, A. di Giorgio, F. Liberati, A. Michiorri, G. Bontron, et al. "Economic model predictive control for the energy management problem of a virtual power plant including resources at different voltage levels". *IET Conference Proceedings* 2023 (6 2023), pp. 2044–2048 (cit. on p. 154).

[234] L. Santosuosso, S. Camal, F. Liberati, A. Di Giorgio, A. Michiorri, and G. Kariniotakis. "Stochastic economic model predictive control for renewable energy and ancillary services trading with storage". *Sustainable Energy, Grids and Networks* 38 (2024), p. 101373 (cit. on pp. 154, 158, 163, 165).

[235] G. Rancilio, A. Rossi, D. Falabretti, A. Galliani, and M. Merlo. "Ancillary services markets in europe: Evolution and regulatory trade-offs". *Renewable and Sustainable Energy Reviews* 154 (2022), p. 111850 (cit. on pp. 155–157).

[236] J. Figgener, P. Stenzel, K.-P. Kairies, J. Linßen, D. Haberschusz, O. Wessels, et al. "The development of stationary battery storage systems in Germany–A market review". *Journal of energy storage* 29 (2020), p. 101153 (cit. on p. 155).

[237] Frontier Economics. "METIS Technical Note T4: Overview of European Electricity Markets". *METIS Tech Notes* 67 (2016) (cit. on p. 155).

[238] T. Kapetanovic, B. M. Buchholz, B. Buchholz, and V. Buehner. "Provision of ancillary services by dispersed generation and demand side response–needs, barriers and solutions". *e & i Elektrotechnik und Informationstechnik* 125 (2008), pp. 452–459 (cit. on p. 155).

[239] V. Ahlqvist, P. Holmberg, and T. P. Tangerås. *Central-versus self-dispatch in electricity markets*. JSTOR, 2018 (cit. on p. 156).

[240] Smart4RES. *Smart4RES: European research project supported by the Horizon 2020 Framework Program*. https://www.smart4res.eu/ (cit. on p. 163).

RÉSUMÉ

La nature stochastique des sources d'énergie renouvelable variables (vRES) pose des défis importants pour leur intégration à grande échelle dans les systèmes électriques. Cela a conduit au développement du paradigme des centrales électriques virtuelles (VPP), qui atténue l'intermittence et la variabilité des vRES en les agrégeant avec des unités pilotables. À mesure que la pénétration des vRES continue de croître, les VPP devraient se développer en taille de portefeuille. Cependant, la dimension du portefeuille ne représente qu'un aspect de la complexité des VPP modernes. Ces systèmes impliquent également des facteurs tels que des dynamiques non linéaires difficiles, plusieurs sources d'incertitude et des contraintes de couplage complexes entre les unités agrégées. Ensemble, ces défis contribuent à l'évolution des VPP en systèmes à grande échelle et dynamiques, avec des dynamiques internes complexes — que l'on désigne ici sous le nom de VPP complexes. Un défi majeur dans le développement des VPP complexes est la nécessité d'outils de prise de décision rapides et évolutifs capables de maintenir à la fois la qualité de la solution et la précision. Pour y répondre, cette thèse introduit un cadre de prise de décision entièrement stochastique à deux niveaux, conçu pour optimiser la participation des VPP aux marchés de l'électricité sur plusieurs étapes temporelles. Le cadre est ensuite entièrement décomposé selon les dimensions des scénarios et spatiale, permettant la création d'un algorithme distribué évolutif garantissant la performance, même pour les modèles VPP à variables entières mixtes. La méthodologie est validée par une étude de cas réelle de l'agrégateur français Compagnie Nationale du Rhône, qui gère un VPP complexe combinant des centrales hydroélectriques à cours d'eau, des actifs éoliens et solaires. Les résultats montrent que ce VPP complexe peut améliorer l'intégration des vRES sans recourir à des solutions de stockage conventionnelles. De plus, les méthodes distribuées proposées répondent efficacement aux complexités du système, offrant des garanties de performance fiables et une évolutivité pour les opérations des VPP.

MOTS CLÉS

Centrales électriques virtuelles; systèmes complexes; optimisation distribuée; optimisation stochastique; hydroélectricité en cascade; commande prédictive à base de modèle; énergie renouvelable; marché de l'énergie; services auxiliaires; stockage.

ABSTRACT

The inherent stochasticity of variable renewable energy sources (vRES) challenges their widespread integration, prompting the emergence of the virtual power plant (VPP) paradigm, which reduces vRES variability through their combined operation with flexible, dispatchable units. As vRES penetration continues to grow, VPPs are expected to expand in portfolio size. However, the portfolio dimension represents only one aspect of the complexity of modern VPPs. These systems also involve factors such as hard nonlinear dynamics, multiple sources of uncertainty, and intricate coupling constraints between aggregated units. Together, these challenges contribute to the evolution of VPPs into large-scale, dynamic systems with complex internal dynamics—referred to here as complex VPPs. A major challenge in the development of complex VPPs is the need for fast, scalable decision-making tools that can maintain both solution quality and accuracy. To address this, this thesis introduces a two-level, scenario-based, fully stochastic decision-making framework designed to optimize VPP participation in the electricity markets across multiple time stages. The framework is then fully decomposed along both the scenario and spatial dimensions, enabling the creation of a scalable distributed algorithm that guarantees performance, even for mixed-integer VPP models. This methodology is validated through a real-world case study from the French aggregator Compagnie Nationale du Rhône, which manages a complex VPP combining run-of-the-river cascaded hydropower plants, wind, and solar assets. The results show that this complex VPP can enhance vRES integration without relying on conventional storage solutions. Furthermore, the proposed distributed methods effectively address system complexities, providing reliable performance guarantees and scalability for complex VPP operations.

KEYWORDS

Virtual power plants; complex systems; distributed optimization; stochastic optimization; cascaded hydropower; model predictive control; renewable energy; energy trading; ancillary services; storage.